Removal of Nitrogen Based Pollutants From the AmmoniaDrive Exhaust

Timo Boxma

Master Thesis

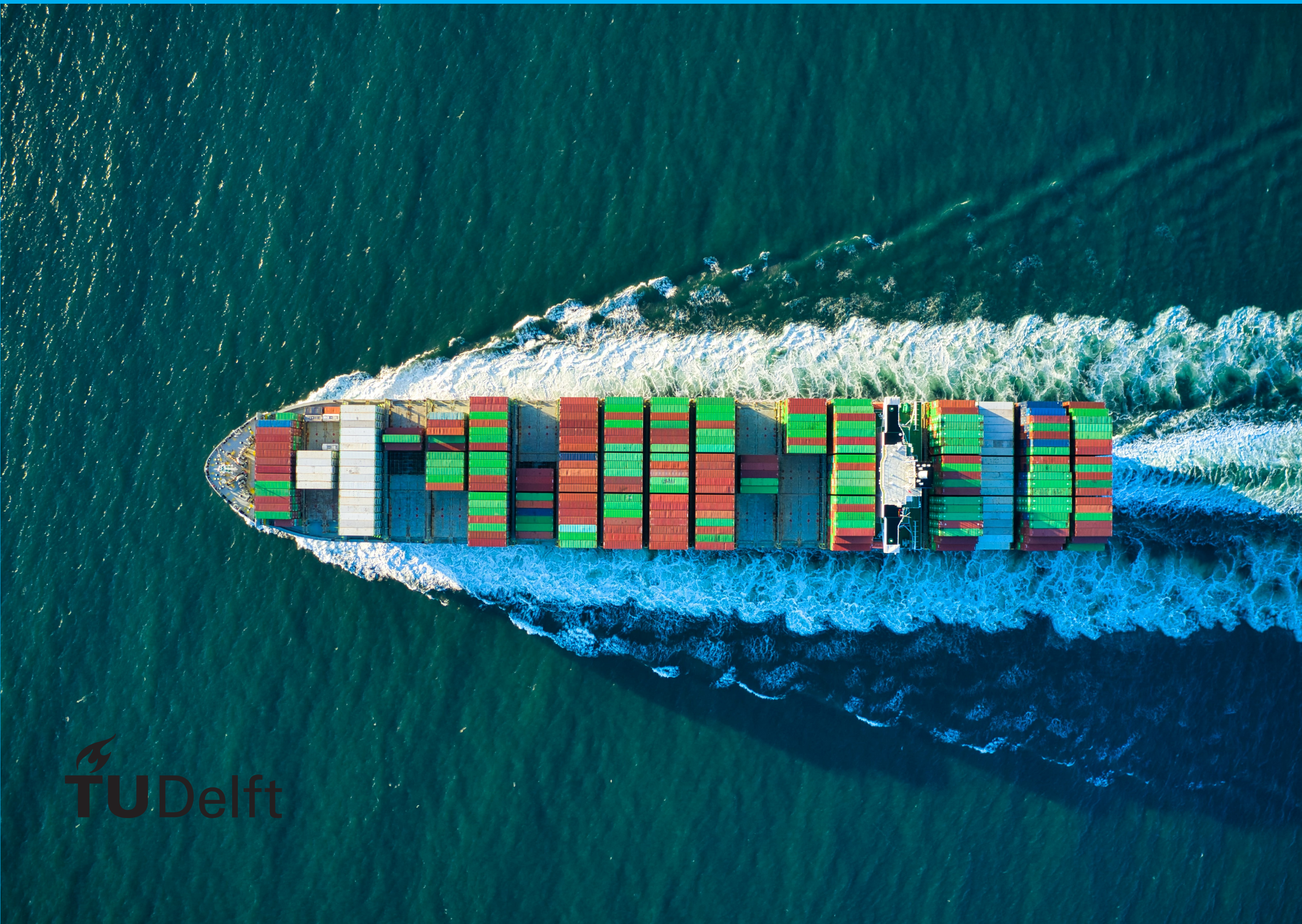

Thesis for the degree of MSc in Marine Technology in the specialization of Marine Engineering

Removal of Nitrogen Based Pollutants From the AmmoniaDrive Exhaust

by

Timo Boxma

This thesis (MT.21.004.m) is classified as confidential in accordance with the general conditions for projects performed by the TUDelft.

19/10/2021

Student number:	4365364	
Author contact e-mail:	timoboxma@hotmail.com	
Thesis number:	MT.21.004.m	
Project duration:	November 2020 – October 2021	
Thesis committee:	Ir. K. Visser,	TU Delft, chair
	Dr. ir. P. De Vos,	TU Delft, supervisor
	Prof. dr. ir. B.J. Boersma,	TU Delft
	Dr. ir. X.L.J. Seykens ,	TNO

TUDelft

Preface

With this thesis, I bring my time as a student to an end. Since I was little, moving things and boats have always fascinated me. Being able to study Maritime Technology was a true gift for me. I hope my thesis brings the AmmoniaDrive one step close to becoming a reality.

First, I want to thank all the members of the comity. Especially Peter, for having a lot of confidence in me. I am very thankful for the collaboration we had. I also want to thank Xander for sharing his knowledge on SCR's and running simulations in the ADVANCE software of TNO.

Finally, I would like to thank my friends and family. I want to specially name my parents, as they have always supported me throughout my entire education. Thank you, Jard, for your mental support and for all the fun activities we did together. I want to thank my friends from the study for all the Froffie we drank in all those years. Finally, my housemates and friends from HYSBAK for all the drinks and laughs we had together.

Timo Boxma
Rotterdam, October 2021

Summary

There is a strong need to reduce greenhouse gas emissions, including those of the maritime sector. To do so, the maritime industry needs to move away from fossil fuels and find different solutions. For deep-sea shipping, using ammonia as a fuel is one of those solutions. The AmmoniaDrive is a promising concept to use ammonia efficiently as a fuel onboard ships. However, there is already concern regarding harmful nitrogen-based emissions: NO_X, NH_3 and N_2O. The first two are a hazard for the local environment and human health, while the latter is a powerful greenhouse gas. Clearly, there is a need to prevent these pollutants from entering the atmosphere.

The removal of harmful emissions from the exhaust pipe can be done by installing after-treatment components. For AmmoniaDrive, the Selective Catalytic Reduction (SCR) is deemed the most useful component. The capability of the SCR to reduce both NO_X and NH_3 simultaneously is a huge benefit. SCR's are currently already used on ships to comply with regulations in the NO_X Emission Control Areas (NECA). In this application, the main objective is to reduce NO_X emissions, and Urea is added to the exhaust to provide the required NH_3 inside the SCR. The SCR's used in ships are currently often Va based. This material is cheap compared to Fe and Cu. Also, it has a high resistance to sulphur, which is often present in current marine fuels. Therefore, the use of NH_3 as fuel opens up the option to use Fe and Cu based SCR's. The Cu type is currently widely used in the automotive industry.

This study conducts experiments on a computer model describing a Va, Fe and Cu SCR. The goal of these experiments is to compare the steady-state performance of each material over a wide range of inlet variables. Most important for the SCR performance are the exhaust gas temperature, the NO_X concentration and the NH_3 concentration. The computer model is a 1-D single-channel model. This means 1 channel of the monolith is modelled and that this channel is discretised along the length of the monolith. Kinetic data from literature was used to determine the reaction rates.

The emission levels leaving the SCR are compared to the TIER III limits, currently in effect in the NECA's. These current limits only regulate the specific NO_X emissions. A new limit, also taking into account NH_3 and N_2O emissions is proposed. This new limit poses a maximum on the specific NO_X and NH_3 emissions combined. Moreover, it limits the N_2O emissions to reduce greenhouse gas emissions. Meeting these new limits is much harder compared to meeting the current regulations.

Due to the good performance of the Cu catalyst at low temperatures, it is considered the best option to reduce the NO_X and NH_3 emissions from the AmmoniaDrive power plant. The Va and Fe catalyst perform well at higher temperatures, but higher temperatures in the exhaust mean the system is less efficient. Removing N_2O from the exhaust is difficult; production of N_2O in the Internal Combustion Engine (ICE) should therefore be avoided. For future research, it is essential to look at the dynamic behaviour of all catalyst types. Furthermore, it is recommended to validate the models using physical tests.

Contents

List of Tables

List of Figures

1

Introduction

”The total annual Green House Gas (GHG) emissions from international shipping should be reduced by at least 50% by 2050 compared to 2008.” This is one of the main goals of IMO to fight global warming. To comply with the Paris agreement, an even larger reduction is needed: 95% compared to 1990 for the transport sector as a whole. Ships can be made to sail more efficiently, or the transport of goods can be organised more efficiently.

However, such ambitious reduction goals can not be met without the use of fossil-free fuels [30] & [60]. Batteries are not likely to become the standard for ships, due to their relatively low energy density and specific energy. The loss of cargo capacity would be too big. Green hydrogen has a high potential for inland and short sea shipping, but is also not likely to become the standard for deep sea. The fuel storage would take too much space, due to the low energy density of hydrogen.

Deep-sea shipping needs other green fuels with higher energy densities and specific energies. These can be carbon-based, such as green diesel or methanol, but can also be carbon-free: like ammonia. Ammonia has been marked by many as a very high potential candidate for deep-sea shipping. For shipping, the costs of ammonia compared to carbon-based green fuels will be similar or even cheaper if the feedstock cost of CO_2 becomes higher [60]. Compared to other fuels, ammonia has a good potential to be produced renewably, and it can easily be stored. These properties are shown in table 1.1 and figure 1.1. When looking at these figures it is important to note that ships often only bunker around 1/3 to 1/2 of their total capacity, which partially reduces the need for such high energy-dense fuels like diesel [60] and opens opportunities for using ammonia.

Table 1.1: Comparison renewable fuels [10]

Fuel type	Specific energy LHV [MJ/kg]	Energy density [GJ/m3]	Renewable synthetic production cost [MJ/MJ]	Storage pressure [bar]	Storage temperature [^{o}C]
Marine Gas Oil	42.7	36.6	n.a.	1	20
Liquid Methane	50	23.4	2.3	1	-162
Ethanol	26.7	21.1	3.6	1	20
Methanol	19.9	15.8	2.6	1	20
Liquid Ammonia	18.6	12.7	1.8	1 or 10	-34 or 20
Liquid Hydrogen	120	8.5	1.8	1	-253
Compressed Hydrogen	120	7.5	1.7	700	20

Ammonia can be directly fuelled into a Solid Oxide Fuel Cell (SOFC) to generate electricity [39]. However, to fully power a ship with a SOFC is less attractive. This is due to its high costs and low power density compared to an ICE. Besides, SOFC’s have a long start-up time and can not cope with fast load changes [3]. Neither is feeding NH_3 directly into an ICE the solution for a marine power plant. Due to slow burning velocity of an ammonia-air flame, some type of flame enhancement is needed for

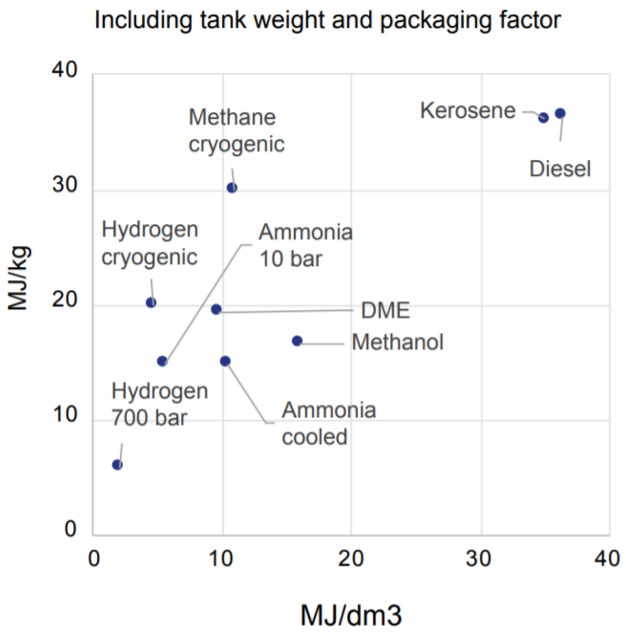

Figure 1.1: Energy density and specific energy of different fuels including tank weight and packaging factor [60].

ammonia to be used as a fuel. This could be done with hydrogen for example [37]. Hydrogen could be directly stored on board, but this poses challenges for storage on ships, due to its low energy density. Another solution is to crack the ammonia and produce hydrogen: something that can be done onboard the ship. AmmoniaDrive takes it even one step further by replacing a cracker by a SOFC, increasing the power plant's efficiency by multiple percent points. This is a result of the electric power produced by the SOFC when generating H_2. An overview of the power plant layout is shown in figure 1.2 [62]. The size of this system is not yet known. However, to perform this thesis, the size and power output of the system is set to be roughly equal to the Wärtsillä 12V31 marine engine.

The combustion of ammonia raises concerns with respect to nitrogen-based pollutants such as NO_X, N_2O and NH_3. They can be measured in the exhaust of multiple experimental NH_3-engines [41], [52], [67], [37]. The nitrogen based pollutants are bad for the local environment, cause global warming, and pose a risk for human health: they clearly should be kept to an absolute minimum. To do so exhaust after treatment will be installed with SCR as the main component, as is the logical choice with the presence of both NO_X and NH_3 in the exhaust. The aim of this thesis is to investigate the potentials for reducing these harmful nitrogen-based emissions using the SCR.

1.1. Objective and Research Questions

Ammonia fuel has a very high nitrogen content and is thus likely to emit large amounts of NO_x: up to 5 times as high as in current marine diesel engines [5]. The ICE is also likely to have un-burned ammonia in the outlet. Both substances are a serious hazard to the (local) environment and are topic of debate for what is known as the "stikstofcrisis" in the Netherlands [32]. In addition, NO_X is also a carcinogenic substance. At last, N_2O emissions are of concern, as this is a very strong greenhouse gas. More than enough reason to eliminate these emissions. This thesis focuses on the removal of these constituents from the exhaust, preventing the pollutants from entering the atmosphere. The main research question is as follows:

To what extend can the harmful nitrogen-based pollutants be removed from the AmmoniaDrive exhaust with existing after treatment components?

To help answer this question, the following sub-questions are proposed.

1. How can the exhaust of AmmoniaDrive be characterised in terms of composition, flow and temperature?
2. What components are currently available for exhaust after treatment and how would they be used in AmmoniaDrive? Can a preliminary setup of components be chosen?
3. Which parameters at the inlet of the SCR have most significant influence on reduction and production of nitrogen based pollutants in the SCR in stead state condition?
4. How do these important parameters influence the performance, i.e. the reduction and production of nitrogen based pollutants, of the SCR in stead state condition?
5. What are the needed outlet conditions from the ICE to ensure sufficient reduction of harmful emissions by the after treatment components in stead state condition?

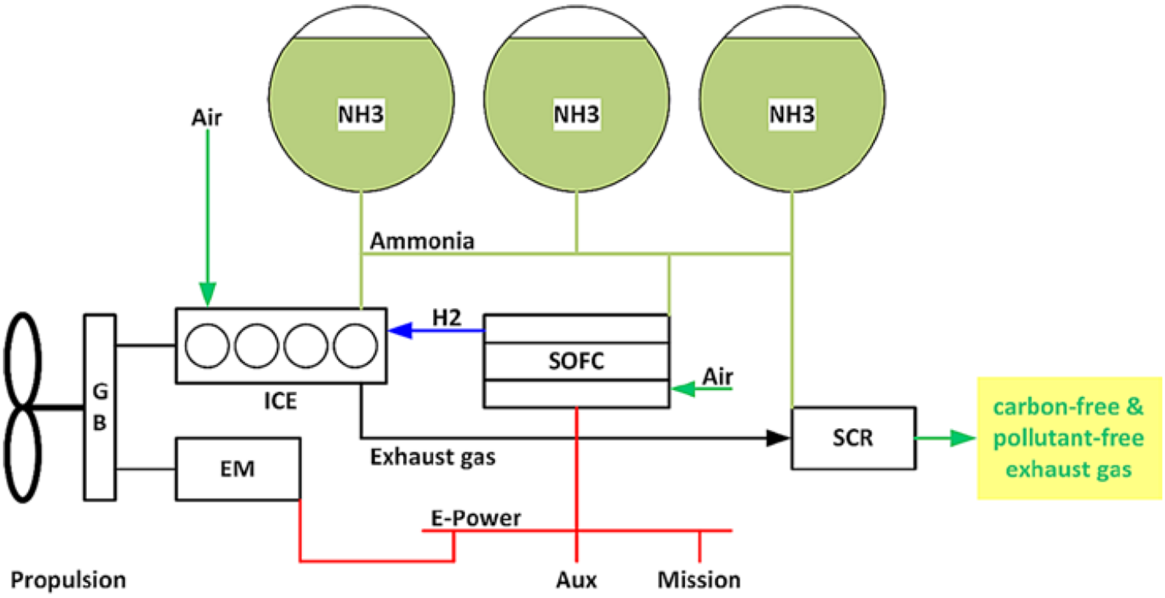

Figure 1.2: Overview of preliminary layout AmmoniaDrive system [62].

2

AmmoniaDrive Exhaust

In this chapter the combustion of ammonia is discussed, the pollutants that can be expected as a result of this chemical process, and their hazards. Next, the other properties of the exhaust are discussed. Finally, the legislation regarding nitrogen-based pollutants is discussed. This chapter comes from the literature report, conducted at the beginning of this thesis [4].

2.1. Ammonia Combustion

The kinetics of ammonia combustion have been widely studied. The overall reaction describing ideal ammonia combustion is as follows:

$$4NH_3 + 3O_2 \leftrightarrow 2N_2 + 6H_2O \tag{2.1}$$

The combustion kinetics have been studied by Duynslaegher et al. [16] at low pressures. She proposes the reaction mechanism shown in figure 2.1. Ammonia combustion at high pressures has been studied by Dai et al. [9]. The used reaction scheme, including the fluxes of more than 5%, is shown in figure 2.2. Although N_2O is not shown in this (due to its small mass flux) it is formed from NH2 and is discussed in the paper itself. Although both reaction mechanisms are different, it gives a preliminary insight into the different paths for ammonia combustion and radicals formed along these paths. From here, it is already possible to see which radicals can become a problem when present in the exhaust. NO, NO_2 and N_2O are all formed during ammonia combustion and are stable and harmful to the environment. As can be predicted when looking at mass fluxes in figure 2.2, NO will be the most dominant radical in the exhaust.

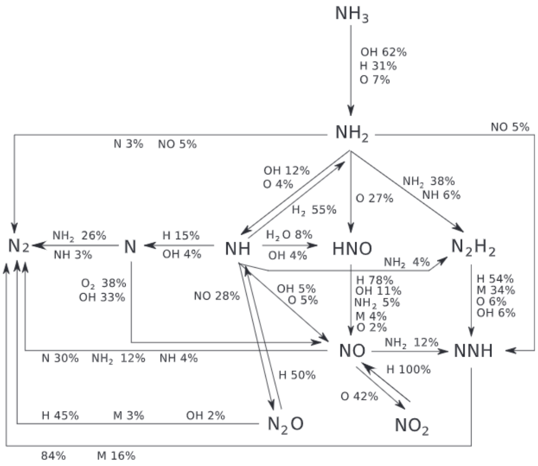

Figure 2.1: Consumption reaction pathways for the modified Konnov mechanism proposed by Duynslaegher et al. [16].

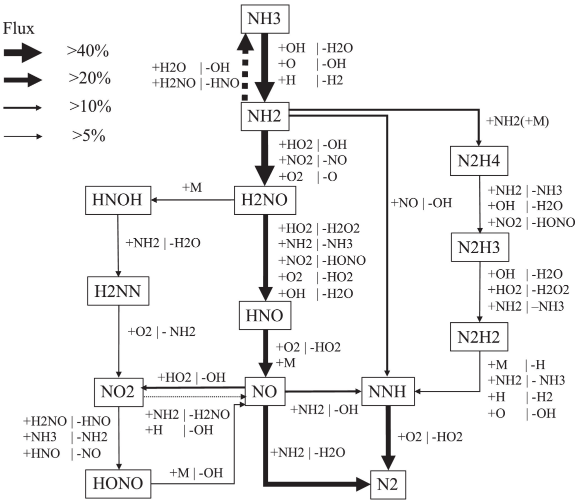

Figure 2.2: Reaction path diagram for pure NH_3 at ϕ=0.5, Tc=1080K, Pc=60bar [9].

2.2. NO_X, N_2O and NH_3

In this section, a more detailed explanation is provided on how the different pollutant emissions are formed and why they are undesired.

2.2.1. NO_X

NO_X is the collective term for NO and NO_2. Although NO is not directly a pollutant, it reacts with oxygen in the atmosphere to form NO_2. NO_2 can react with oxygen (O_2) molecules in the air to form ozone (O_3) and cause acid rain. The formation of ozone leaves a NO molecule, which again reacts to NO_2, after which the process starts over again [20]. One might think the ratio between NO and NO_2 is not of great importance, as NO is oxidised to NO_2 after all. This is however not true. The functioning of the after-treatment system is highly dependent on these ratios, which is further discussed in 3.3.
In combustion engines NO_X is formed via three different mechanisms: thermal, prompt and fuel NO_X. The quantities in which they are formed, depend mainly on temperature and residence time in the combustion chamber [33].

Thermal NO_X is formed in very hot parts of the combustion chamber. Nitrogen and oxygen from the air react with one another to form NO. This reaction is called the Seldovich mechanism and is shown in the two reactions below. Thermal NO_X often starts to form around 1900-2000K and above.

$$\begin{aligned} O + N_2 &\leftrightarrow NO + N \\ N + O_2 &\leftrightarrow NO + O \end{aligned} \tag{2.2}$$

The prompt NO_X is formed in rich sections of the fuel combustion. This means it is mainly present in direct injection engines, such as conventional diesels. It uses radicals such as CH, HCN, NCO HN and N to form NO_X. Of course, the radicals containing a carbon atom are only applicable to hydrocarbon fuels. This phenomenon is more important when the combustion temperature is too low for thermal NO_X to be formed.

The last mechanism converts nitrogen atoms in the fuel directly to NO_X. Fuel NO_X is formed when the nitrogen atoms in the fuel react with the oxygen in the air. This mechanism is already a large contributor of NO_X emissions for some hydrocarbon fuels, especially fuels such as heavy fuel oil that contain relatively high nitrogen contents, and are used in marine vessels. Clearly, the nitrogen content in ammonia is very high, which will make fuel NO_X a large contributor.

2.2.2. NH_3

The NH_3 emitted by the engine is directly related to the combustion efficiency of the engine. NH_3 causes damage to the environment and can be toxic to people [69]. Currently, agriculture is the main source of NH_3, but transportation and power plants using SCR systems are also an increasing source of NH_3. The use of NH_3 as a main fuel could lead to a further increase in pollution if no proper measures are taken.

High concentrations of NH_3 can be found in the exhaust if the engine is operated in rich condition, due to the lack of available oxygen molecules to react with. In other engines running a premix of air and fuel, a portion will always remain unburned. Wall wetting is one of the mechanisms for fuel to stay unburned. However, as ammonia is already gaseous at ambient conditions, this mechanism is unlikely to contribute in the case of ammonia combustion [67].

Other sources of unburned fuel are trapped fuel inside the combustion chamber crevices and fuel near the cylinder wall. The latter is likely to suffer from flame quenching due to the relatively cold cylinder walls. The amount of unburned fuel in crevices increases with the pressure, and thus compression ratio, inside the combustion chamber [67].

2.2.3. N_2O

N_2O is a major problem as it is a strong greenhouse gas: the global warming potential (GWP) of N_2O is very high at 298 CO_2 equivalents! [21]. This means one kg of N_2O contributes just as much to the greenhouse effect as 298 kg of CO_2. Clearly, emitting larger quantities of this substance would disregard the benefits of having a CO_2 free power plant. N_2O has two sources in AmmoniaDrive: the ICE and the after-treatment components. Westlye, Ivarsson, and Schramm [67] suggest N_2O is formed when unburned ammonia from the crevices reacts with the NO in the cylinder during the expansion stroke. The following two reactions are believed to be responsible for the N_2O formation at low and high temperatures respectively:

$$NH_2 + NO_2 \leftrightarrow N_2O + H_2O \tag{2.3}$$

$$NH + NO \leftrightarrow N_2O + H \tag{2.4}$$

The N_2O can not only be emitted by the ICE, but can also be formed along the different catalytic components in the exhaust treatment [1] & [26]. A more detailed explanation of these mechanisms is discussed in 3.

2.3. Regulations

Currently, the MARPOL annex IV regulates the NO_x emissions for merchant ships. The limits in place are presented in table 2.1 [29]. Whilst the TIER II limits apply worldwide, the Tier III limits are only applicable in Emission Control Areas (ECA) [27]. For this study, TIER III limits will be used as a standard, as AmmoniaDrive ships should be able to operate in those ECAs. This means that if an engine speed of 750 RPM (Wartsilla 31V12) is adopted, the maximum allowable NO_X emission would be $9 \cdot 750^{-0.20} = 2.4\ [g/kWh]$. For the engines presented in chapter 2.4 the limits would be $9 \cdot 1000^{-0.20} = 2.3\ [g/kWh]$ and $9 \cdot 1500^{-0.20} = 2.1\ [g/kWh]$ for the engines running at 1000 and 1500 RPM respectively.

Table 2.1: NO_x emission limit by IMO. [29]

Tier	Ship construction date on or after	Total weighted cycle emission limit (g/kWh)		
		n = engine's rated speed (rpm)		
		n < 130	n = 130 - 1999	n ≥ 2000
I	01-Jan-00	17	$45 \cdot n^{-0.20}$	9.8
II	01-Jan-11	14.4	$44 \cdot n^{-0.23}$	7.7
III	01-Jan-16	3.4	$9 \cdot n^{-0.20}$	2

The IMO does not yet impose any limits on NH_3 emissions by ships. It is however likely that such limits will be implemented in the IMO regulations once ammonia becomes a more widely available and used fuel by ships.

As the IMO regulations are often slow, it is also interesting to have a look at the more progressive emission limits for heavy-duty road vehicles sold in the EU. The limits are regulated under EURO 6 and limit the emissions for both NO_X and ammonia. The limits on NO_X are much lower than those posed by the IMO: 0.4 and 0.46 g/kWh for steady-state and transient testing respectively. The limit on ammonia is set at 10 ppm [14]. Although future shipping regulations are likely to allow higher values, a similar order size should be achieved by AmmoniaDrive after treatment.

2.4. AmmoniaDrive Outlet

As the AmmoniaDrive is still a non-existing drive, the exact composition of the exhaust gas is unknown. However, an estimate should be made to further investigate the feasibility of eliminating the harmful emissions. The following outlet parameters of the ICE are considered to be of great importance:

- Exhaust composition
- Exhaust temperature
- Exhaust flow

2.4.1. Composition

As discussed in chapter 2.1 the expected compounds in the exhaust are N_2, O_2, H_2O, NO, NO_2, N_2O, and NH_3. The concentrations of N_2, O_2, and H_2O can be calculated using the standard composition of air and the overall reaction for complete ammonia combustion as shown in reaction 2.1. Standard air consists of 21% oxygen, 78% nitrogen and 1% other by volume [19]. For convenience, 21% oxygen and 79% nitrogen is assumed. The composition of the non-toxic components can thus be easily approximated using the equations below. In this approximation, a complete combustion is assumed (which is of course incorrect, but gives the needed level of detail):

$$\begin{aligned} x_{O_2} &= \frac{21 - 21\phi}{100 + \phi\left(21 + 14x_{fuel,NH_3}\right)} \\ x_{N_2} &= \frac{79 + 14\phi x_{fuel,NH_3}}{100 + \phi\left(21 + 14x_{fuel,NH_3}\right)} \\ x_{H_2O} &= \frac{42\phi}{100 + \phi\left(21 + 14x_{fuel,NH_3}\right)} \end{aligned} \tag{2.5}$$

The levels of NO, NO_2, N_2O, and NH_3 are less easily determined. Studies of the levels of these substances in the exhaust of an ammonia hydrogen engine have been performed by Westlye, Ivarsson, and Schramm [67], Pochet, Jeanmart, and Contino [52] and Lhuillier et al. [42]. A short overview of the type of engine and the exhaust levels are shown in table 2.2.

Table 2.2: Hydrogen ammonia engines

Author	Westlye et al. [67]	Lhuillier et al. [42]	Pochet et al. [67]
Ignition	SI	SI	HCCI
Cylinders [#]	1	1	1
η [%]	20-40	39	37
H2 fraction [-]	0.2	0-60	0.06-1
Volume [cc]	612	400	436
Speed [RPM]	1000	1500	1500
NO [ppm]	1000-5000	186-9280	1000-6000
NO_2 [ppm]	10-150	0-500	
N_2O [ppm]	10-40	3-95	significant
NH_3 [ppm]	1000-3000	1100-20000	0-6000
CR [-]	7-15	10.5	21.9
ϕ [-]	0.7-1	0.6-1.2	0.1-0.6
T_{exh} [K]	675-800	675-825	450-600

Both SI engines show relatively little NO_X production when operated at stoichiometric or rich conditions. Furthermore the NO_X is dominated by NO. NO emissions are generally in the order size of 1000s of ppm, and so is NH_3. It is important to note that the researchers found feasible operating conditions with a NH_3/NO_X ratio close to 1 in the exhaust, which would be beneficial for the after-treatment system. NO_2 is only in the order size of 10s of ppm, and the same applies to N_2O.

The Homogeneous Charge Compression Ignition (HCCI) engine shows roughly equal amounts of NO_X and NH_3 in the exhaust. Large differences can however be seen for the NO_2/NO ratio and N_2O levels. Pochet, Jeanmart, and Contino [52] reports the NO measurements to be flawed by N_2O, as the UV spectrometer used, can not separate the two. N_2O emissions are very high due to the relatively cold temperatures (below 1400K) in the cylinder. Under these conditions, it is not possible to fully oxidise NH_3. Even when the combustion temperature is further increased, wall quenching will always reduce this combustion temperature locally.

Obviously, the engines shown in table 2.2 are very different from marine engines such as the Wärtsilä 31V12. How the levels of the different pollutants will scale is very difficult, if not impossible to predict at this stage. The vastly different size and speed of the engine change important NO_X parameters, such as burning temperature and residence time. The pollutant levels found in the small engines will be used throughout the research as it is the best option for now.

2.4.2. Exhaust Temperature

Temperature is one of the key aspects when it comes to the after-treatment of the exhaust [70]. The engines presented in table 2.2 also show an exhaust temperature. Both SI ignited engines show an increase in exhaust temperature with an increase of ϕ. The lowest value found in the HCCI engine by Pochet, Jeanmart, and Contino [52] corresponds to pure hydrogen combustion, while the upper limit corresponds to 95% ammonia mixture by volume.

These smaller engines have actual measurements. These physical experiments are very valuable. On a marine scale, multiple computational studies have been performed. The company Proton Ventures B.V. has studied a compression ignition type engine running on ammonia for marine purposes. The rated power of this engine was 8MW. As part of this project, they had the goal to perform experimental data to validate the efficiency of the model and to register the emissions. However, the available software at that time was not powerful enough to estimate such emissions. Although not realistic, the model assumed complete combustion. With this condition, the exhaust temperature was calculated at ca.296 ^oC [22].

Recently Zheng [74] studied the combustion of hydrogen ammonia blends in internal combustion engines on marine size. In his findings, he concluded HCCI to be a very promising technique for an ammonia-hydrogen engine. The exhaust temperature in this research ranged from 550 to 650 K. Unfortunately, pollutant concentrations were not calculated in this research.

Combining the previous data, it can be concluded that large differences in exhaust temperature exist. The HCCI and compression ignition type engines have a lower exhaust temperature compared to the SI engines. Despite the differences, all temperatures are within the working ranges of SCR systems.

2.4.3. Flow

The exhaust flow of an ammonia engine will be different compared to the exhaust flow of a conventional diesel powerplant. This has consequences for the flow resistance and allowable pollutant concentrations in the exhaust. The latter is due to the fact that emission limits are measured in gr/kWh. If the Wärtsilä 12V31 is taken as a reference, an order of magnitude of the airflow can be estimated. First the equivalence ratio of the engine is determined using the data from table 2.3 [64] and table 2.4. The used calculation method is shown below [33]:

$$\begin{aligned}
\phi^{-1} &= \left(\frac{A}{F}\right)\cdot\left(\frac{F}{A}\right)_s = \left(\frac{f_{air}}{f_{fuel}}\right)\cdot\left(\frac{F}{A}\right)_s \\
\phi^{-1} &= \left(\frac{f_{exh}-f_{fuel}}{f_{fuel}}\right)\cdot\left(\frac{F}{A}\right)_s = \left(\frac{f_{exh}}{f_{fuel}}-1\right)\cdot\left(\frac{F}{A}\right)_s \\
\phi &= \left(\left(\frac{f_{exh}}{SFC\cdot P}-1\right)\left(\frac{F}{A}\right)_s\right)^{-1} \approx 0.4 \text{ for all operating conditions}
\end{aligned} \tag{2.6}$$

Table 2.3: Wartsila 12V31 operating conditions [64].

Power [kW]	sfc [g/kWh]	f_{exh} [kg/s]
7080	169.6	12.6
6018	167.7	10.68
5310	171.7	10.08
3540	179	7.44

Next, an estimate can be made for the ammonia hydrogen engines. The efficiency and thus in going chemical energy will be roughly the same for all concepts. Looking at the stoichiometric ratios and Lower Heating Value (LHV) of the different fuels, it becomes clear that similar mass flows can be expected in the exhaust regardless of the fuel used. Hydrogen is not taken into account here, as it is only a small fraction of the fuel on mass base. Ammonia SI engines will run close to an equivalence ratio of 1, but slightly lean [42] and the HCCI engines close to 0.2/0.3 [52], [74]. The expected mass flow through the after-treatment system will thus be around 2 times smaller for the ammonia SI engine and up to 2 times larger for the HCCI engine, compared to the conventional diesel engine. It is important to note that the lower mass flow of the SI engine is beneficial as much higher pollutant concentrations (measured in ppm) are allowed, compared to the HCCI engine, when looking at the same g/kWh emission levels.

Table 2.4: Stoichiometric air to fuel ratios of MDO and NH_3

	$\left(\frac{A}{F}\right)_S$ [kg/kg]	LHV [MJ/kg]	$\frac{LHV}{\left(\frac{A}{F}\right)_S+1}$ [Mj/kg]	Ref
MDO	14.5	42.7	2.8	[36]
NH_3	6.06	18.8	2.7	[74], [61]

3

Exhaust After-Treatment

This chapter comes from the literature report, conducted at the beginning of this thesis [4]. The allowable limits for ships and trucks are very different, as explained in chapter 2.3. As a result, both after-treatment systems are also very different. In this section, a short overview of a common layout system for both applications will be given. The focus will be centred around a system with SCR. Other options would include a three-way catalyst as is common in stoichiometric operated cars. This option is not considered as it does not break down NH_3 and does not convert NO_X when oxygen is present in the exhaust [12].

3.1. Common Layout Ships

The after-treatment system for modern ships often consist of two main components: the scrubber and SCR unit. A schematic overview, such as provided by Wärstilä is shown in figure 3.1. The scrubber is installed to reduce sulphur oxide emissions. As of 2020 stricter regulations are enforced regarding sulphur emissions by ships. Globally only 0.5% sulphur content is allowed in the fuel, or a scrubber has to clean the exhaust, to reach similar levels of sulphur [28]. In the ECAS this level is even as low as 0.1% sulphur. When switching to ammonia as a fuel, as is with all synthetic fuels [60], no sulphur will be present in the fuel and thus the exhaust. As a result, the need to have a scrubber installed will be completely eliminated.

A SCR reactor is installed to reduce the NO_X emitted by the ship. The NO_X reacts with NH_3 over a catalytic surface and forms N_2 and H_2O. A more detailed explanation of the working principles of the SCR is given later in this chapter. The ammonia required for this reaction is injected into the exhaust in the form of Urea. A solution of 40% urea in water is most commonly used in the shipping industry [5]. The solution is non-toxic and non-combustible in contrast to ammonia and is, therefore, more easily stored onboard. Once injected into the exhaust stream the water vaporises and the urea is decomposed into NH_3 and CO_2. This decomposition is a very important process and requires a temperature of 180/200 or higher [70] & [51]. The AmmoniaDrive will most likely use NH_3 directly as it is already stored as fuel onboard the ship. As a result, the after-treatment system will not struggle with the partial decomposition of urea.

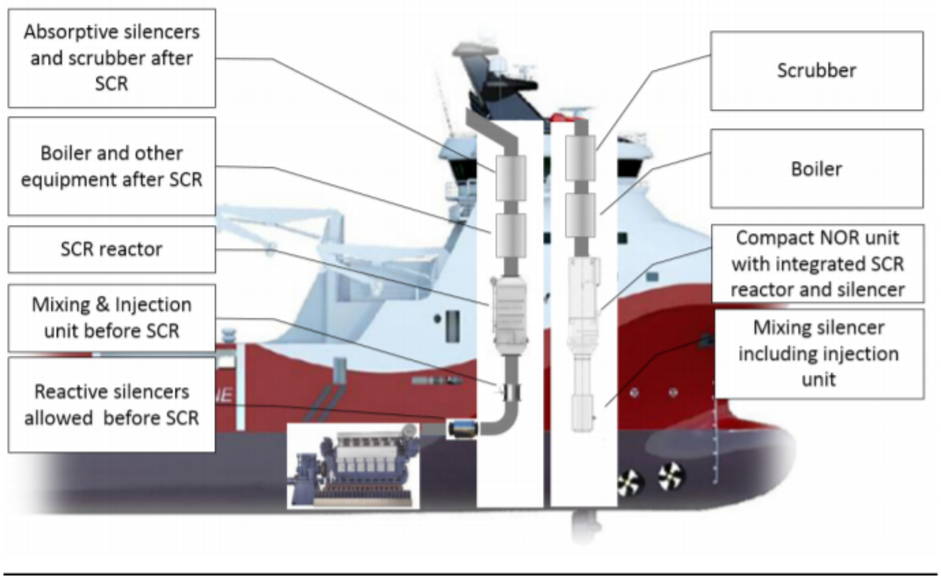

Figure 3.1: Exhaust after-treatment onboard ships, overview of Wärtsilä [65]

3.2. Common Layout Road Vehicle

The current allowable emissions for road transportation are much lower than that of shipping. As a result, the after-treatment systems installed are also much more extensive. An overview of the standard exhaust cleaning system for EURO 6 heavy-duty diesel exhaust is shown in figure 3.2. It differs greatly from the system presented in figure 3.1. Firstly, there is no scrubber or other device to remove SO_X content. SO_X is not even presented as a harmful substance. This is due to the very low sulphur contents of today's fuels for road vehicles. First, the exhaust passes a Diesel Oxidation Catalyst (DOC). This catalyst burns hydrocarbons that have slipped through the ICE. This is of course not relevant for the AmmoniaDrive, but it also converts a large portion of NO into NO_2, which can be very beneficial as it enables more active reaction mechanisms. A more detailed explanation is given in chapter 3.3. It also raises the temperature slightly which helps the SCR reactions. Although a larger SCR would give the same result [23].

Next down the line, the Diesel Particulate Filter (DPF) is installed. This filter eliminates the Particulate Matter (PM) from the exhaust. In the AmmoniaDrive context, a DPF is less relevant. The burning of fuel will not produce PM, however, a particulate filter would be useful for wear from the engine and lubricant oils. As the DPF has only little significance with respect to AmmoniaDrive, it is not further discussed.

Before the exhaust enters the SCR, Urea is added to the exhaust gas. Urea decomposes into ammonia and carbon dioxide, and NH_3 is used as a reducing agent in the SCR. The exhaust now enters the SCR. The ammonia reacts with the NO and NO_2 and produces water and nitrogen. This component will be key in reducing the harmful emissions in the AmmoniaDrive exhaust, as it is currently the only working mechanism to reduce the NO_X and NH_3 content simultaneously. To effectively do so, often a slight excess of ammonia is entering into the SCR. This excess ammonia is broken down in the Ammonia Slip Catalyst (ASC). The amount of excess ammonia is still unknown: at one far end extra ammonia will have to be added before the SCR and thus low quantities will have to be broken down. At the other far end, large quantities coming from the engine will have to be further decomposed in the ASC.

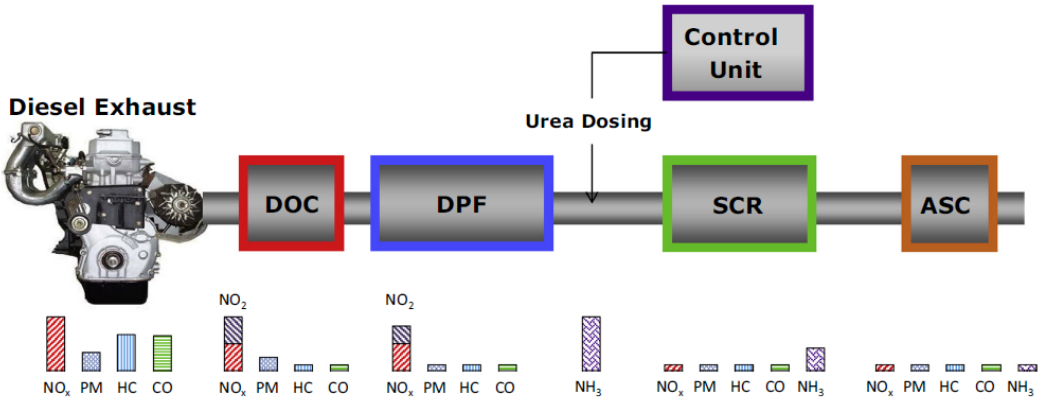

Figure 3.2: The standard Euro VI diesel engine exhaust gas cleaning system. The bars below the catalysts represent the effect each catalyst has on the composition of the exhaust gases [1]

3.3. After Treatment Components

In this section, a more detailed explanation of the different components and their reaction mechanisms is given.

3.3.1. DOC

The (Diesel Oxidation Catalyst) DOC has been applied in road vehicles over the last 40 years. The DOC usually uses platinum as a catalytic material and has a strong oxidising nature [2]. The main function of the DOC is to oxidise the hydrocarbons and CO in the exhaust. Both reactions are shown in reaction scheme 3.1 and 3.2 respectively. The AmmoniaDrive itself will not emit any hydrocarbons, and as a result, the DOC will and can not be used in this way.

$$C_nH_{2m} + \left(n + \frac{m}{2}\right) O_2 \rightarrow CO_2 + H_2O \tag{3.1}$$

$$2CO + O_2 \rightarrow 2CO_2 \tag{3.2}$$

Due to the strong oxidising nature of the catalyst, not only hydrocarbons and carbon monoxide are oxidised, but also the other substances in the exhaust. This is one of the main reasons why they are currently not installed in marine applications. The high sulphur content of marine fuels becomes problematic as H_2SO_4, also known as sulphuric acid, is formed in the DOC according to reaction 3.3 [13].

$$\begin{gathered} 2SO_2 + O_2 \rightarrow 2SO_3 \\ SO_3 + H_2O \rightarrow H_2SO_4 \ (sulphuric\ acid) \end{gathered} \tag{3.3}$$

Sulphuric acid is a very corrosive and aggressive acid. However, without the presence of sulphur in the fuel, this is not a problem anymore. One of the great benefits of the DOC is the conversion of NO into NO_2 as shown in reaction 3.4. The presence of NO_2 promotes the fast SCR reaction 3.8 as is explained later in this chapter. The elevated NO_2 content is even of such high importance, DOC systems are often optimised for NO_2 production [13].

$$2NO + O_2 \rightarrow 2NO_2 \tag{3.4}$$

Although lacking proper documentation of NH_3 oxidation over a DOC, it is very likely to happen [70]. Both ASC and DOC are platinum-based catalysts, therefore the same oxidation mechanisms are expected for both catalysts, as shown in reaction 3.14, 3.15 and 3.16. The NH_3 oxidation is a waste of fuel as it is also needed in the SCR. Moreover, it could produce N_2O and NO_X! For both reasons, a DOC is currently not seen as a vital component for the exhaust after-treatment of AmmoniaDrive.

3.3.2. SCR

SCR is a widely adopted device to deNO$_X$ the exhaust gasses of ships, cars and other lean operated engines. The first SCR systems on ships were installed around 1990 and have now become the main device to reduce NO$_X$ emissions from lean operated engines [15]. Although SCRs are not the only solution to reduce NO$_X$ content in the exhaust, they are in this thesis considered the only logical option for AmmoniaDrive. Other solutions applied in the automotive industry are the Three-Way Catalyst (TWC) and Lean NO$_X$ trap. The former is used in stoichiometric operated engines and reduces the hydrocarbons, carbon monoxide and NO$_X$ simultaneously. They lose conversion efficiency quickly when the engine is not operated at stoichiometric condition and are thus deemed not suitable [59] & [12]. The Lean NO$_X$ Trap (LNT) is mainly used in light-duty diesel vehicles [58]. The NO$_X$ is ”trapped” on a substrate, which is regenerated by introducing hydrocarbons into the LNT. This is usually done by running a few rich cycles in the engine for 1-10 seconds every 60-120 seconds. Compared to a SCR it provides a less cost-effective solution and is less efficient. However, it has the benefit of eliminating the need for carrying an extra reducing agent in a separate tank. Clearly, this benefit does not apply to AmmoniaDrive as NH$_3$ is already present in the exhaust and directly available as fuel. In the case of AmmoniaDrive, it would also be possible to regenerate the trap with hydrogen instead of hydrocarbons. This regeneration would also produce N$_2$O and NH$_3$, which must be reduced again down the line [6]. Furthermore, it requires the FC to produce more hydrogen, which is not beneficial for the fuel consumption and system size. Combining these facts, the LNT is not considered to be a suitable solution for the AmmoniaDrive.

Inside the SCR multiple reactions are taking place. The most important ones are those where NH$_3$ reacts with NO and NO$_2$. Before this can happen the NH$_3$ has to be absorbed on the monolith. The absorption en desorption of NH$_3$ goes via the following reaction scheme [1], where S denotes a free surface and the * absorbed ammonia:

$$NH_3 + S \leftrightarrow NH_3^* \tag{3.5}$$

This reaction depends, just like all reactions, on the temperature of the monolith. All materials can store more NH$_3$ at lower temperatures and less at higher temperatures. The storage of ammonia takes place on the so-called Lewis and Brønsted acid sites. The Lewis sites can accept electrons from the NH$_3$ molecules to bond, while the Brønsted sites donate a proton to the NH$_3$ molecule. The Lewis site provides a weaker bond for ammonia, while the Brønsted provides a stronger bond. The amount of available sites is dependent on the used catalytic material. It is also important to note that NH$_3$ is not the only substance in the exhaust which can bind with the acid sites: H$_2$O and OH can also take the place of NH$_3$, leaving no or fewer sites for the NH$_3$ to bond. [55] & [5]

The buffer of ammonia provides clear advantages and disadvantages. If the catalyst can store a lot of NH$_3$ it is less sensitive to changes in the inlet concentrations. However, the system becomes much more sensitive to changes in inlet temperature (related to load changes in the engine). The increase in temperature will lead to a larger release of NH$_3$ molecules if the buffer capacity is larger [35].

Once the ammonia is absorbed it can react with the other substances present in the exhaust. According to Lezcano-Gonzalez et al. [40] & Liu, Zhao, and Lee [43] the NH$_3$ molecules stored on the Brønsted sites react very slowly compared to the ones stored on the Lewis sites and thus have only little contribution to the SCR process. The reactions can be split into a set of desired and a set of undesired reactions. The desired reactions convert the harmful NO and NO$_2$ into the harmless N$_2$ and H$_2$O. There are three of them, and are often referred to as slow, standard and fast SCR and are shown in reaction scheme 3.6, 3.7 and 3.8 respectively [5].

$$8NH_3^* + 6NO_2 \rightarrow 7N_2 + 12H_2O + 8S \tag{3.6}$$

$$4NH_3^* + 4NO + O_2 \rightarrow 4N_2 + 6H_2O + 4S \tag{3.7}$$

$$2NH_3^* + NO + NO_2 \rightarrow 2N_2 + 3H_2O + 2S \tag{3.8}$$

The medium SCR reaction needs O$_2$, but its rate is not reduced as long as the oxygen content is above 2% in the exhaust [73]. The temperature of the monolith and catalytic material influence greatly what reactions take place. This is discussed in more detail later in this chapter. The consumption of NH$_3$ with respect to NO_X is 1:1 for the medium and fast SCR reaction. For the slow reaction this ratio is equal to 4:3. As mentioned earlier, the ratio between NO_2 and NO is very important. If the ratio is closer to 1 nearly all NO_X and NH_3 will react via the fast SCR reaction, resulting in higher conversion efficiencies.

Next, there are the undesired reactions. In the case of high sulphur content fuels, the SO_2 in the exhaust can be absorbed by the catalyst and react later on with the ammonia. In AmmoniaDrive this is clearly not a problem. The absorbed ammonia can react in multiple undesirable ways [5]. Firstly it can oxidise as shown in reaction scheme 3.9. The NO that is produced, can still be broken down further downstream. It is undesirable as it consumes NH_3 and thus increases the use of reducing agent. However, in AmmoniaDrive it could be a useful reaction as it is a functioning mechanism to get rid of excess NH_3. Next, the ammonia can react with NO_2 to form ammonium nitrate, as presented in reaction scheme 3.10. This reaction mainly occurs at low temperatures, but can be a problem as it causes solid deposition on the washcoat. Finally, the ammonia can react with NO to form N_2O, following reaction scheme 3.11. This is a major problem as it is a strong greenhouse gas, and can not be broken down any further down the line.

$$4NH_3^* + 5O_2 \rightarrow 4NO + 6H_2O + 4S \tag{3.9}$$

$$2NH_3^* + 2NO_2 \rightarrow NH_4NO_3 + N_2 + H_2O + 2S \tag{3.10}$$

$$4NH_3^* + 4NO + 3O_2 \rightarrow 4N_2O + 6H_2O + 4S \tag{3.11}$$

3.3.3. SCR MATERIALS

Commercial SCR catalyst beds come mainly in three different types: Copper (Cu), Iron (Fe) and Vanadium (Va) catalyst. They all have different properties, drawbacks and advantages.

Vanadium

V_2O_5/TiO_2 promoted with WO_3 is currently widely adopted in industry and the predominant choice for marine applications [44]. This is a result of the high sulphur resistance and low cost of the material. The former is clearly not a driving force for AmmoniaDrive. However, the price tag could be one. Compared to the Cu and Fe SCR, the vanadium-based SCR provides a much cheaper solution. On the downside, the optimal working range is relatively small at 300-400 ^oC. The formation of N_2O and ammonia oxidation according to reaction 3.11 and 3.9 respectively, becomes significant above 400 ^oC. The formation of ammonia nitrate, following reaction 3.10, plays a role below 200 ^oC. If the exhaust gas entering the catalyst is above 500 ^oC, the catalyst starts to release V into the environment. This does not only reduce the working of the catalyst, but is also highly toxic and carcinogenic. This toxicity also presents difficulties when handling the material for maintenance purposes. [43]. When it comes to buffer capacity of NH_3, the vanadium catalyst can store the least of the three [70].

Cu-Zeolite

Copper zeolites are generally used when very high conversion rates are required, but comes at a high financial cost [70]. The NO_X conversion rates surpass the other catalysts, especially at lower temperatures [24]. The optimal NO_X conversion ranges from 175-300 ^oC [51]. This can also bee seen in figure 3.3. When operating at higher temperatures the oxidation of NH_3 increases, which leaves less NH_3 for the desired SCR reactions [40]. The temperature can be much further increased before thermal degradation takes place: temperatures up to 750 ^oC do no permanent damage [43]. The Cu-zeolites are also less sensitive to changing NO_2/NO_X ratios. The conversion efficiencies at low NO_2/NO_X ratios are almost as high as those found at a ratio of 0.5 [24]. In conventional heat engine systems, multiple problems can arise when using the Cu catalyst. The hydrocarbons and sulphur compounds can form bonds with the Cu sites, resulting in so-called poisoning of the catalyst. The catalyst can be cleaned, by removing the compounds from the inlet and raising the temperature significantly. If the inlet temperature of the system is too low, the urea can form deposits on the catalyst, blocking the active sites [51]. Luckily, all these problems do not occur in the AmmoniaDrive, as these compounds are not used. The buffer capacity of the Cu zeolite is very large: around 4 times higher than Fe, posing difficulties in handling temperature fluctuations as explained earlier [51]. Some N_2O formation can be expected over the CU catalyst, although quite low. Only 10s of ppm are found in the exhaust with 500 ppm NO and NH_3 at the inlet. A peak in N_2O formation is seen around 350 ^oC.

Fe-zeolite

The Fe catalyst is, just like the Cu SCR, based on a zeolite carrier. Compared to the other options, it provides the "in-between solution", when it comes to cost and NO_X conversion [70]. It can not handle the presence of hydrocarbon compounds in the exhaust, as this results in HC poisoning. Sulphur is less of a problem [51]. The typical working range of this catalyst is relatively wide and ranges from 350 to 550 ^oC, as can be seen in figure 3.3. Of the three options considered it is the best performing catalyst at high temperatures. Thermal degradation does not occur up to temperatures of 670 ^oC [51]. The catalyst is very sensitive to changing NO_2/NO_X ratios as shown in figure 3.4. A ratio of 0.5 would be ideal, but as discussed earlier, not the expected ratio of the AmmoniaDrive. The ammonia buffer of Fe catalysts is significantly lower than that of Cu, around four times. [51]. The Fe-zeolites outperform the other catalysts when it comes to N_2O formation. N_2O is produced over the catalyst surface, but can also be broken down from temperatures of 250 ^oC and above, providing a net zero output. This reduction takes place via reaction mechanisms 3.12 and 3.13 [73].

$$2N_2O \rightarrow 2N_2 + O_2 \tag{3.12}$$

$$3N_2O + 2NH_3 \rightarrow 4N_2 + 3H_2O \tag{3.13}$$

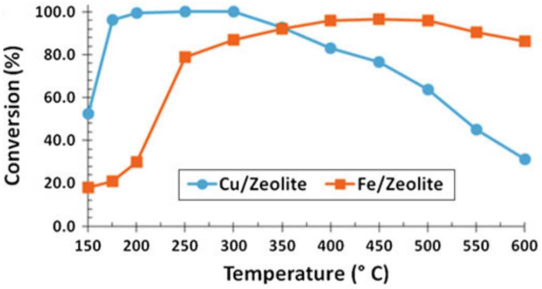

Figure 3.3: NO_X conversion efficiencies of CU and Fe-zeolites with ANR = 1 [51]

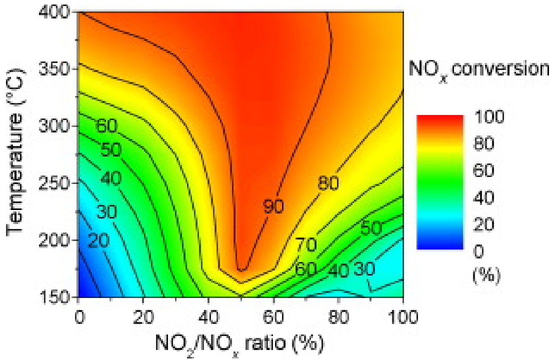

Figure 3.4: Map of NO_X conversion vs NO_2/NO_X ratio and temperature, on Fe/ZSM-5. [31]

3.3.4. ASC

Ideally, the amount of NH_3 inserted in the SCR would be fully consumed. However, in practice a slight overdose of NH_3 is needed inside the SCR to achieve full NO_X reduction. As a result NH_3 will be leaving the SCR and needs to be removed before the exhaust gasses are released into the environment. The solution is to place an Ammonia Slip Catalyst (ASC) after the SCR. The ASC itself has a monolithic structure, like the SCR, and can exist of multiple catalytic components, which will be discussed in more detail in this chapter [52] & [26]. Currently, this component is most often not installed on ships. It should not be used in combination with high sulphur content fuels, just like the DOC [5]. The formation of sulphuric acid as shown in reaction 3.3 should be avoided. In the context of AmmoniaDrive, there is less control over the NH_3 concentrations entering the SCR, as it can already be present in large amounts coming out of the ICE. This increases the need for an ASC in the AmmoniaDrive concept.

ASC is actually a reactor capable of containing multiple different catalysts: an Ammonia Oxidation Catalyst (AMOX) and SCR. The AMOX uses mostly Platinum Group Metal (PGM) as catalytic materials to promote the oxidation of NH_3. Metals in this group are amongst others platinum, palladium and rhodium. [11]. Just like in the SCR, the ammonia first needs to be adsorbed in by the catalyst bed, before taking part in one of the oxidation reactions. The desired reaction taking place in the ASC is shown in reaction 3.14 [26].

$$4NH_3 + 3O_2 \rightarrow 2N_2 + 6H_2O \tag{3.14}$$

However, the selectivity towards N_2 of a Pt catalyst is quite poor. As a result N_2O and NO_X can also be formed. The formation of N_2O is shown in reaction 3.15, which reaches a maximum between 225-300 ^oC. The formation of NO_X is shown in reaction 3.16 and 3.17. The formation of NO_X starts to become a problem when temperatures higher than 250 ^oC are reached. [26]. In figure 3.5 the different yields are plotted as a function of temperature.

$$4NH_3 + 4O_2 \rightarrow 2N_2O + 6H_2O \tag{3.15}$$

$$4NH_3 + 5O_2 \rightarrow 4NO + 6H_2O \tag{3.16}$$

$$2NO + O_2 \leftrightarrow 2NO_2 \tag{3.17}$$

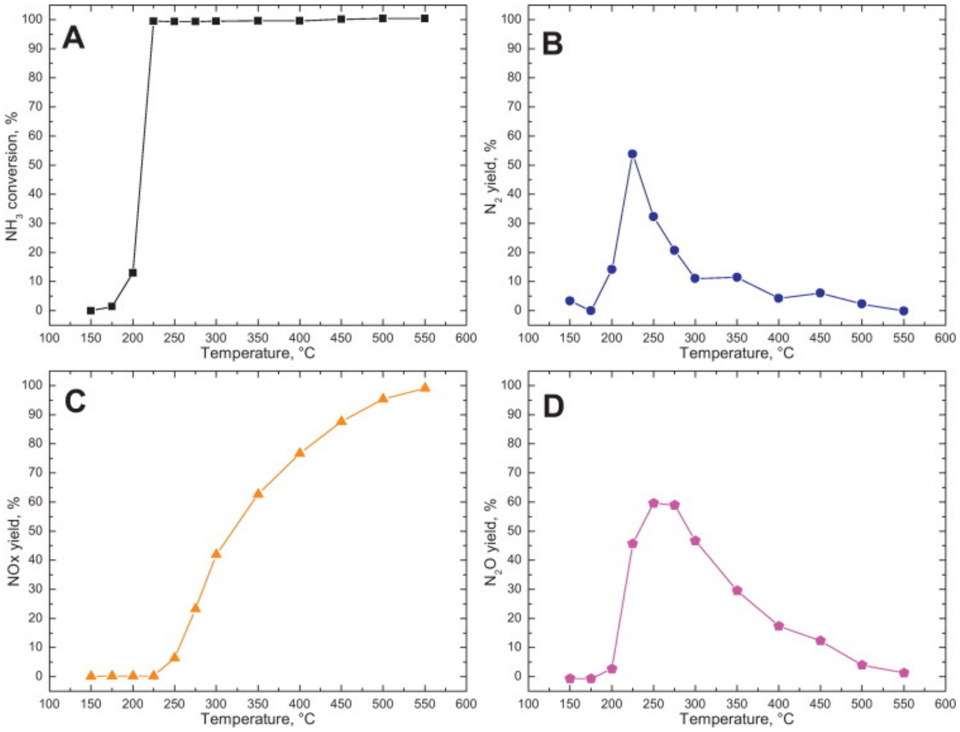

Figure 3.5: NH3 oxidation on PGM catalyst [7].

Clearly, the production of NO_X and N_2O in the last exhaust treatment component is problematic as they will be released into the environment. The performance of the ASC can be improved by introducing an SCR and AMOX catalyst into the ASC. The SCR will promote the SCR reactions (reaction 3.6,3.7 and 3.8), reducing the NO_X output of the ASC. The integration of the SCR catalyst can be done in different ways. The SCR can be mixed into the AMOX, creating a single mixed layer. Next, the SCR catalyst can be stacked onto the AMOX making a dual-layer configuration. Finally, the two previous options can be combined: a SCR catalyst on top of a mixed layer, creating a hybrid dual layer. These three configurations are shown in figure 3.6, but more setups could be thought of. The selectivity towards N_2 can easily be well over 60% using an AMOX+SCR catalyst [26] & [7].

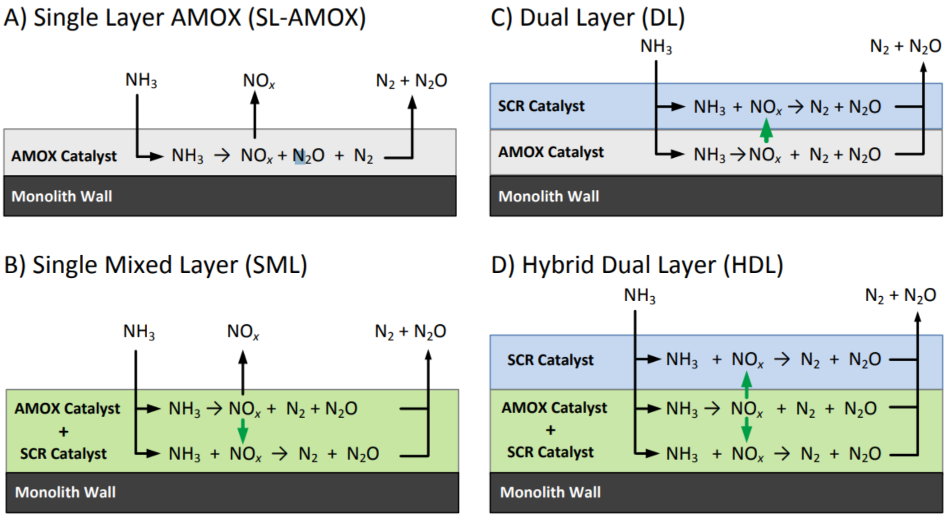

Figure 3.6: Ammonia slip catalyst configurations [26].

Besides the freedom of choice in layer configuration, different SCR materials can be chosen as well. For example the work of Hansen [26] focuses primarily on Cu-zeolite, while the work of Colombo et al. [7] focuses on Fe-zeolites. The former could be a better way to promote low-temperature activity. While the latter should be able to further reduce the formation of N_2O, based on the findings in the previous section.

4

Geometry

This chapter comes from the literature report, conducted at the beginning of this thesis [4]. To properly model a SCR or ASC, one first has to understand its geometry. Catalysts come in multiple types, namely pellets, powders and monolithic structures. The latter provide Superior mass transportation, lower pressure drop, thermal stability, and mechanical strength. Thus, monolithic structures are the best option for exhaust after treatment components [25]. The monolith consists of a single block with multiple channels (most often square) on the inside. An example is shown in figure 4.1.

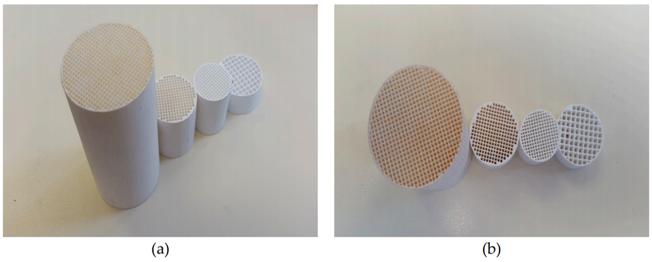

Figure 4.1: Monoliths with different cell densities: (a) side view; (b) top view [25].

The monolith itself is either entirely made from the catalytic material, resulting in an extruded monolith. Or, the monolith is made from a carrier material, providing mechanical strength. The monolith is then later powder or washcoated to apply the catalytic layer. In this case the monolith is most often made from a ceramic or metallic material. The former benefits from a more porous structure which makes it easier for the coating to stick and have good thermal stability. The latter provides a higher mechanical strength, better heat transfer, a lower pressure drop and smaller volume [25].

Most marine SCR systems consist of multiple washcoated monoliths placed after one another, as shown in figure 4.2a. An example of a monolith layer is shown in figure 4.2b.

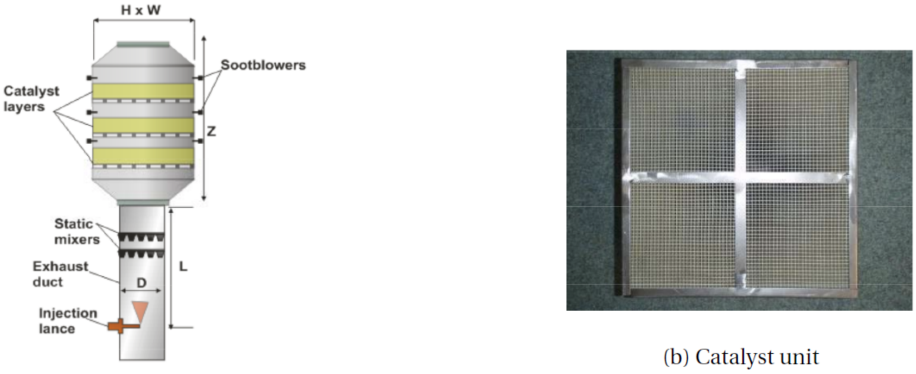

(a) SCR reactor

(b) Catalyst unit

Figure 4.2: Marine SCR system [5].

All catalysts require a support material, the actual catalyst is only present in a few percent mass fraction. The support material has to have a high surface area and good thermal stability [26]. A common support material for the Vanadia catalyst is TiO_3 [5]. The Cu and Fe SCR catalyst use zeolites as a support material. Specific examples of zeolites are ZSM-5, SAPO-34 and SSZ-13 [73]. The PGM oxidation catalyst, as present in the AMOX is often supported on a Al_2O_3 material [26]. The catalytic surface at its most detailed level is shown in figure 4.3 and 4.4. Both figures show a Scanning Electron Microscope (SEM) image of a VO_5-WO_3/TiO_3 and Cu ZSM-5 catalyst surface respectively. In these images the porous nature of the different catalytic surfaces is clearly visible. When zooming out it is possible to see how the washcoat is attached to the monolith. Figure 4.5 shows a microscopic view of a monolith cross section. In this image it is clearly shown, that the flow channels are not actually square, but have rounded edges. This is an inevitable effect of the way a washcoat is applied.

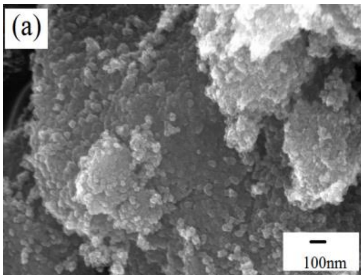

Figure 4.3: SEM image of VO_5-WO_3/TiO_3 catalyst surface [57]

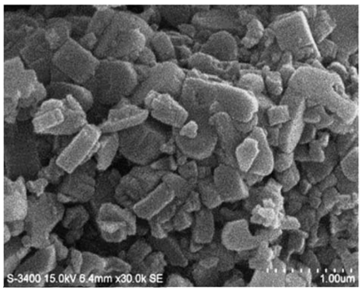

Figure 4.4: SEM image of Cu ZSM-5 catalyst surface [38]

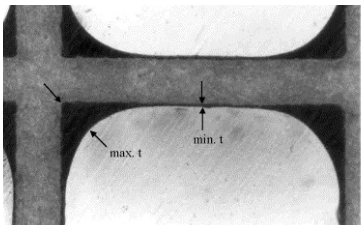

Figure 4.5: Cross section of ZSM-5 washcoat on monolith [71].

A schematic cross section of the monolith is shown in figure 4.6, both an extruded and washcoated catalyst are shown in this figure. The differences in channel geometry can clearly be seen in these cross sections. Using the schematic drawing in figure 4.7, it is possible to define some of the important geometric properties [68] & [5].

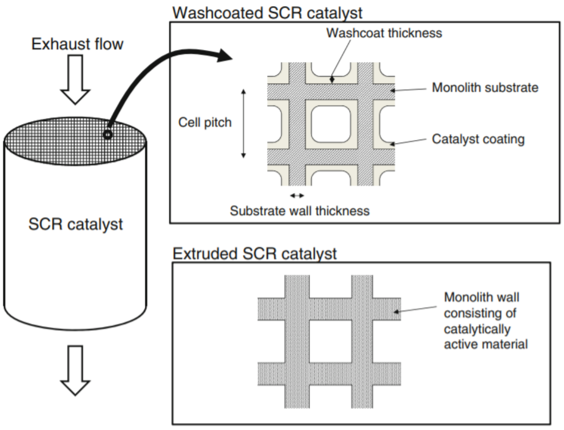

Figure 4.6: Monolith cross section [51].

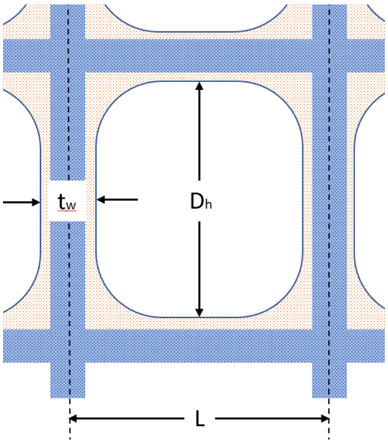

Figure 4.7: Dimensions of monolith cross section.

The cell density N is often expressed in cells per square inch (CPSI) and is calculated using the cell spacing L, using the following formula:

$$N = \frac{1}{L^2} \tag{4.1}$$

The open frontal area (OFA) is calculated using the cell density (N), cell spacing (L) and wall thickness (t). This is shown in the equation below:

$$OFA = N \cdot (L - t_w)^2 \tag{4.2}$$

The hydraulic diameter (d_h) is defined as a function of cell spacing and wall thickness:

$$d_h = L - t_w \tag{4.3}$$

The Geometric Surface Area (G_a) is defined as a function of the open frontal area and the hydraulic diameter:

$$G_a = 4\frac{OFA}{d_h} \tag{4.4}$$

When increasing the cell density, both the pressure drop and GSA are increased. Larger channels are used when high levels of soot and/or dust can be expected in the exhaust. This helps the channels from becoming blocked [34]. Common values for marine applications are around 100 CPSI [72] & [5]. However, AmmoniaDrive might benefit from a higher cell density as clogging by soot is not limiting any longer.

5

Modelling Approach

As explained before, the testing will be done on a computer model. This chapter explains step by step how the model was built. Building a model can be very complex and mistakes are easily made. To better guide this process the ”9 step method” is used to systematically build a suitable model [8]. This method consists of the following steps:

1. Purpose
2. System border & variables
3. Relevant phenomena
4. Hypotheses & assumptions
5. Submodels
6. Conservation laws & relations
7. Simplifications
8. Implementation
9. Simulation, validation and application

The rest of this chapter will elaborate on each step in the same order as presented here. The last step will be presented in the next chapter as it is a slightly more elaborate step compared to the others.

5.1. Step 1, Purpose

Before a model can be built it is important to define the purpose of the model. By doing so, it becomes easier to determine which parts need more detail and which parts can have more simplifications. In short, **the models should be able to predict the nitrogen based pollutant levels at the outlet (NO, NO_2, NH_3 & N_2O) of the SCR over a range of inlet variables**. The level of detail should be such that a comparative study can be conducted regarding workable inlet conditions and how the different materials compare to one another. It is possible to construct a 0-D, 1-D, 2-D or 3-D model. A 0D model is not ideal in this case as concentrations would not be able to vary along the length of the catalyst. The 1D model does have this capability. If differences in the radial direction, for example due to heat loss at the housing of the reactor, must be taken into account a 2-D model should be used. Finally, it is also possible to compute a 3-D model if these radial changes are non uniform, which could be a result of non uniform inflow. The 2 and 3-D models require a lot of computational power and could be of interest in a final design phase of components. For this study a 1-D model is assumed to provide the proper balance between accuracy and computational speed.

The 1-D model already contains quite a few states and although the results to be obtained are steady state, a dynamic model is built. If the model has no dynamics, it becomes extremely hard, if not impossible, to solve at once. The model will therefore be a dynamic model.

5.2. Step 2, System Border and Variables

Before the model is built, it is important to clearly define the boundaries of the model and the variables crossing these boundaries. A schematic drawing of the SCR indicating the boundary is shown in figure 5.1. The model consists of two catalytic layers and a void in between. The exhaust flow (indicated with green arrows) crosses the model boundaries. The variables describing the flow at the in- and outlet are shown in table 5.1, the subscript E stands for "entering" and L for "leaving". P denotes the pressure, f the mass flow and T the temperature. These three values are single scalars. X_j and ppm_j are both vectors. The first is used to express the mass fraction of O2, N2 and H2O in the bulk phase, the latter is used to express the molar fractions of NO, NO_2, NH_3 and N_2O.

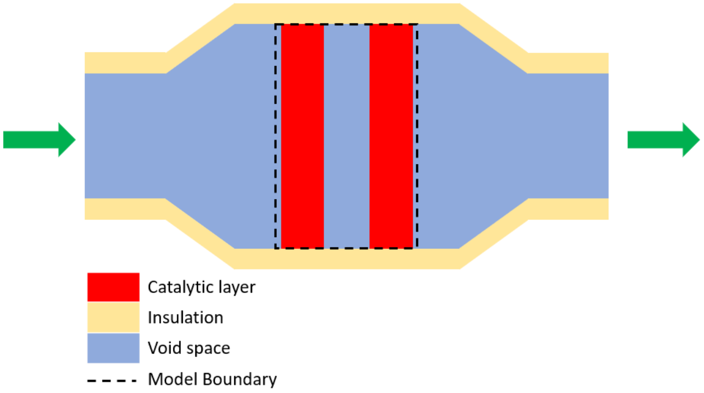

Figure 5.1: Schematic drawing of SCR, showing the model boundaries.

Table 5.1: Border variables.

Inlet	Outlet
P_E	P_L
f_E	f_L
T_E	T_L
$ppm_{j,E}$	$ppm_{j,L}$
$X_{j,E}$	$X_{j,L}$

5.3. Step 3, Relevant Phenomena

Next, it is important to list the relevant phenomena taking place inside the model. The relevant phenomena inside this model are:

- Heat transfer
- Heat storage
- Mass transfer
- Mass storage
- Pollutant transfer
- Pollutant storage
- Chemical reactions
- No work
- No Phase change

5.4. Step 4, Hypotheses and Assumptions

The hypotheses and assumptions on which the model is built, are listed in step 4. Hypotheses, in contrast to assumptions, can be falsified or verified afterwards. The following hypotheses are made:

- Laminar flow along the entire length of the channel.
  The laminar flow hypothesis can easily be checked. The highest change for turbulent flow will occur at full scale testing, an equivalence ratio of 0.2 and an inlet temperature of 100 ^{o}C. Testing showed that in this condition the mass flow is equal to 26.4 kg/s, the hydraulic diameter is 2.2 mm, the cross section is 4.13 m2 and the void fraction 0.774. For this check the dynamic viscosity of

air is used, which is 21.74 μPas [17]. The Reynolds number is described by the following equation [50]:

$$\begin{aligned} Re &= \frac{\rho \cdot v \cdot d_h}{\mu} \\ &= \frac{f \cdot d_h}{A_{cs} \cdot \epsilon \cdot \mu} \\ &= \frac{26.4 \cdot 0.0022}{4.13 \cdot 0.774 \cdot 2.17e-05} \\ &= 835 \end{aligned} \tag{5.1}$$

The Reynolds number is smaller than 2300, which indicates the flow is laminar.

- Fully developed flow for heat and mass transfer is assumed along the full length of the channel. As a result of this hypothesis the asymptotic values for both the Nusselt and Sherwood number can be used [49].

  To verify this hypothesis the thermal entrance length (L$_{eh}$) is calculated in equation 5.2. This is the length required for the Nusselt number to decrease within 5% of its fully developed value [50]. This calculation requires the Prandtl number. For this case the Prandtl number used, is for air at 300 K and is equal to 0.7 [18].

$$\begin{aligned} L_{eh}(5\%) &= 0.017 \cdot Re \cdot Pr \cdot d_h \\ &= 0.017 \cdot 835 \cdot 0.7 \cdot 0.0022 \\ &= 0.022m \end{aligned} \tag{5.2}$$

  Compared to the length of the monolith itself, this means the flow is fully developed within 7% of the channel length. The entrance effects for heat and mass transfer are therefore neglected in the channel.

Next to the hypothesis, a number of assumptions were made:

- The exhaust gas behaves as an ideal gas.
- The monolith has a constant cross section.
- Adiabatic process.
- Same friction coefficient for all materials
- The channels inside the monolith are perfectly square.
- Solely convection as transport mechanism for bulk flow in monolith channel.
- Perfectly mixed concentrations and heat inside each cell of the monolith channel.
- Perfectly mixed concentrations and heat inside void space.

5.5. Step 5, Sub-models

During this step, the setup of the model is made: the model is divided into smaller sub-models and information flows are determined. The model is built with resistive and storage elements (both noted with R and S respectively). The storage modules make use of an integrator to ”store” the relevant quantity. To transport a quantity from one storage module to another, a resistive block is used. This model makes use of three different domains: mass, heat and pollutants.

On a top level the model is divided into three sub models: two monolith layers and one void space. This setup is shown in figure 5.2. The monolith layer acts as a resistive element for mass transport, whilst the void is a storage for mass, heat and pollutants. The pollutant concentrations are either indicated with $c_{j,E}$ or $Y_{j,E}$. The first is measured in mol/m^3 and is used for the Va model. The latter is measured in mol/mol and is used for the Fe and Cu model. This difference is a result of the kinetic data provided by Åberg et al. [1] and Metkar, Balakotaiah, and Harold [47].

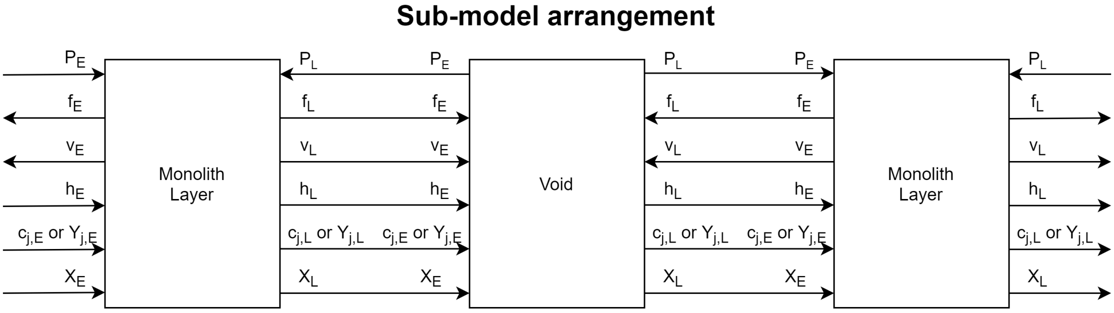

Figure 5.2: Top level sub-models

The Void model sub-model is opened in figure 5.3. In this sub-model a storage element for heat, mass and pollutants are present. Heat, mass and pollutants are all transported with the gas flow through the two adjacent monoliths.

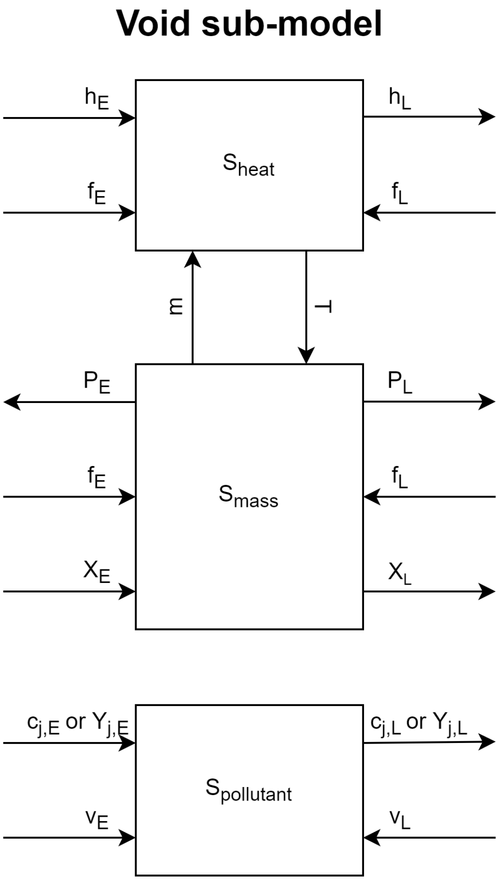

Figure 5.3: Void sub-model

The monolith layers are a bit more complex. At the top a resistive mass flow element is shown. Using this block, both mass flow and flow speed are determined, these two parameters are also important for the transport of heat and pollutants. One resistive flow module was chosen over the entire length of the monolith to reduce the stiffness and number of states of the model. Both heat and concentrations are discritised in length. The pollutant levels are discritised in length to realise higher accuracy. As both reaction rates and transport mechanisms inside the washcoat are dependent on the washcoat temperature, the heat is also discritised along the length of the monolith. Heat in the gas phase is transported with the mass flow in the monolith channel. From the gas, heat is transferred from and to the monolith. Inside the monolith itself conduction can also transfer heat to and from the adjacent cells.

The pollutants in the bulk phase are transported with the volume flow inside the monolith channel. In the channel pollutants can be transferred to and from the washcoat. Here, they can take part in one of the reaction mechanisms and NH_3 can be stored on the active sites. The Va model uses one concentration in the washcoat element, while the Fe and Cu models are also discritised in the y-direction. Diffusion is the transport mechanism for the pollutants inside the washcoat. It is important to note that monolith temperature is an important parameter in the pollutant balance and is used to determine transport properties as well as reaction rates. The monolith sub-models for Va, Fe and Cu are shown on the two following pages.

Monolith layer sub-model (for Va)

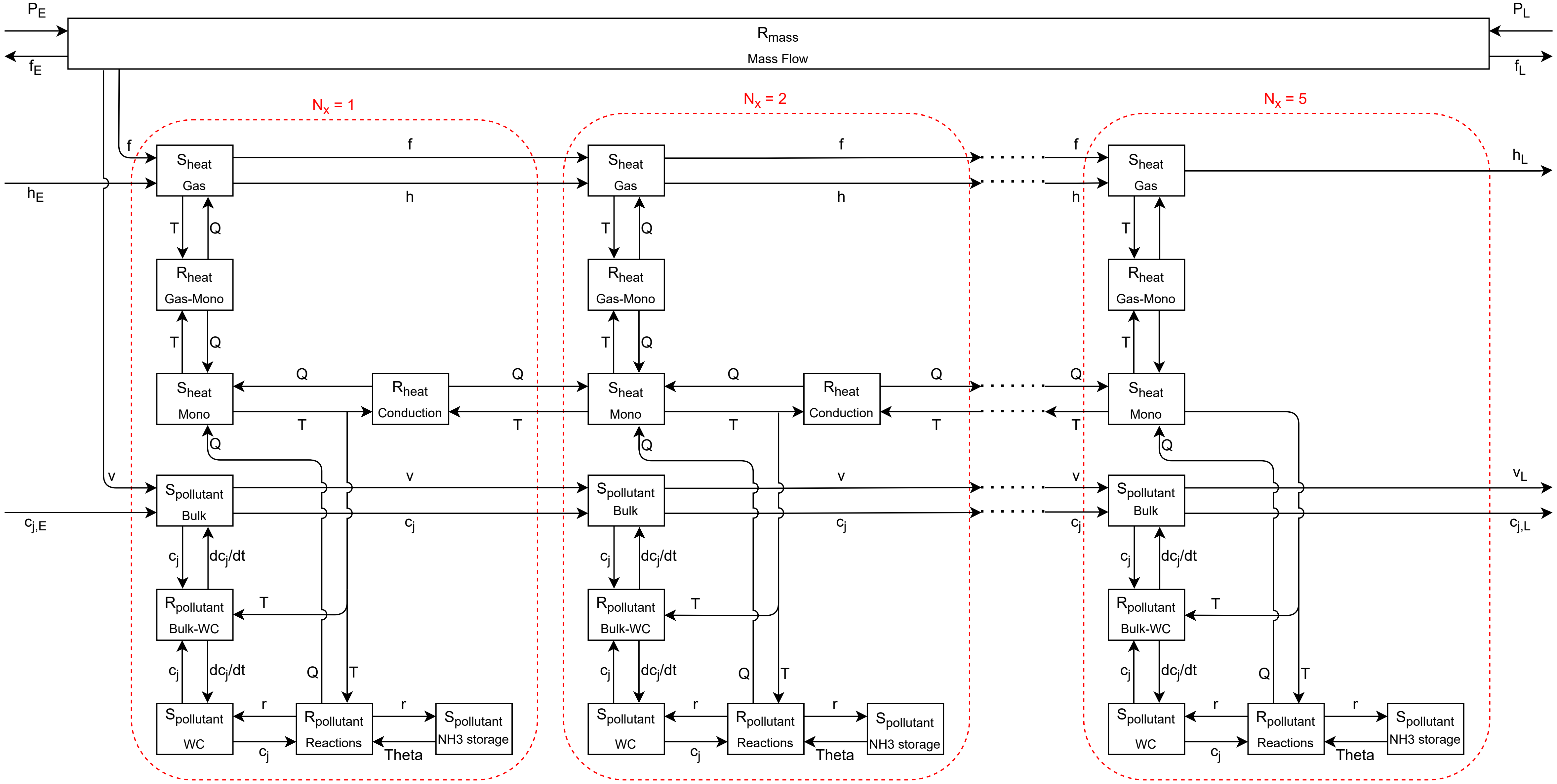

Monolith layer sub-model (for Fe and Cu)

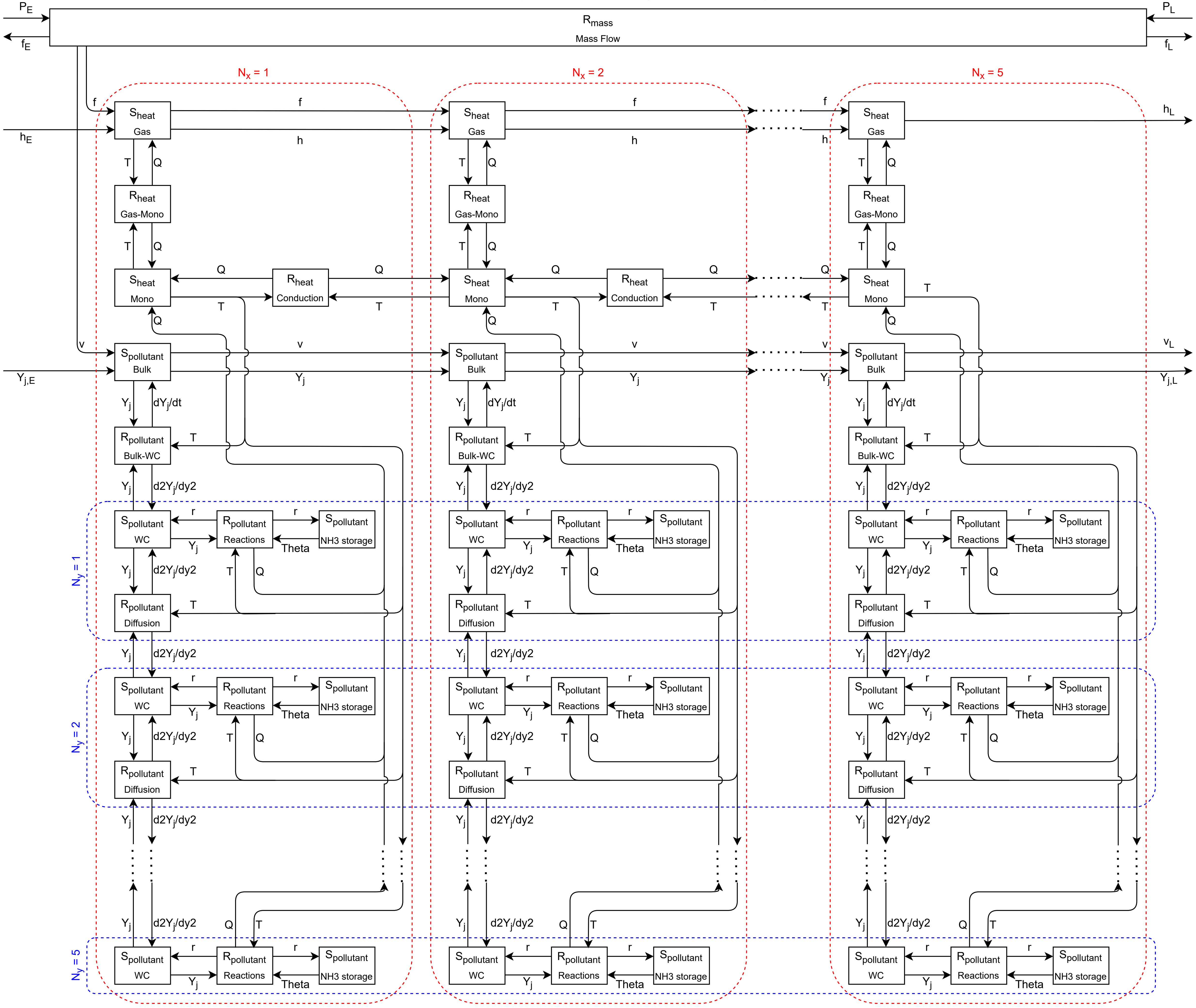

5.6. Step 6, Conservation Laws and Relations

Each block as presented in Step 5 has formulas implemented. In this step all relations and conservation laws are presented and explained, block by block.

5.6.1. Void

First the used formulas as implemented in the Void sub-model are discussed.

Mass Storage

A mass balance is used to monitor the accumulation of mass in the volume elements. The conservation of mass, as implemented in the model, is expressed in equation 5.3 and is equal to zero in steady state conditions [56]:

$$\frac{\partial m}{\partial t} = f_E - f_L \tag{5.3}$$

In which m is the mass and f the mass flow.

The pressure is calculated in using the ideal gas law [56]:

$$P = \frac{m \cdot R_s \cdot T}{V_{void}} \tag{5.4}$$

In the equation above, P is the pressure, m the mass, R_s the specific gas constant, T the temperature and V_{void} the volume of the void space.

The implementation of these formulas in Simulink can be seen in figure C.1.

Heat Storage

The internal energy of a system is defined by:

$$dU = \partial Q - \partial W \tag{5.5}$$

In which Q is the heat and W the work.
Stapersma [56] shows that the equation above can be rewritten in the following form to monitor the temperature:

$$m \cdot c_v \cdot \frac{\partial T}{\partial t} = f_E \cdot (h_E - u) - f_L \cdot (h_L - u) \tag{5.6}$$

In which c_v is the specific heat capacity for constant volume, h the enthalpy and u the specific internal energy.
The specific internal energy can be calculated using the following formula:

$$d_u = \int c_v \cdot dT \tag{5.7}$$

The implementation in Simulink can be seen in figure C.2.

Pollutant Storage

The different pollutants are also stored in the void space. They are transported by the incoming and leaving bulk flow. The balance used for the Va model is shown in equation 5.8, the equation used in the Fe and Cu model is shown in 5.9.

$$\frac{\partial c_j}{\partial t} = \frac{\epsilon}{L_{void}} \left(c_{j,E} \cdot v_E - c_{j,L} \cdot v_L\right) \tag{5.8}$$

$$\frac{\partial Y_j}{\partial t} = \frac{\epsilon}{L_{void}} \left(Y_{j,E} \cdot v_E - Y_{j,L} \cdot v_L\right) \tag{5.9}$$

In the equations above c_j and Y_j are the pollutant concentrations, L_void the length of the void space and v the velocity.
The implementation in Simulink can be seen in figure C.3.

5.6.2. Monolith Layer

In this section the formulas used in the monolith sub-model are discussed.

Mass Flow, Resistive

The pressure drop over a channel can be described by the following equation [50]:

$$\Delta P = \phi_f \cdot \left(\frac{L_m}{d_h}\right) \cdot \frac{1}{2} \cdot \rho \cdot v^2 \tag{5.10}$$

In the equation above ϕ_f is the friction factor, d_h the hydraulic diameter, L_m the length of the monolith and v the velocity. By describing the pressure drop in this manner, the inlet and outlet pressure drops are bundled in the friction coefficient. Furthermore, it is assumed the flow has a constant speed and density over the resistive element: the change in density as a result of the pressure drop and temperature increase are neglected. Thereby the acceleration pressure drop is also neglected. The change in the composition of bulk gasses (O2, N2 and H2O) is also neglected due to the relatively low concentrations of pollutants (below one percent) [5].
The formula, as given in 5.10, can be rewritten so it can be used to determine the mass flow in the model:

$$f_E = A_{cs} \cdot \epsilon \cdot \sqrt{\frac{d_h}{\phi_f \cdot L_m}} \cdot \frac{P_E}{\sqrt{R_{s,E} \cdot T_E}} \cdot \sqrt{2} \cdot \sqrt{1 - \frac{P_L}{P_E}} \tag{5.11}$$

Where A_{cs} the total cross-section area of the SCR, ϵ the void fraction of the catalyst, d_h the hydraulic diameter, ϕ_f the friction factor and L_m the length of the monolith. The entering properties of the fluid were used to determine the average values along the length of the catalyst. The accumulation of mass inside the monolith channel is neglected, so:

$$f_L = f_E \tag{5.12}$$

The flow velocity inside the monolith channel is calculated using the following equation, it is assumed the density and thus velocity do not change along the catalyst length:

$$v_E = \frac{\dot{m}}{\rho_E \cdot A_{sc} \cdot \epsilon} \tag{5.13}$$

In which the density ρ_E is calculated using:

$$\rho_E = \frac{P_E}{R_E \cdot T_E} \tag{5.14}$$

The outlet velocity of the Va model is equal to the inlet velocity:

$$v_L = v_E \tag{5.15}$$

The outlet velocity of the resistive mass flow block of the Fe and Cu model uses a different outlet velocity. An adjustment is made for the difference in temperature and pressure for the in and outlet. The outlet velocity of the Fe and Cu model is shown in equation 5.16. Note that this correction factor is only used to correct the flow velocity leaving the monolith, it is not used to change the flow velocity inside the monolith itself.

$$v_L = \frac{T_L}{T_E} \cdot \frac{P_E}{P_L} \cdot v_E \tag{5.16}$$

The implementation of these formulas in Simulink can be seen in figure C.4 (Va model) and C.5 (Fe and Cu model).

Gas Temperature, Storage

The temperature balance used for the bulk gas is shown in equation 5.17. The first term on the right hand side represents the convective transport of heat along the channel of the monolith, the second term describes the heat transferred from the monolith structure to the bulk gas phase.

$$m_b \cdot c_{p,b} \cdot \frac{\partial T_b}{\partial t} = f_E \cdot h_E - f_L \cdot h_L + \dot{Q}_{m\to b} \tag{5.17}$$

m_b is the mass of bulk gas present in each cell, $c_{p,b}$ the heat capacity of the bulk phase and $\dot{Q}_{m\to b}$ the heat transferred from the monolith to the gas phase.
The implementation of these formulas in Simulink can be seen in figure C.8.

Monolith Temperature, Storage

The temperature balance used for the monolith is shown in the equation 5.18. All heat released by the reactions is absorbed by the monolith. This is partly a mathematical trick to create a less stiff model due to the higher heat capacity and mass of the monolith compared to the bulk gas. More heat flows to and from the monolith cell due to conduction inside the monolith and via heat exchange with the bulk gas.

$$A_{cs} \cdot (1-\epsilon) \cdot \int \rho_m \, dx \cdot c_{p,m} \cdot \frac{\partial T_m}{\partial t} = \dot{Q}_{reaction} + \dot{Q}_{cond} + \dot{Q}_{b\to m} \tag{5.18}$$

In the equation above, ρ_m is the density of the monolithic structure, $c_{p,m}$ the heat capacity of the monolith material, $\dot{Q}_{reaction}$ represents the heat released by the reactions, $\dot{Q}_{cond}$ the conductive heat flow inside the monolith structure and $\dot{Q}_{b\to m}$ the heat exchange between the gas bulk phase and the monolith structure.
In this block, the heat released by the reactions is also calculated. This is done using the following equation:

$$\Delta H_i = H_{i,products} - H_{i,reactants} \tag{5.19}$$

The implementation of these formulas in Simulink can be seen in figure C.8.

Heat Exchange Gas-Monolith, Resistive
The heat exchanged between the bulk gas and monolith is described as follows:

$$\dot{Q}_{b\to m} = A_{cs} \cdot G_a \cdot \int h_{b\to m} \cdot \left(T_{g,i} - T_{m,i}\right)\ dx \tag{5.20}$$

$$\dot{Q}_{m\to b} = -\dot{Q}_{b\to m} \tag{5.21}$$

In the equation above G_a is the area to surface ratio and $h_{b\to m}$ the heat transfer coefficient. The latter is defined as follows:

$$h_{b\to m} = \frac{Nu \cdot \lambda_b}{d_h} \tag{5.22}$$

Where Nu is the Nusselt number and λ_b the thermal conductivity of the bulk gas.
The implementation of these formulas in Simulink can be seen in figure C.7.

Heat Conduction Monolith, Resistive
The heat conduction inside the monolith structure in longitudinal direction can be described by the following equation:

$$\dot{Q}_{cond} = A_{cs} \cdot (1-\epsilon) \cdot \lambda_m \cdot \frac{\partial T_m}{\partial x} \tag{5.23}$$

In the equation above, λ_m describes the thermal conductivity of the monolith structure.
The implementation of these formulas in Simulink can be seen in figure C.6.

Concentration Balance Pollutants in Bulk Phase, Storage
In the bulk phase two mechanisms create a change in concentration. First the convection of pollutants in the bulk flow is important (first term of right hand side). Next to this pollutant particles are exchanged with the washcoat (second term of the right hand side). The Va model keeps track of the pollutants in mol/m3, the equation is as follows:

$$\frac{\partial c_{j,b}}{\partial t} = -v \cdot \frac{\partial c_{j,b}}{\partial x} + \dot{c}_{j,wc\to b} \tag{5.24}$$

Here $c_{j,b}$ represents the pollutant concentration in the bulk phase, while $\dot{c}_{j,wc\to b}$ represents the exchange of pollutants from the washcoat to the bulk phase.
The Fe and Cu model keep track of the pollutants in molar fractions. The balance used, is shown in the equation below:

$$\frac{\partial Y_{j,b}}{\partial t} = -v \cdot \frac{\partial Y_{j,b}}{\partial x} + \dot{Y}_{j,wc\to b} \tag{5.25}$$

The implementation of these formulas in Simulink can be seen in figure C.10 (Va model) and C.11 (Fe and Cu model).

Pollutant Exchange Washcoat-Bulk, Resistive
In this block the exchange of pollutants between the washcoat and bulk phase is covered. The Va model has one concentration in the washcoat and therefore uses a slightly different approach compared to the Fe and Cu model, this model calculates a concentration gradient inside the washcoat.
The pollutant exchange in the Va model is described in the following way:

$$\dot{c}_{j,b\to wc} = \frac{4 \cdot k_{g,j}}{d_{hyd}} \cdot \left(c_{i,b} - c_{i,wc}\right) \tag{5.26}$$

$$\dot{c}_{j,wc\to b} = -\dot{c}_{j,b\to wc} \tag{5.27}$$

In this equation $k_{g,j}$ represents the mass transfer coefficient, this is calculated in the following way:

$$k_{g,j} = \frac{Sh \cdot D_{f,j}}{d_h} \tag{5.28}$$

Where Sh is the Sherwood number and $D_{f,j}$ the diffusivity of each pollutant in the bulk mixture.
The pollutants going from the washcoat to the bulk phase is described by the following equation in the Fe and Cu model:

$$\dot{Y}_{j,b\rightarrow wc} = \frac{-4 \cdot k_{g,j}}{d_{hyd}} \cdot \left(Y_{j,b} - Y_{j,wc}\big|_{y=0}\right) \tag{5.29}$$

The concentration in the washcoat depends on the double derivative of the concentration in the y-direction. Therefore this block also calculates the derivative of Y at y = 0:

$$k_{g,j} \cdot \left(Y_{j,b} - Y_{j,wc}\big|_{y=0}\right) = -D_{e,j} \cdot \frac{\partial Y_{j,wc}}{\partial y} \text{ at } y = 0 \tag{5.30}$$

The implementation of these formulas in Simulink are integrated in different blocks in Simulink. The concentration exchange of the Va model can be found in figure C.10 and C.12. The concentration exchange of the Fe and Cu model is can be found in C.11 and C.15.

Pollutant Concentration Washcoat, Storage
The Va model uses the balance shown in equation 5.31. The first term on the right hand side of the equation represents the exchange of pollutants with the bulk phase and the second term the change in concentration due to the reactions taking place.

$$\frac{\partial c_{j,wc}}{\partial t} = \dot{c}_{j,b\rightarrow wc} + \sum_i v_j r_i\left(T, \theta, c_{j,wc}\right) \tag{5.31}$$

The concentration storage in the Fe and Cu washcoat is governed by the following equation:

$$\epsilon_{wc} \cdot \frac{\partial Y_{j,wc}}{\partial t} = \frac{1}{C_{Tm}} \cdot \left(\sum_i v_j r_i\left(T, \theta, Y_{j,wc}\right)\right) + D_{e,j} \cdot \frac{\partial^2 Y_{j,wc}}{\partial y^2} \tag{5.32}$$

ϵ_{WC} is the washcoat porosity, $C_T m$ is the total molar concentration, v the stoichiometric coefficient, r the reaction rate and D_e the effective diffusivity. A ratio of D_e/D_f of 90 was used.
The implementation of these formulas in Simulink can be seen in figure C.12 (Va model) and C.13 (Fe and Cu model).

Pollutant Diffusion in Washcoat, Resistive
This block calculates the derivative of $X_{j,wc}$ over y and is only used for the Fe and Cu balance. The following equation is used:

$$\frac{\partial^2 Y_{j,wc,i}}{\partial y^2} = \frac{Y_{j,wc,i-1} - 2 \cdot Y_{j,wc,i} + Y_{j,wc,i+1}}{dy^2} \tag{5.33}$$

To solve this equation a boundary condition is required on both ends of the washcoat thickness. At y = 0, this boundary condition is presented by equation 5.30. At the full thickness of the washcoat the following boundary condition holds:

$$\frac{\partial Y_{j,wc}}{\partial y} = 0 \text{ at } y = R_{\Omega 2}, \tag{5.34}$$

(5.35)

The implementation of these formulas in Simulink can be seen in figure C.15 for both the Fe and Cu model

Pollutant Reaction, Resistive

In this block the different reactions are modelled. They are modelled using the Arrhenius equation as shown below [47] & [1]:

$$k_i = k_{0,i} \cdot exp\left(\frac{-E_i}{\overline{R} \cdot T_{WC}}\right) \tag{5.36}$$

Where $k_{0,i}$ is the pre-exponential factor of reaction i, E_i is the activation energy of reaction i, $\overline{R}$ is the universal gas constant, and T is the reaction temperature.

To model the actual reaction rates, the vanadium model has a slightly different approach from the Fe and Cu model. The first uses the bulk concentrations measured in mol/m3, while the latter two make use of the mole fraction by volume inside the washcoat. The way reaction rates are modelled in the Va model is shown in equation 5.37. The formula used for the Fe and Cu catalyst is shown in 5.38.

$$r_i = k_i \cdot \prod_{i=1}^{N} c_j \tag{5.37}$$

$$r_i = k_i \cdot \prod_{i=1}^{N} Y_j \tag{5.38}$$

The specific rate expressions per reaction are shown in table 5.2.

Table 5.2: Rate expressions

Number	Reaction	Rate expression Va	Rate expression Fe & Cu
R1	$NH_3 + S \leftrightarrow NH_3^*$	$k_{1f}(1-\theta)C_{NH_3,b} - k_{1r}\theta$	$k_{1f}X_{\mathrm{NH_3}}(1-\theta) - k_{1r}\theta$
R2.1	$2\ NH_3^* + 1.5\ O_2 \rightarrow N_2 + 3\ H_2O + 2\ S$	n.a.	$k_{2.1f}X_{\mathrm{O_2}}\theta$
R2.2	$2\ NH_3^* + 5/2\ O_2 \rightarrow 2\ NO + 3\ H_2O + 2\ S$	$k_{2.2f}\theta$	n.a.
R3	$NO + 1/2\ O_2 \leftrightarrow NO_2$	n.a.	$k_{3f}X_{\mathrm{O_2}}^{1/2}X_{\mathrm{NO}} - k_{3r}X_{\mathrm{NO_2}}$
R4	$4\ NH_3^* + 4\ NO + O_2 \rightarrow 4\ N_2 + 6\ H_2O + 4\ S$	$k_{4f}C_{NO,b}\theta$	$\frac{k_{4f}X_{\mathrm{NO}}\theta}{1+K^*X_{\mathrm{NH_3}}}$
R5	$2\ NH_3^* + NO + NO_2 \rightarrow 2\ N_2 + 3\ H_2O + 2\ S$	$k_{5f}C_{NO,b}C_{NO_2,b}\theta$	$k_{5f}X_{\mathrm{NO}}X_{\mathrm{NO_2}}\theta$
R6	$4\ NH_3^* + 3\ NO_2 \rightarrow 3.5\ N_2 + 6\ H_2O + 4\ S$	n.a.	$k_{6f}X_{\mathrm{NO_2}}\theta$
R7	$2\ NH_3^* + 2\ NO_2 \rightarrow N_2 + NH_4NO_3 + H_2O + 2\ S$	n.a.	$k_{7f}X_{\mathrm{NO_2}}\theta$
R8	$NH_4NO_3 \rightarrow N_2O + 2\ H_2O$	n.a.	$k_{8f}X_{\mathrm{NH_4NO_3}}$
R9	$2\ N_2O \rightarrow 2\ N_2 + O_2$	n.a.	$k_{9f}X_{\mathrm{N_2O}}$
R10	$2\ NH_3^* + 3\ N_2O \rightarrow 4\ N_2 + 3H_2O + 2\ S$	n.a.	$k_{10f}X_{\mathrm{N_2O}}\theta$
R11	$2\ NH_3^* + 2\ NO_2 \rightarrow N_2 + N_2O + 3\ H_2O + 2\ S$	$k_{11f}C_{NO_2,b}\theta$	$k_{11f}X_{\mathrm{NO_2}}\theta$

The implementation of these formulas in Simulink can be seen in figure C.16 (Va model) and C.17 (Fe and Cu model).

Pollutant NH_3 Storage, Storage
The ammonia stored on the active sites is expressed as a cover fraction Θ, ranging from 0 to 1. More ammonia is stored as a result of the adsorption reaction. The adsorbed ammonia can then react via one of the other reaction mechanisms.

$$C_{st}\frac{\partial \Theta_{NH_3}}{\partial t} = \sum_i v_{NH_3} r_i \left(T, \theta, Y_{j,wc}\right) \tag{5.39}$$

C_{st} is the total available active sites on the catalyst, this is 270, 2000 and 4000 [mol/m3] for the Va, Fe and Cu catalysts respectively.
The implementation of these formulas in Simulink can be seen in figure C.14 for all models.

5.6.3. Constants and flow numbers

Many blocks make use of certain constants, such as heat capacity and diffusivity. This subsection covers how these numbers can be calculated.

Thermodynamic Properties
The polynomial data as presented by Mcbride et al. [46] were used to determine the heat capacity, enthalpy and thermal conductivity of each component. The used formulas are shown in equation 5.40, 5.41 and 5.42 respectively. The used coefficients can be found in Appendix B.

$$\frac{c_p(T)}{\overline{R}} = a_1 + a_2 \cdot T + a_3 \cdot T^2 + a_4 \cdot T^3 + a_5 \cdot T^4 \tag{5.40}$$

$$\frac{H(T)}{\overline{R}} = b_1 + a_1 \cdot T + a_2 \cdot \frac{T^2}{2} + a_3 \cdot \frac{T^3}{3} + a_4 \cdot \frac{T^4}{4} + a_5 \cdot \frac{T^5}{5} \tag{5.41}$$

$$ln(\lambda) = A \cdot ln(T) + \frac{B}{T} + \frac{C}{T^2} + D \tag{5.42}$$

To determine the thermodynamic and transport properties of the bulk phase, only the mayor components are considered: O_2, N_2 and H_2O. The contribution of the pollutants have been neglected as they do not make up more than 0.5% of the mixture at most (When pollutant levels hit 5000 ppm). The heat capacity, enthalpy and thermal conductivity of the bulk mixture were determined using mole fractions, the formulas are shown in equation 5.43, 5.44 and 5.45 respectively [53].

$$c_{p,b} = \sum_i Y_i \cdot c_{p,i} \tag{5.43}$$

$$h_b = \sum_i Y_i \cdot h_i \tag{5.44}$$

$$\lambda_b = \sum_i Y_i \cdot \lambda_i \tag{5.45}$$

Using the isobaric heat capacity (c_p) it is possible to determine the isochoric heat capacity (c_p), the used formula is:

$$c_v = R_s - c_p \tag{5.46}$$

Diffusivity
To determine the diffusivity during verification of the Fe and Cu model, the expressions as presented by Metkar, Balakotaiah, and Harold [47] are used to determine the diffusivity of all pollutants in Argon. During the actual testing of the SCR, the diffusivity of each pollutant in air was used. To approximate this, the method of Wilke and Lee as presented in Poling, Prausnitz, and O'connell [53] was used. The method uses an empirical correlation to describe the diffusion coefficient:

$$D_{\mathrm{AB}} = \frac{\left[3.03 - \left(0.98/M_{\mathrm{AB}}^{1/2}\right)\right]\left(10^{-3}\right)T^{3/2}}{PM_{\mathrm{AB}}^{1/2}\sigma_{\mathrm{AB}}^{2}\Omega_{D}} \tag{5.47}$$

In this equation the D_{AB} is binary diffusion coefficient of A in substance B, measured in [cm^2/s], M_A & M_B the molecular weights in [g/mol] of A & B respectively and P the pressure in [bar].

M_{AB}, $\varepsilon_{\mathrm{AB}}$ and σ_{AB} are described by the following three equations:

$$M_{AB} = 2[(1/M_A) + (1/M_B)]^{-1} \tag{5.48}$$

$$\varepsilon_{\mathrm{AB}} = (\varepsilon_{\mathrm{A}}\varepsilon_{\mathrm{B}})^{1/2} \tag{5.49}$$

$$\sigma_{\mathrm{AB}} = \frac{\sigma_{\mathrm{A}} + \sigma_{\mathrm{B}}}{2} \tag{5.50}$$

Ω_D can be described using the Lennard Jones potentials [53]:

$$\Omega_D = \frac{A}{(T^*)^{\mathrm{B}}} + \frac{C}{\exp(DT^*)} + \frac{E}{\exp(FT^*)} + \frac{G}{\exp(HT^*)} \tag{5.51}$$

The values used in the polynomial coefficients used in the equation above can be found in appendix B.

Nusselt and Sherwood number

The Nusselt and Sherwood number do depend on the x coordinate. However, as a fully developed flow is assumed in the entire monolith channel, asymptotic value can be used. For square channels the following values are assumed [50]:

$$Nu_{\infty} = 2.976 \tag{5.52}$$

$$Sh_{\infty} = 2.976 \tag{5.53}$$

Specific gas constant

The specific gas constant R can be calculated using the universal gas constant and molar mass.The equation is as follows:

$$R = \frac{\overline{R}}{M} \tag{5.54}$$

The molar mass can be calculated using either one of two equations as shown below:

$$M = \sum_{j=1}^{nc} M_j \cdot Y_j \tag{5.55}$$

$$\frac{1}{M} = \sum_{j=1}^{nc} \frac{X_j}{M_j} \tag{5.56}$$

5.7. Step 7, Simplifications

Not all physical processes are modelled into the finest details, a number of simplifications were made. The simplifications are listed below:

- Mass accumulation inside monolith channel can be neglected.

- Density and thus flow velocity inside flow channel are constant.
- Heat capacity, heat transfer and enthalpy only defined by bulk species.
- The diffusivity of the different pollutants is calculated in air.
- No heat transfer through the insulation of the SCR reactor.
- All NH4NO3 is converted into N_2O.
  As a result reaction 7 and 8 are taken together as reaction 11. Reaction 7 is taken as the limiting reaction.

5.8. Step 8, Implementation

The models are built in Matlab Simulink R2020b and the ODE15s solver is used to solve them. The models are built up in the same way as discussed in step 5. Screen shots of the model are shown in Appendix C. To discretise the monolith layer in x direction and the washcoat in y direction, the ”For Each” block in Simulink was used. This block allows to create a for loop inside the Simulink model.

The Fe and Cu model require the concentration of each pollutant to determine the exchange rate of pollutants between the washcoat and bulk concentrations (as can be seen in equation 5.30 and 5.29). This is approximated by linear extrapolation:

$$Y_{j,wc}|_{y=0} = 1.5 \cdot Y_{j,wc}|_{N_y=1} - 0.5 \cdot Y_{j,wc}|_{N_y=2} \tag{5.57}$$

Most gas properties, such as heat capacity and diffusivity, are implemented in a simplified way. To reduce computational effort, a second order polynomial was fitted to the data. This polynomial is implemented in the model.

From the simplification ”All NH4NO3 is converted into N_2O” it is possible to remove NH4NO3 from the pollutant balance. This was done by creating reaction 11 as shown in table 5.2. The pre exponential factor and activation energy of reaction 7 are adopted for this reaction.

$$\begin{aligned}
\mathrm{R7}&: 2NH_3* + 2NO_2 \rightarrow N_2 + NH_4NO_3 + H_2O + 2S \\
\mathrm{R8}&: NH_4NO_3 \rightarrow N_2O + 2H_2O \\
\mathrm{R11}&: 2NH_3* + 2NO_2 \rightarrow N_2 + N_2O + 3H_2O + 2S
\end{aligned}$$

The equilibrium of the NO oxidation (reaction 3) comes from Metkar, Balakotaiah, and Harold [48]. The equilibrium consists of multiple reaction sub-reactions. The overall equilibrium constant was calculated beforehand and implemented as a look-up table.

6

Verification

The last, but very important step, is to do the verification and validation of the model. Verification shows that the equations are solved right, while validation is a process that shows the right equations are solved [54]. To properly do the latter, experimental testing is required. This is out of the scope of this thesis, therefore, only verification is done.

6.1. Comparison with Original Paper.

Before the models can be further used, they are compared to their sources: The papers providing the kinetic data.

6.1.1. Vanadium

The paper of Åberg et al. [1] uses three tests. During the first test only diluted NH_3 is fed to the SCR, in the second test a feed of NH_3 and NO with an ANR of 1 and finally a feed of NH_3 and NO with an ANR of 1.2. To replicate the tests, the data presented in table 6.2 is used. It is important to know that the actual flow rate is unknown. The paper states "space velocities in the order of 40,000 h^{-1}" are used. To match the flow rates as close as possible, a space velocity of 40,000 h^{-1} is used for these experiments. An overview of the used geometric parameters is shown in table 6.2. Both 3, 5 and 10 cells in x direction are considered. The computation times required for the 15 validation experiments are shown in table 6.1. This time is needed to run all 15 experiments on 6 cores (Intel(R) Core(TM) i7-8750H CPU @ 2.20GHz 2.21 GHz) simultaneously.

Table 6.1: Computation time for Va model.

N_X	Computation time
3	0:30
5	0:35
10	1:26

Table 6.2: Geometric and flow parameters used for validation of Va model

Parameter	Symbol	Value	Unit
Number of Layers		1	#
Cell density	CPSI	270	#/in^2
Wall thickness	t_w	0.015	in
Diameter monolith	D	4.83	cm
Length Monolith	L_m	0.08	m
SCR void fraction	ϵ	0.56	-
Space Velocity	SV	40,000	1/h

The results of the diluted NH_3, ANR = 1 and ANR 1.2 are shown in figure 6.1, 6.2 and 6.3 respectively. The trends match the reference material. However, the results differ more when the temperature increases. This could partly be a result of the unknown exact mass flow through the SCR in the reference material.

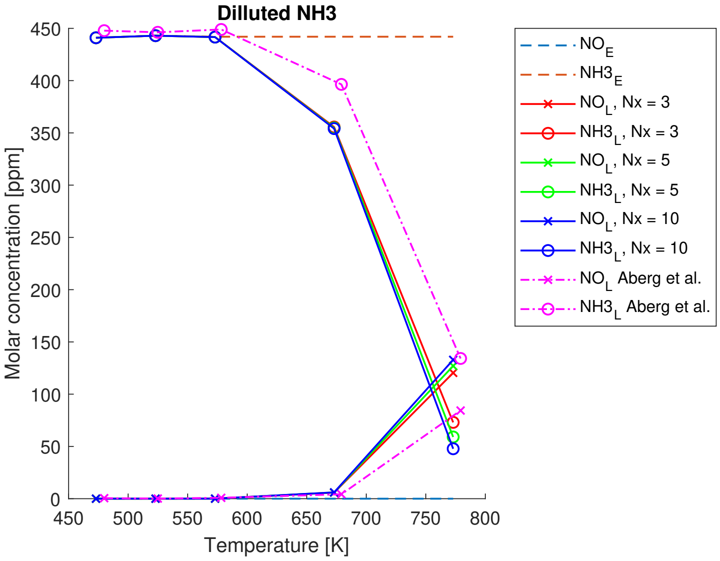

Figure 6.1: Diluted NH_3 verification experiment for Va model.

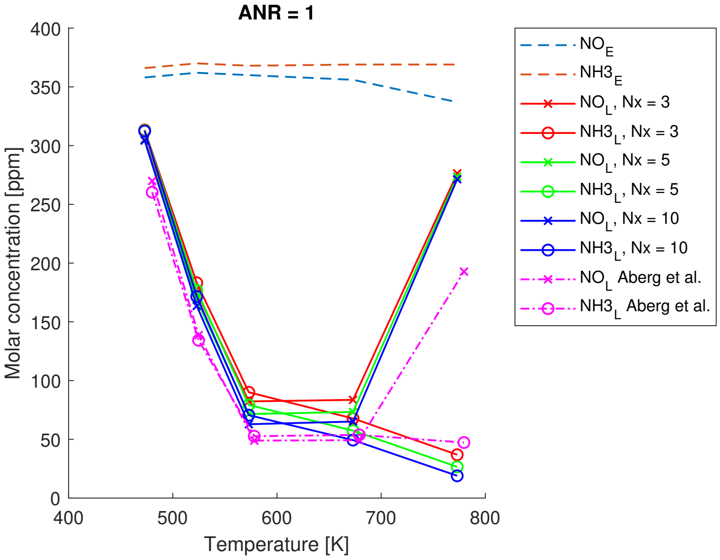

Figure 6.2: ANR = 1 verification experiment for Va model.

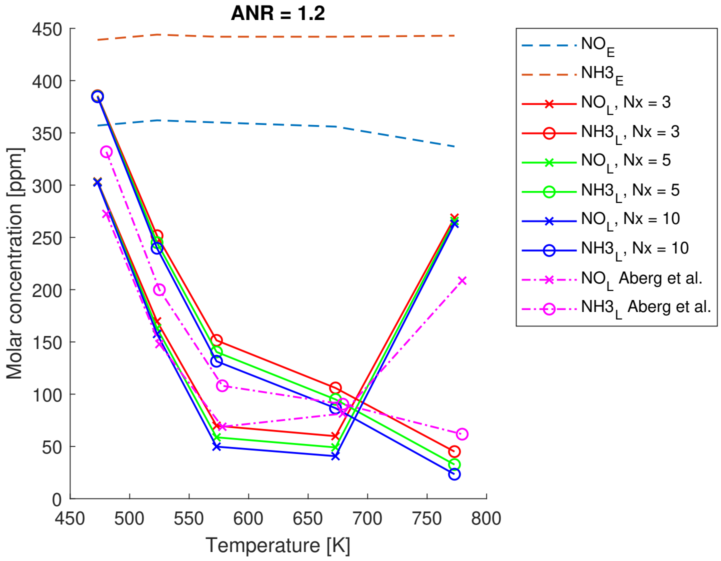

Figure 6.3: ANR = 1.2 verification experiment for Va model.

6.1.2. Fe and Cu Model

The first step is to see if the results of the Fe and Cu match the results of the source paper of Metkar, Balakotaiah, and Harold [47]. To do so multiple experiments, matching the validation experiments from the paper itself are performed. First a constant feed containing 500 ppm NH_3 is examined, then a constant feed containing 500 ppm NO, finally a feed with 500 ppm NH_3 and 500 ppm NO. Some of the geometric properties used for these experiments were not directly given in the paper and had to be constructed from other data in the paper. The generation of heat was neglected during this verification step (in line with the paper). Furthermore, the tests are conducted with Argon as carrier gas and therefore use different values for diffusivity. The used relations are shown in table 6.3. The other geometric and flow parameters are shown in table 6.4.

Table 6.3: Diffusivity in Argon

Gas	Diffusivity (m^2/s)
NO	1.2365e-9 $\cdot T^{1.7006}$
NO_2	7.9236e-10 $\cdot T^{1.7297}$
NH_3	1.215e-9 $\cdot T^{1.7389}$
N_2O	8.1452e-10 $\cdot T^{1.7314}$

Table 6.4: Geometric and flow parameters used for validation of Fe and Cu model

Parameter	Symbol	Value	Unit
Number of Layers		1	#
Washcoat thickness	$R_{\Omega 2}$	5.00E-05	m
Cell density	CPSI	400	#/in^2
Wall thickness	t_w	0.007	in
Diameter monolith	D	0.81	cm
Length Monolith	L_m	0.02	m
Washcoat porosity	ϵ_{WC}	0.4	-
SCR void fraction	ϵ	0.742	-
Volumetric flow rate	Q	1000	ml/min
Velocity in channel	u	0.45	m/s at 300 K

The results of the first two experiments are shown in figure 6.4, the third experiment is shown in figure 6.5. Small differences can be seen, but overall the trend follows the source paper very closely. To perform all three tests, 63 runs have to be performed to get a data point every 50 ^{o}C. The time consumed by the computer to perform these 63 runs on 6 cores (Intel(R) Core(TM) i7-8750H CPU @ 2.20GHz 2.21 GHz) simultaneously, is shown in table 6.5 and table 6.6 for the Fe and Cu catalyst respectively. The Fe model takes significantly longer to solve, compared to the Cu model. This is a result of the more complex reaction mechanism taking place in the Fe catalyst. The higher level of complexity also requires a smaller maximum relative error in the solver. Taking these computation times and accuracy of the computations, Nx=5 and Ny = 5 is used in further calculations.

Table 6.5: Computation time for Fe model

Computation time		N_X		
		3	5	10
N_Y	3	3:49	9:44	53:16
	5	7:20	15:26	1:13:50
	10	31:21	55:51	3:47:00

Table 6.6: Computation time for Cu model

Computation time		N_X		
		3	5	10
N_Y	3	1:22	2:56	12:01
	5	2:13	5:14	20:47
	10	7:01	14:37	53:49

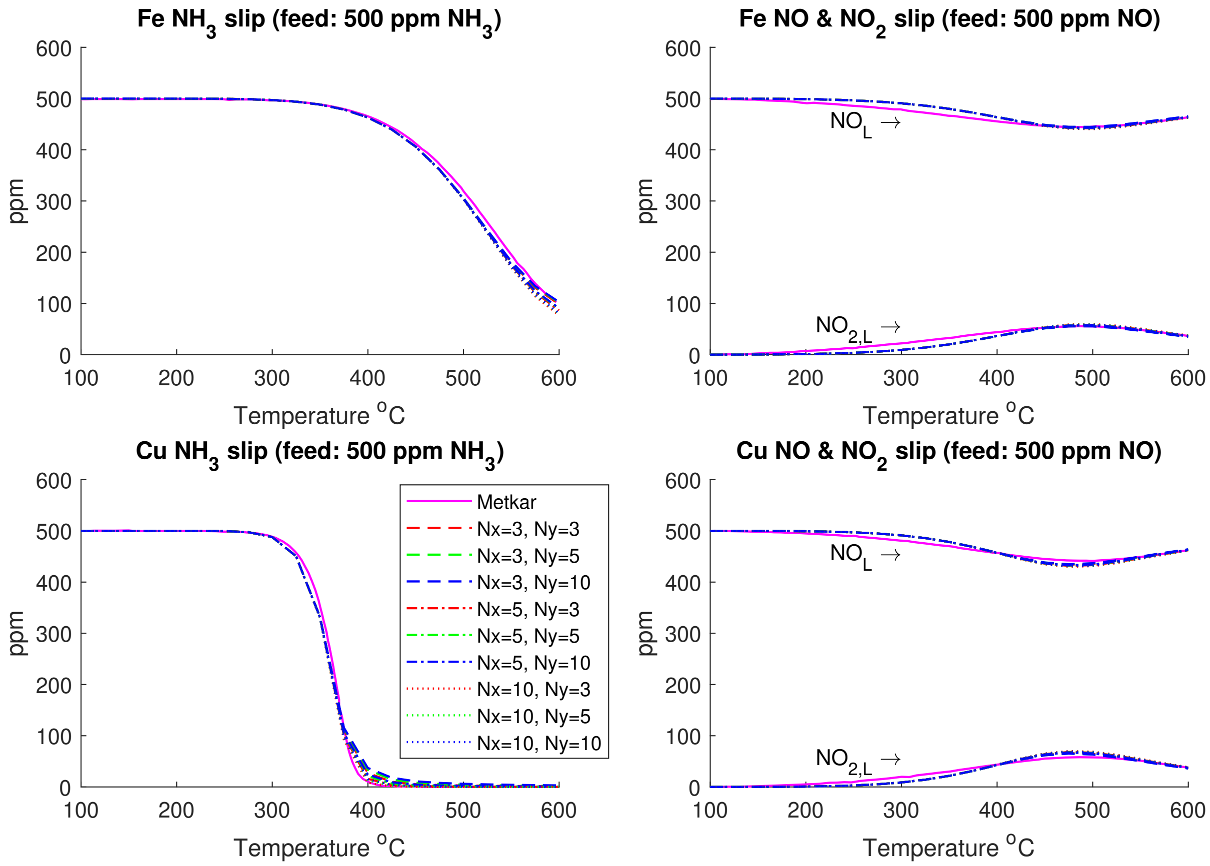

Figure 6.4: Diluted NH$_3$ and Diluted NO verification experiment for Fe and Cu model.

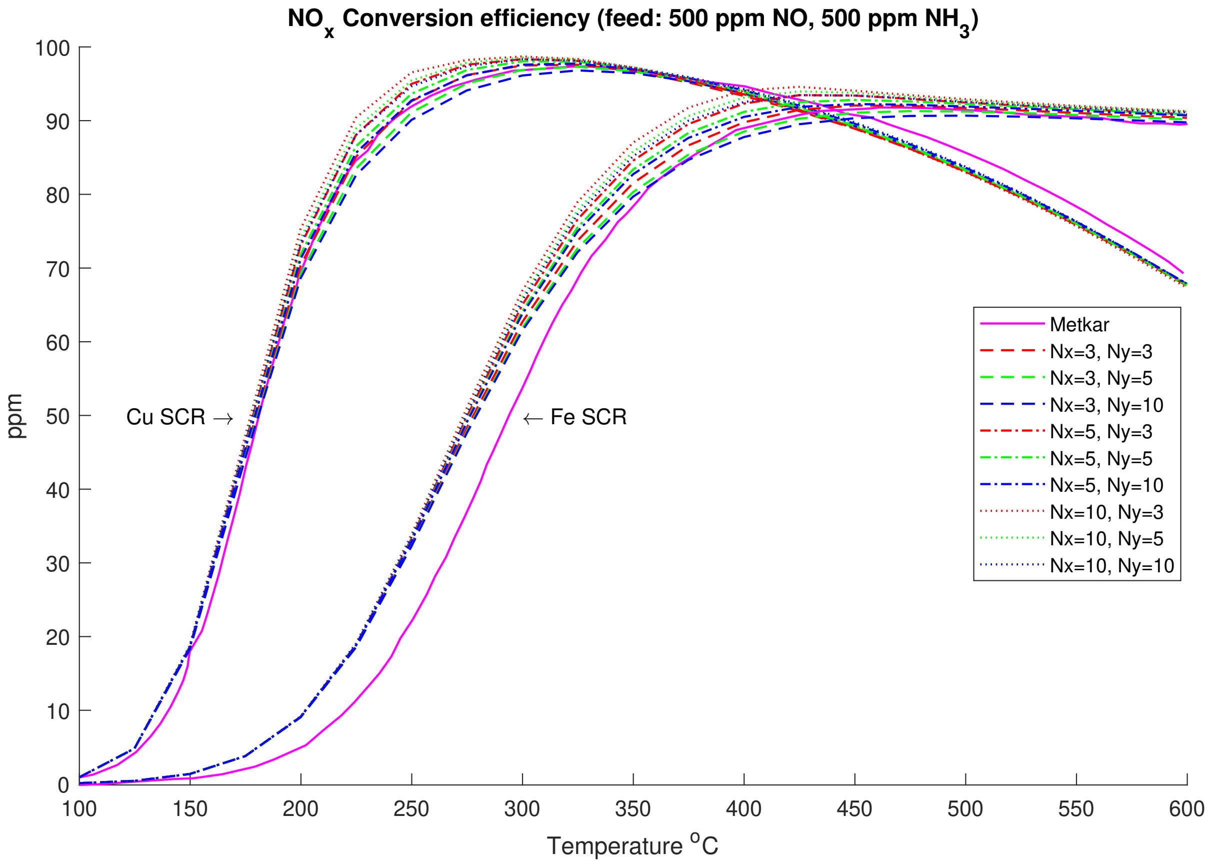

Figure 6.5: NO conversion verification experiment for Fe and Cu model.

6.2. Batch Reactor

For the sake of this experiment it is assumed that the monolith layer is not part of a flow reactor, but a batch reactor. By doing so, it is possible to see if the correct amount of NH_3 is absorbed and reacts, with the corresponding volume of the reactor. The dimensions of this batch reactor correspond to the ones shown in table 6.7. Clearly, this ”test” is not a proper physical test, as transport and heat coefficients change when there is no flow. However, it does show if the correct amounts of pollutants react. This helps to confirm the model was constructed correctly.

Table 6.7: Dimensions of batch reactor.

Variable	Value	Unit
L	1	[m]
B	1	[m]
t_w	0.012	[inch]
cpsi	100	[#/inch2]
eps	0.7744	[-]

With these values it is fairly easy to come up with a simple test case and the theoretical and actual amount of NH_3 that reacted inside the reactor. To do so it is assumed all NH_3 reacts if an initial ANR of 1:1 is used. This is a valid assumption as NO can not react without NH_3, while NH_3 can oxidise solely and irreversibly. This is also the reason a ANR greater than 1 is often used to break down all NO_x in an SCR. First, the maximal theoretical amount of NH_3 that is able to react is determined. This is shown in equation 6.1. In this case, an initial concentration of 1000 ppm NO and 1000 ppm NH_3 is assumed.

$$NH_{3,theoretical} = A_{cs} \cdot L \cdot \epsilon \cdot \frac{P}{R_u \cdot T} \cdot ppm \cdot 1e-6 \\ = 0.01887 mol \tag{6.1}$$

Next, it is possible to check how much NH_3 has reacted in the models. For both Fe and Cu, the kinetic data is based on mol/s/m3washcoat. Therefore the total amount of NH_3 reacting is governed by the following equation:

$$NH_{3,model} = A_{cs} \cdot G_a \cdot \int_0^\infty \int_0^L \int_0^{R_{\Omega 2}} (r_{ads} - r_{des}) dy \cdot dx \cdot dt \\ = 0.01887 mol \; for \; both \; Fe \; and \; Cu \tag{6.2}$$

for Va the equation is slightly different. The volume over which must be integrated is not that of the washcoat itself, but the volume of the channels:

$$NH_{3,model} = A_{cs} \cdot eps \cdot \int_0^\infty \int_0^L (r_{ads} - r_{des}) dx \cdot dt \\ = 0.01887 mol \; for \; Va \tag{6.3}$$

All models consume the maximum theoretical amount as can be expected. This verification step helped to debug errors in the heat generated in the SCR reactor, as well as faults in the transport coefficients.

6.3. TNO Model

TNO offers a Cu model, that can be used to see how well data from Metkar, Balakotaiah, and Harold [47] can be scaled. The same tests as with the small scale verification, but with different geometry and higher inlet concentrations are performed. The used geometry is equal to the geometry presented in table 7.2. There is one other difference: The experiments of Metkar use a NO_2/NO_X ratio of 0, while these experiments use a NO_2/NO_X ratio of 0.075. The results of the experiments are shown in figure 6.6 and 6.7.

Looking at the diluted NH_3 experiment in figure 6.4, certain similarities and differences can be seen between the two models. Both models show no oxidation in the lower temperature range. In the higher temperature range all NH_3 is oxidised. The oxidation of NH_3 is shows a strong increase over a short temperature interval. The location of this interval is located at a higher temperature for the TNO model. The diluted NO_X experiment shows a large difference with the TNO model. The kinetic data provided by Metkar includes the oxidation of NO to NO_2, the TNO model does not. The result is a different shaped curvature, as NO is converted into NO_2 with an optimum around 425/450 ^{o}C.

Figure 6.5 shows the TNO model predicts around a 10% higher conversion efficiency at lower temperatures. For both models a sharp increase is seen in conversion efficiency in the range from 100 to 200 ^{o}C. At higher temperatures the conversion efficiency the model start to decrease, while the conversion efficiency of the TNO model stays near 100 %. From literature it can however be expected that the conversion energy drops slightly at higher temperatures [47] & [51].

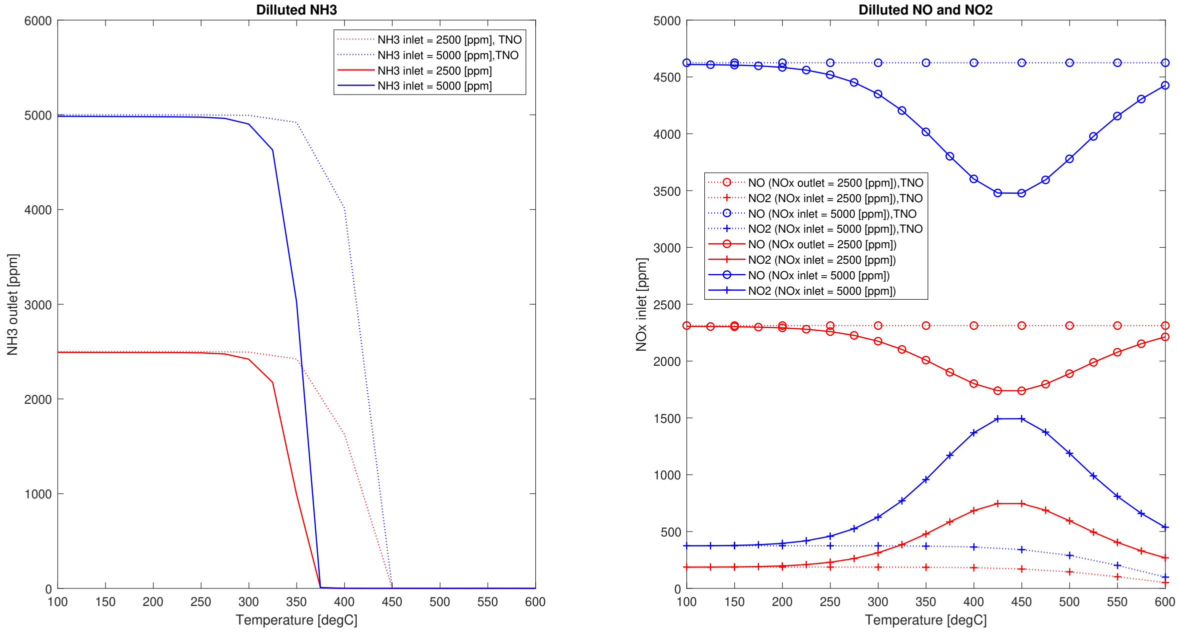

Figure 6.6: Diluted NH_3 (left) and diluted NO_X (right) validation experiment for Cu model.

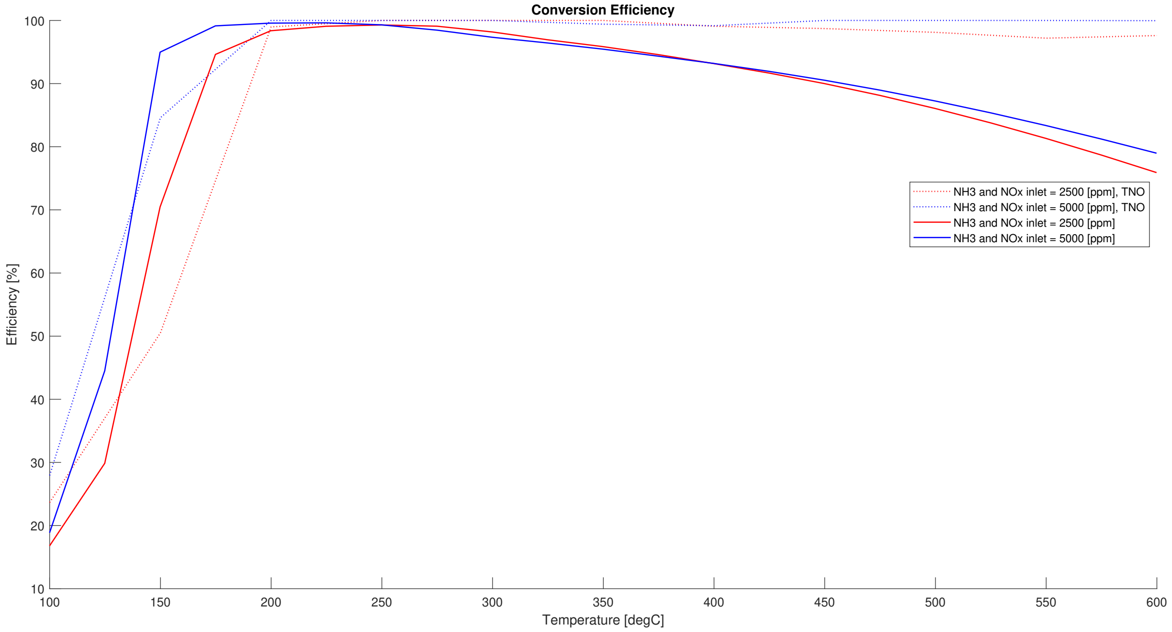

Figure 6.7: NO_X conversion verification experiment for Cu model.

7

Test Setup and Schematic

This chapter first discusses the full scale setup and dimensions used for testing. Furthermore, the maximum allowed emissions for NO_X, NH_3 and N_2O are discussed.

7.1. Full Scale Dimensions

To size the SCR for full scale operation, multiple sources were consulted. To size the width of the SCR, table 7.1 was used. It shows for a 7300 kW engine, a SCR with a cross section of 2.44*2.44 m is needed. This measurement also includes a 15 cm thick insulation on both sides, as well as a packaging factor of 0.95 as a result of stacking multiple modules side by side [5]. The width of the catalytic layer as used in the model is therefore determined in the following way:

$$\begin{aligned} B &= (B_{tot} - 2 \cdot t_{insulation}) \cdot PF \\ &= (2.44 - 2 \cdot 0.15) \cdot 0.95 \\ &= 2.033\ [m] \end{aligned} \tag{7.1}$$

ϕ_f is determined using equation 5.11 with a pressure drop of 1500 Pa over the 2 layers combined at full load of a Wartsila 12V31. This corresponds to a mass flow of 12.6 kg/s, 266 ^oC at the inlet of the SCR [63].

For the monolith layer itself, marine standards are maintained. This means that the cell density is relatively low and thus the hydraulic diameter is high. This geometry is useful when high amounts of soot can be expected in the exhaust, to prevent clogging of the channels. When switching from HFO or diesel to NH_3 as fuel, soot will also be removed from the exhaust. This will allow for smaller channels, however, for this study the cell density will remain 100 cpsi.
An overview of the used parameters together with their source is shown in table 7.2.

7.2. Input variables

The engines as presented in 2 show a great variety for important inlet parameters of the SCR. The most important parameters, used to define the flow out of the engine and into the SCR are: temperature, NO_X concentration, NH_3 concentration, equivalence ratio, NO_2/NO_X ratio and N_2O concentration. The upper and lower limits used during testing are shown in table 7.3. The range used is in line with the findings as presented in chapter 2. These engines are not marine size engines, but small experimental engines. As a result, the actual concentrations of pollutants leaving the ICE in the AmmoniaDrive might be different. It is likely to assume that they will be within the range as presented in this table.
The experiments to be carried out will be steady state. Initially no concentration or ammonia coverage is present in the SCR. At the start of the experiment a certain set of NO, NO_2, NH_3 and N_2O concentrations are introduced at the inlet and maintained at this level for 3000s. After this duration steady state is achieved and the outlet concentrations at this moment in time defines the steady state capabilities of the SCR.

Table 7.1: SCR dimensions of Wärtsilä [66].

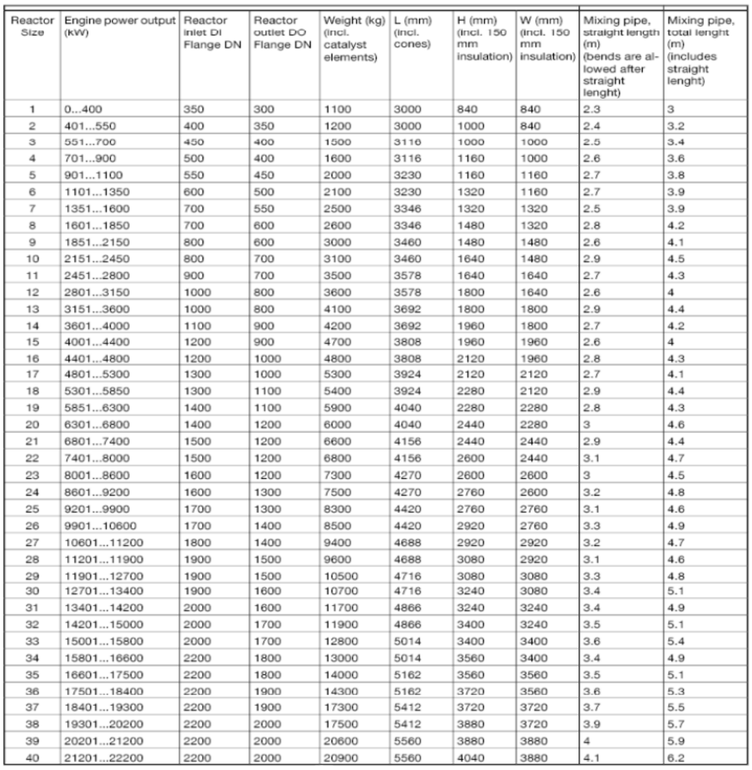

Reactor Size	Engine power output (kW)	Reactor inlet DI Flange DN	Reactor outlet DO Flange DN	Weight (kg) (incl. catalyst elements)	L (mm) (incl. cones)	H (mm) (incl. 150 mm insulation)	W (mm) (incl. 150 mm insulation)	Mixing pipe, straight length (m) (bends are allowed after straight lenght)	Mixing pipe, total lenght (m) (includes straight lenght)
1	0...400	350	300	1100	3000	840	840	2.3	3
2	401...550	400	350	1200	3000	1000	840	2.4	3.2
3	551...700	450	400	1500	3116	1000	1000	2.5	3.4
4	701...900	500	400	1600	3116	1160	1000	2.6	3.6
5	901...1100	550	450	2000	3230	1160	1160	2.7	3.8
6	1101...1350	600	500	2100	3230	1320	1160	2.7	3.9
7	1351...1600	700	550	2500	3346	1320	1320	2.5	3.9
8	1601...1850	700	600	2600	3346	1480	1320	2.8	4.2
9	1851...2150	800	600	3000	3460	1480	1480	2.6	4.1
10	2151...2450	800	700	3100	3460	1640	1480	2.9	4.5
11	2451...2800	900	700	3500	3578	1640	1640	2.7	4.3
12	2801...3150	1000	800	3600	3578	1800	1640	2.6	4
13	3151...3600	1000	800	4100	3692	1800	1800	2.9	4.4
14	3601...4000	1100	900	4200	3692	1960	1800	2.7	4.2
15	4001...4400	1200	900	4700	3808	1960	1960	2.6	4
16	4401...4800	1200	1000	4800	3808	2120	1960	2.8	4.3
17	4801...5300	1300	1000	5300	3924	2120	2120	2.7	4.1
18	5301...5850	1300	1100	5400	3924	2280	2120	2.9	4.4
19	5851...6300	1400	1100	5900	4040	2280	2280	2.8	4.3
20	6301...6800	1400	1200	6000	4040	2440	2280	3	4.6
21	6801...7400	1500	1200	6600	4156	2440	2440	2.9	4.4
22	7401...8000	1500	1200	6800	4156	2600	2440	3.1	4.7
23	8001...8600	1600	1200	7300	4270	2600	2600	3	4.5
24	8601...9200	1600	1300	7500	4270	2760	2600	3.2	4.8
25	9201...9900	1700	1300	8300	4420	2760	2760	3.1	4.6
26	9901...10600	1700	1400	8500	4420	2920	2760	3.3	4.9
27	10601...11200	1800	1400	9400	4688	2920	2920	3.2	4.7
28	11201...11900	1900	1500	9600	4688	3080	2920	3.1	4.6
29	11901...12700	1900	1500	10500	4716	3080	3080	3.3	4.8
30	12701...13400	1900	1600	10700	4716	3240	3080	3.4	5.1
31	13401...14200	2000	1600	11700	4866	3240	3240	3.4	4.9
32	14201...15000	2000	1700	11900	4866	3400	3240	3.5	5.1
33	15001...15800	2000	1700	12800	5014	3400	3400	3.6	5.4
34	15801...16600	2200	1800	13000	5014	3560	3400	3.4	4.9
35	16601...17500	2200	1800	14000	5162	3560	3560	3.5	5.1
36	17501...18400	2200	1900	14300	5162	3720	3560	3.6	5.3
37	18401...19300	2200	1900	17300	5412	3720	3720	3.7	5.5
38	19301...20200	2200	2000	17500	5412	3880	3720	3.9	5.7
39	20201...21200	2200	2000	20600	5560	3880	3880	4	5.9
40	21201...22200	2200	2000	20900	5560	4040	3880	4.1	6.2

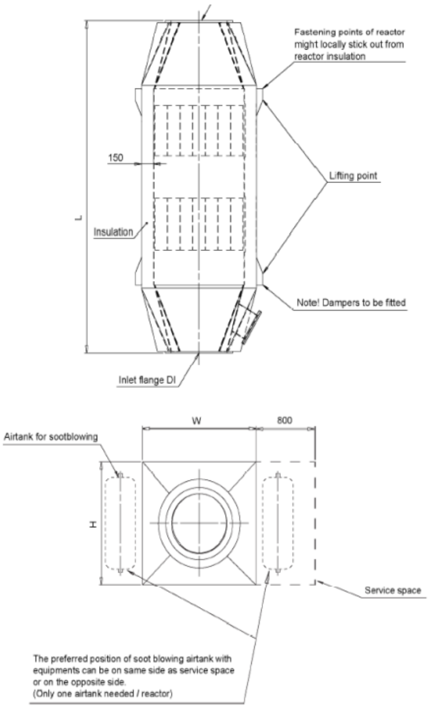

The preferred position of soot blowing airtank with equipments can be on same side as service space or on the opposite side.
(Only one airtank needed / reactor)

7.3. Feasible Operating Range

After understanding how and why the SCR behaves as it does, it is possible to examine where the feasible operating range of the SCR is. This range is defined as the set of input variables that provide NO, NO_2, NH_3 and N_2O concentration levels at the outlet of the SCR below the legal or desired limits.

7.3.1. NO_X and NH_3

The combined limit for NO and NO_2 is currently covered by the TIER III limit for NO_X emissions. This is 2.4 g NO_X/kWh if the rotational speed of a Wartsila 12V31 engine is adopted. Currently, no limits are in place for NH_3 emissions by ships. However, as NH_3 becomes a widely adopted fuel, it is likely some limit will be introduced. As the problems caused by NH_3 emissions are similar to those caused by NO_X emissions, it is logical to limit the two together. The newly proposed limit, limits the combined specific emission of NO_X and NH_3 to 2.4 g/kWh.

Table 7.2: Marine size SCR parameters.

Parameter	Symbol	Value	Unit	Source
Number of Layers		2	#	[66] & [65]
Washcoat thickness	$R_{\Omega 2}$	1.00e-04	m	[1]
Cell density	CPSI	100	#/inch2	[5]
Wall thickness	t_w	0.012	inch	[5]
Hydraulic diameter	d_h	0.0022	m	
Width monolith	B	2.033	m	[66], [65] & [5]
Length Monolith	L_m	0.3	m	[5]
length void	L_{void}	0.5	m	[5]
friction coefficient	ϕ_f	0.505	-	[63] & [65]

Table 7.3: Range inlet variables

Variable	Lower limit	Upper limit	Unit
T_E	100	600	[^{o}C]
NO$_X$	0	5000	[ppm]
NH$_3$	0	5000	[ppm]
ϕ	0.2	0.9	[-]
$^{NO_2}/_{NO_X}$	0	0.15	[-]
N$_2$O	0	100	[ppm]

7.3.2. N$_2$O

There is no legal limit on the maximum allowable N$_2$O emission (yet). However it is a highly potent greenhouse gas as discussed earlier. So the AmmoniaDrive power plant should emit only little, if it wants to have a "green" status. The CO2 emissions of a ship, measured in g/kWh, can be determined, using the following equation:

$$\begin{aligned} specific\ CO_2\ emission &= sfc * \frac{kg_{CO_2}}{kg_{diesel}} \\ &= 170 * 3.16 \\ &= 537\ [g/kWh] \end{aligned} \tag{7.2}$$

In the equation above, sfc represents the specific fuel consumption [36] and $\frac{kg_{CO_2}}{kg_{diesel}}$ the amount of CO2 emitted per kg diesel burned. The used molecular formula for diesel was $C_{12}H_{36}$.

The maximum specific emission of N$_2$O is shown in the equation below. It is assumed the reduction of green house gas is 90% compared to a conventional diesel power plant and the GWP of N$_2$O is 282 times that of CO2.

$$\begin{aligned} N_2O\ limit &= \frac{g_{CO_2}/kWh \cdot (1 - reduction)}{GWP_{N_2O}} \\ &= \frac{537 \cdot (1 - 0.9)}{282} \\ &= 0.19\ [g/kWh] \end{aligned} \tag{7.3}$$

The limit is fairly low. If the power plant operates at an equivalence ratio of 0.55, this limit translates into 23 ppm.

8

Results

This chapter presents the results of the carried out tests. The first step is to examine in more detail which inlet parameters have the most effect on the NO_X, NH_3 and N_2O concentrations at the outlet of the SCR. Next will be to examine how these inlet parameters influence the concentrations at the outlet of each SCR type. It will be discussed which reactions and processes take place inside the SCR. Finally, a more all-encompassing comparison will be done, here the feasible operating range of the different SCR types will the examined.

8.1. Relevant Parameters

This section is divided according to the different pollutants: first NO_X is discussed, later NH_3 and finally N_2O emission.

8.1.1. NO_X

The figures in appendix D show the interaction between the different input parameters and NO_X concentrations at the outlet. Further explanation on how to properly read these plots is given in the appendix.

When looking at the plots, multiple things become clear. First of all, temperature is a key player for all materials. Va shows a more pronounced optimum around 300/400 ^oC. Fe and Cu on the other hand do not start to perform worse when the temperature rises significantly. Furthermore, the increase in NO_X concentration at the inlet leads to more NO_X concentration at the outlet. Important to note is the non-zero output of NO_X with zero NO_X input for the Va catalyst, this is a result of the oxidation of NH_3 and will be discussed in detail in the following section. At last, the NH_3 concentration at the inlet IS an important parameter for all catalysts. This is logical as NH_3 is needed to break down NO_X via the standard or fast SCR reaction.

The equivalence ratio, NO_2/NO_X ratio and N_2O concentrations at the inlet make little difference. The first matters little when looking at concentrations, measured in ppm. This is however not the case when measuring emissions in g/kWh, further explanation will be given in chapter 8.3. The main change is the different mass flow, thus flow velocity and therefore residence time inside the SCR. The fact that changing residence time does not result in a performance loss, could tell that the SCR is oversized. An oversized SCR is a problem when designing and optimising a system, as it results in a system that is too big and too expensive. The steady state NO_X conversion is not negatively influenced by an oversized SCR.

The NO_2/NO_X ratio is an important parameter when looking at a greater interval: the diesel oxidation catalyst is often optimised for a 50% ratio after all. The higher NO_2 content allows for the fast SCR reaction to take place. This reaction does not only allow for faster conversion, but also conversion at lower temperatures. For the relative small interval of 0-0.15, considered in this study, the effect is only marginal.

N2O concentration at the inlet shows little to no influence at all to the NO_X emission. This is logical as no interaction between NO or NO_2 and N_2O is present. When studying the different reaction mechanisms, it can even be seen that only on the Fe catalyst, the N_2O can react with NH_3. The fact that the N_2O concentration at the inlet does not influence the NO_X concentration at the outlet on the Fe catalyst, shows that NH_3 is more likely to react with NO_X instead of N_2O. This claim will be further substantiated in the following sections.

8.1.2. NH_3

The plots as shown in appendix Eshows how the different parameters influence the NH_3 concentrations at the outlet of the SCR. Further explanation on how to read these plots is given in the appendix itself.

Once again, the inlet temperature is a very important parameter for all SCR types as it controls the reaction rates inside the SCR. The NH_3 concentration at the outlet decreases as the inlet temperature rises. Both the Va and Cu SCR do not emit any more NH_3 at temperatures above 475 ^oC. The Fe catalyst reaches this point at higher temperatures and might still emit small amounts of NH_3 at 600 ^oC. The amount of NO_X at the inlet is also an important parameter, that changing the NH_3 concentration at the outlet. The standard and fast SCR reactions are important reactions taking place in the SCR and as they both consume NO_X and NH_3, they lower the NH_3 concentration at the outlet. The NH_3 concentration itself at the inlet of the SCR is obviously an important parameter to determine the amount of NH_3 at the outlet: the NH_3 that was unable to react inside the SCR will leave at the outlet.

In line with the NO_X concentrations leaving the SCR, the equivalence ratio, NO_2/NO_X ratio and N_2O concentration at the inlet make little difference in the NH_3 concentration leaving the SCR. However the fact that the SCR is oversized needs a footnote. Although this is not a problem when looking at steady state NH_3 emissions of the SCR, it is highly undesirable when the SCR operates in transient conditions. The large SCR is able to hold large amounts of NH_3. If the temperature increases, a large amount of this NH_3 is released from the active sites and leaves the SCR. This could very well result in an overrun of the allowable NH_3 concentrations at the outlet of the SCR.

8.1.3. N_2O

Looking at the figures in appendix F, it becomes clear the Va and Cu catalyst can not break down the N_2O that enters the SCR. The Va catalyst produces extra N_2O under certain conditions: high inlet temperatures and relatively larger inlet concentrations of NO_2, also NH_3 is required. Extra NO_X and a higher NO_2/NO_X ratio at the inlet lead to higher NO_2 concentrations at the inlet. As a result the N_2O production increases.

The Cu catalyst does not produce any extra N_2O. The interaction plot shows no variation over all inlet variables, except for N_2O.

The Fe catalyst shows the ability to reduce the N_2O concentrations entering the SCR. The inlet temperature is an important parameter in this case as the reduction of N_2O requires high temperatures. The NH_3 concentration is also of importance as it is one of the breakdown mechanisms of N_2O is by reacting with bonded NH_3. However, it is also possible for the N_2O to be broken down without NH_3.

8.2. Detailed Catalyst Behaviour

This section looks with more detail into how the inlet temperature, NO_X concentration and NH_3 concentration affect the nitrogen-based pollutant levels leaving the SCR. First, the Va catalyst is discussed, later the Fe catalyst and finally the Cu catalyst.

8.2.1. Va Catalyst

First the NO_X concentration leaving the Va SCR is shown in figure 8.1.
Looking at the zero NH_3 inlet, it becomes clear NO_X can not be broken down without NH_3. This trend also continues for the other NH_3 inlet concentrations, where only as much NO_X can react as NH_3 is injected. The plots at $NH_{3,E}$ = 1000 and 2000 ppm show an optimum around 300-400 ^oC. As the NH_3 concentration is further increased, this optimum starts to move to the lower inlet temperatures. This is

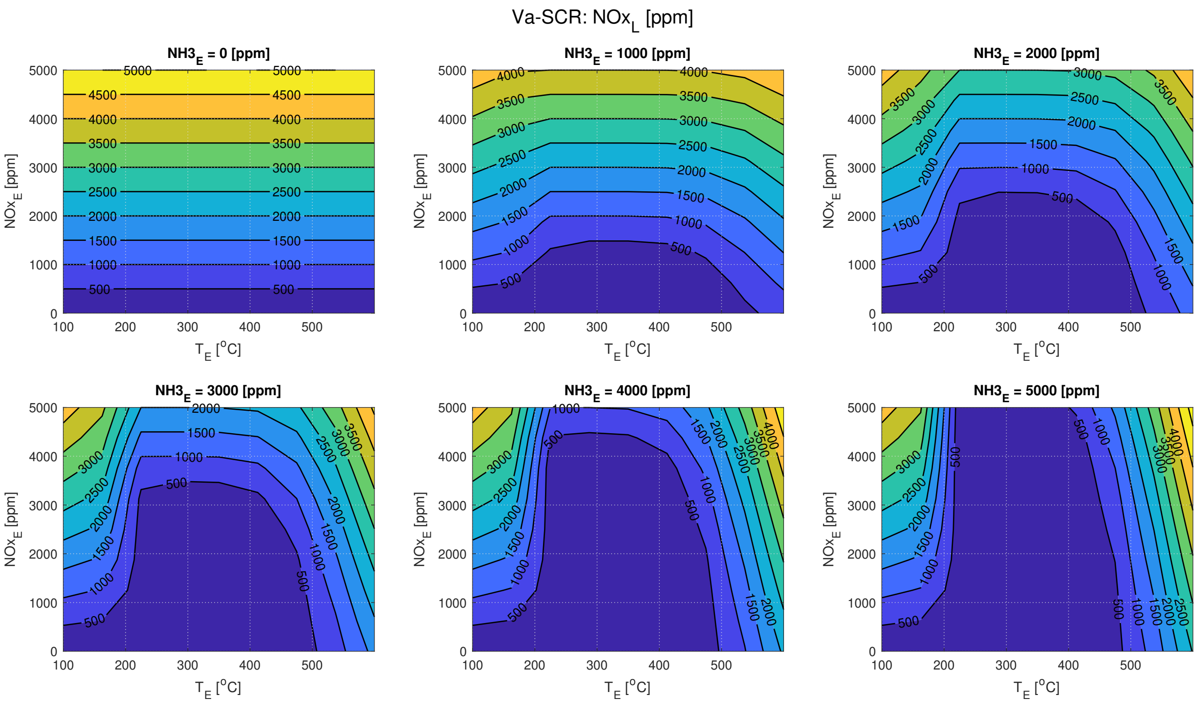

Figure 8.1: NO$_X$ concentrations at outlet Va-SCR (N$_2$O$_E$ = 100 [ppm], ϕ = 0.55, $^{NO_2}/_{NO_X}$ = 0.075).

a result of the generated heat inside the SCR. In the most extreme cases, a temperature increase of 60 ^{o}C can be seen over the SCR. When too high temperatures are reached, NH$_3$ starts to oxidise. This is problem becomes very prominent above 400-500 ^{o}C. As this happens (according to reaction 2.2) NO is formed. As a result, it is possible to emit more NO$_X$ than goes into the SCR.

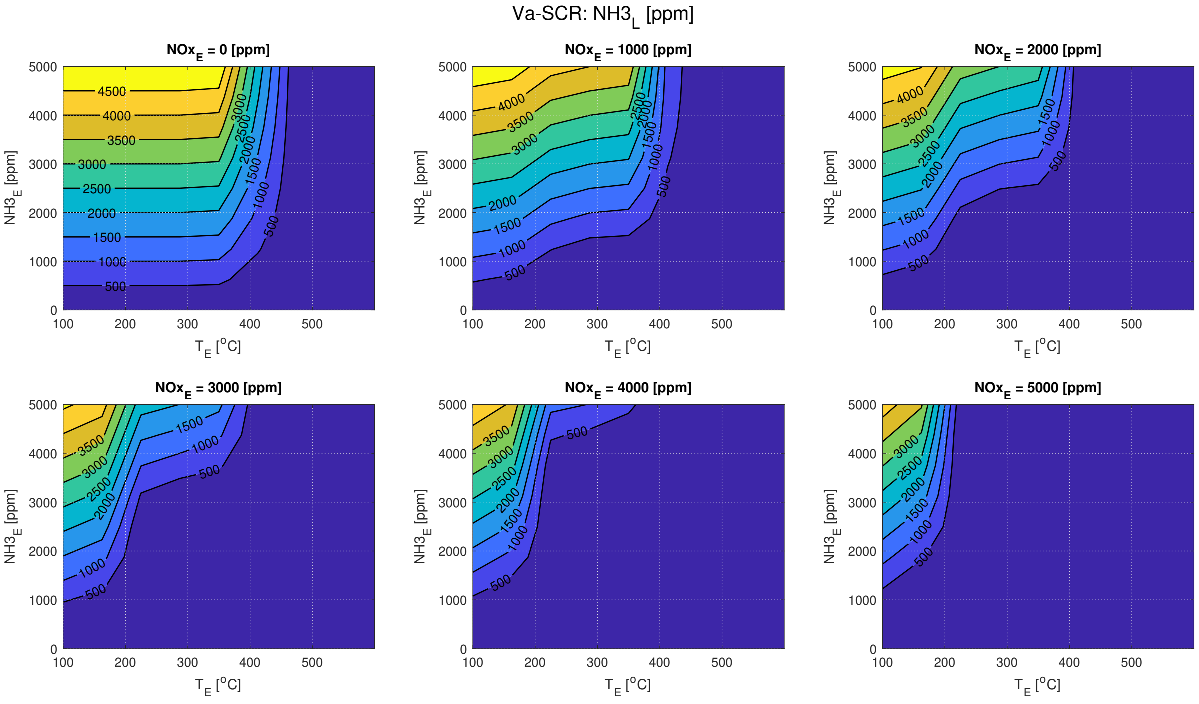

Figure 8.2: NH$_3$ concentrations at outlet Va-SCR (N$_2$O$_E$ = 100 [ppm], ϕ = 0.55, $^{NO_2}/_{NO_X}$ = 0.075).

When looking at figure 8.2, it is possible to gain more insight into the oxidation of NH$_3$. Looking at the NO$_{X,E}$ = 0ppm, a decline in NH$_3$ emission occurs from temperatures of 350 ^{o}C and up, all NH$_3$

emissions are eliminated from 450 ^oC and above. When NO_X concentrations at the inlet are increased, the effects of the normal and fast SCR reaction become evident: between 250 and 350 ^oC, NH_3 reacts with the available NO_X in the reactor. Looking at figure 8.1 $NH_{3,E}$ = 5000 it is possible to conclude that in the range of 350-450 ^oC, the NO created by NH_3 oxidation is also broken down by the standard SCR reaction.

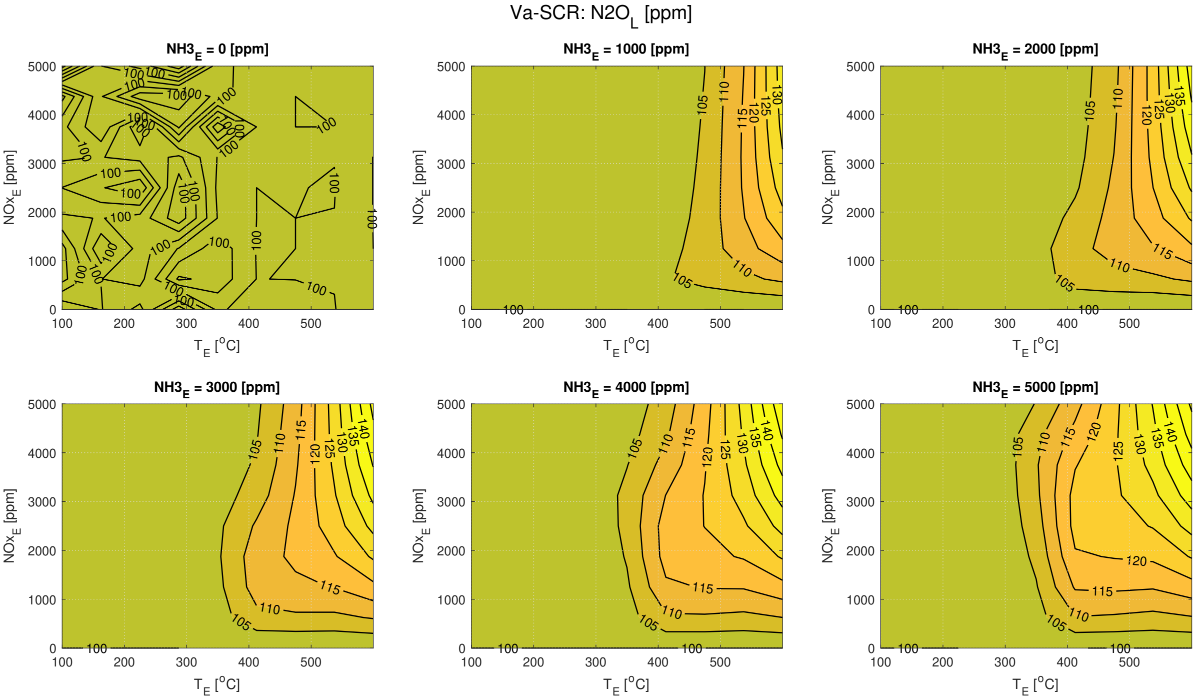

Figure 8.3: N_2O concentrations at outlet Va-SCR (N_2O_E = 100 [ppm], ϕ = 0.55, $^{NO_2}/_{NO_X}$ = 0.075).

The production of N_2O by the Va catalyst is shown in figure 8.3. The figure shows the Va catalyst is not able to reduce the N_2O coming into the SCR, instead, it produces extra N_2O. With an increasing amount of NH_3 at the inlet of the SCR, the N_2O production inside the SCR also increases. Depending on the NH_3 inlet concentration the production starts around 400-500 ^oC. The maximum production is around 30/40 ppm. The effect of changing NO_X inlet concentrations (and thus NO_2 inlet concentrations), becomes more pronounced at temperatures above 500 ^oC.

8.2.2. Fe catalyst

Looking at figure 8.4 $NH_{3,E}$ = 0 ppm, it becomes clear NO_X is not broken down without the presence of NH_3. The other plots in this figure show that lower concentrations of NH_3 and NO_X react well from 300 C and higher. With high concentrations of NH_3 and NO_X at the inlet it is possible to push this limit down to 250 ^oC and higher, as a result of the large amounts of heat generated in the reactions. The actual temperature of the washcoat surface, where the reactions take place, can easily be 60 C higher than the inlet temperature. The performance of the NO_X reduction, as was seen for the Va catalyst is not present here. This phenomenon has two explanations. First, in contrast to the Va catalyst, the oxidation of NH_3 does not result in the production of NO, but N2. Second, the SCR reactions are always preferred over the direct oxidation of NH_3, leaving enough NH_3 to react with the NO_X.

Looking at figure 8.5 $NO_{X,E}$ = 0ppm, it can be seen that NH_3 oxidation starts to occur from 300 ^oC on. However, full oxidation of all NH_3 requires much higher temperatures: almost 600 ^oC. With an increasing concentration of NO_X at the inlet a shift becomes clear: first, the NO_X and NH_3 react at temperatures below 250 ^oC, beyond this temperature oxidation removes the leftover NH_3.

Figure 8.6 shows the capability of the Fe catalyst to break down N_2O. If 100 ppm N_2O is introduced in the inlet feed of the SCR, reduction occurs from 400 ^oC and full reduction is achieved far above 500 deg C if the ANR is around 1 or lower. As the SCR reactions are faster, all reduction has to occur without

NH_3 (reaction 9). If the ANR is above 1, the faster reaction where N_2O reacts with NH_3 (reaction 10) takes over. Reduction then starts around 300 ^oC and full reduction is achieved well below 500 ^oC.

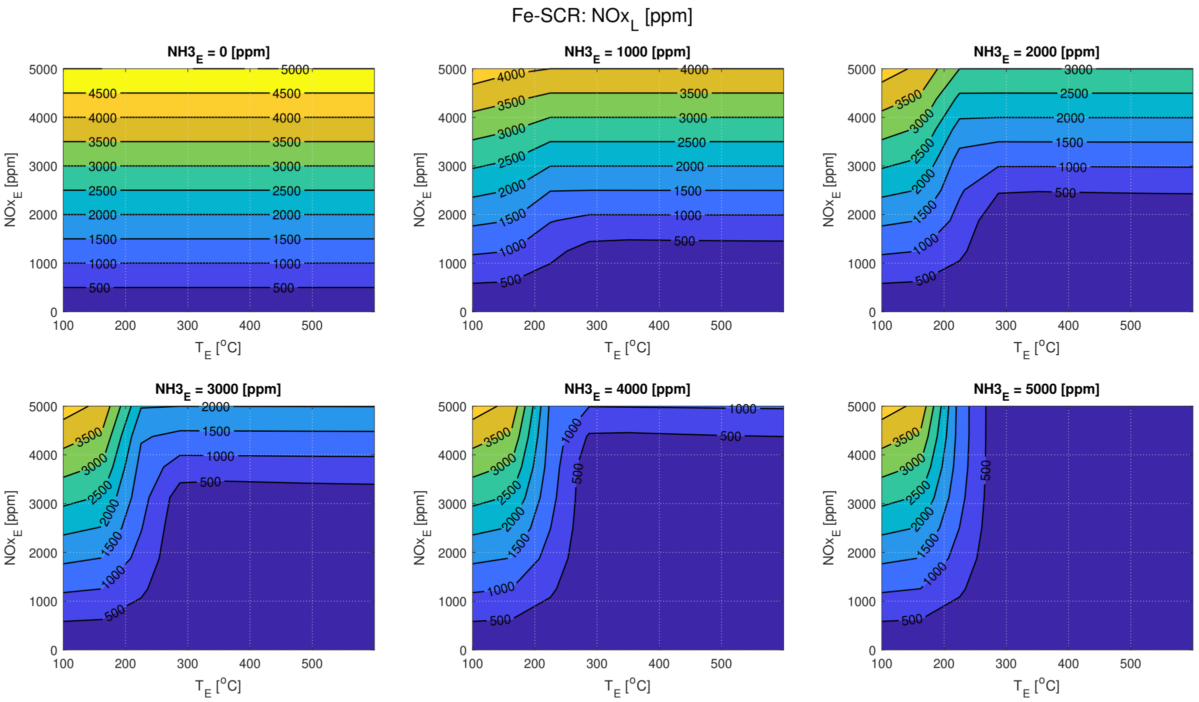

Figure 8.4: NO_X concentrations at outlet Fe-SCR (N_2O_E = 100 [ppm], ϕ = 0.55, $^{NO_2}/_{NO_X}$ = 0.075).

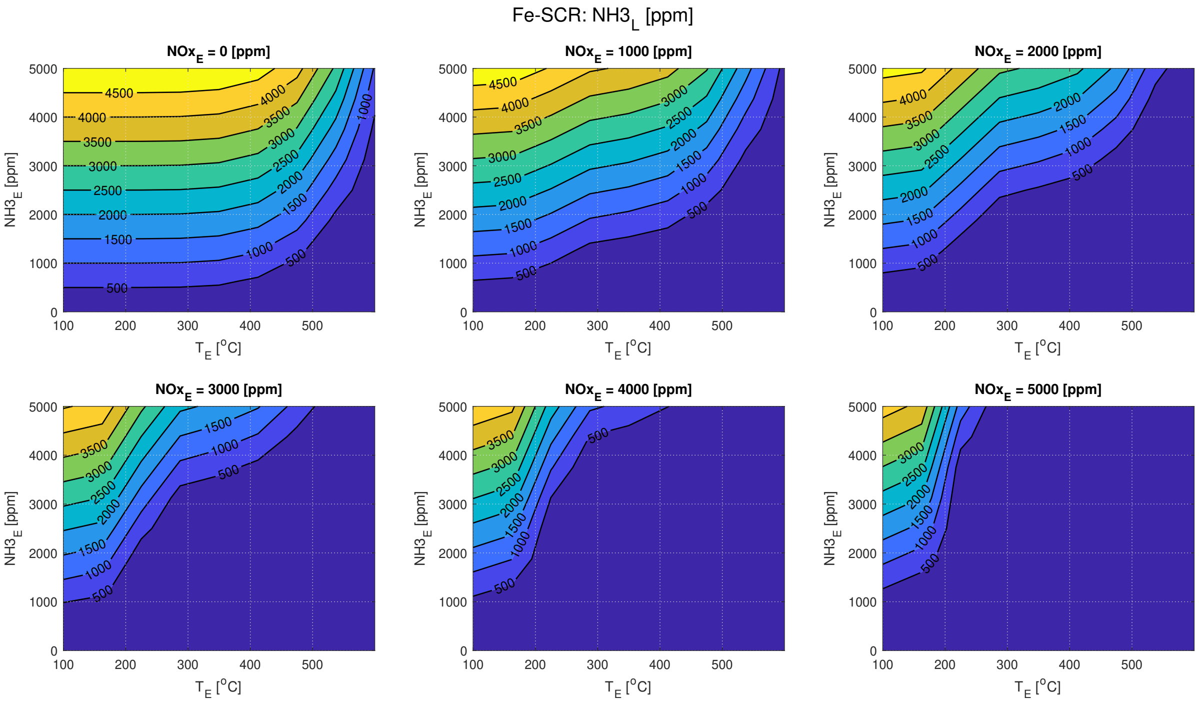

Figure 8.5: NH_3 concentrations at outlet Fe-SCR (N_2O_E = 100 [ppm], ϕ = 0.55, $^{NO_2}/_{NO_X}$ = 0.075).

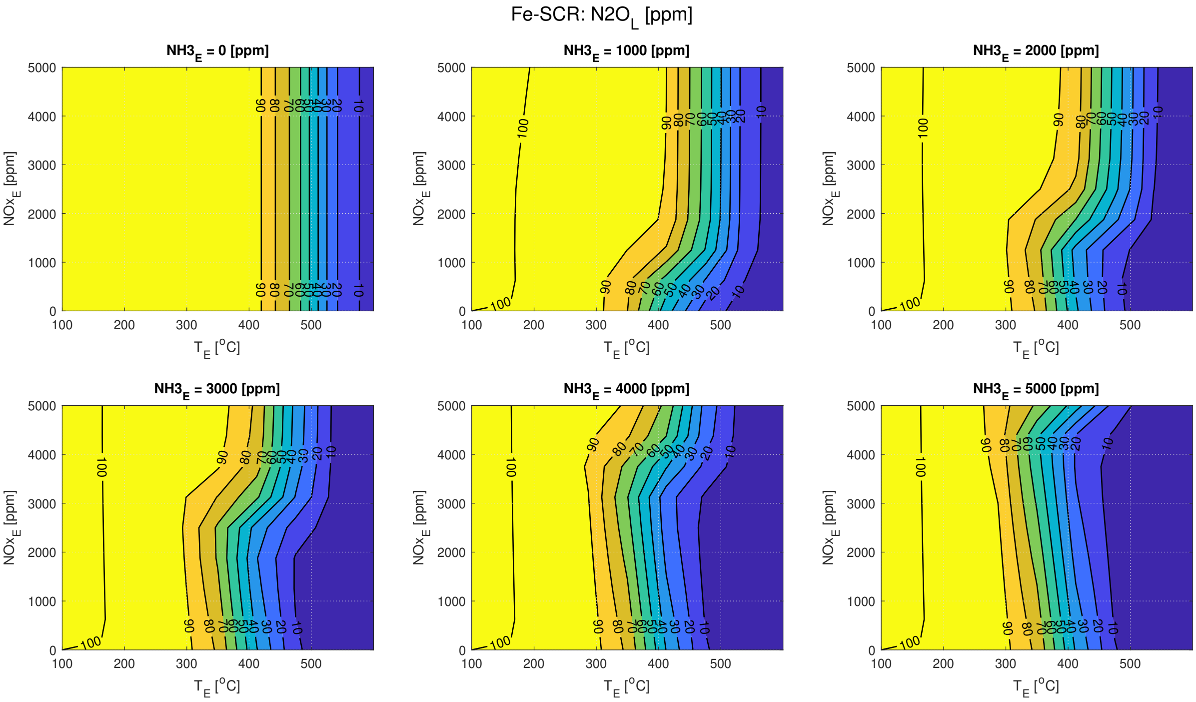

Figure 8.6: N_2O concentrations at outlet Fe-SCR (N_2O_E = 100 [ppm], ϕ = 0.55, $^{NO_2}/_{NO_X}$ = 0.075).

8.2.3. Cu catalyst

Figure 8.7 $NH_{3,E}$ = 0 ppm, shows that neither the Cu catalyst is able to reduce NO_X by itself. When NH_3 in introduced at the inlet of the SCR, reduction of the NO_X already takes place at very low temperatures. Looking the graphs, it can be seen that reduction takes place from 100 ^oC and full conversion takes place from 200 ^oC and higher. At higher concentrations, this limit can be as low as 150 ^oC, due to the heat produced by the reactions. At higher temperatures, 400 ^oC and above, the conversion efficiency starts to reduce slightly. This is not because NH_3 starts to oxidise into NO as happens in the Va SCR, but because NH_3 oxidises into N2 and is not "available" anymore for the normal or fast SCR reaction.

Figure 8.8 $NO_{X,E}$ = 0ppm shows no NH_3 is oxidised below 300 ^oC. Between 300 and 400 ^oC the NH_3 is oxidised partly and no NH_3 leaves the exhaust above 400 ^oC. When NO_X is introduced at the inlet, NO_X and NH_3 start to react (as was visible in figure 8.4). This normal or fast SCR takes place between 150-200 ^oC. The NH_3 exhaust concentrations leaving the SCR remain constant between 200 and 300 ^oC. Above these temperatures, the remaining NH_3 is oxidised in the SCR.

The production of N_2O inside the Cu catalyst is shown in figure 8.9. Looking at the different plots it becomes obvious the N_2O production inside the Cu based SCR can be neglected: no extra N_2O is produced in all operating conditions. On the other hand, the Cu catalyst is also not able to break down any N_2O coming into the SCR.

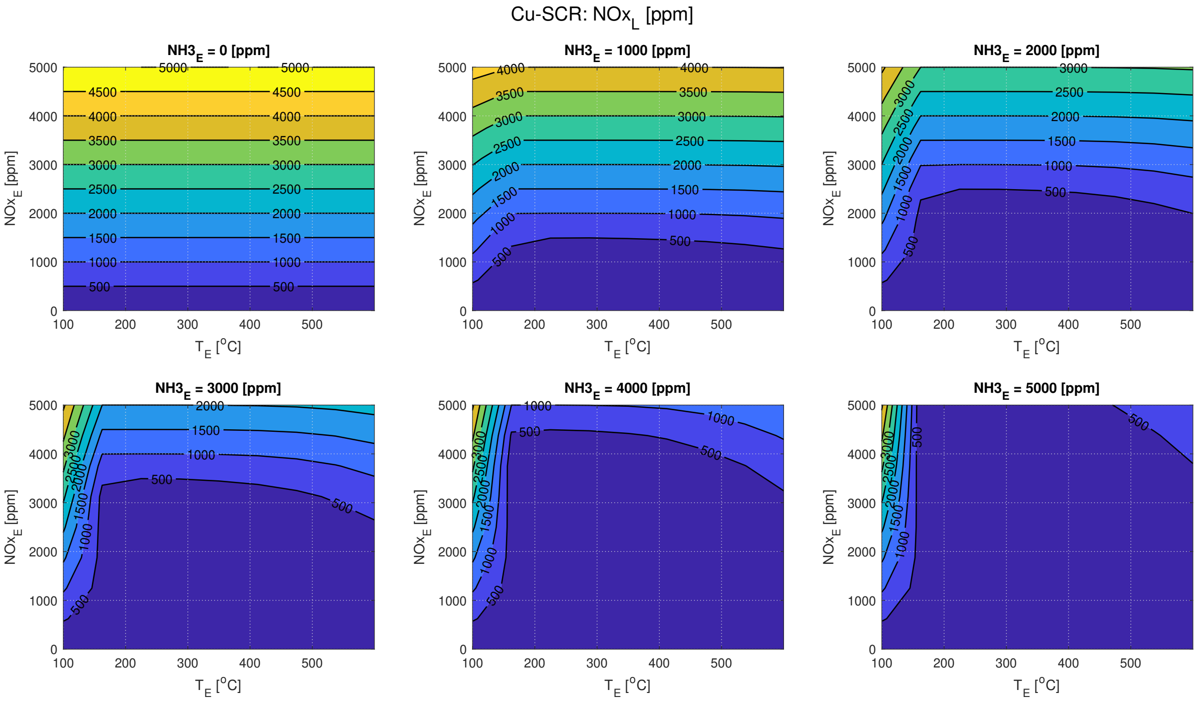

Figure 8.7: NO$_X$ concentrations at outlet Cu-SCR (N$_2$O$_E$ = 100 [ppm], ϕ = 0.55, ${}^{NO_2}/_{NO_X}$ = 0.075).

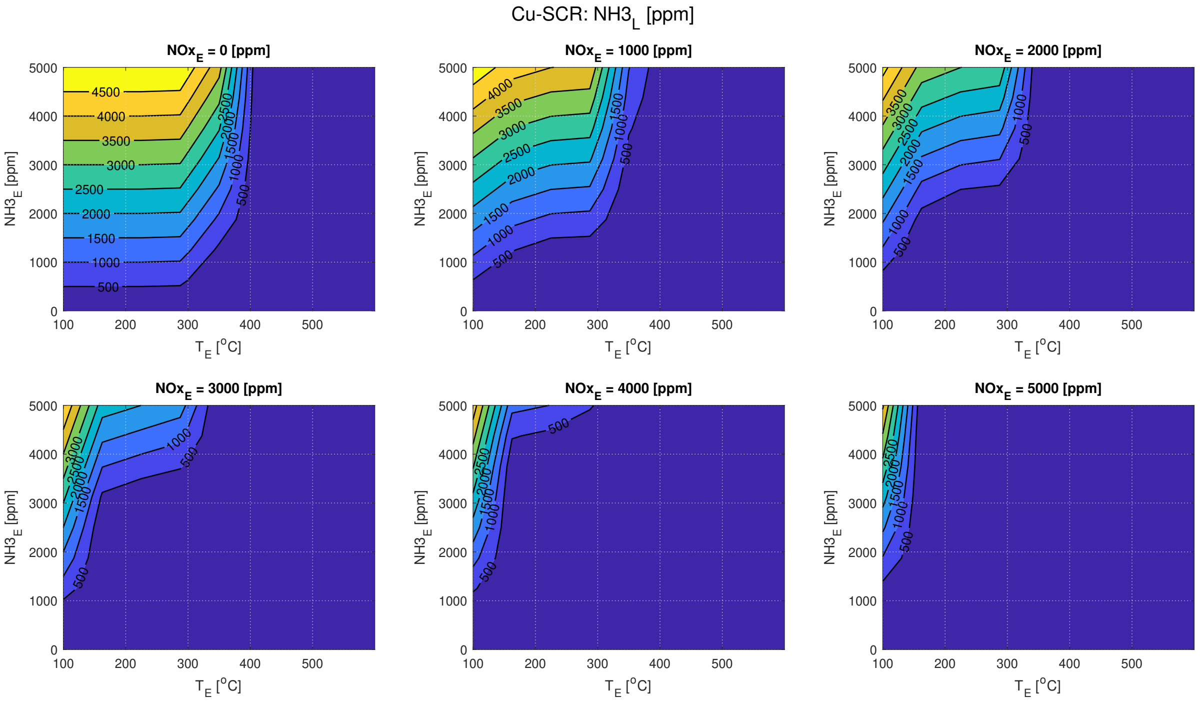

Figure 8.8: NH$_3$ concentrations at outlet Cu-SCR (N$_2$O$_E$ = 100 [ppm], ϕ = 0.55, ${}^{NO_2}/_{NO_X}$ = 0.075).

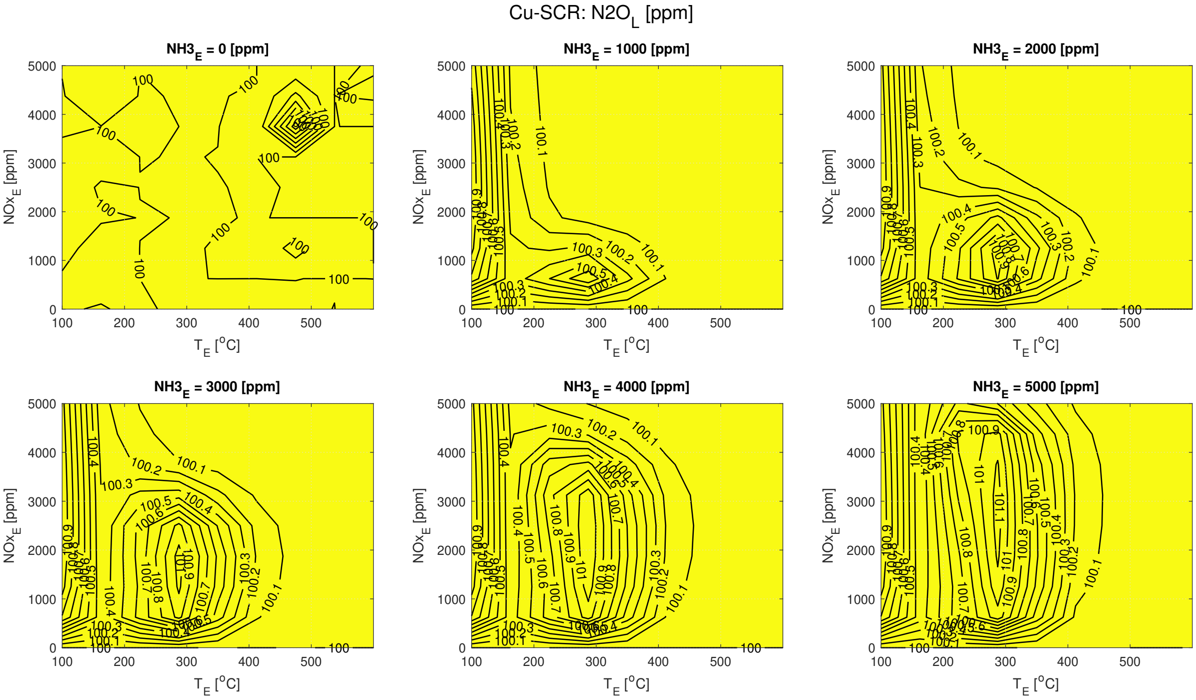
Cu-SCR: $N2O_L$ [ppm]

$NH3_E$ = 0 [ppm]

$NH3_E$ = 1000 [ppm]

$NH3_E$ = 2000 [ppm]

$NH3_E$ = 3000 [ppm]

$NH3_E$ = 4000 [ppm]

$NH3_E$ = 5000 [ppm]

Figure 8.9: N_2O concentrations at outlet Cu-SCR (N_2O_E = 100 [ppm], ϕ = 0.55, $^{NO_2}/_{NO_X}$ = 0.075).

8.3. Feasible Operating Range

Now that understanding is gained on how the SCR behaves, it is time to look at the working range, i.e. where the limits as discussed in chapter 7.3 are not exceeded. First, the three different materials will be compared to one another, with an equivalence ratio of 0.55, a NO_2/NO_X ratio of 0.075 and zero N_2O at the inlet. Later the effect of changing the equivalence ratio is discussed. At last, the effect of N_2O at the inlet of the SCR is discussed.

The green area represents the area where the NO_X, NH_3 and N_2O levels are below the newly specified levels. The yellow area represents NO_X emission levels below the current IMO standard for TIER III. Obviously, all operating conditions in the green area also meet the current IMO standards for NO_X. In the red area, the new and current limits are not met.

The plots shown in this chapter have the inlet temperature on the x-axis and the inlet NO_X concentration on the y-axis. Different variables on the x and y axis are shown in appendix J.

8.3.1. Va Catalyst

The results for the Va catalyst are shown in figure 8.10. The Va catalyst shows a very narrow band in which it can operate. It becomes clear that the NH_3 and NO_X concentrations need to roughly match 1 on 1 when they enter the SCR. At the lower temperatures (below 250 ^oC), too little NO_X and NH_3 will react, while at higher temperatures (above 450 ^oC) the NH_3 molecules will oxidise and form NO. As a result, the NO_X concentration at the outlet will become too high again.

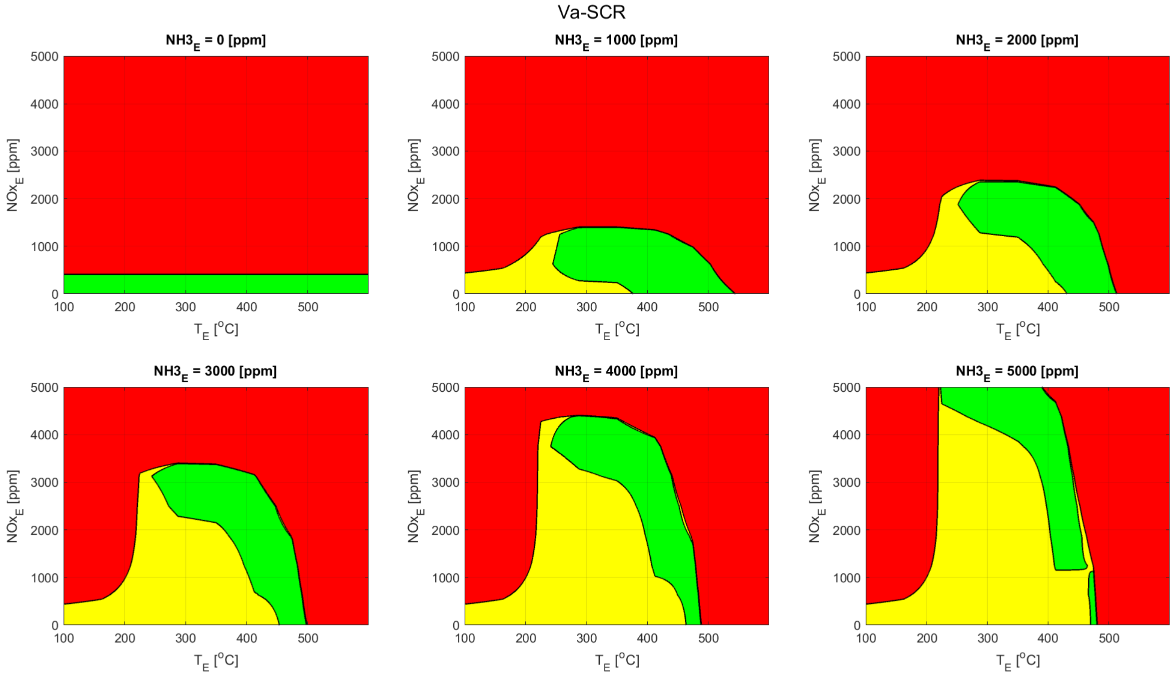

Figure 8.10: Operating range Va-SCR (N_2O_E = 0 [ppm], ϕ = 0.55, $^{NO_2}/_{NO_X}$ = 0.075).

8.3.2. Fe Catalyst

The feasible operating range of the Fe catalyst is shown in figure 8.11. If the ratio between $NO_{X,E}$ and $NH_{3,E}$ is roughly 1:1, all temperatures above 300 ^oC will provide sufficient reduction. If there is more NO_X at the inlet of the SCR than NH_3, the NO_X emissions will stay too high. If an access of NH_3 is going into the SCR, relatively high temperatures (sometimes above 500 ^oC) are needed to oxidise all NH_3.

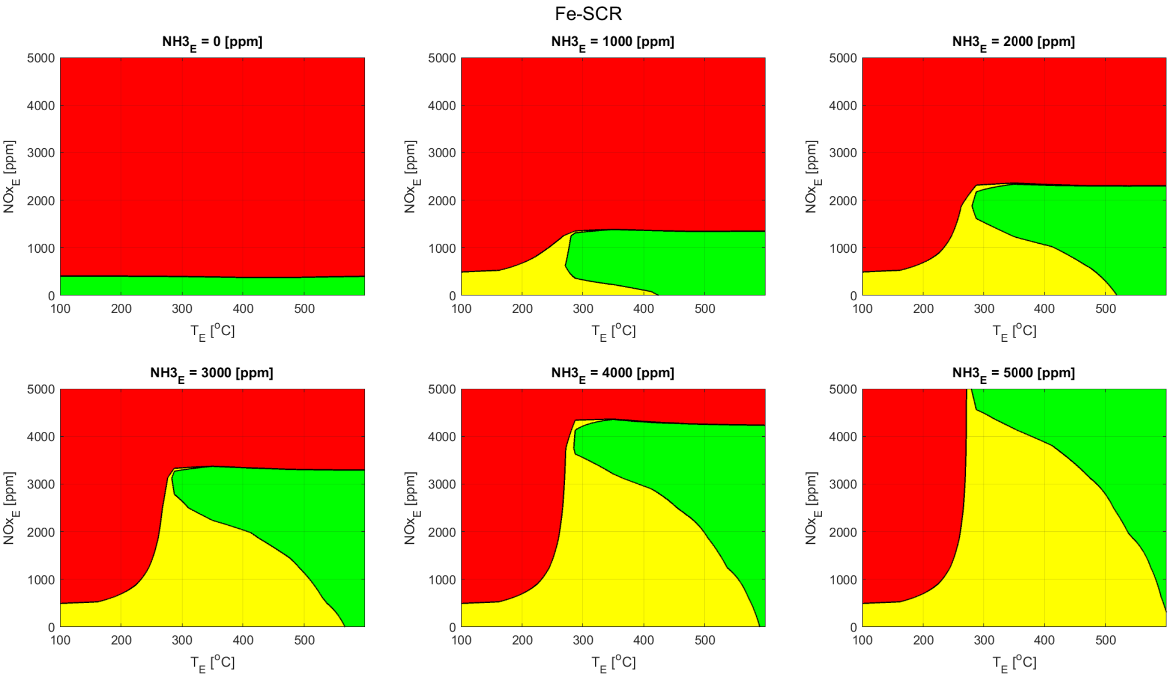

Figure 8.11: Operating range Fe-SCR (N_2O_E = 0 [ppm], ϕ = 0.55, $^{NO_2}/_{NO_X}$ = 0.075).

8.3.3. Cu Catalyst

At last, the response of the Cu catalyst is shown in figure 8.12. The Cu catalyst can operate with very low inlet temperatures: with an ANR of 1, temperatures of 200 ^{o}C are already sufficient. If the inlet temperature is further increased, a higher ANR is needed to reduce the NO$_X$ to acceptable levels. At temperatures above 350 ^{o}C the Cu SCR can deal with large access amounts of NH_3. The oxidation of NH_3 into N2 is already strong enough to reduce any quantity of NH_3 to acceptable levels.

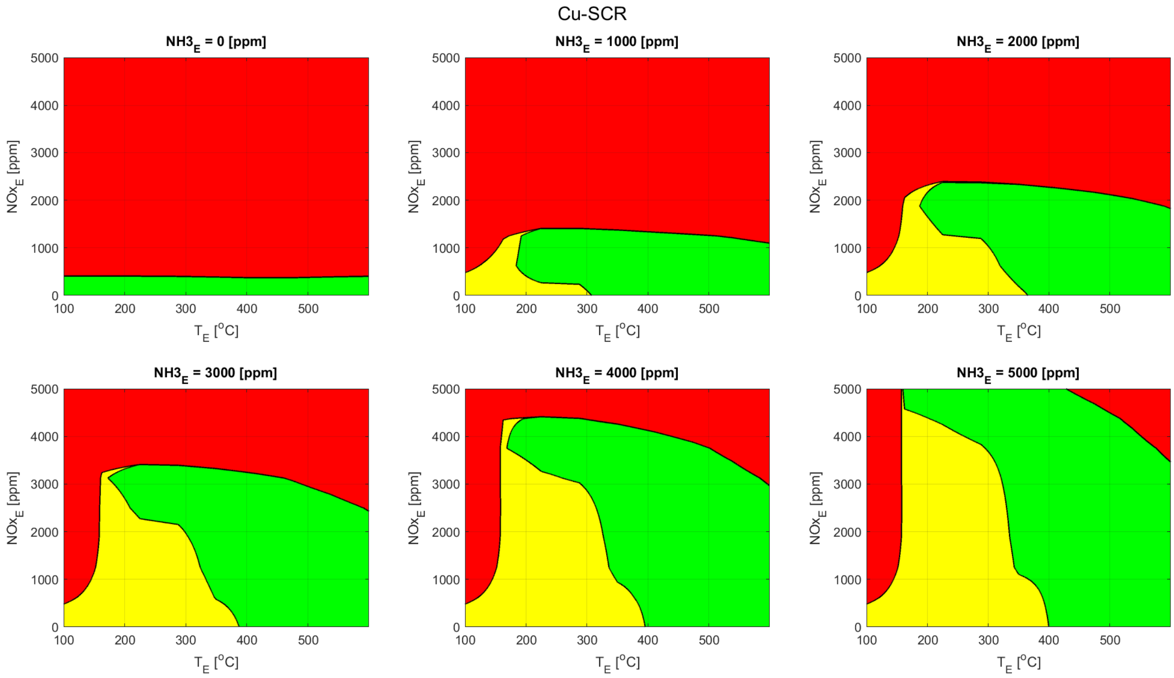

Figure 8.12: Operating range Cu-SCR (N$_2$O$_E$ = 0 [ppm], ϕ = 0.55, $^{NO_2}/_{NO_X}$ = 0.075).

8.3.4. Effect of Equivalence Ratio

The equivalence ratio has only little to no effect on the performance of the SCR itself. However,the effect on the specific emissions of the system is significant. In figure 8.13, 8.14 and 8.15 the effect of a changing equivalence ratio for the Va, Fe and Cu catalyst respectively is shown. These figures represent an inlet flow with 3750 ppm NH$_3$. More figures, showing more NH$_3$ inlet concentrations are shown in appendix J. The increasing equivalence ratio allows the SCR to work over a wider range of inlet NO$_X$, NH$_3$ and temperature. As the equivalence ratio increases, the mass flow through the system decreases. As a result, the same concentration of pollutants will result in a different specific emission of pollutants.

The figures show a much wider feasible range at an equivalence ratio of 0.9 than at 0.2 for all materials. At 0.2, the Va catalyst can only meet current standards, while the Fe and Cu catalyst require relatively high temperatures to meet both current and newly set limits.
At the equivalence ratio of 0.55, the Va catalyst is able to operate with both the current and newly proposed limits. The Fe catalyst has reduced operating temperature with ANR close to 1 and can also meet the new standards with a high surplus of NH$_3$ at high temperatures.
The Cu catalyst is able to operate at both lower and higher temperatures if the ANR is close to 1. With a surplus of NH$_3$, the green and yellow areas are extended into the higher temperature range.
Going from 0.55 to 0.9, the minimum temperature, with ANR close to 1, does not go down significantly for all three catalysts. However, the inlet range for NO$_X$ widens significantly at this point.

At high temperatures (above 450 ^{o}C for Fe and above 350 ^{o}C for Cu) and with a significant surplus of NH$_3$, the performance starts to decrease slightly when going from ϕ = 0.55 to ϕ = 0.9. In this range, a significant amount of NH$_3$ needs to oxidise to meet the new limits. The oxidation requires O$_2$ and due to the lower concentration coming out of the engine, the system is less able to do so. The Va catalyst does not show this behaviour. It is questionable if this is physically correct or a modelling mistake. The reactions in the Va model are, in contrast to the Fe and Cu model, independent of O$_2$ concentrations.

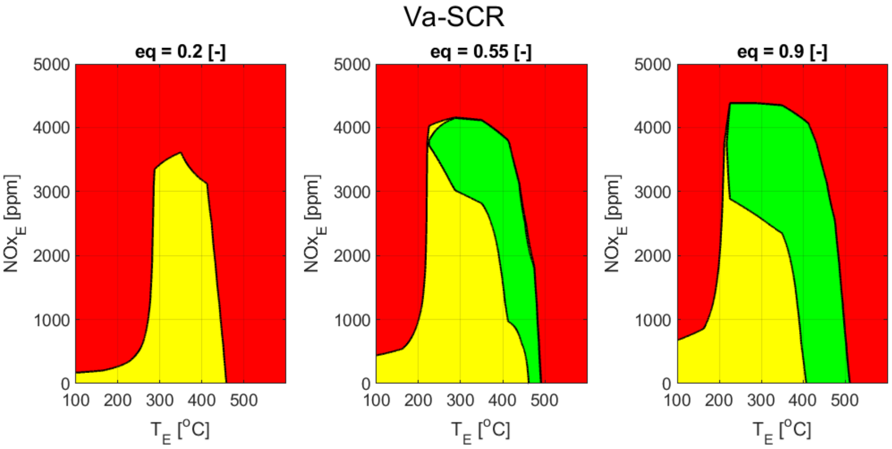

Figure 8.13: Operating range Va-SCR (N_2O_E = 0 [ppm], $NH_{3,E}$ = 3750 [ppm], ${}^{NO_2}/{}_{NO_X}$ = 0.075).

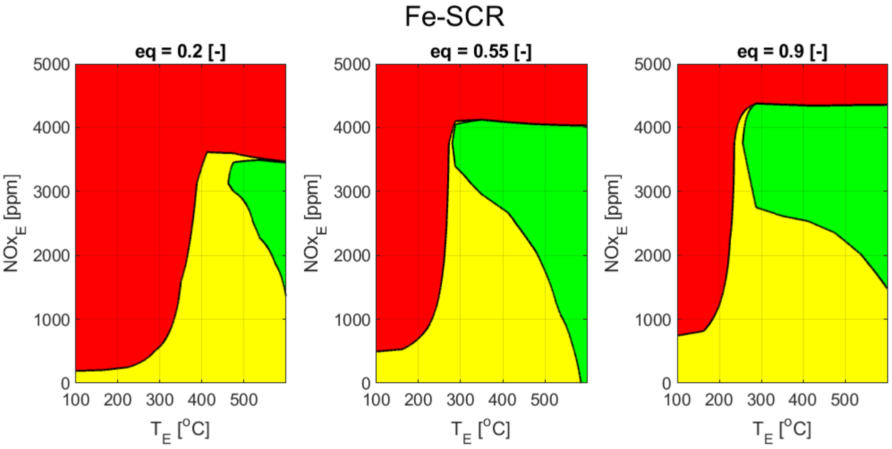

Figure 8.14: Operating range Fe-SCR (N_2O_E = 0 [ppm], $NH_{3,E}$ = 3750 [ppm], ${}^{NO_2}/{}_{NO_X}$ = 0.075).

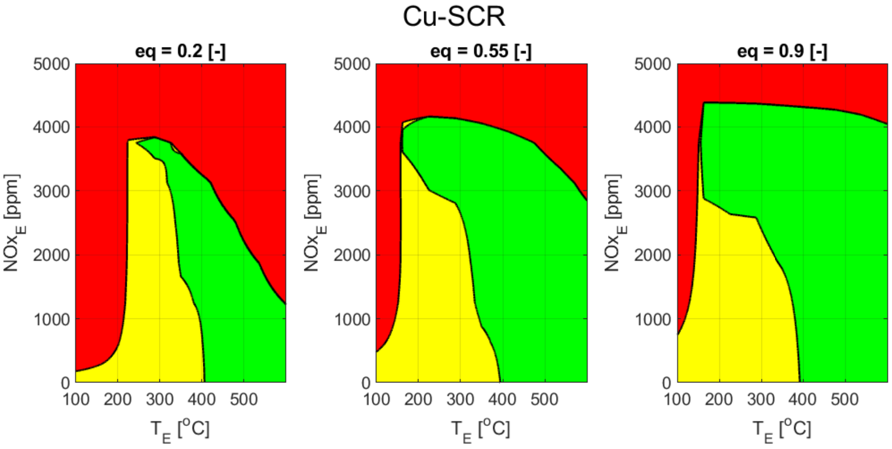

Figure 8.15: Operating range Cu-SCR (N_2O_E = 0 [ppm], $NH_{3,E}$ = 3750 [ppm], ${}^{NO_2}/{}_{NO_X}$ = 0.075).

8.3.5. Effect of N_2O

The presence of N_2O in the exhaust coming from the ICE can be problematic. Both the Va and Cu catalyst type can not break down this molecule and it will pass right through the reactor. The Va catalyst will even produce additional N_2O in the high temperature range.

For this example, 100 ppm N_2O is introduced in the inlet feed of the SCR. Both the Va and Cu catalyst will have no feasible operating range with the newly defined standards. The Fe catalyst is able to break down N_2O and the feasible operating range is shown in figure 8.16. The yellow area is identical to the one shown in figure 8.11 as this includes no limits for N_2O. The feasible operating range with the newly proposed limits is reduced significantly. Only at temperatures above 400/450 ^{o}C the catalyst is able to reduce the N_2O to acceptable levels. Exhaust temperatures this high are highly undesirable as it means the AmmoniaDrive is a rather inefficient driveline.

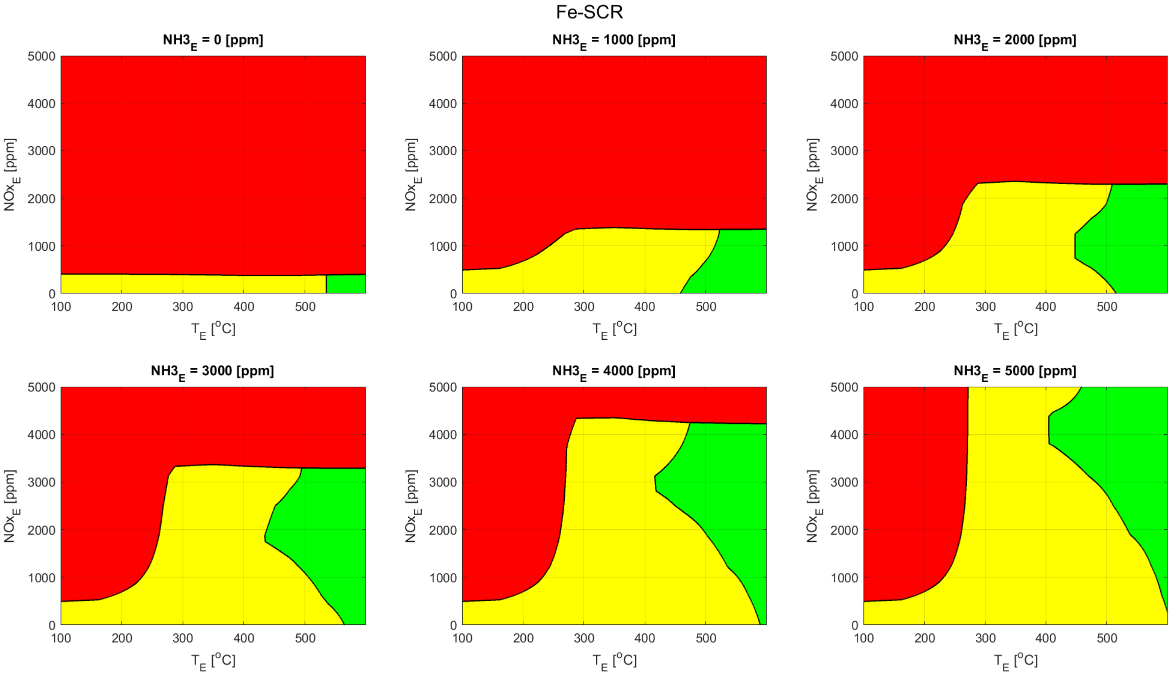

Figure 8.16: Operating range Fe-SCR (N_2O_E = 100 [ppm], ϕ = 0.55, $^{NO_2}/_{NO_X}$ = 0.075).

9

Conclusions

This study aimed to investigate to what extent the harmful nitrogen-based pollutants can be removed from the AmmoniaDrive exhaust with existing after-treatment components. The levels should be reduced to at least the legal standards while providing a significant reduction in greenhouse gasses emitted by the AmmoniaDrive power plant concept. To answer this question, the sub-questions posed in chapter 1 will be answered. The first two sub-questions are answered in the literature report [4].

9.1. Findings from Literature Studies

A NH_3 fuelled ICE will undoubtedly emit significant quantities of NO_X and NH_3, and possibly N_2O. Based on experimental NH_3 engines, high concentrations in the order size of 1000s ppm of NO and NH_3 can be expected. The NO_2 and N_2O emissions are expected to be relatively low at 10s ppm. The expected exhaust temperature and flow differ significantly with SI on end and HCCI on the other. The former is characterised by high temperatures and a low mass flow, and the latter with lower temperatures and higher mass flows. This is mainly a result of the vastly different equivalence ratios used in the different engine types. Up to a certain extent, higher temperatures are usually beneficial to the after-treatment components. The mass flow is essential as it influences the maximum allowable concentrations in the exhaust. Important is that all experimental engines showed good lean operating performance, as excess oxygen is needed for the after-treatment components to function.

Based on the gained knowledge regarding the ICE outlet conditions and different after-treatment components it is possible to choose a first setup for the after-treatment system. The most suitable components for AmmoniaDrive are expected to be an SCR and ASC. The SCR is generally composed of three different materials. Vanadium based catalysts are currently the predominant choice for marine applications due to their low cost and high sulphur resistance. The absence of other pollutants, like sulphur, in the exhaust opens the way for different catalyst types to be used as well. The other catalyst types to be further examined for AmmoniaDrive are Cu and Fe-zeolites. As ammonia slip from the ICE gives less control over the NH_3 concentration in the exhaust, an ASC is also needed. A pure AMOX ASC does not seem ideal as it could produce large amounts of NO_X and N_2O. Better selectivity towards N_2 in the ASC can be achieved by introducing a SCR active catalyst as well. This could be, amongst others, a mixed layer and stacked layer.

9.2. Working Principals of the SCR

The questions on which inlet parameters are important for the operation of the SCR (question 3) and how these parameters influence the operation of the SCR (question 4) are answered in this section. As the two questions are closely intertwined, the findings answering them both are listed here together:

- Inlet temperature of the SCR is a crucial parameter and determines mainly if and how well the SCR will function. The Va catalyst has a narrow temperature range (250-400 ^oC) in which it performs well, the Fe catalyst performs well at higher temperatures (above 300 ^oC), and the Cu catalyst starts working at very low temperatures (200^oC).

- None of the SCR materials can break down NO_X without the help of NH_3. The high NH_3 and NO_X concentrations are not a problem, as long as the ANR is close to one or larger.
- The Va catalyst can only cope with a surplus of NH_3 in a small temperature window: below 400 ^oC the NH_3 is not converted, and above 450 ^oC the NH_3 is converted into NO. The Va catalyst can not cope well with a surplus of NH_3 as the oxidation of NH_3 produces NO. The Fe and Cu catalysts produce N_2 when NH_3 is oxidised and can therefore cope with a large surplus. At higher inlet temperatures (above 500 ^oC for the Fe catalyst and 350 ^oC for the Cu catalyst), all leftover NH_3 is oxidised.
- The equivalence ratio does not influence the SCR performance: this shows the SCR is oversized. This does not make much difference for this study as only steady-state performance is the object of this research. Although the SCR behaviour itself does not change, there is a significant difference in emissions measured in g/kWh. This is a result of the change in airflow through the ICE when operating at different equivalence ratios.
- Generally speaking, the NO_2/NO_X ratio is an important parameter to determine the SCR performance as it promotes the fast SCR reaction. In this setup, that is not the case. The low ratio, ranging from 0-0.15, looked at in this research does not significantly influence the SCR performance.
- Non of the catalytic types produced significant amounts of N_2O. This follows from the fact that N_2O is formed from NO_2 and the inlet concentrations of the latter are relatively low. However, once N_2O is present in the exhaust coming from the ICE, only the Fe catalyst can break down the N_2O at high temperatures: 450/500 ^oC.
- The heat released by the reactions at higher inlet concentrations does not shift the feasible operating temperature down.

9.3. Recommendations for ICE

From an engine perspective, it is also possible to draw conclusions. These conclusions are only applicable for a steady-state situation.

- A high equivalence ratio is desired. Due to the different exhaust flows out of the engine when changing the equivalence ratio, the same concentration of pollutants in the exhaust flow will result in different specific emissions (g/kWh). One important side note: access oxygen is still a must for the SCR to operate.
- The production of N_2O during combustion in the ICE should be avoided as it is challenging to get rid of. This is only possible if the exhaust gas temperature exceeds 450 ^oC and the ANR exceeds 1. If the ANR is below 1, temperatures of 550 ^oC are needed.
- An ANR of slightly over 1 is desired to reduce NO_X and NH_3 emissions.
- Lower exhaust temperatures from the ICE, 150-300 ^oC, require a Cu catalyst and an ANR of around 1 to reduce any amount of NO_X and NH_3.
- Medium exhaust temperatures, 250-400 ^oC, allow for all catalyst types to be used if the ANR is around 1. If the ANR is above 1 and the temperature at the high end of this range (350-400 ^oC), the Cu catalyst can reduce the surplus of NH_3.
- High exhaust temperatures, above 400 ^oC, require a Fe catalyst if the ANR is around 1. For a higher ANR, a Cu catalyst is preferred.
- The high inlet concentrations of NO_X and NH_3 itself are not a problem as long as the ANR is not below 1. The heat generated by the reactions has little effect on the optimal inlet temperature of the SCR.
- An ANR below 1 does not work. This scenario requires the injection of extra NH_3 before the SCR to increase the ANR. This reduces the fuel efficiency of the system.

10

Discussion and Recommendations

To limit the scope of this thesis, certain boundaries have been set, and assumptions were made. Future research will have to complement the work done so far. Some of the most important recommendations are listed below.

- The used kinetic data, for the Va model on the one hand and the Fe and Cu models, on the other hand, comes from different papers/research groups. The focus of each paper was different: fast simulation for the Va model and mixing of different catalytic materials for the Fe and Cu model. As a result, other reaction mechanisms are implemented. The research will benefit if kinetic data comes from one research group with one goal.
- The used kinetic data is calibrated on different sized SCR's. The Va data is based on a truck size, while the Fe and Cu models are based on a laboratory scaled setup. Although the data uses washcoat concentrations and can thus be changed in size by adjusting the mass transport coefficient, it is not ideal. A full-scale validation of each material would be desirable. Ideally, this data would also be used to create the kinetic data for the models.
- This research focuses on steady-state results. A dynamic analysis also needs to be conducted. The assumption that the SCR is oversized might cause problems for dynamic loading. The shifts in temperature can cause problems for the NH_3 storage on the SCR and release significant quantities of NH_3 into the environment.
- This research only looks into a sole SCR catalyst. In addition, an ASC could be introduced. Also, the injection of extra NH_3 before the SCR could be looked into as both options will increase the operating range of the SCR.
- Besides introducing different components before and after the catalyst, the SCR could also have a different layout. Different SCR materials could be stacked after one another, different washcoats can be stacked on top of each other, or mixed washcoats could be created. A thorough study could be conducted on how to combine the benefits of the different catalytic materials into one SCR.
- The adopted limit for NH_3 is not existing yet. A more thorough environmental study should dictate the desired limits for any future ammonia fuelled driveline.
- The current study only provides an analysis of the SCR performance. For the AmmoniaDrive to become a success, other aspects are essential as well. The financial part is important. The Va catalyst is the cheapest out of the three, Cu the most expensive, and Fe in the middle. An optimisation for the size and cost of the SCR system could be interesting as well. Important parameters in this study could, amongst others, include the material, cell density and length of the catalytic layers.

Nomenclature

Abbreviations

AMOX	Ammonia Oxidation Catalyst
ANR	Ammonia to NO$_X$ Ratio
ASC	Ammonia Slip Catalyst
ASC	Ammonia Slip Catalyst
DOC	Diesel Oxidation Catalyst
DPF	Diesel Particulate Filter
GHG	Green House Gas
GWP	Global Warming Potential
HCCI	Homogeneous Charge Compression Ignition
ICE	Internal Combustion Engine
LHV	Lower Heating Value
LNT	Lean NO$_X$ Trap
NECA	NO$_X$ Emission Control Area
PGM	Platinum Group Metal
PM	Particulate Matter
SCR	Selective Catalytic Reduction
SEM	Scanning Electron Microscope
SOFC	Solid Oxide Fuel Cell
TWC	Three Way Catalyst

Greek Symbols

ϵ	void fraction	[m/s]
ϵ_{WC}	washcoat porosity	[-]
λ	thermal conductivity	[W/m K]
μ	dynamic viscosity	[Pa s]
ϕ	equivalence ratio	[-]
ϕ_f	friction factor	[-]
ρ	density	[kg/m^3]

Roman Symbols

$\dot{Q}$	heat flux	[J/s]

A_{cs}	cross section area monolith layer	[m^2]
c_j	molar concentration	[mol/m^3]
c_p	specific heat capacity	[J/kg K]
C_{Tm}	total molar concentration	[mol/m^3]
c_v	specific heat capacity	[J/kg K]
d_h	hydraulic diameter	[m]
D_e	effective diffusivity	[m^2/s]
D_f	diffusivity	[m^2/s]
E	activation energy	[J/mol]
f	mass flow	[kg/s]
GSA	geometric surface area	[-]
H	enthalpy	[J]
h	heat transfer coefficient	[W/m^2 K]
h	specific enthalpy	[J/kg]
k	rate constant	[variable]
k_0	pre-exponential factor	[variable]
k_g	mass transfer coefficient	[m/s]
L	cell spacing	[in or m]
L_{eh}	thermal entrance length	[m]
L_m	length of monolith	[m]
L_{void}	length of void	[m]
m	mass	[kg]
N	cell density	[CPSI]
Nu	Nusselt number	[-]
OFA	open frontal area	[in or m]
P	power	[kW]
P	pressure	[Pa]
Pr	Prandtl number	[-]
Q	heat	[J]
R	universal gas constant	[J/mol/K]
r	reaction rate	[mol/m^3/s]
$R_{\Omega 2}$	washcoat thickness	[m]
R_s	specific gas constant	[J/kg K]
Re	Reynolds number	[-]

sfc	specific fuel consumption	[g/kWh]
Sh	Sherwood number	[-]
T	temperature	[K]
t	time	[s]
t_w	wall thickness	[in or m]
U	internal energy	[J]
u	specific internal energy	[J/kg]
v	stoichiometric coefficient	[-]
v	velocity	[m/s]
V_{void}	volume of void	[m^3]
W	work	[J]
X_j	mass fraction	[-]
Y_j	molar fraction	[-]

Other Symbols

b	bulk phase
E	Entering
L	Leaving
m	monolith
wc	washcoat

References

[1] Andreas Åberg et al. “Parameter estimation and analysis of an automotive heavy-duty SCR catalyst model”. In: *Chemical Engineering Science* 161 (2017), pp. 167–177. ISSN: 00092509. DOI: `10.1016/j.ces.2016.12.024`.

[2] Tahrizi Andana et al. “Advances in Cleaning Mobile Emissions: NOx-Assisted Soot Oxidation in Light-Duty Diesel Engine Vehicle Application”. In: *Horizons in Sustainable Industrial Chemistry and Catalysis329*. Turin, 2019. Chap. 16, pp. 329–352. URL: `https://reader.elsevier.com/reader/sd/pii/B9780444641274000161?token=75068118A12D3DE859F616D1BEBF7FE350088D69`

[3] L. van Biert et al. *A review of fuel cell systems for maritime applications*. Sept. 2016. DOI: `10.1016/j.jpowsour.2016.07.007`.

[4] T Boxma. *Removal of nitrogen based pollutants from the AmmoniaDrive exhaust Literature Report*. Tech. rep. 2021.

[5] Federico Cattaneo. *Selective Catalytic Reduction System for Marine Applications Dynamic Modelling and System Integration*. Tech. rep. Delft: Technical University Delft, Mar. 2018. URL: `http://repository.tudelft.nl/.`.

[6] Robert D. Clayton, Michael P. Harold, and Vemuri Balakotaiah. “Performance Features of Pt/BaO lean NOx trap with hydrogen as reductant”. In: *AIChE Journal* 55.3 (Mar. 2009), pp. 687–700. ISSN: 00011541. DOI: `10.1002/aic.11710`.

[7] Massimo Colombo et al. “Experimental and modeling study of a dual-layer (SCR+PGM) NH3 slip monolith catalyst (ASC) for automotive SCR aftertreatment systems. Part 1. Kinetics for the PGM component and analysis of SCR/PGM interactions”. In: *Applied Catalysis B: Environmental* 142-143 (Oct. 2013), pp. 861–876. ISSN: 09263373. DOI: `10.1016/j.apcatb.2012.10.031`.

[8] Piero Colonna. *The 9-step Method*. 2020.

[9] Liming Dai et al. “Experimental and numerical analysis of the autoignition behavior of NH3 and NH3/H2 mixtures at high pressure”. In: *Combustion and Flame* 215 (May 2020), pp. 134–144. ISSN: 15562921. DOI: `10.1016/j.combustflame.2020.01.023`. URL: `www.elsevier.com/locate/combustflame`.

[10] Niels De Vries. “Safe and effective application of ammonia as a marine fuel”. PhD thesis. Delft: Delft University of Technology, 2019. URL: `https://repository.tudelft.nl/`.

[11] Dieselnet.com. *Catalytic Coating & Materials*. 2005. URL: `https://dieselnet.com/tech/cat_mat.php`.

[12] Dieselnet.com. *Diesel Catalysts*. 2016. URL: `https://dieselnet.com/tech/cat_diesel.php`.

[13] Dieselnet.com. *Diesel Oxidation Catalyst*. 2018. URL: `https://dieselnet.com/tech/cat_doc.php`.

[14] Dieselnet.com. *Emission Standards: Europe: Heavy-Duty Truck and Bus Engines*. 2019. URL: `https://dieselnet.com/standards/eu/hd.php`.

[15] Dieselnet.com. *SCR Systems for Diesel Engines*. 2005. URL: `https://dieselnet.com/tech/cat_scr_diesel.php`.

[16] Catherine Duynslaegher et al. “Modeling of ammonia combustion at low pressure”. In: *Combustion and Flame* 159.9 (Sept. 2012), pp. 2799–2805. ISSN: 00102180. DOI: `10.1016/j.combustflame.2012.06.003`. URL: `http://dx.doi.org/10.1016/j.combustflame.2012.06.003`.

[17] Engineering ToolBox. *Air - Dynamic and Kinematic Viscosity*. 2003. URL: `https://www.engineeringtoolbox.com/air-absolute-kinematic-viscosity-d_601.html?vA=100&units=C#`.

[18] Engineering ToolBox. *Air - Prandtl Number*. 2018. URL: `https://www.engineeringtoolbox.com/air-prandtl-number-viscosity-heat-capacity-thermal-conductivity-d_2009.html`.

[19] engineeringtoolbox.com. *Air - Composition and Molecular Weight*. 2003. URL: `https://www.engineeringtoolbox.com/air-composition-d_212.html`.

[20] Environmental Protection Agency. *Nitrogen Oxides (NOx), Why and How They Are Controlled*. Tech. rep. 2020. URL: `http://www.epa.gov/ttn/catc`.

[21] epa.gov. *Understanding Global Warming Potentials | Greenhouse Gas (GHG) Emissions | US EPA*. 2020. URL: `https://www.epa.gov/ghgemissions/understanding-global-warming-potentials`.

[22] Giorgio Fagioli. *Personal communication*. Rotterdam, 2021.

[23] Pär L.T. Gabrielsson. "Urea-SCR in automotive applications". In: *Topics in Catalysis* 28.1-4 (2004), pp. 177–184. ISSN: 10225528. DOI: `10.1023/B:TOCA.0000024348.34477.4c`. URL: `https://link.springer.com/article/10.1023/B:TOCA.0000024348.34477.4c`.

[24] Feng Gao et al. "A comparative kinetics study between Cu/SSZ-13 and Fe/SSZ-13 SCR catalysts". In: *Catalysis Today* 258 (May 2015), pp. 347–358. ISSN: 09205861. DOI: `10.1016/j.cattod.2015.01.025`. URL: `http://dx.doi.org/10.1016/j.cattod.2015.01.025`.

[25] Sandeeran Govender and Holger B. Friedrich. *Monoliths: A review of the basics, preparation methods and their relevance to oxidation*. Feb. 2017. DOI: `10.3390/catal7020062`.

[26] Thomas Klint Hansen. *Development of New Diesel Oxidation and NH3 Slip Catalysts*. Tech. rep. 2017. URL: `www.dtu.dk`.

[27] IMO. *Emission Control Areas (ECAs) designated under MARPOL Annex VI*. 2020. URL: `https://www.imo.org/en/OurWork/Environment/Pages/Emission-Control-Areas-(ECAs)-designated-under-regulation-13-of-MARPOL-Annex-VI-(NOx-emission-control).aspx`.

[28] IMO. *IMO 2020 – cutting sulphur oxide emissions*. 2019. URL: `https://www.imo.org/en/MediaCentre/HotTopics/Pages/Sulphur-2020.aspx`.

[29] IMO. *Nitrogen Oxides (NOx) – Regulation 13*. 2019. URL: `https://www.imo.org/en/OurWork/Environment/Pages/Nitrogen-oxides-(NOx)-%E2%80%93-Regulation-13.aspx`.

[30] IMO. *Reducing greenhouse gas emissions from ships*. 2019. URL: `https://www.imo.org/en/MediaCentre/HotTopics/Pages/Reducing-greenhouse-gas-emissions-from-ships.aspx`.

[31] Masaoki Iwasaki and Hirofumi Shinjoh. "A comparative study of "standard", "fast" and "nO2" SCR reactions over Fe/zeolite catalyst". In: *Applied Catalysis A: General* 390.1-2 (Dec. 2010), pp. 71–77. ISSN: 0926860X. DOI: `10.1016/j.apcata.2010.09.034`.

[32] J.W. Remkes et al. *Niet alles kan*. Tech. rep. Adviescollege Stikstofproblematiek, Sept. 2019.

[33] Bengt Johansson et al. *Combustion Enginges*. Vol. 1. Media-Tryck Lund, 2016.

[34] Johnson Matthey. *SCR catalyst - SINOX® honeycomb | Johnson Matthey*. 2020. URL: `https://matthey.com/en/products-and-services/emission-control-technologies/stationary-emissions-control/scr-catalyst-sinox-honeycomb`.

[35] Michael Kleemann et al. "Investigation of the ammonia adsorption on monolithic SCR catalysts by transient response analysis". In: *Applied Catalysis B: Environmental* 27.4 (Aug. 2000), pp. 231–242. ISSN: 09263373. DOI: `10.1016/S0926-3373(00)00158-2`.

[36] Hans Klein Woud and Douwe Stapersma. *Design of Propulsion and Electric Power Generation Systems*. 2012th ed. London: IMarEST, 2002.

[37] Hideaki Kobayashi et al. "Science and technology of ammonia combustion". In: *Proceedings of the Combustion Institute* 37.1 (2019), pp. 109–133. ISSN: 15407489. DOI: `10.1016/j.proci.2018.09.029`. URL: `www.sciencedirect.comwww.elsevier.com/locate/proci`.

[38] Shuangshuang Lai et al. “The promotional role of Ce in Cu/ZSM-5 and in situ surface reaction for selective catalytic reduction of NOx with NH3”. In: *RSC Advances* 5.110 (Oct. 2015), pp. 90235–90244. ISSN: 20462069. DOI: 10.1039/c5ra12505g.

[39] James. Larminie and Andrew. Dicks. *Fuel cell systems explained*. J. Wiley, 2003, p. 406. ISBN: 047084857X.

[40] I. Lezcano-Gonzalez et al. “Determining the storage, availability and reactivity of NH3 within Cu-Chabazite-based Ammonia Selective Catalytic Reduction systems”. In: *Physical Chemistry Chemical Physics* 16.4 (Jan. 2014), pp. 1639–1650. ISSN: 14639076. DOI: 10.1039/c3cp54132k.

[41] Charles Lhuillier et al. *Experimental study on ammonia/hydrogen/air combustion in spark ignition engine conditions*. 2020. URL: https://www.sciencedirect.com/science/article/pii/S0016236120304439.

[42] Charles Lhuillier et al. “Experimental study on ammonia/hydrogen/air combustion in spark ignition engine conditions”. In: *Fuel* 269 (2020). ISSN: 00162361. DOI: 10.1016/j.fuel.2020.117448. URL: https://www.sciencedirect.com/science/article/pii/S0016236120304439.

[43] Yu Liu, Jun Zhao, and Jong-Min Lee. “Conventional and New Materials for Selective Catalytic Reduction (SCR) of NO _{<i>x</i>}”. In: *ChemCatChem* 10.7 (Apr. 2018), pp. 1499–1511. ISSN: 18673880. DOI: 10.1002/cctc.201701414. URL: http://doi.wiley.com/10.1002/cctc.201701414.

[44] Mathias Magnusson, Erik Fridell, and Hanna H. Ingelsten. *The influence of sulfur dioxide and water on the performance of a marine SCR catalyst*. 2012. URL: https://reader.elsevier.com/reader/sd/pii/S0926337311004280?token=01BBAB7400AD681CE66EE3100842A149703FCA3C53B

[45] MathWorks. *Interaction plot for grouped data - MATLAB interactionplot - MathWorks Benelux*. 2021. URL: https://nl.mathworks.com/help/stats/interactionplot.html.

[46] Bonnie J Mcbride et al. *NASA Technical Memorandum 4513 Coefficients for Calculating Thermodynamic and Transport Properties of Individual Species*. Tech. rep. 1993.

[47] Pranit S. Metkar, Vemuri Balakotaiah, and Michael P. Harold. “Experimental and kinetic modeling study of NO oxidation: Comparison of Fe and Cu-zeolite catalysts”. In: *Catalysis Today*. Vol. 184. 1. 2012. DOI: 10.1016/j.cattod.2011.11.032.

[48] Pranit S. Metkar, Vemuri Balakotaiah, and Michael P. Harold. “Experimental and kinetic modeling study of NO oxidation: Comparison of Fe and Cu-zeolite catalysts”. In: *Catalysis Today*. Vol. 184. 1. Elsevier, Apr. 2012, pp. 115–128. DOI: 10.1016/j.cattod.2011.11.032.

[49] Pranit S. Metkar, Michael P. Harold, and Vemuri Balakotaiah. “Experimental and kinetic modeling study of NH3-SCR of NOx on Fe-ZSM-5, Cu-chabazite and combined Fe- and Cu-zeolite monolithic catalysts”. In: *Chemical Engineering Science* 87 (Jan. 2013), pp. 51–66. ISSN: 00092509. DOI: 10.1016/j.ces.2012.09.008.

[50] A.F. Mills. *Basic Heat and Mass Transfer*. 2nd ed. Harlow: Pearson, 2014.

[51] Isabella Nova and Enrico Tronconi. *Urea-SCR Technology for deNOx After Treatment of Diesel Exhausts*. 2014.

[52] Maxime Pochet, Hervé Jeanmart, and Francesco Contino. “A 22:1 Compression Ratio Ammonia-Hydrogen HCCI Engine: Combustion, Load, and Emission Performances”. In: *Frontiers in Mechanical Engineering* 6 (2020). ISSN: 2297-3079. DOI: 10.3389/fmech.2020.00043.

[53] Bruce E Poling, John M Prausnitz, and John P O’connell. *THE PROPERTIES OF GASES AND LIQUIDS*. fith edition. New York: McGRAW-HILL, 2001. ISBN: 0071499997. DOI: 10.1036/0070116822.

[54] Patrick J Roache. “Verification of Codes and Calculations”. In: *AIAA JOURNAL* 36.5 (1998).

[55] Eser Semih. *Bronsted and Lewis Acid Sites | FSC 432: Petroleum Refining*. 2020. URL: https://www.e-education.psu.edu/fsc432/content/bronsted-and-lewis-acid-sites.

[56] D Stapersma. *Diesel Engines Volume 5 Thermodynamical Principles I*. Jan. 2010.

[57] Ping Tao et al. *Effects of V 2 O 5 and WO 3 loadings on the catalytic performance of V 2 O 5-WO 3 /TiO 2 catalyst for SCR of NO with NH 3*. Tech. rep. X. 2017.

[58] Total Lubricants. *LNT: SCR'S LITTLE BROTHER*. 2017. URL: `https://www.lubricants.total.com/news-press-releases/lnt-scrs-little-brother`.

[59] Umicore. *Three-way catalyst (TWC) | Automotive Catalysts*. 2021. URL: `https://ac.umicore.com/en/technologies/three-way-catalyst/`.

[60] Karin Van Kranenburg et al. *E-FUELS: TOWARDS A MORE SUSTAINABLE FUTURE FOR TRUCK TRANSPORT, SHIPPING AND AVIATION*. Tech. rep. 2020.

[61] Matthias Veltman Song-Charng Kong and Robert Bosch LLC. *Department of Mechanical Engineering Developing Fuel Injection Strategies for Using Ammonia in Direct Injection Diesel Engines*. Tech. rep. Ames: Iowa State University, 2012. URL: `www.me.iastate.edu`.

[62] Peter de Vos. "AmmoniaDrive: a solution for zero-emission shipping?!" In: *SWZ Maritime* 141.3 (2020), pp. 36–37. URL: `https://research.tudelft.nl/en/publications/ammoniadrive-a-solution-for-zero-emission-shipping`.

[63] Wärtsilä. *Engine Online Configurator | Wärtsilä*. 2021. URL: `https://www.wartsila.com/marine/engine-configurator`.

[64] Wärtsilä. *Wärtsilä 31 - Product guide*. Tech. rep. 2019.

[65] Wärtsilä. *Wärtsilä Environmental Product Guide*. Tech. rep. 2017.

[66] Wärtsilä. *Wärtsilä NO X Reducer Wärtsilä NO X Reducer Environmental Efficiency*. 2011.

[67] Fredrik R. Westlye, Anders Ivarsson, and Jesper Schramm. "Experimental investigation of nitrogen based emissions from an ammonia fueled SI-engine". In: *Fuel* 111 (2013), pp. 239–247. ISSN: 00162361. DOI: `10.1016/j.fuel.2013.03.055`. URL: `http://dx.doi.org/10.1016/j.fuel.2013.03.055`.

[68] Jimmie L Williams. *Monolith structures, materials, properties and uses*. Tech. rep. 2001, pp. 3–9.

[69] www.eea.europa.eu. *Ammonia (NH3) emissions — European Environment Agency*. 2015. URL: `https://www.eea.europa.eu/data-and-maps/indicators/eea-32-ammonia-nh3-emissions-1`.

[70] Xander Seykens. *Personal communication*. Rotterdam, 2021.

[71] Juan M. Zamaro, Maria A. Ulla, and Eduardo E. Miró. "Zeolite washcoating onto cordierite honeycomb reactors for environmental applications". In: *Chemical Engineering Journal* 106.1 (Jan. 2005), pp. 25–33. ISSN: 13858947. DOI: `10.1016/j.cej.2004.11.003`.

[72] Dimitrios Zarvalis et al. *Investigation of SCR Catalysts for Marine Diesel Applications*. 2017. URL: `https://www.jstor.org/stable/pdf/26422556.pdf?refreqid=excelsior%3Ab02bdd1e1f71c1427c26b461c004e73f`.

[73] Dong Zhang and Ralph T Yang. "N 2 O Formation Pathways over Zeolite-Supported Cu and Fe Catalysts in NH 3-SCR". In: (2018). DOI: `10.1021/acs.energyfuels.7b03405`. URL: `https://pubs.acs.org/sharingguidelines`.

[74] Xiao Sen Zheng. *An investigation of hydrogen-ammonia combustion inside internal combustion engines*. Tech. rep. 2020. URL: `http://repository.tudelft.nl/.`.

A

Kinetic data

In this appendix the numerical values for the kinetic data is shown.

Table A.1: Pre exponential factors.

	Va		Fe		Cu	
	value	unit	value	unit	value	unit
$\mathrm{k}_{0,1f}$	372	[1/s]	1.70E+08	[mol/m3/s]	6.68E+07	[mol/m3/s]
$\mathrm{k}_{0,1b}$	7.40E+06	[1/s]	3.00E+13	[mol/m3/s]	4.00E+15	[mol/m3/s]
$\mathrm{k}_{0,2.1f}$	n.a.		7.17E+07	[mol/m3/s]	5.56E+16	[mol/m3/s]
$\mathrm{k}_{0,2.2f}$	1.64E+16	[mol/m3/s]	n.a.		n.a.	
$\mathrm{k}_{0,3f}$	n.a.		1.00E+07	[mol/m3/s]	5.10E+07	[mol/m3/s]
$\mathrm{k}_{0,4f}$	4.58E+08	[1/s]	1.50E+10	[mol/m3/s]	7.08E+13	[mol/m3/s]
$\mathrm{k}_{0,5f}$	1.57E+12	[m3/mol/s]	5.70E+17	[mol/m3/s]	1.00E+18	[mol/m3/s]
$\mathrm{k}_{0,6f}$	n.a.		2.13E+16	[mol/m3/s]	1.96E+17	[mol/m3/s]
$\mathrm{k}_{0,7f}$	n.a.		1.23E+08	[mol/m3/s]	2.28E+08	[mol/m3/s]
$\mathrm{k}_{0,8f}$	n.a.		3.50E+08	[mol/m3/s]	1.25E+08	[mol/m3/s]
$\mathrm{k}_{0,9f}$	n.a.		4.50E+11	[mol/m3/s]	n.a.	
$\mathrm{k}_{0,10f}$	n.a.		1.65E+10	[mol/m3/s]	n.a.	
$\mathrm{k}_{0,11f}$	1.10E+14	[1/s]	1.23E+08	[mol/m3/s]	2.28E+08	[mol/m3/s]

Table A.2: Activation energy.

	Va [kJ/mol]	Fe [kJ/mol]	Cu [kJ/mol]
E_{1f}	0	0	0
E_{1b}	67.8 (1-0.18θ)	145.9 (1-0.97θ)	145.9 (1-0.97θ)
$\mathrm{E}_{2.1f}$	n.a.	90.8	178.8
$\mathrm{E}_{2.2f}$	221.1	n.a.	n.a.
E_{3f}	n.a.	48	56
E_{4f}	75.3	70.5	89.1
E_{5f}	73.6	69.9	77.1
E_{6f}	n.a.	140.3	136.3
E_{7f}	n.a.	40	43
E_{8f}	n.a.	37	41.5
E_{9f}	n.a.	128	n.a.
E_{10f}	n.a.	90	n.a.
E_{11f}	140	40	43

B

Gas data

In this appendix the numerical values of the coefficients used in the polynomials of equation 5.40, 5.41, 5.42 and 5.51.

Table B.1: Nasa Polynomial coefficients [46].

	O_2	N_2	H_2O	NO	NO_2	NH_3	N_2O
a_1	3.782E+00	3.531E+00	4.199E+00	4.219E+00	3.944E+00	4.302E+00	2.257E+00
a_2	-2.997E-03	-1.237E-04	-2.036E-03	-4.640E-03	-1.585E-03	-4.771E-03	1.130E-02
a_3	9.847E-06	-5.030E-07	6.520E-06	1.104E-05	1.666E-05	2.193E-05	-1.367E-05
a_4	-9.681E-09	2.435E-09	-5.488E-09	-9.341E-09	-2.048E-08	-2.299E-08	9.682E-09
a_5	3.244E-12	-1.409E-12	1.772E-12	2.806E-12	7.835E-12	8.290E-12	-2.931E-12
b_1	-1.064E+03	-1.047E+03	-3.029E+04	9.845E+03	2.897E+03	-6.748E+03	8.742E+03
A	8.160E-01	9.431E-01	1.554E+00	n.a.	n.a.	n.a.	n.a.
B	-3.437E+01	1.228E+02	6.611E+01	n.a.	n.a.	n.a.	n.a.
C	2.279E+03	-1.184E+04	5.597E+03	n.a.	n.a.	n.a.	n.a.
D	1.005E+00	-1.067E-01	-3.926E+00	n.a.	n.a.	n.a.	n.a.

Table B.2: Lennard Jones potential coefficients [53]

coefficient	value
A	1.06036
B	0.15610
C	0.19300
D	0.47635
E	1.03587
F	1.52996
G	1.76474
H	3.89411

C

Model Implementation

In this appendix snapshots of the model are included. The snapshots show how the formulas from chapter 5 are implemented.

C.1. Void

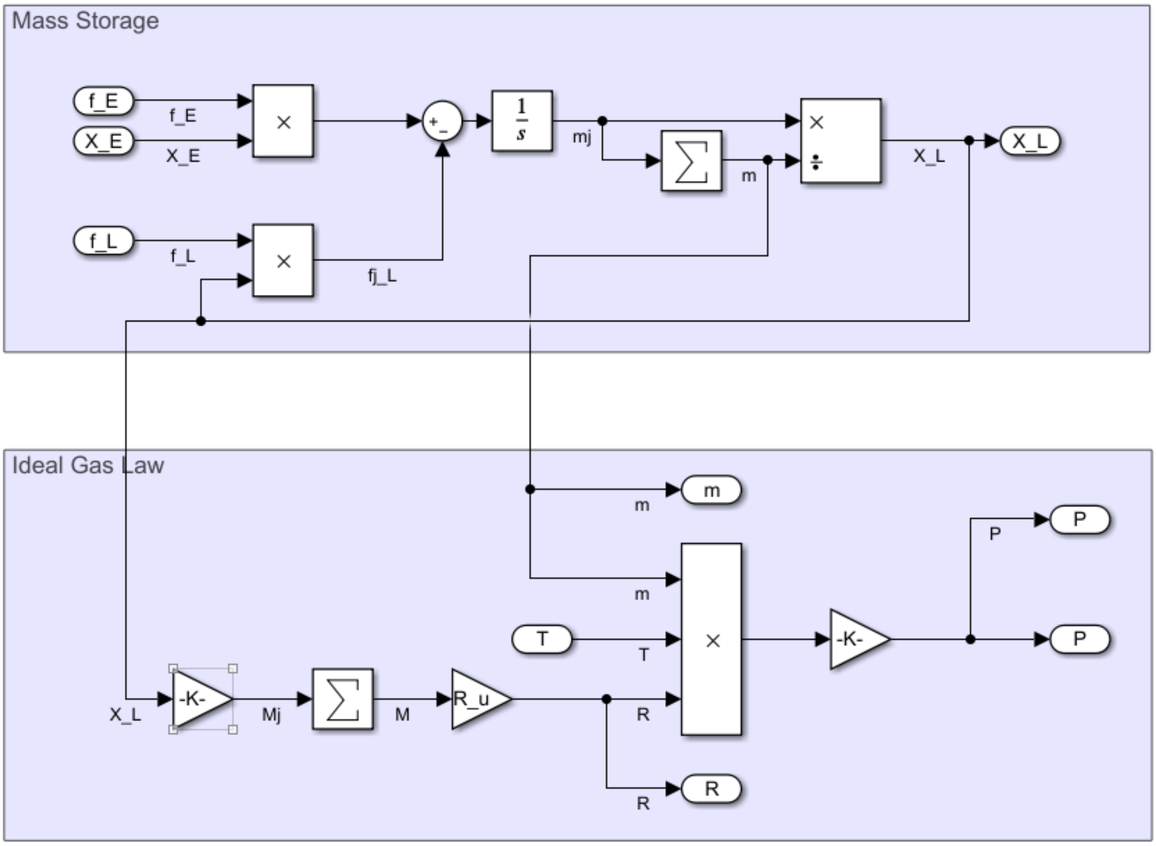

Figure C.1: Mass storage in void sub-model

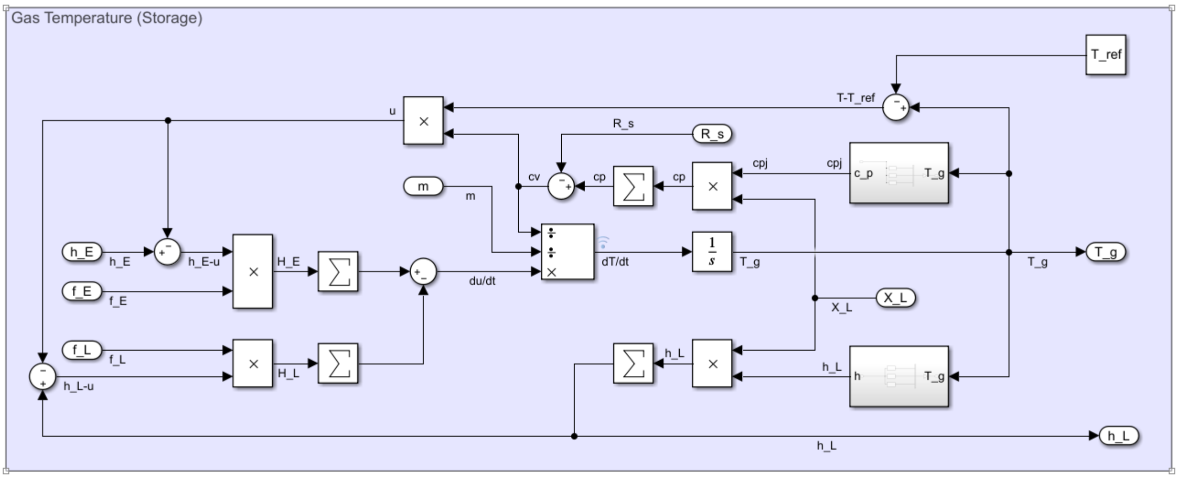

Figure C.2: Gas temperature in void sub-model.

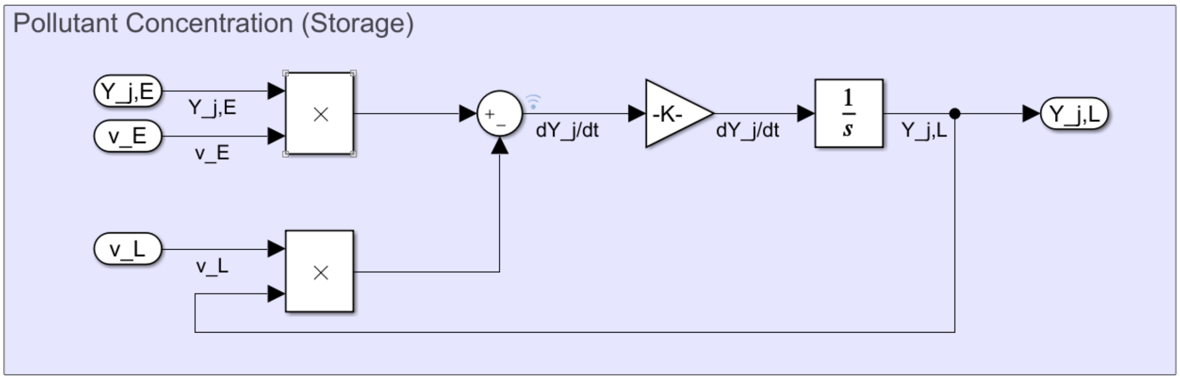

Figure C.3: Pollutant concentration in void sub-model.

C.2. Monolith

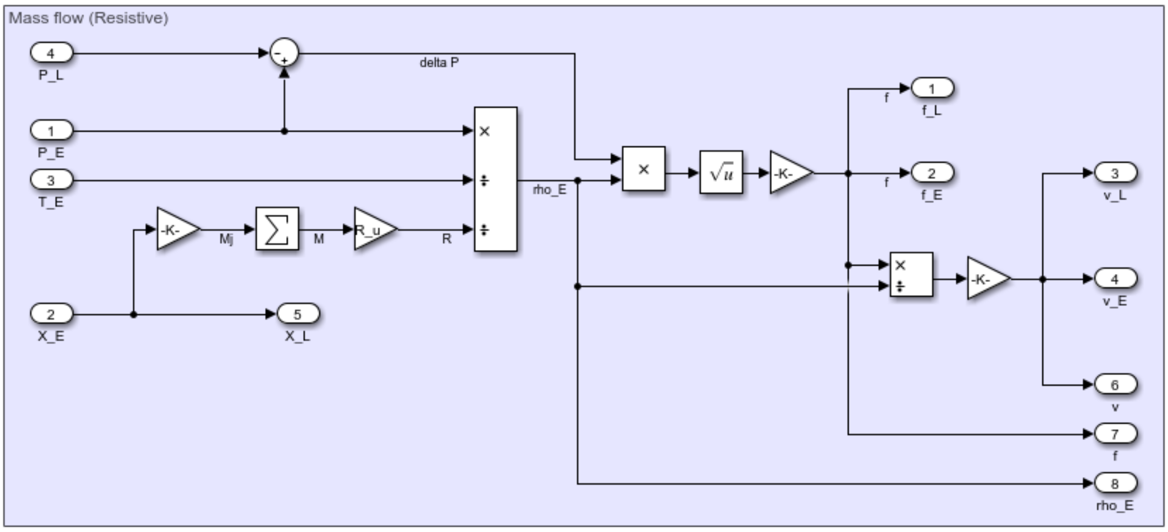

Figure C.4: Mass flow in Va model.

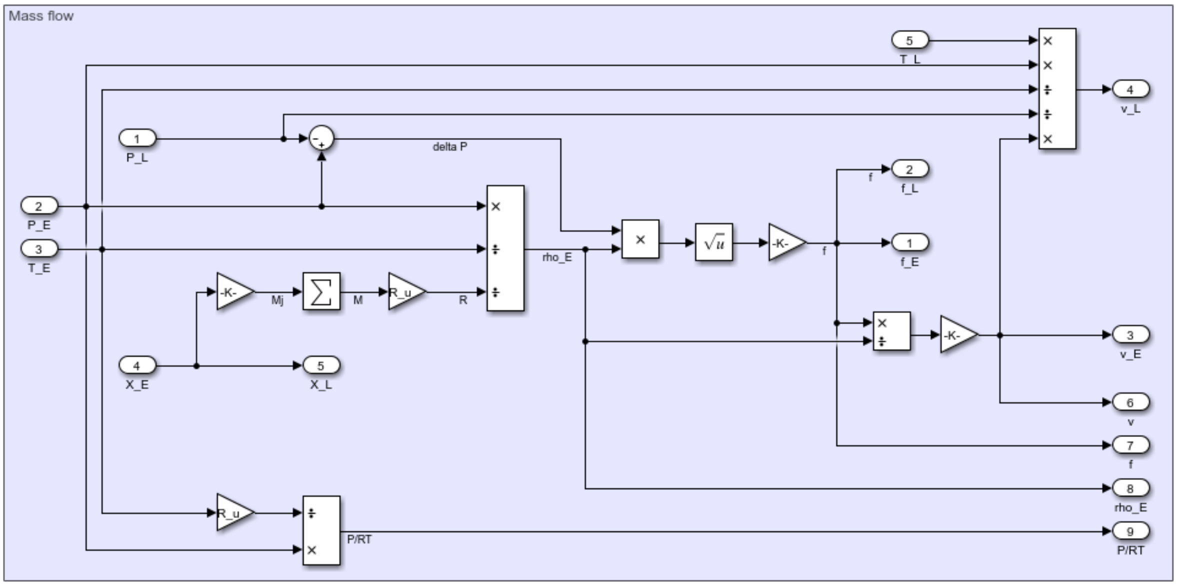

Figure C.5: Mass flow in Fe and Cu model.

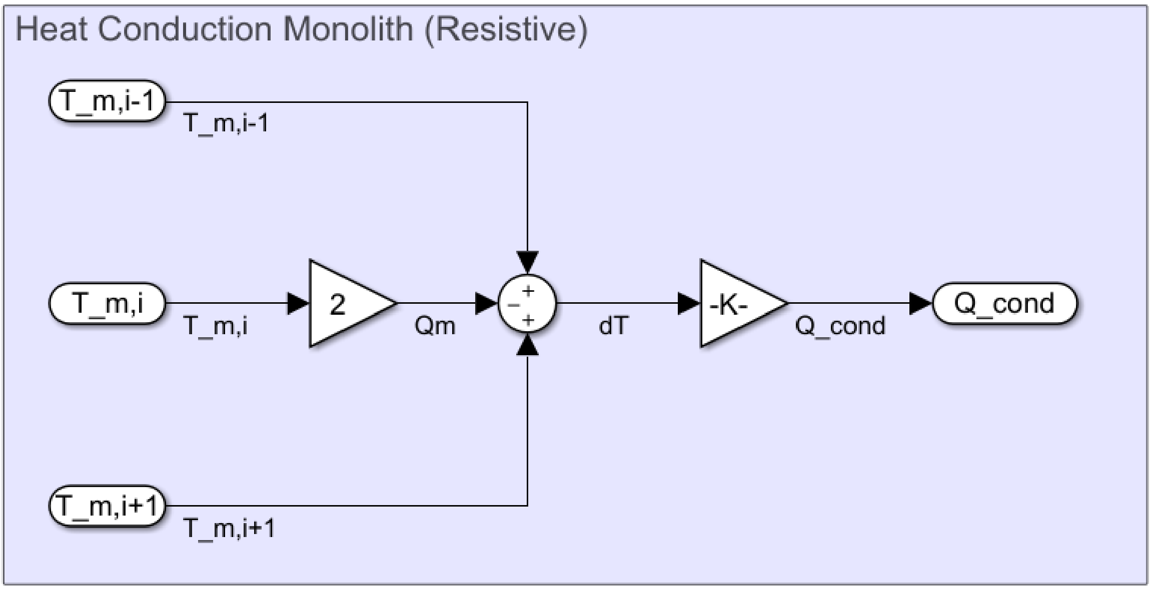

Figure C.6: Conductive heat transfer in all models.

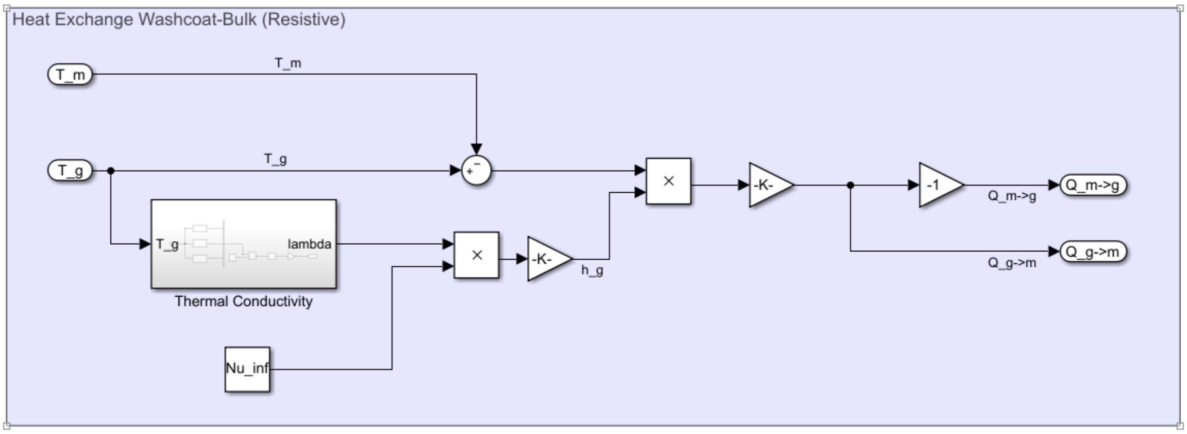

Figure C.7: Heat exchange between monolith and bulk gas in all models.

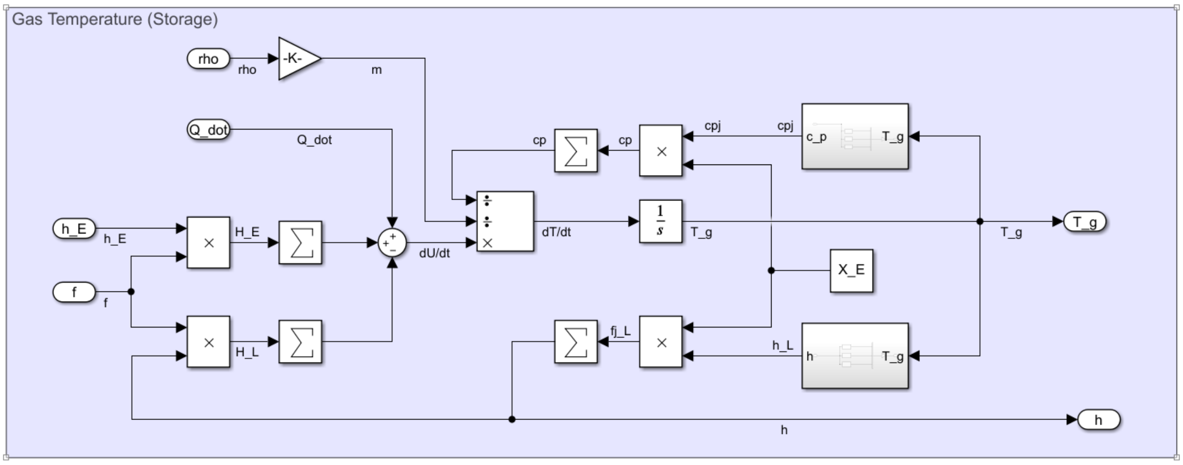

Figure C.8: Temperature balance of bulk gas in all models.

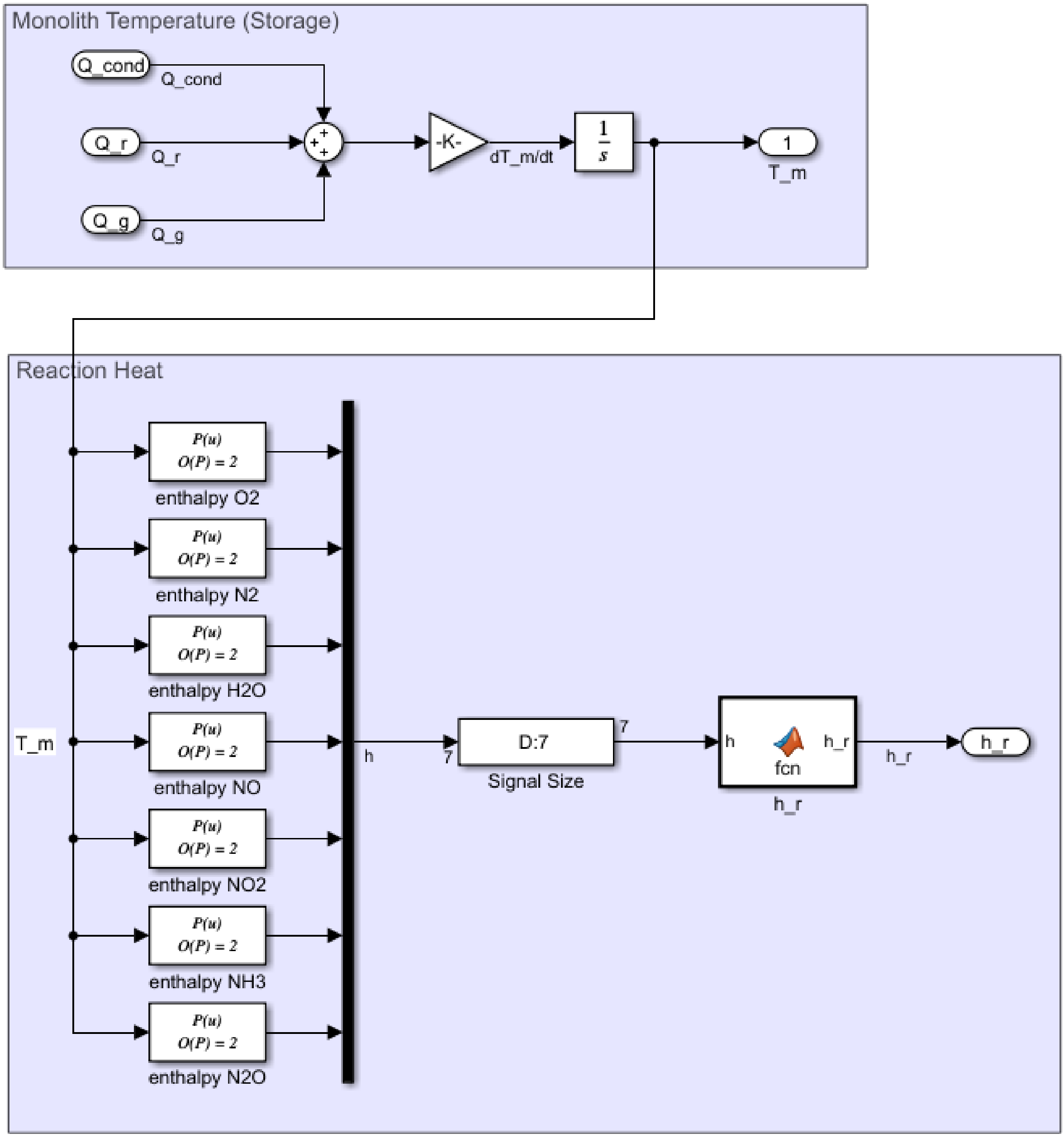

Figure C.9: Temperature balance of monolith in all models.

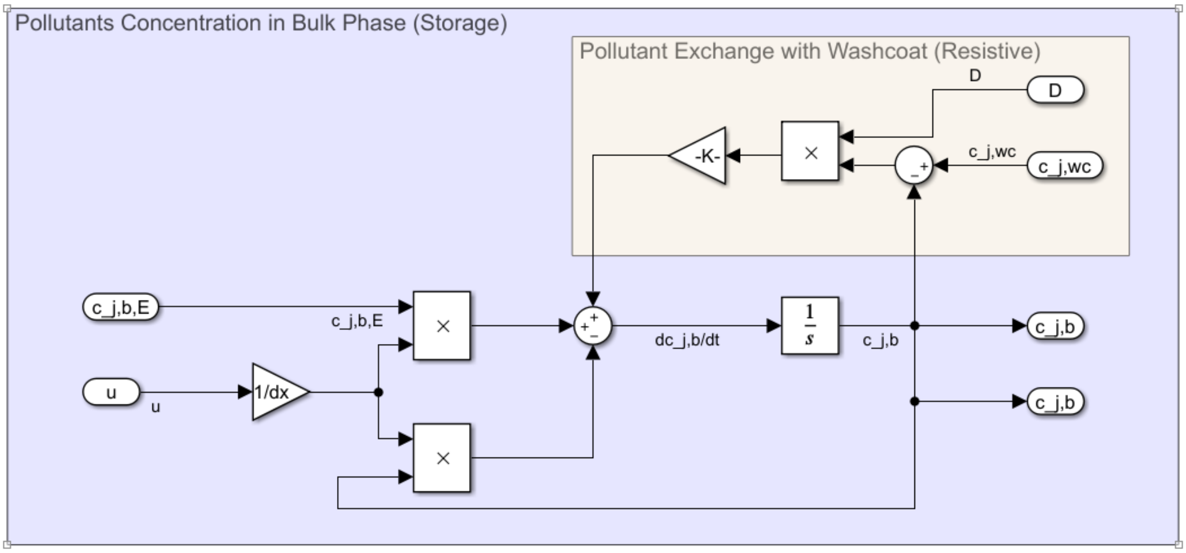

Figure C.10: Pollutant concentration in bulk phase in Va model.

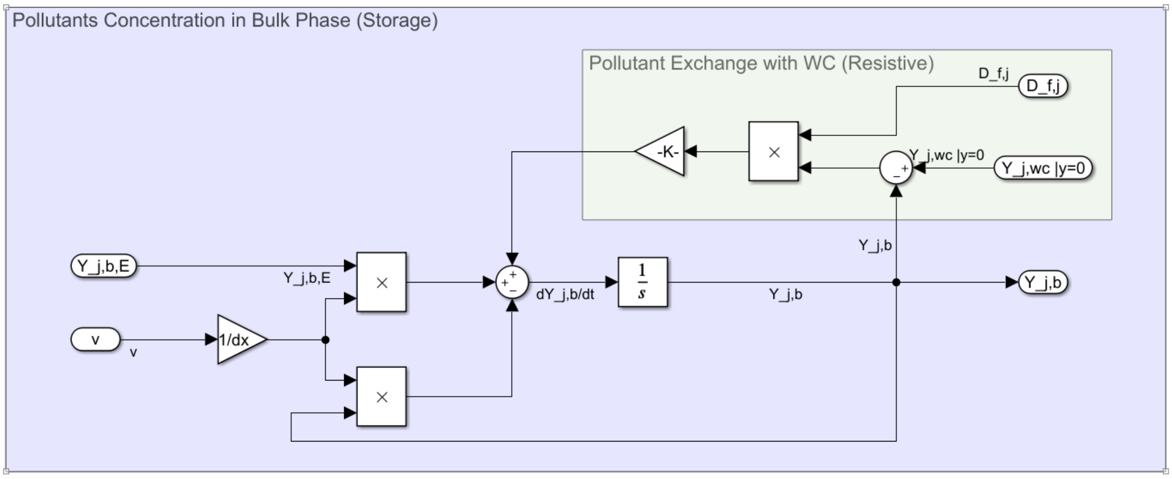

Figure C.11: Pollutant concentration in bulk phase in Fe and Cu model.

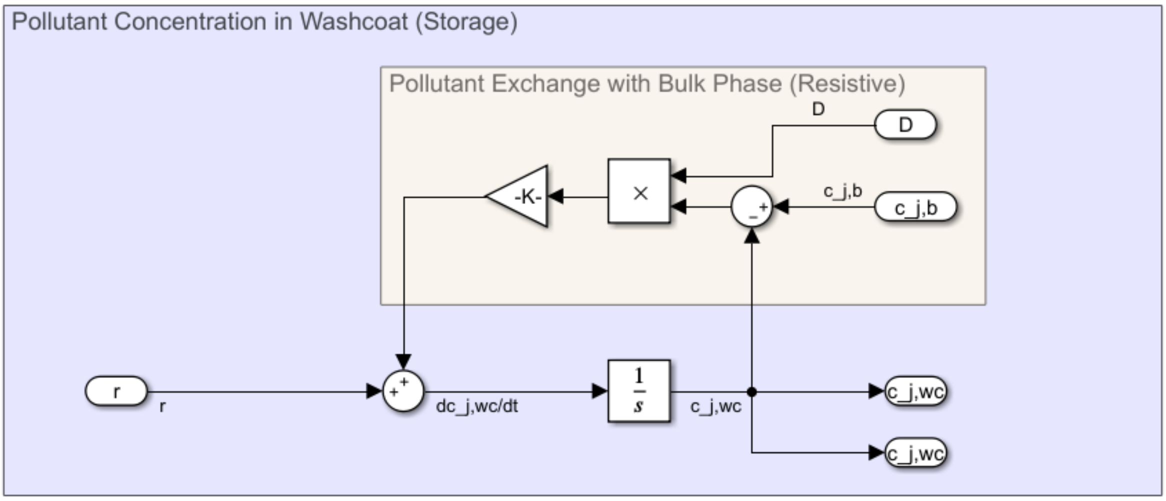

Figure C.12: Pollutant concentration in washcoat in Va model.

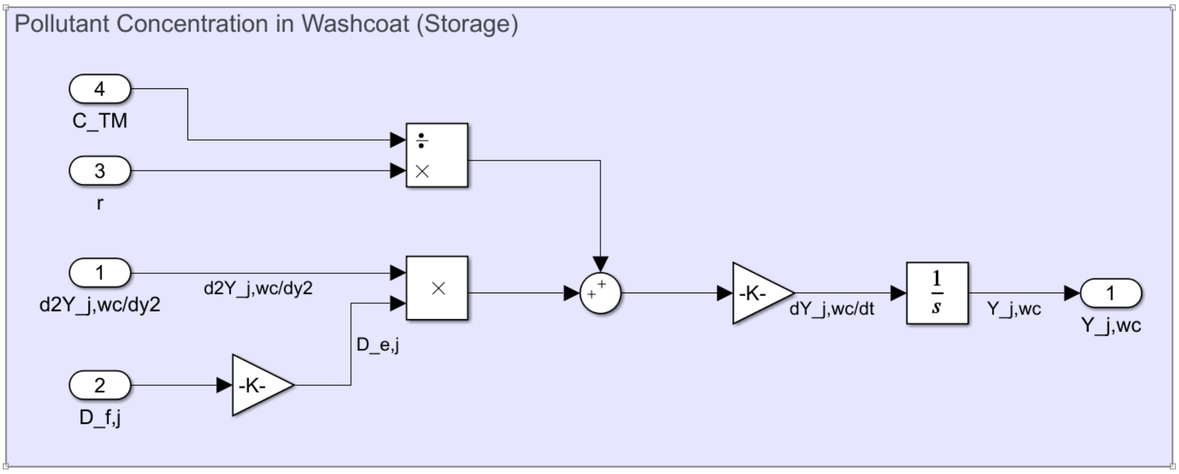

Figure C.13: Pollutant concentration in washcoat in Fe and Cu model.

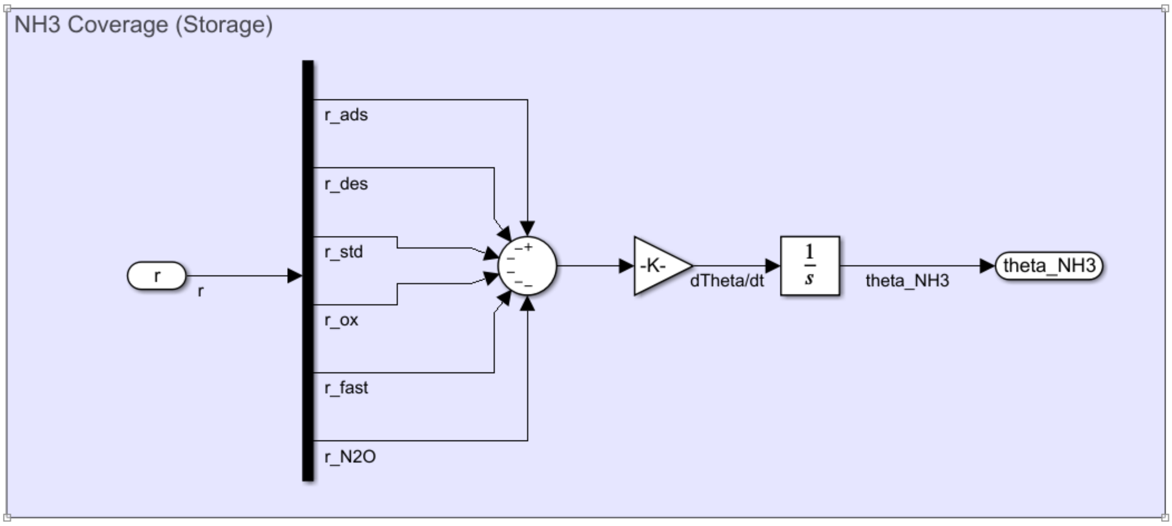

Figure C.14: NH_3 coverage in all models.

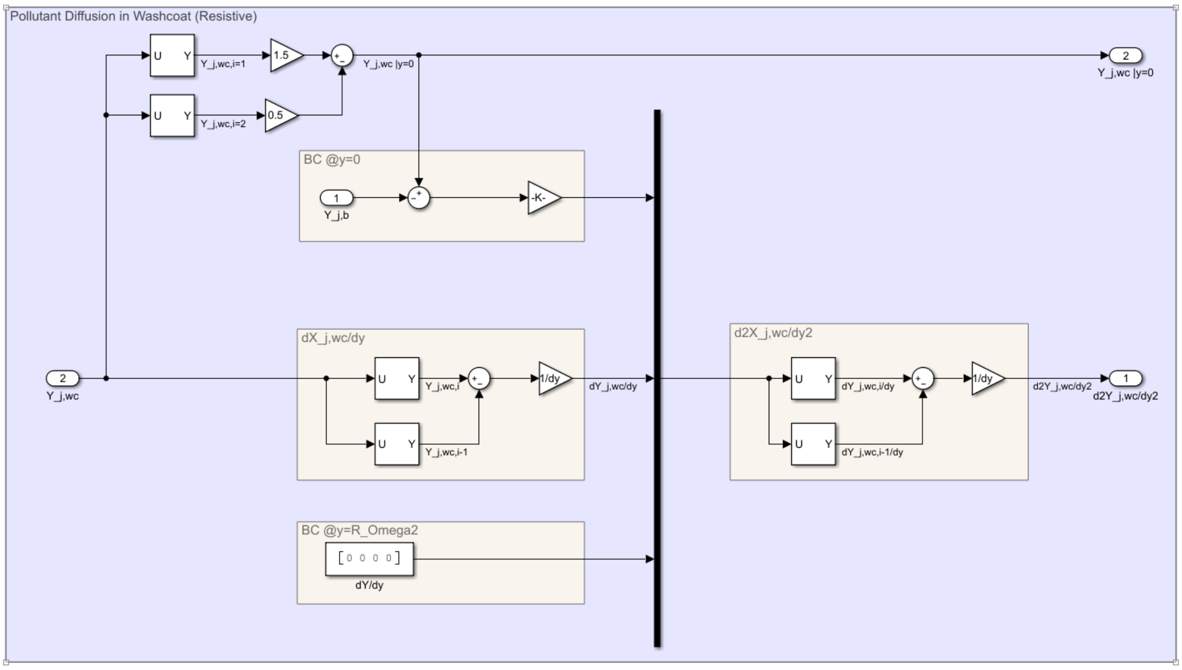

Figure C.15: Diffusion inside washcoat in Fe and Cu model.

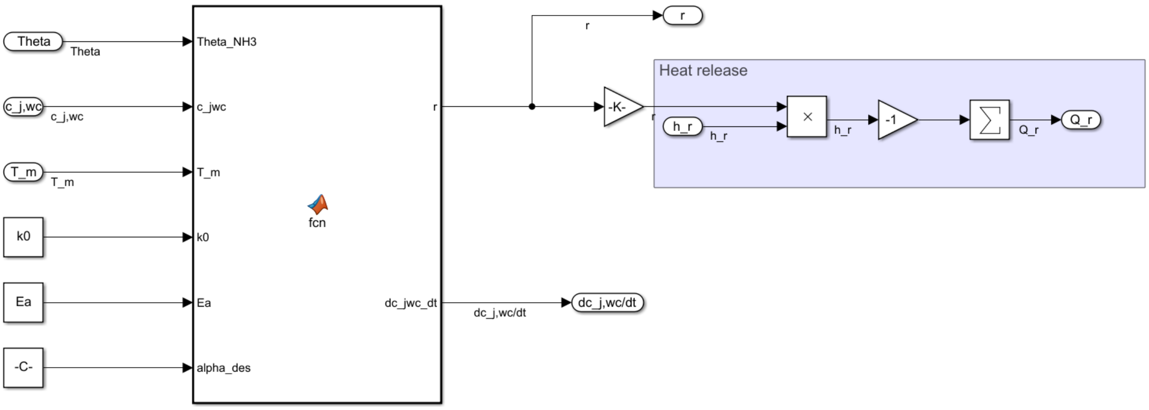

Figure C.16: Reaction rates and heat released by reactions in Va model

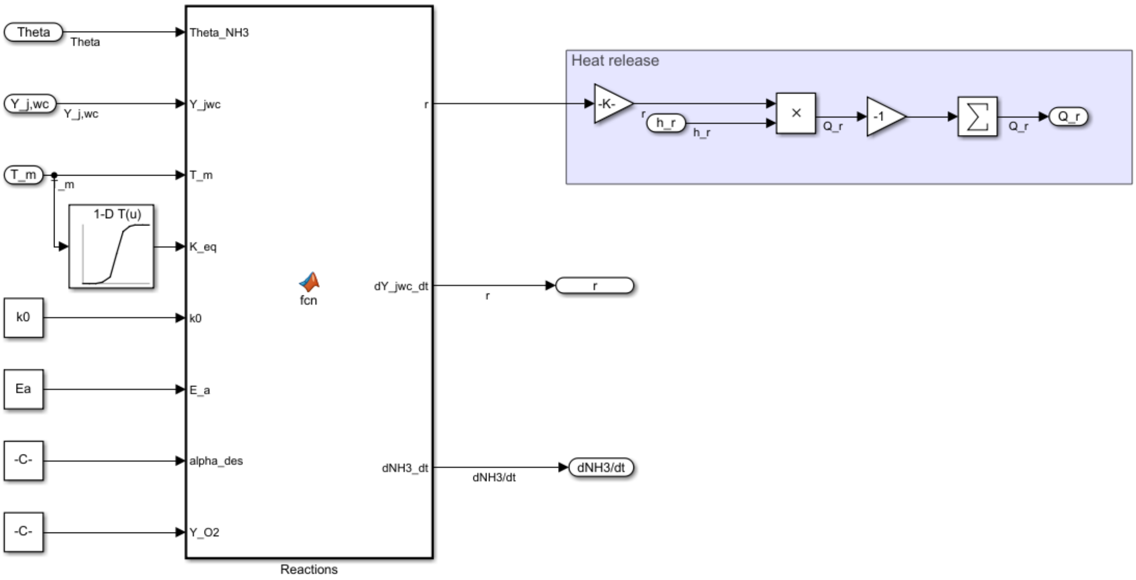

Figure C.17: Reaction rates and heat released by reactions in Fe and Cu model.

D

NO$_X$ Interaction plot

In this appendix interaction plots are shown, they help to gain better insight on how the the input variables influence pollutant levels at the outlet of the SCR.
The interaction plot is a matrix plot. The different input variables are printed on the diagonal of the matrix. The plot at off-diagonal position (i,j) is the interaction of the two variables whose names are given at row diagonal (i,i) and column diagonal (j,j), respectively [45]. On the y axis the outlet NOx concentration [ppm] is shown. The x-axis shows the range over which the column variable was tested. On the right, the different tested values for the row variable are shown.

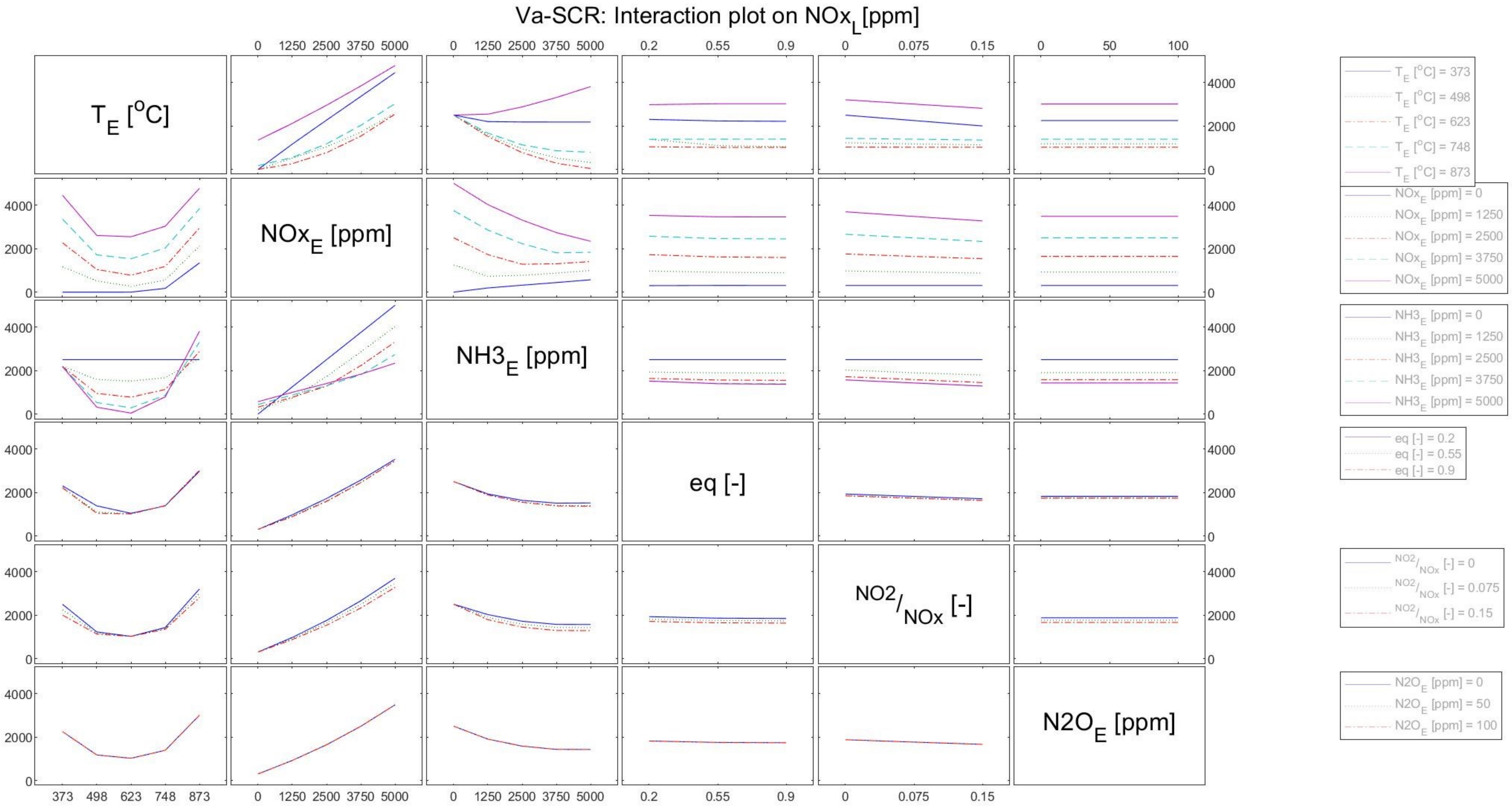
Va-SCR: Interaction plot on NOx_L [ppm]
T_E [^oC]
NOx_E [ppm]
$NH3_E$ [ppm]
eq [-]
$^{NO2}/_{NOx}$ [-]
$N2O_E$ [ppm]
373 498 623 748 873
0 1250 2500 3750 5000
0.2 0.55 0.9
0 0.075 0.15
0 50 100
0 2000 4000
T_E [^oC] = 373
T_E [^oC] = 498
T_E [^oC] = 623
T_E [^oC] = 748
T_E [^oC] = 873
NOx_E [ppm] = 0
NOx_E [ppm] = 1250
NOx_E [ppm] = 2500
NOx_E [ppm] = 3750
NOx_E [ppm] = 5000
$NH3_E$ [ppm] = 0
$NH3_E$ [ppm] = 1250
$NH3_E$ [ppm] = 2500
$NH3_E$ [ppm] = 3750
$NH3_E$ [ppm] = 5000
eq [-] = 0.2
eq [-] = 0.55
eq [-] = 0.9
$^{NO2}/_{NOx}$ [-] = 0
$^{NO2}/_{NOx}$ [-] = 0.075
$^{NO2}/_{NOx}$ [-] = 0.15
$N2O_E$ [ppm] = 0
$N2O_E$ [ppm] = 50
$N2O_E$ [ppm] = 100

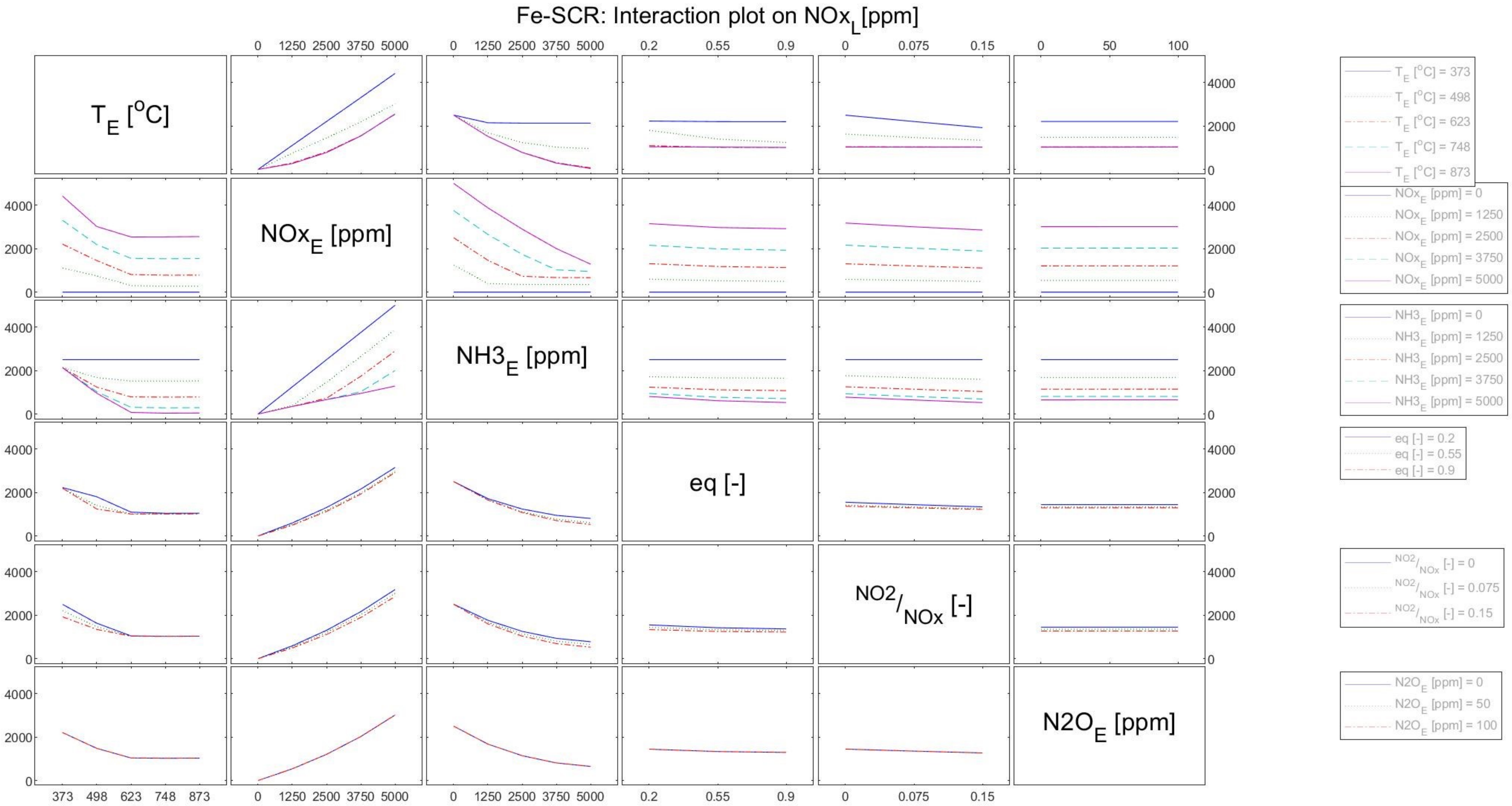
Fe-SCR: Interaction plot on NOx$_L$ [ppm]
T$_E$ [°C]
NOx$_E$ [ppm]
NH3$_E$ [ppm]
eq [-]
NO2/NOx [-]
N2O$_E$ [ppm]
373 498 623 748 873
0 1250 2500 3750 5000
0 1250 2500 3750 5000
0.2 0.55 0.9
0 0.075 0.15
0 50 100
0 2000 4000
T$_E$ [°C] = 373
T$_E$ [°C] = 498
T$_E$ [°C] = 623
T$_E$ [°C] = 748
T$_E$ [°C] = 873
NOx$_E$ [ppm] = 0
NOx$_E$ [ppm] = 1250
NOx$_E$ [ppm] = 2500
NOx$_E$ [ppm] = 3750
NOx$_E$ [ppm] = 5000
NH3$_E$ [ppm] = 0
NH3$_E$ [ppm] = 1250
NH3$_E$ [ppm] = 2500
NH3$_E$ [ppm] = 3750
NH3$_E$ [ppm] = 5000
eq [-] = 0.2
eq [-] = 0.55
eq [-] = 0.9
NO2/NOx [-] = 0
NO2/NOx [-] = 0.075
NO2/NOx [-] = 0.15
N2O$_E$ [ppm] = 0
N2O$_E$ [ppm] = 50
N2O$_E$ [ppm] = 100

Cu-SCR: Interaction plot on NOx_L [ppm]

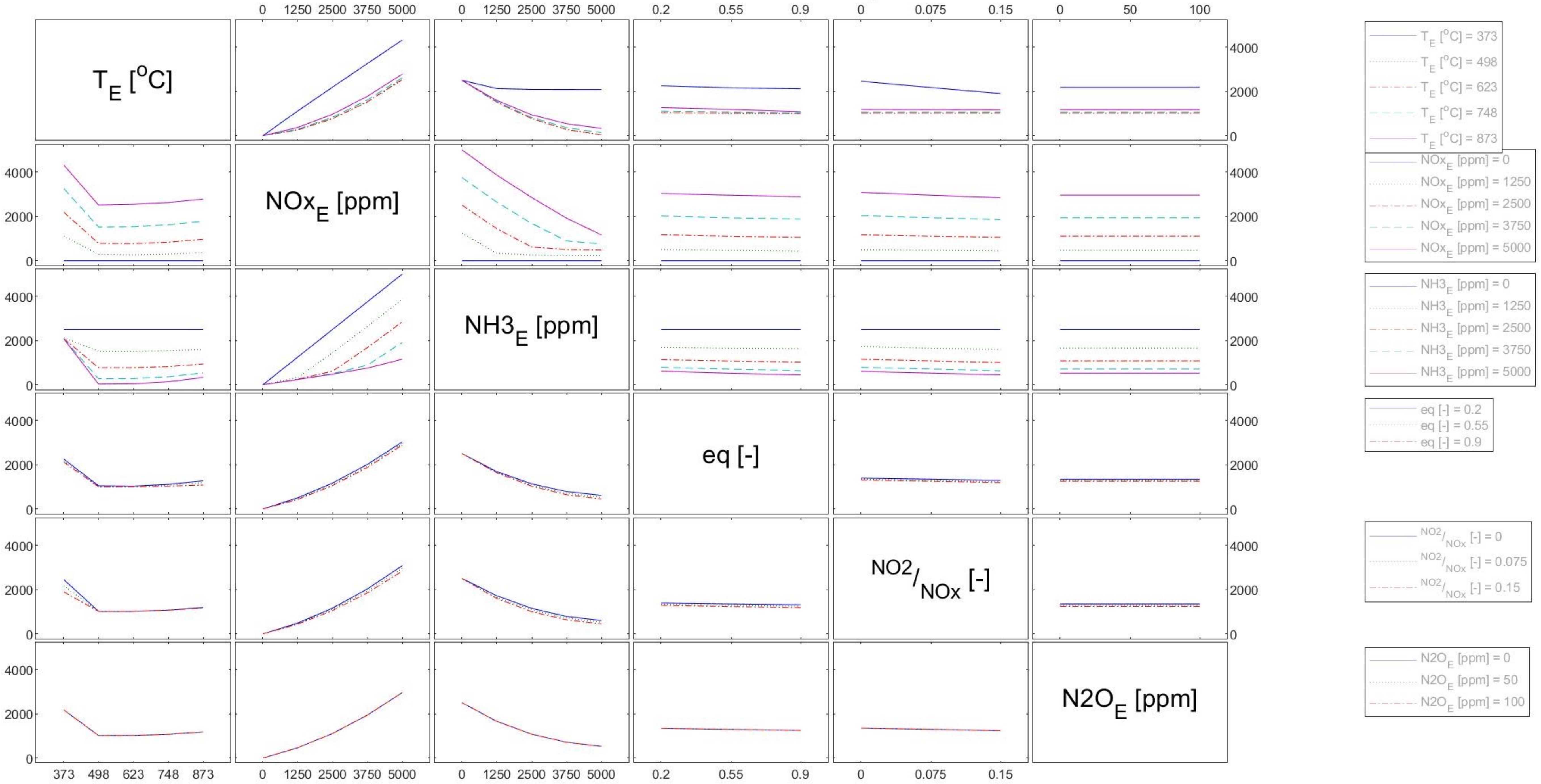

E

NH_3 Interaction plot

In this appendix interaction plots are shown, they help to gain better insight on how the the input variables influence pollutant levels at the outlet of the SCR.
The interaction plot is a matrix plot. The different input variables are printed on the diagonal of the matrix. The plot at off-diagonal position (i,j) is the interaction of the two variables whose names are given at row diagonal (i,i) and column diagonal (j,j), respectively [45]. On the y axis the outlet NH3 concentration [ppm] is shown. The x-axis shows the range over which the column variable was tested. On the right, the different tested values for the row variable are shown.

Va-SCR: Interaction plot on $NH3_L$ [ppm]

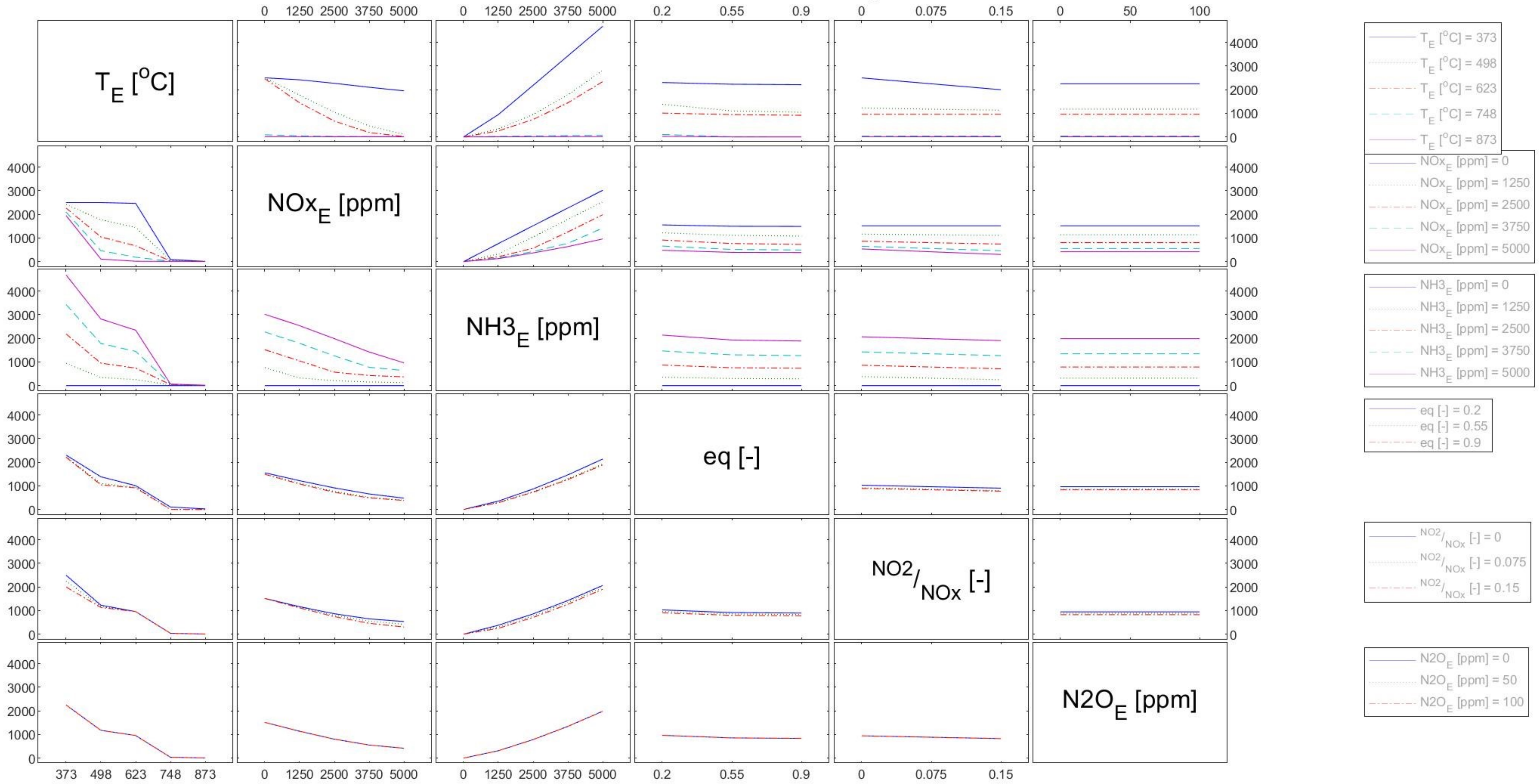

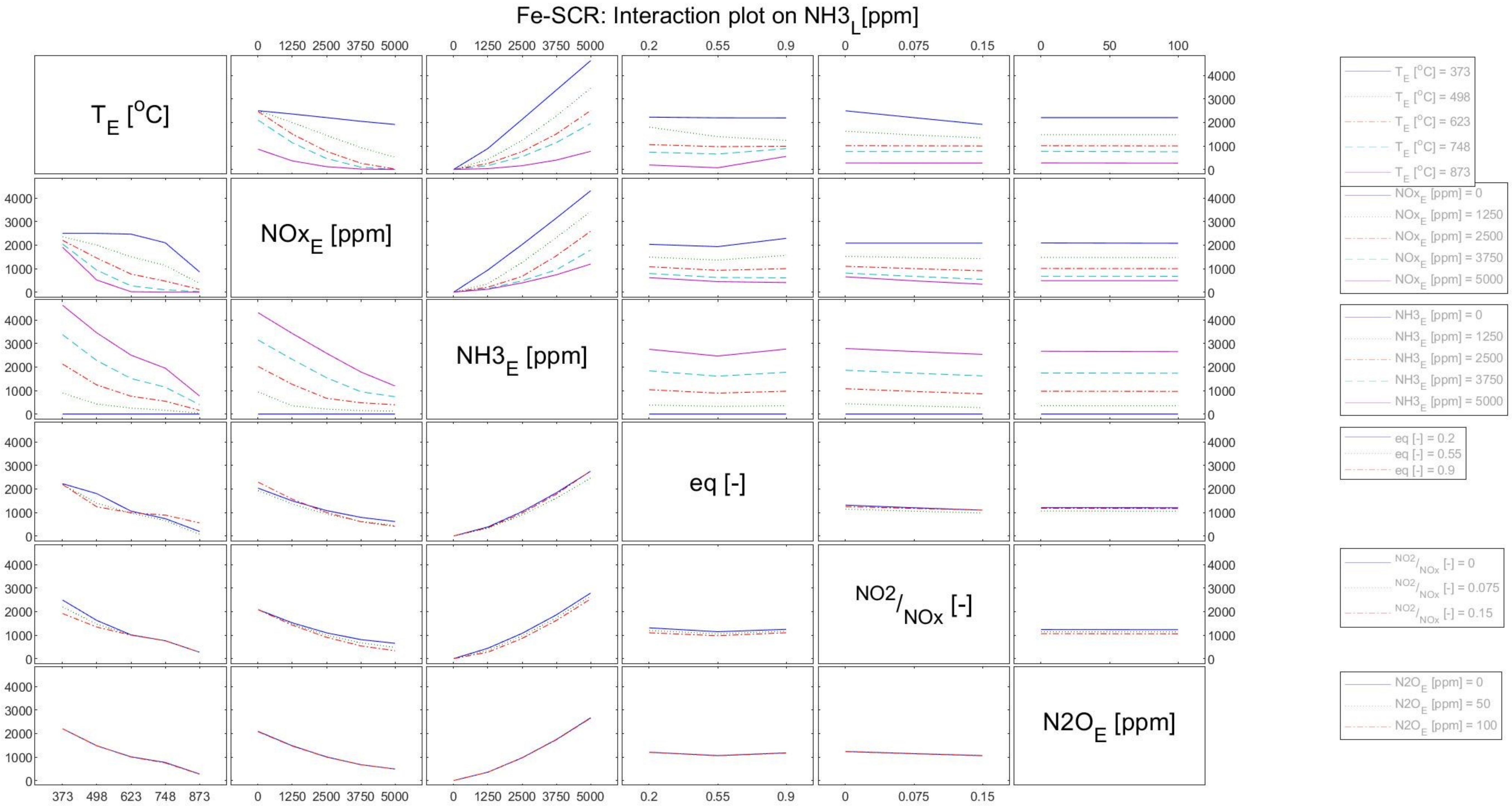

Fe-SCR: Interaction plot on $NH3_L$ [ppm]

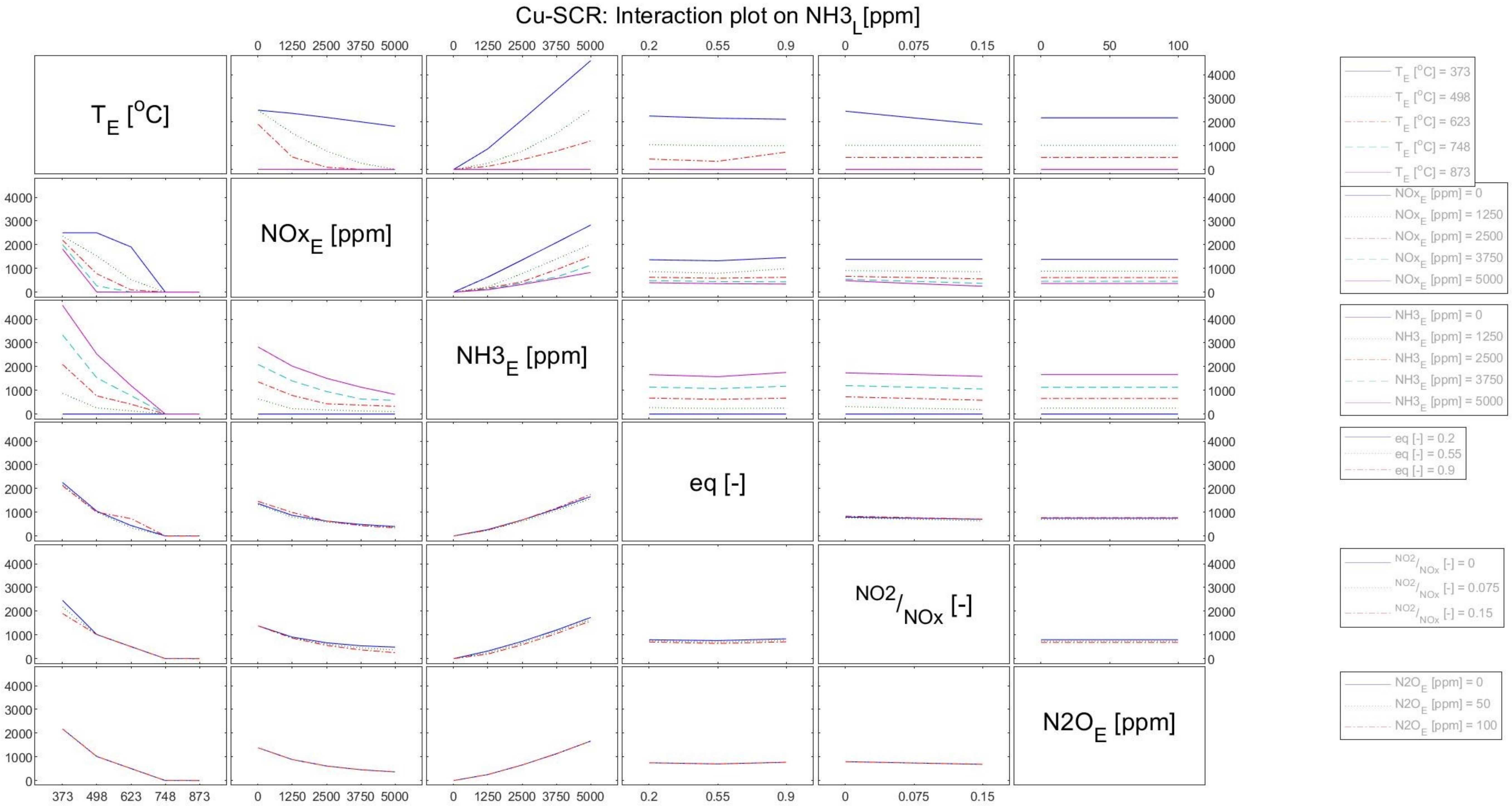
Cu-SCR: Interaction plot on NH3$_L$ [ppm]
T$_E$ [^{o}C]
NOx$_E$ [ppm]
NH3$_E$ [ppm]
eq [-]
NO2/NOx [-]
N2O$_E$ [ppm]
373 498 623 748 873
0 1250 2500 3750 5000
0.2 0.55 0.9
0 0.075 0.15
0 50 100
0 1000 2000 3000 4000
T$_E$ [^{o}C] = 373
T$_E$ [^{o}C] = 498
T$_E$ [^{o}C] = 623
T$_E$ [^{o}C] = 748
T$_E$ [^{o}C] = 873
NOx$_E$ [ppm] = 0
NOx$_E$ [ppm] = 1250
NOx$_E$ [ppm] = 2500
NOx$_E$ [ppm] = 3750
NOx$_E$ [ppm] = 5000
NH3$_E$ [ppm] = 0
NH3$_E$ [ppm] = 1250
NH3$_E$ [ppm] = 2500
NH3$_E$ [ppm] = 3750
NH3$_E$ [ppm] = 5000
eq [-] = 0.2
eq [-] = 0.55
eq [-] = 0.9
NO2/NOx [-] = 0
NO2/NOx [-] = 0.075
NO2/NOx [-] = 0.15
N2O$_E$ [ppm] = 0
N2O$_E$ [ppm] = 50
N2O$_E$ [ppm] = 100

F

N_2O Interaction plot

In this appendix interaction plots are shown, they help to gain better insight on how the the input variables influence pollutant levels at the outlet of the SCR.
The interaction plot is a matrix plot. The different input variables are printed on the diagonal of the matrix. The plot at off-diagonal position (i,j) is the interaction of the two variables whose names are given at row diagonal (i,i) and column diagonal (j,j), respectively [45]. On the y axis the outlet N2O concentration [ppm] is shown. The x-axis shows the range over which the column variable was tested. On the right, the different tested values for the row variable are shown.

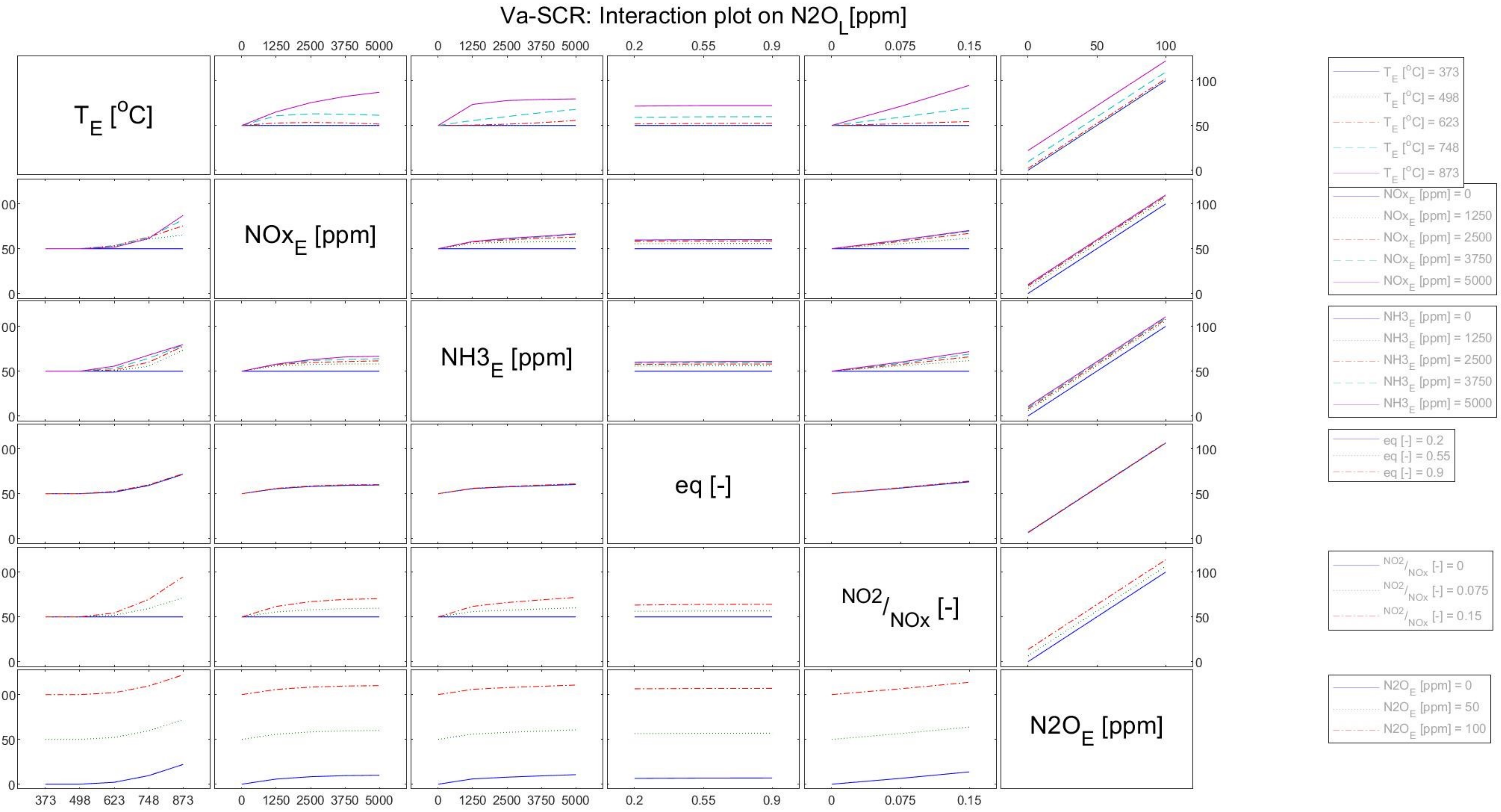
Va-SCR: Interaction plot on $N2O_L$ [ppm]
T_E [°C]
NOx_E [ppm]
$NH3_E$ [ppm]
eq [-]
$^{NO2}/_{NOx}$ [-]
$N2O_E$ [ppm]
373 498 623 748 873
0 1250 2500 3750 5000
0.2 0.55 0.9
0 0.075 0.15
0 50 100
0 50 100
T_E [°C] = 373
T_E [°C] = 498
T_E [°C] = 623
T_E [°C] = 748
T_E [°C] = 873
NOx_E [ppm] = 0
NOx_E [ppm] = 1250
NOx_E [ppm] = 2500
NOx_E [ppm] = 3750
NOx_E [ppm] = 5000
$NH3_E$ [ppm] = 0
$NH3_E$ [ppm] = 1250
$NH3_E$ [ppm] = 2500
$NH3_E$ [ppm] = 3750
$NH3_E$ [ppm] = 5000
eq [-] = 0.2
eq [-] = 0.55
eq [-] = 0.9
$^{NO2}/_{NOx}$ [-] = 0
$^{NO2}/_{NOx}$ [-] = 0.075
$^{NO2}/_{NOx}$ [-] = 0.15
$N2O_E$ [ppm] = 0
$N2O_E$ [ppm] = 50
$N2O_E$ [ppm] = 100

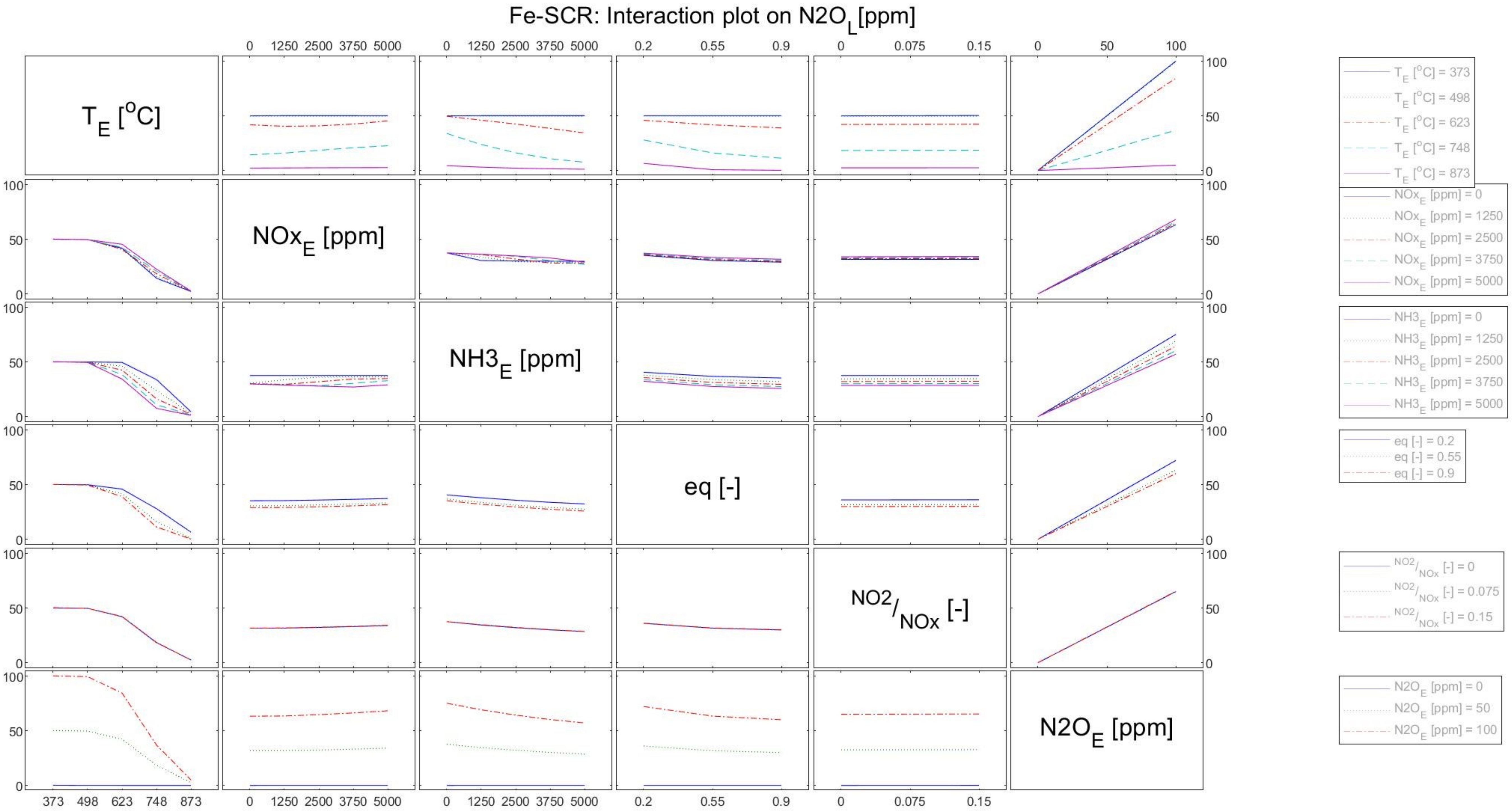
Fe-SCR: Interaction plot on N2O$_L$ [ppm]
T$_E$ [^{o}C]
NOx$_E$ [ppm]
NH3$_E$ [ppm]
eq [-]
NO2/NOx [-]
N2O$_E$ [ppm]
0 1250 2500 3750 5000
0.2 0.55 0.9
0 0.075 0.15
0 50 100
373 498 623 748 873
T$_E$ [^{o}C] = 373
T$_E$ [^{o}C] = 498
T$_E$ [^{o}C] = 623
T$_E$ [^{o}C] = 748
T$_E$ [^{o}C] = 873
NOx$_E$ [ppm] = 0
NOx$_E$ [ppm] = 1250
NOx$_E$ [ppm] = 2500
NOx$_E$ [ppm] = 3750
NOx$_E$ [ppm] = 5000
NH3$_E$ [ppm] = 0
NH3$_E$ [ppm] = 1250
NH3$_E$ [ppm] = 2500
NH3$_E$ [ppm] = 3750
NH3$_E$ [ppm] = 5000
eq [-] = 0.2
eq [-] = 0.55
eq [-] = 0.9
NO2/NOx [-] = 0
NO2/NOx [-] = 0.075
NO2/NOx [-] = 0.15
N2O$_E$ [ppm] = 0
N2O$_E$ [ppm] = 50
N2O$_E$ [ppm] = 100

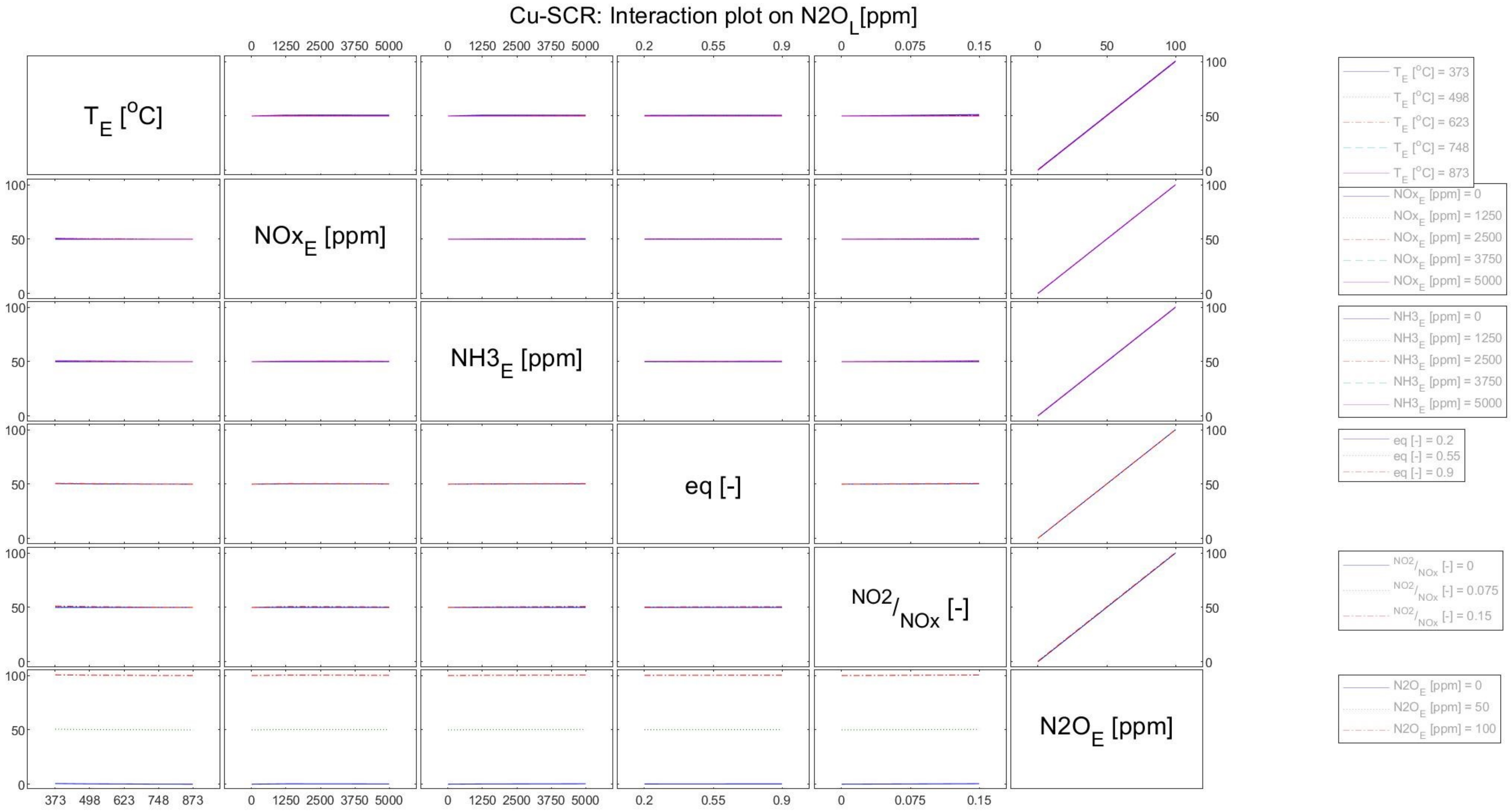

Cu-SCR: Interaction plot on $N2O_L$ [ppm]

G

Va Parameter Effect

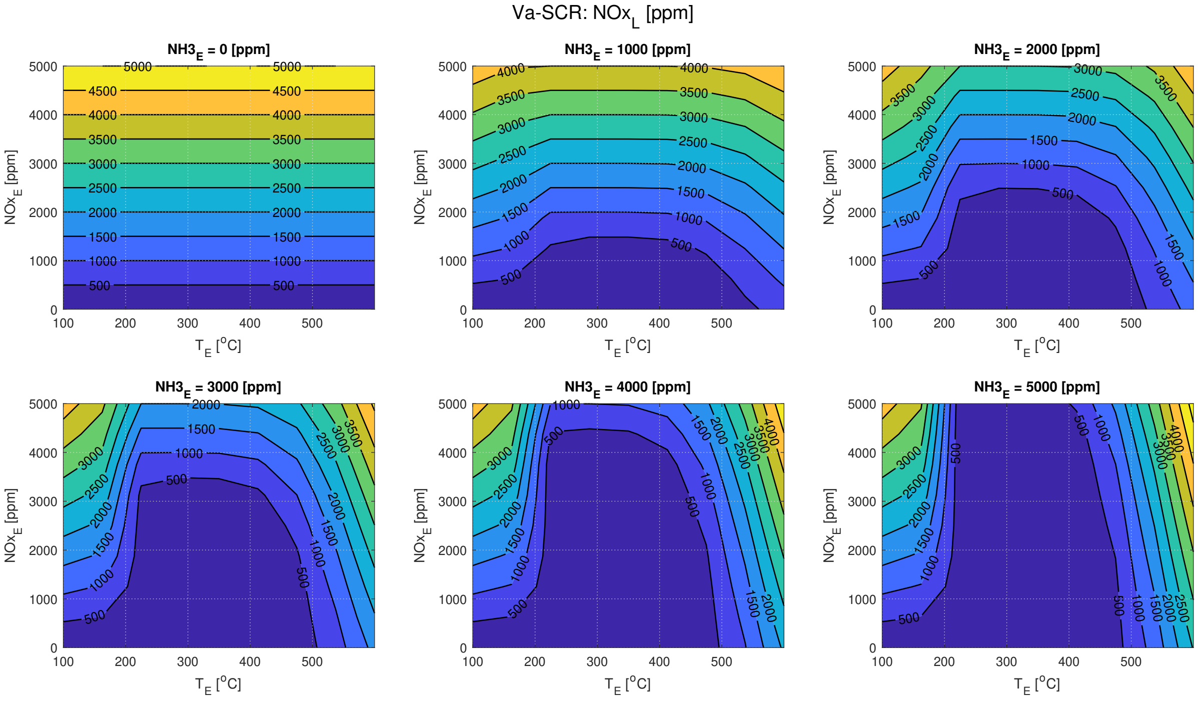

Figure G.1: NO$_X$ concentrations at outlet Va-SCR (N$_2$O$_E$ = 100 [ppm], ϕ = 0.55, $^{NO_2}/_{NO_X}$ = 0.075).

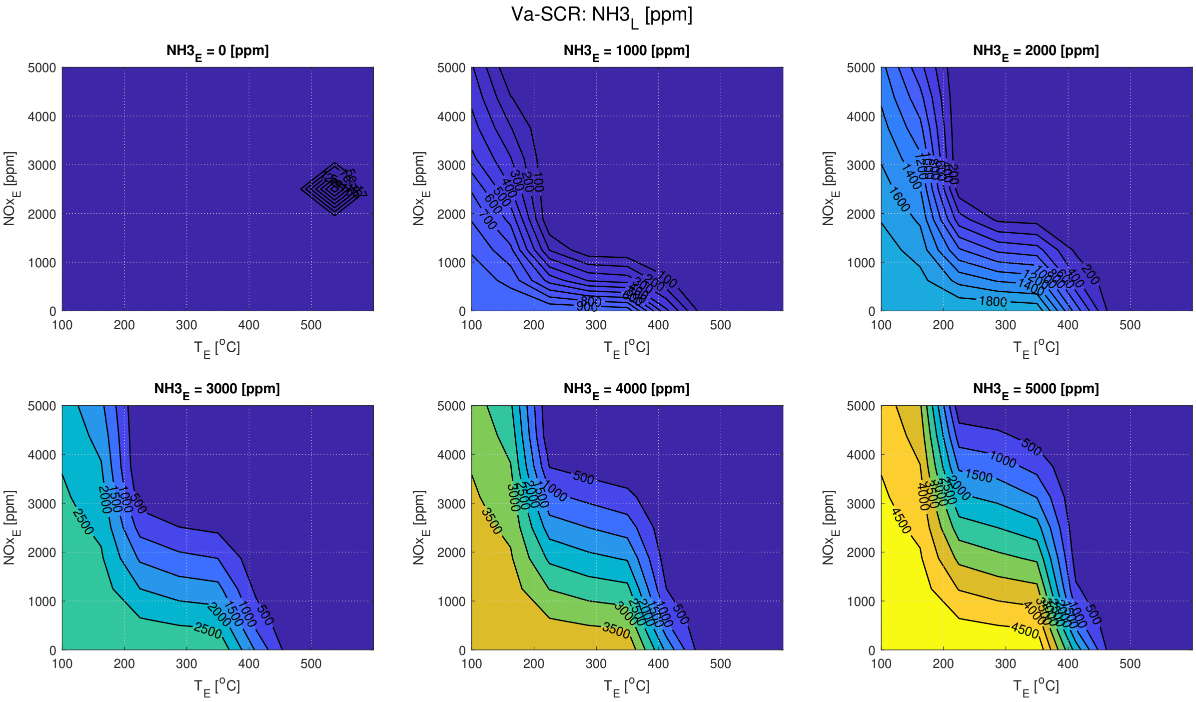

Figure G.2: NH_3 concentrations at outlet Va-SCR (N_2O_E = 100 [ppm], ϕ = 0.55, $^{NO_2}/_{NO_X}$ = 0.075).

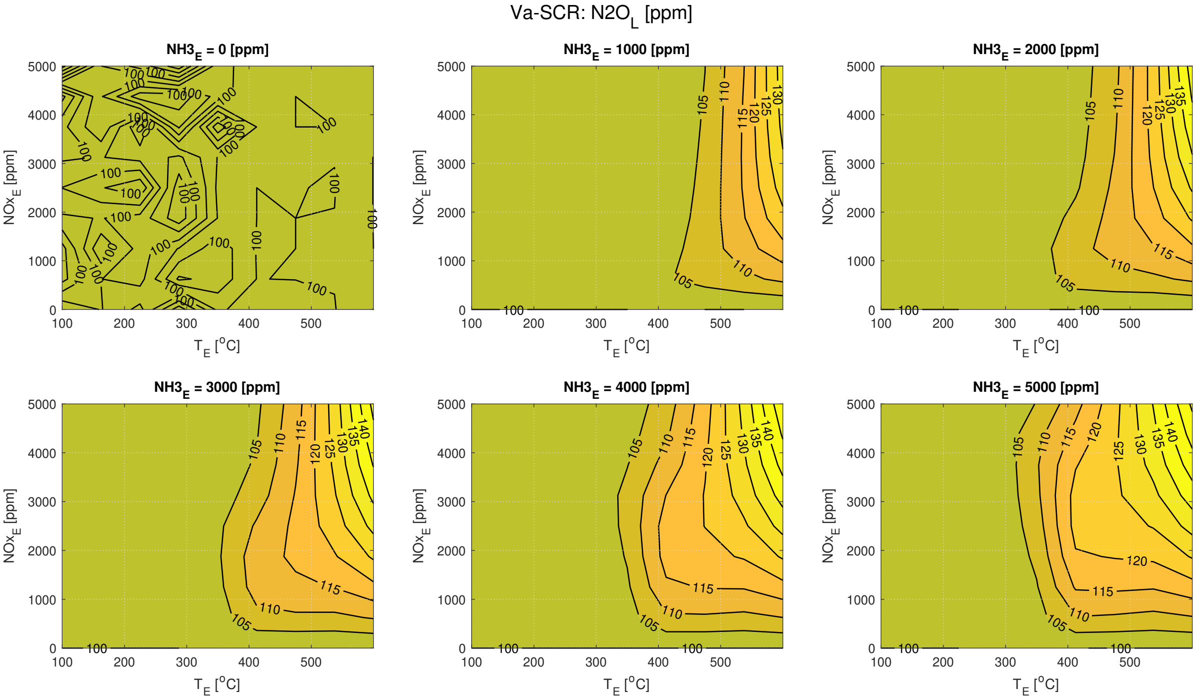

Figure G.3: N_2O concentrations at outlet Va-SCR (N_2O_E = 100 [ppm], ϕ = 0.55, $^{NO_2}/_{NO_X}$ = 0.075).

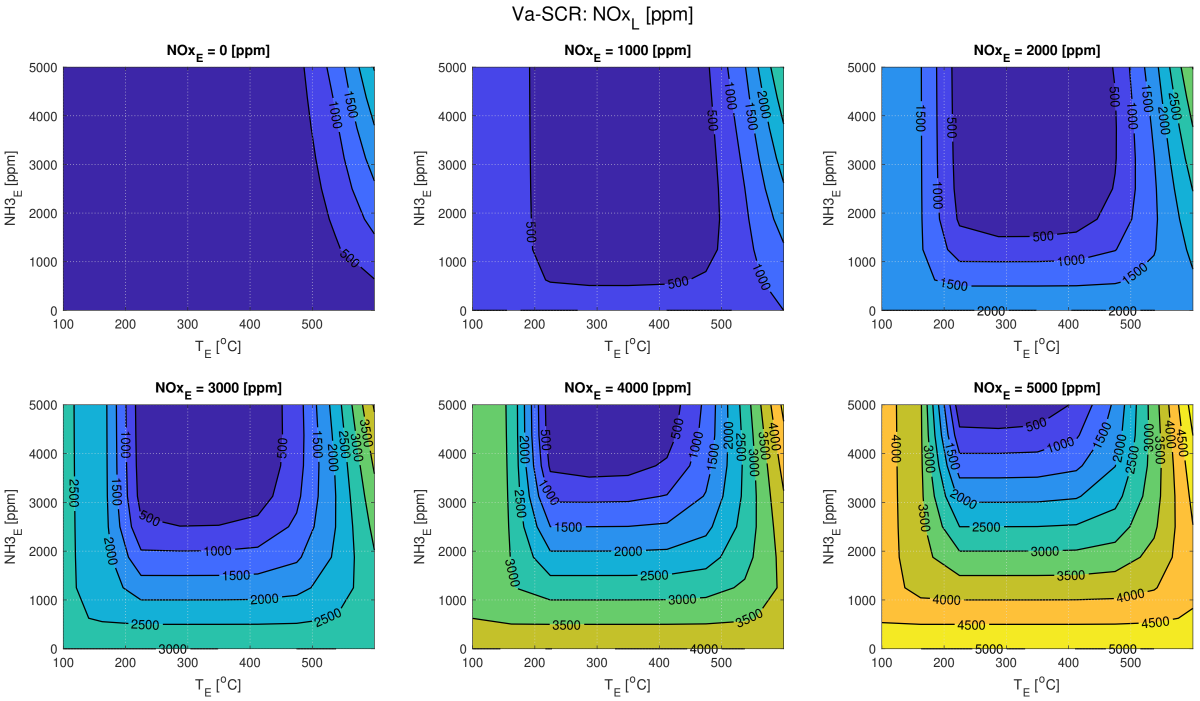

Figure G.4: NO$_X$ concentrations at outlet Va-SCR (N$_2$O$_E$ = 100 [ppm], ϕ = 0.55, $^{NO_2}/_{NO_X}$ = 0.075).

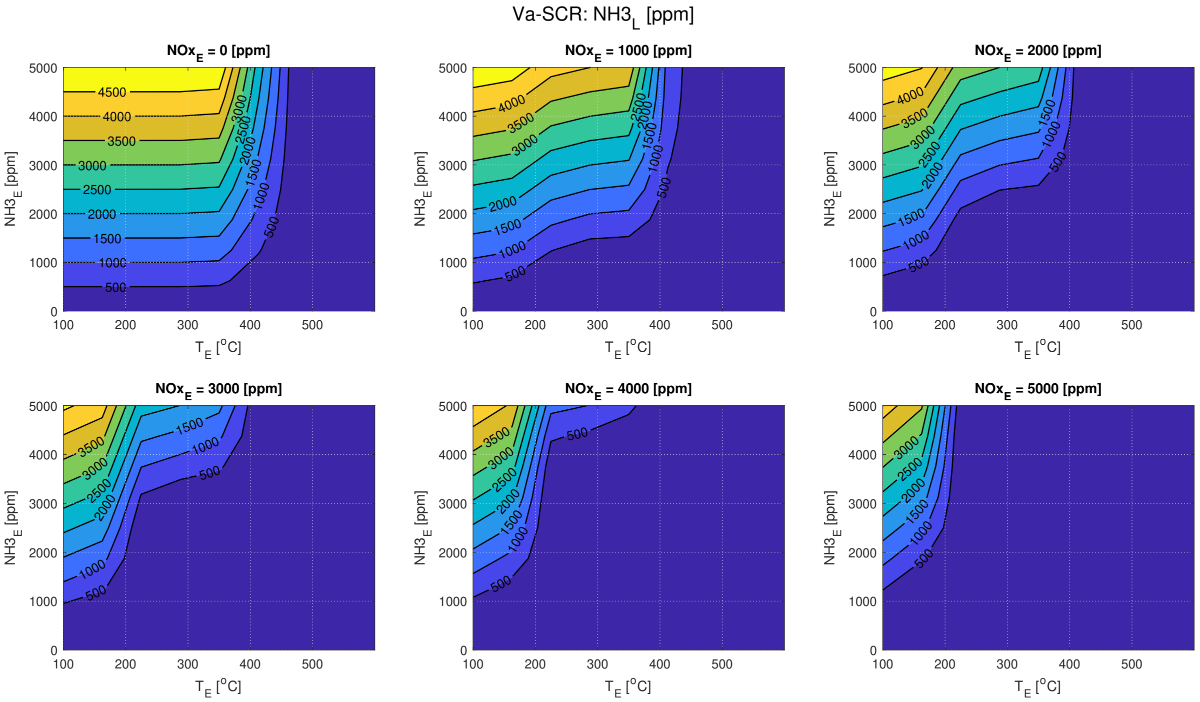

Figure G.5: NH$_3$ concentrations at outlet Va-SCR (N$_2$O$_E$ = 100 [ppm], ϕ = 0.55, $^{NO_2}/_{NO_X}$ = 0.075).

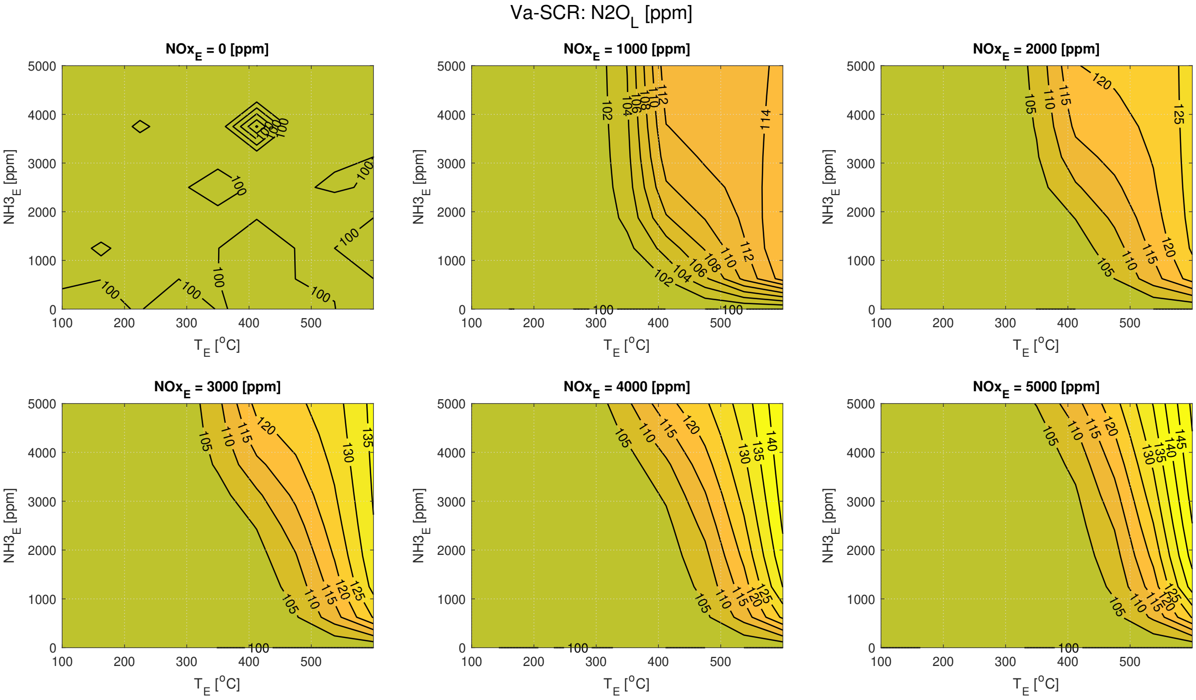

Figure G.6: N_2O concentrations at outlet Va-SCR (N_2O_E = 100 [ppm], ϕ = 0.55, $^{NO_2}/_{NO_X}$ = 0.075).

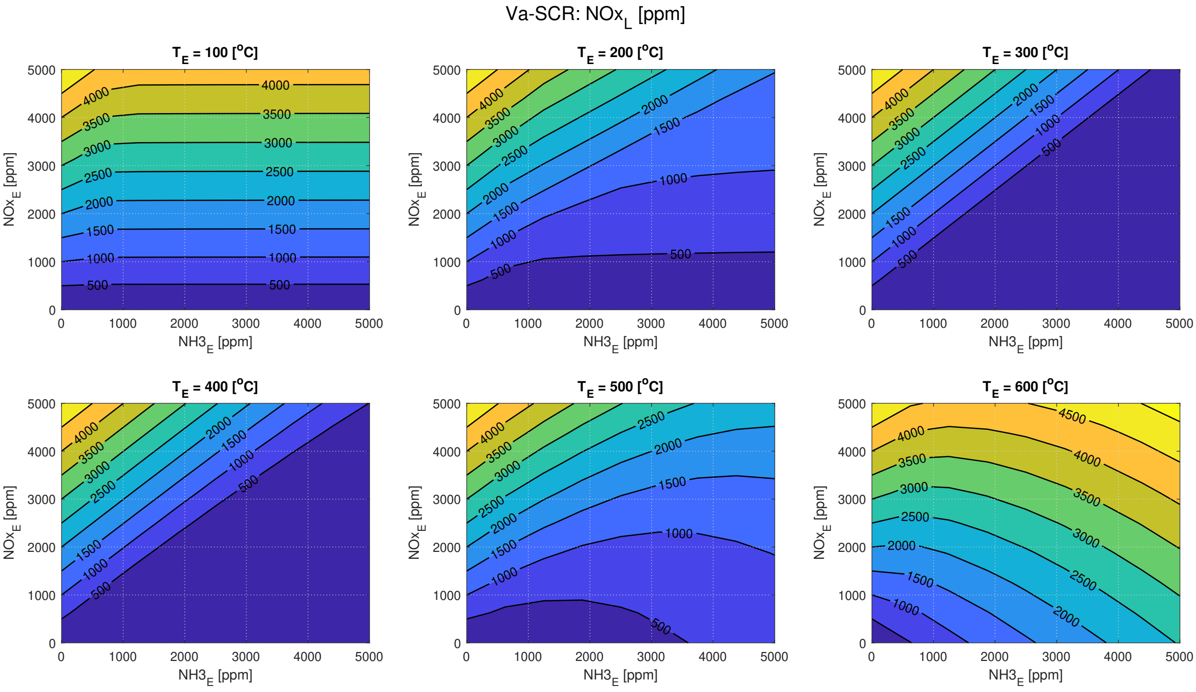

Figure G.7: NO_X concentrations at outlet Va-SCR (N_2O_E = 100 [ppm], ϕ = 0.55, $^{NO_2}/_{NO_X}$ = 0.075).

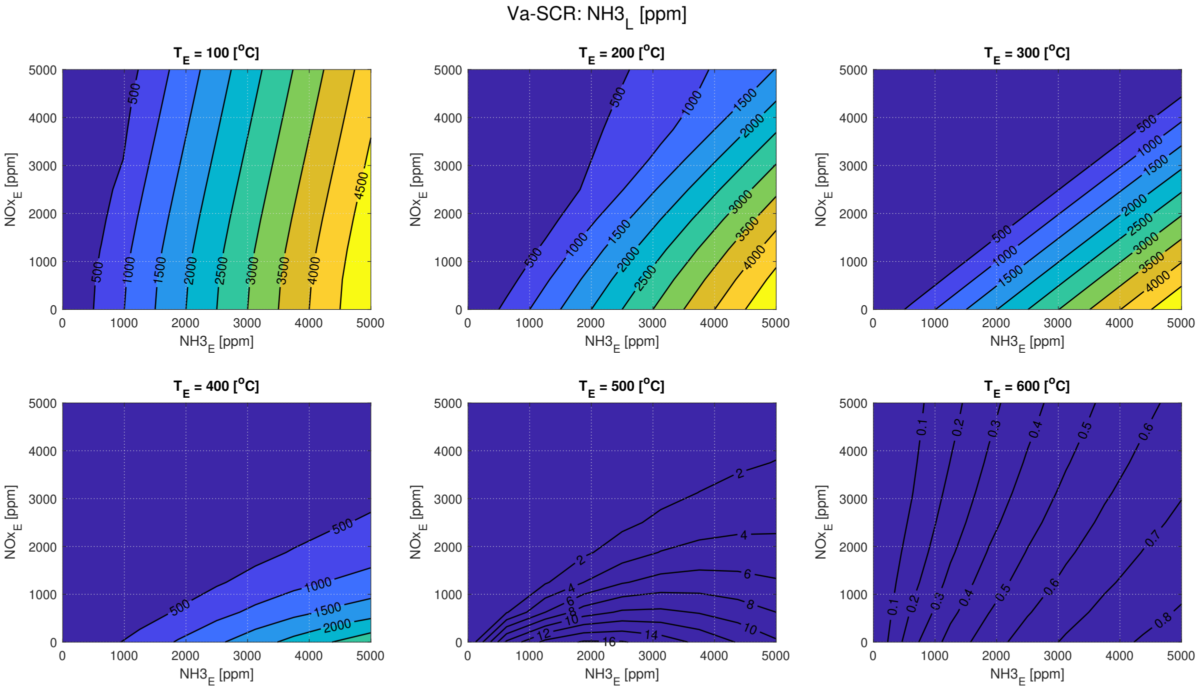

Figure G.8: NH_3 concentrations at outlet Va-SCR (N_2O_E = 100 [ppm], ϕ = 0.55, $^{NO_2}/_{NO_X}$ = 0.075).

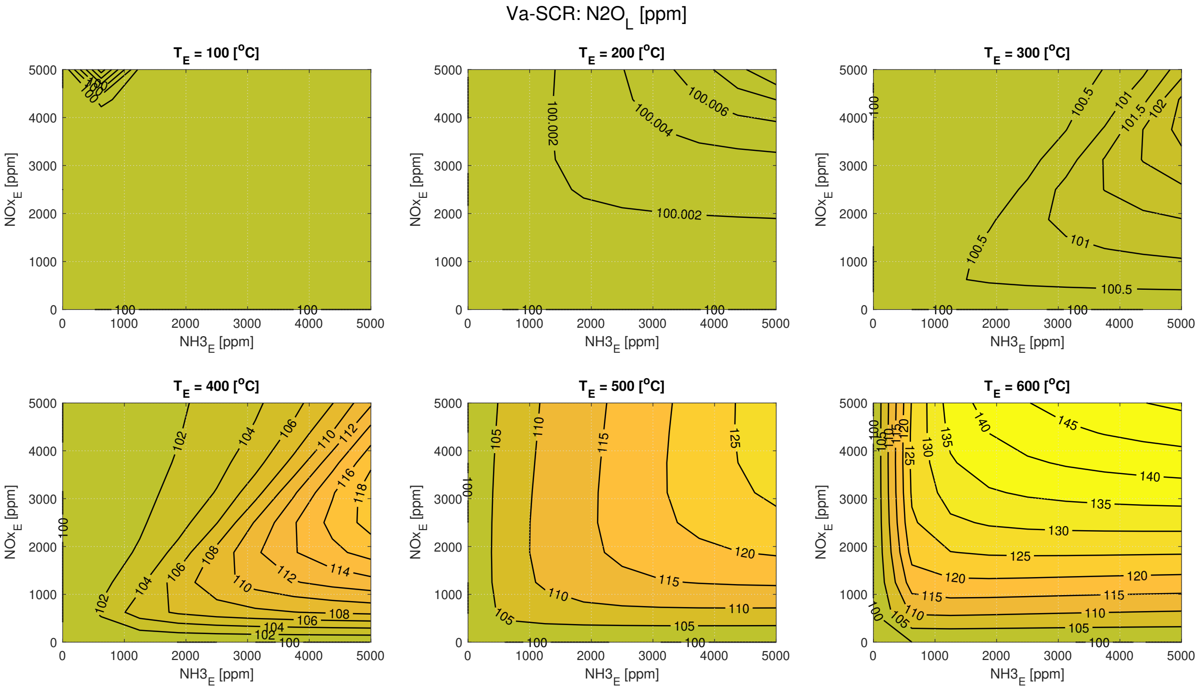

Figure G.9: N_2O concentrations at outlet Va-SCR (N_2O_E = 100 [ppm], ϕ = 0.55, $^{NO_2}/_{NO_X}$ = 0.075).

H

Fe Parameter Effect

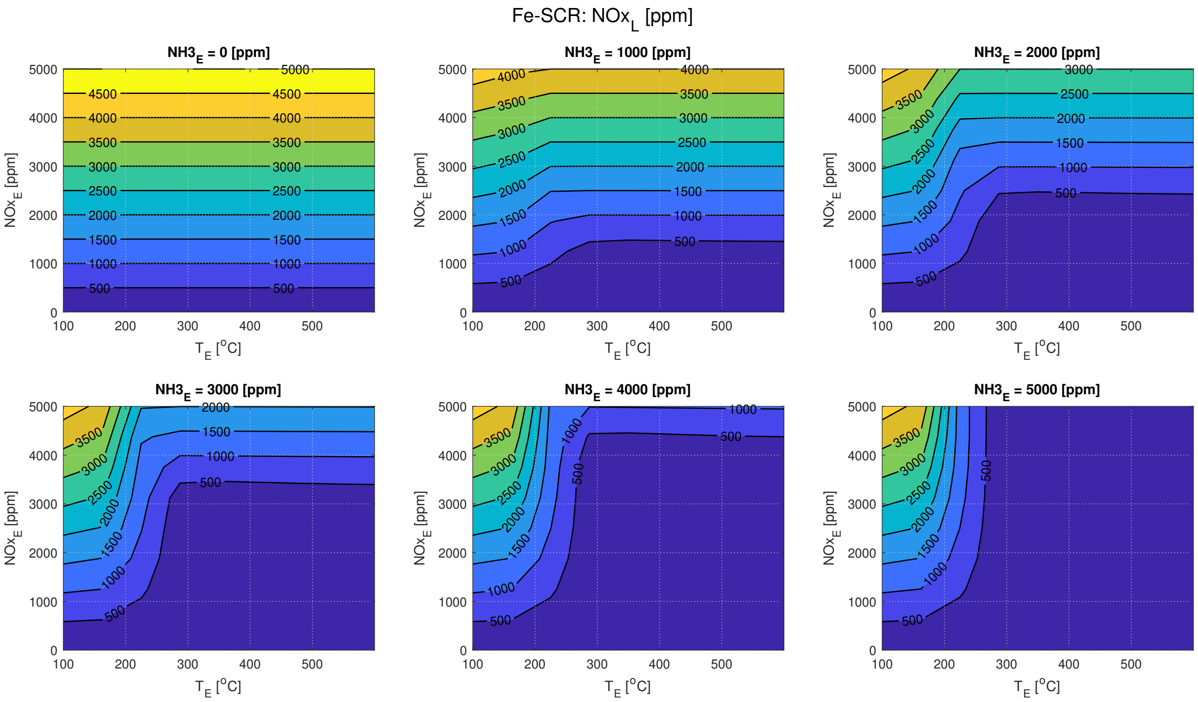

Figure H.1: NO$_X$ concentrations at outlet Fe-SCR (N$_2$O$_E$ = 100 [ppm], ϕ = 0.55, $^{NO_2}/_{NO_X}$ = 0.075).

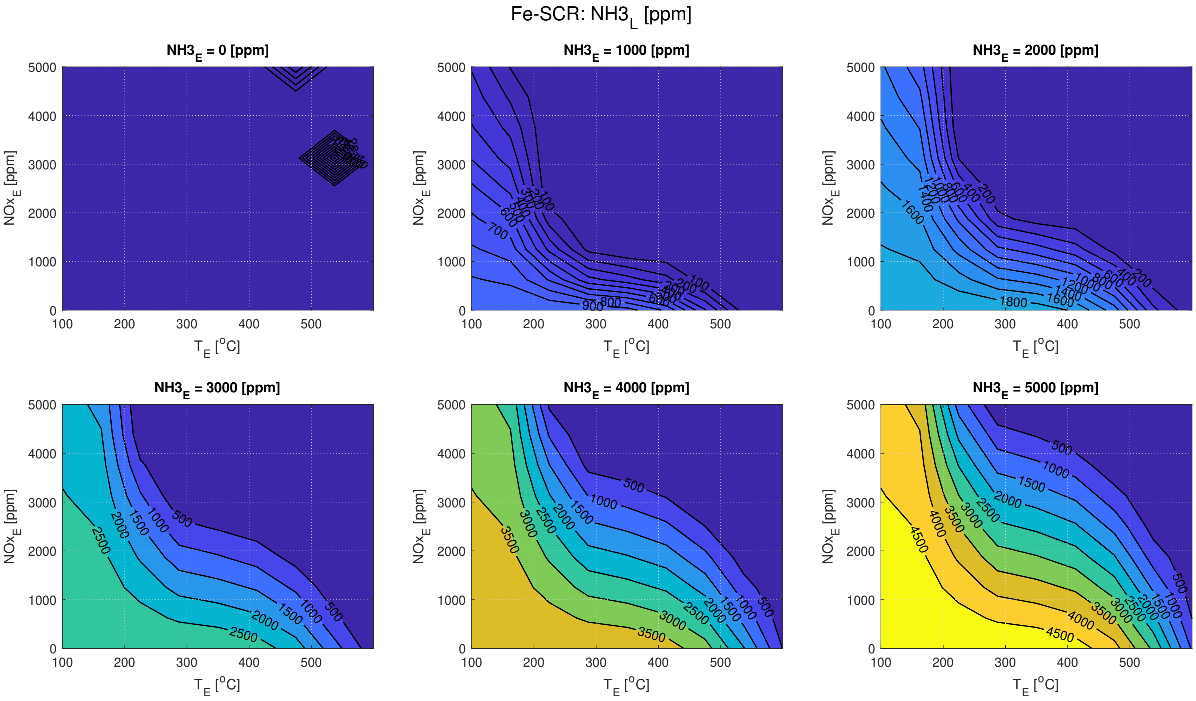

Figure H.2: NH$_3$ concentrations at outlet Fe-SCR (N$_2$O$_E$ = 100 [ppm], ϕ = 0.55, $^{NO_2}/_{NO_X}$ = 0.075).

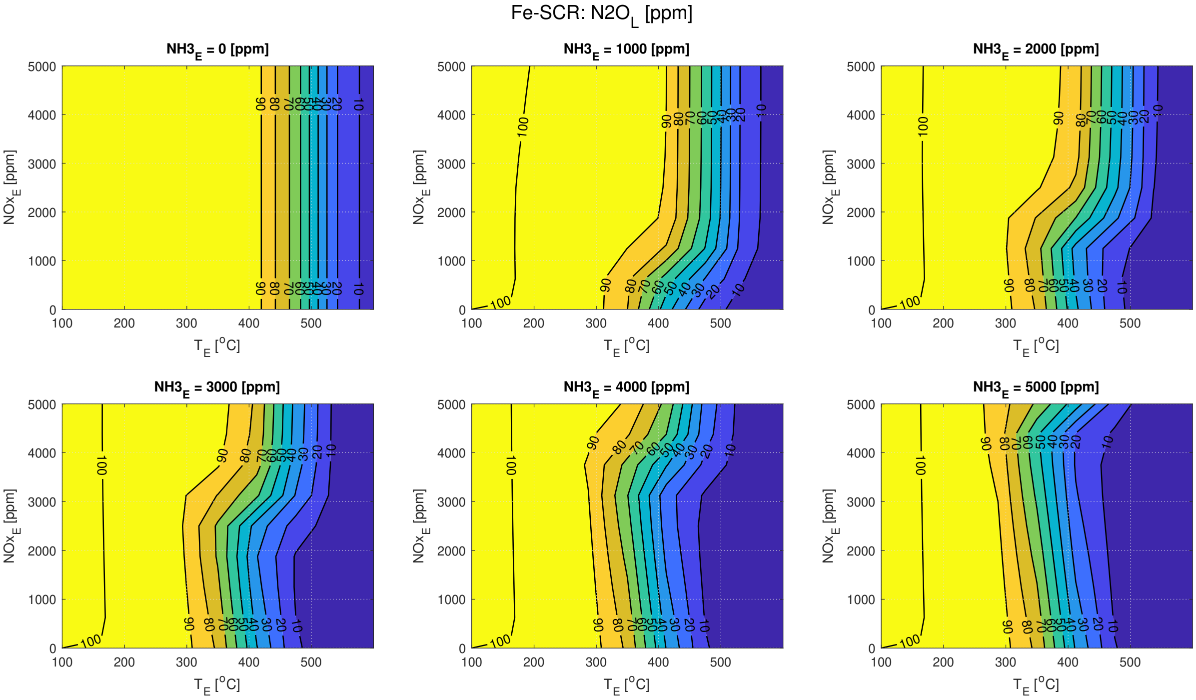

Figure H.3: N$_2$O concentrations at outlet Fe-SCR (N$_2$O$_E$ = 100 [ppm], ϕ = 0.55, $^{NO_2}/_{NO_X}$ = 0.075).

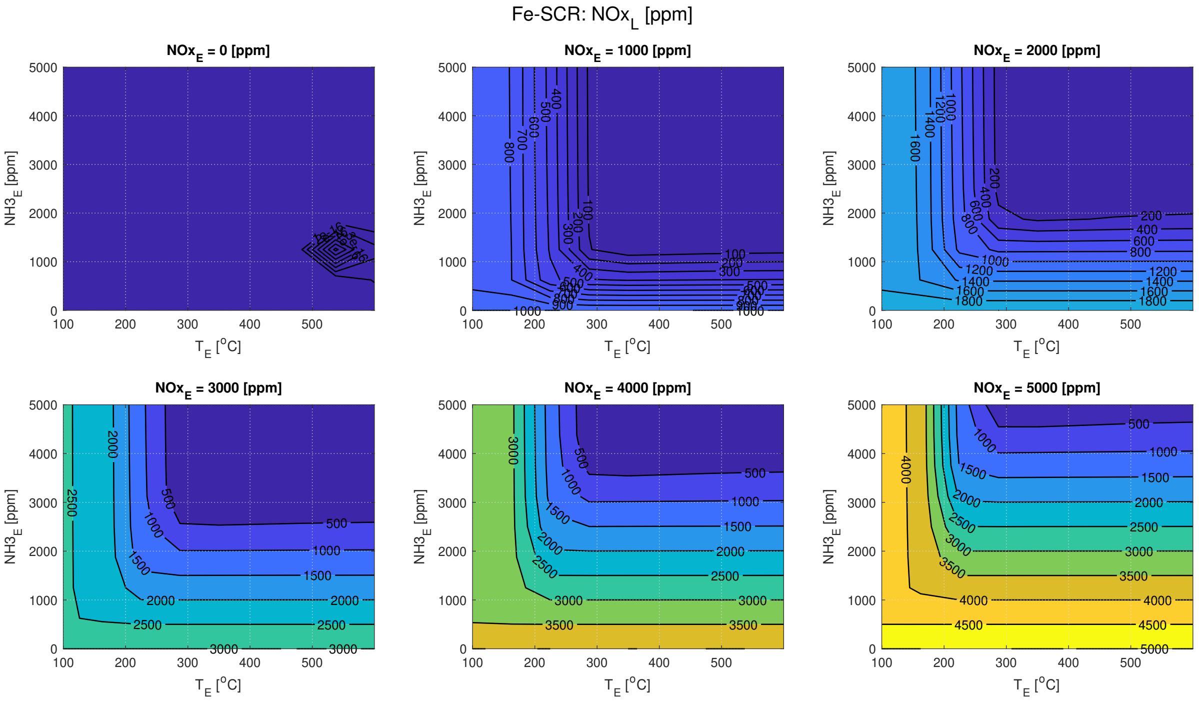

Figure H.4: NO$_X$ concentrations at outlet Fe-SCR (N$_2$O$_E$ = 100 [ppm], ϕ = 0.55, ${}^{NO_2}/_{NO_X}$ = 0.075).

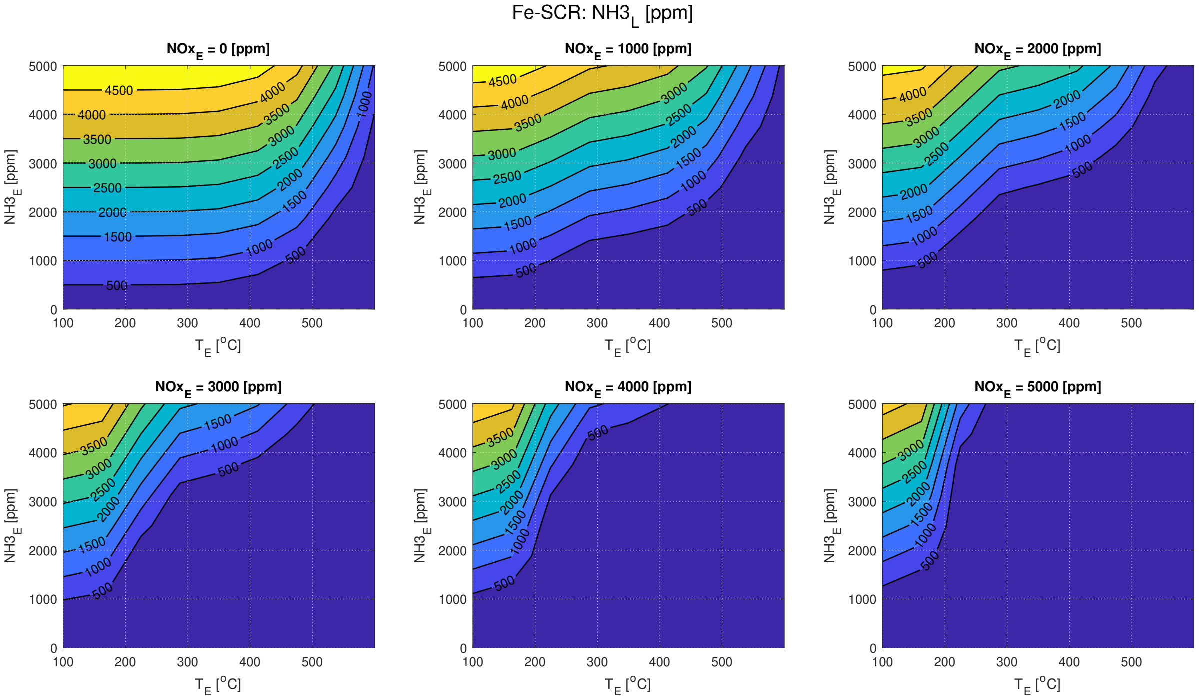

Figure H.5: NH$_3$ concentrations at outlet Fe-SCR (N$_2$O$_E$ = 100 [ppm], ϕ = 0.55, ${}^{NO_2}/_{NO_X}$ = 0.075).

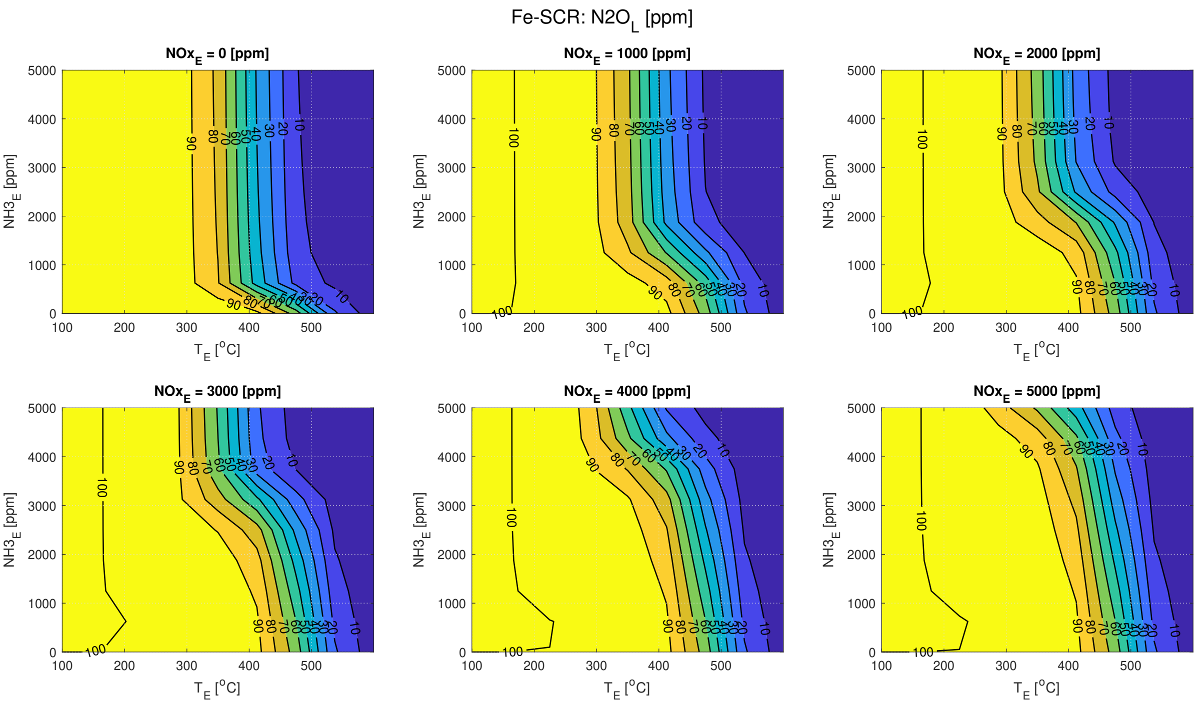

Figure H.6: N_2O concentrations at outlet Fe-SCR (N_2O_E = 100 [ppm], ϕ = 0.55, $^{NO_2}/_{NO_X}$ = 0.075).

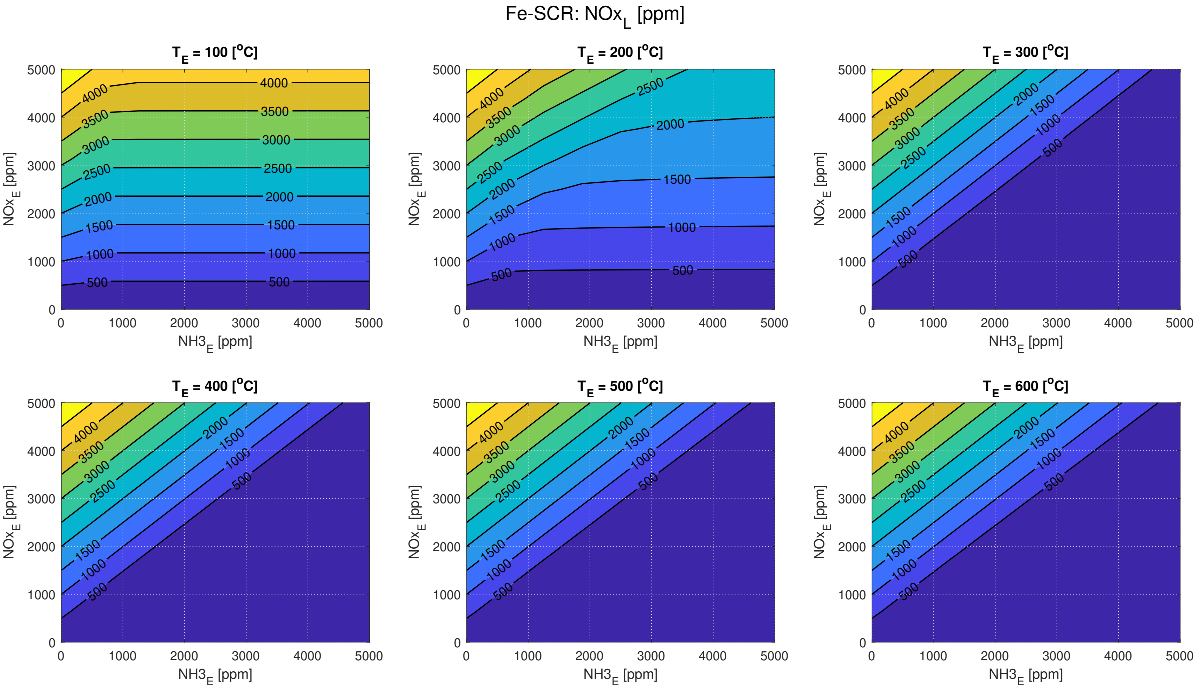

Figure H.7: NO_X concentrations at outlet Fe-SCR (N_2O_E = 100 [ppm], ϕ = 0.55, $^{NO_2}/_{NO_X}$ = 0.075).

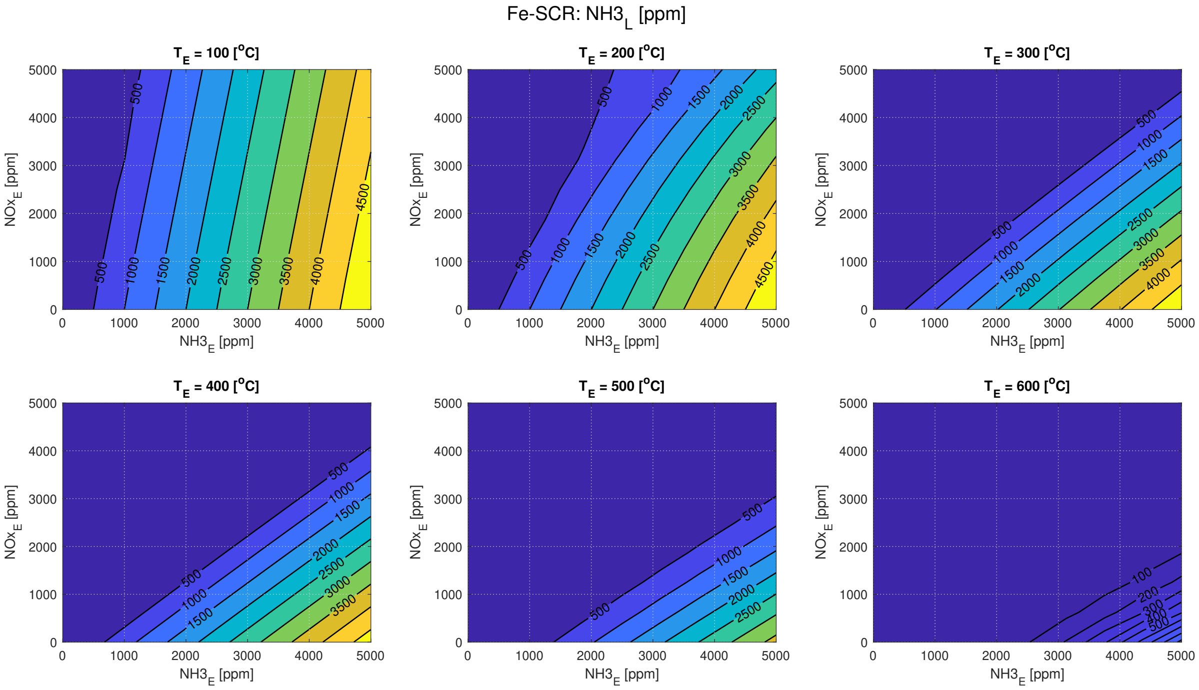

Figure H.8: NH_3 concentrations at outlet Fe-SCR (N_2O_E = 100 [ppm], ϕ = 0.55, ${}^{NO_2}/_{NO_X}$ = 0.075).

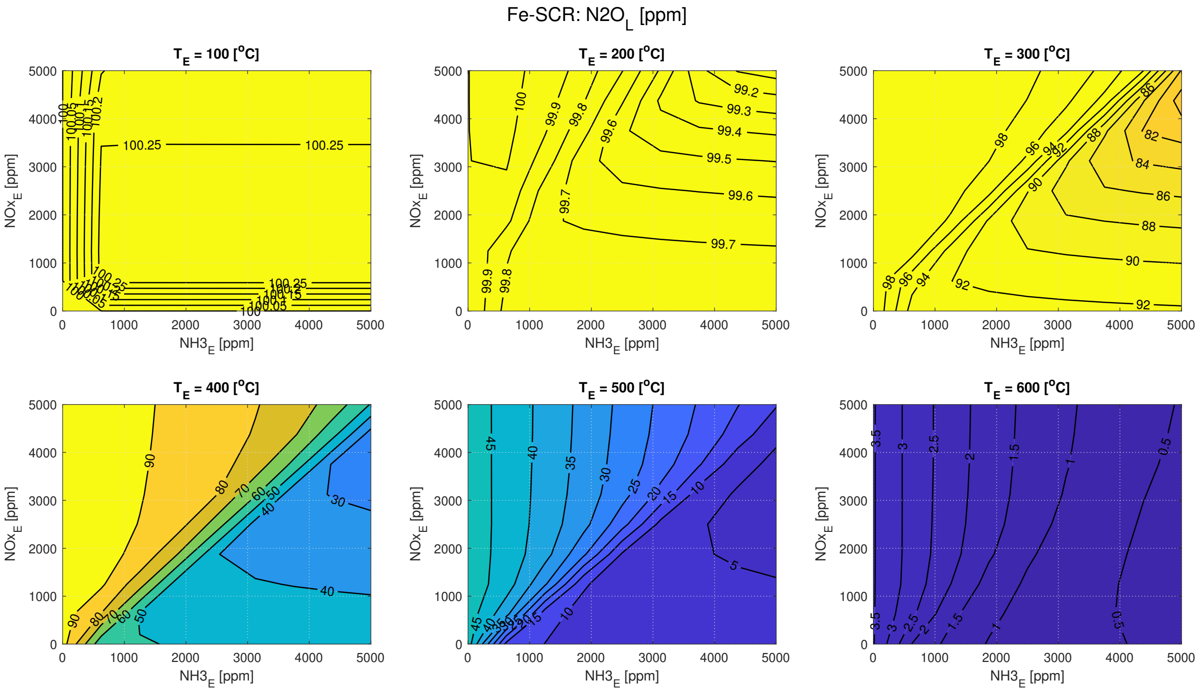

Figure H.9: N_2O concentrations at outlet Fe-SCR (N_2O_E = 100 [ppm], ϕ = 0.55, ${}^{NO_2}/_{NO_X}$ = 0.075).

Cu Parameter Effect

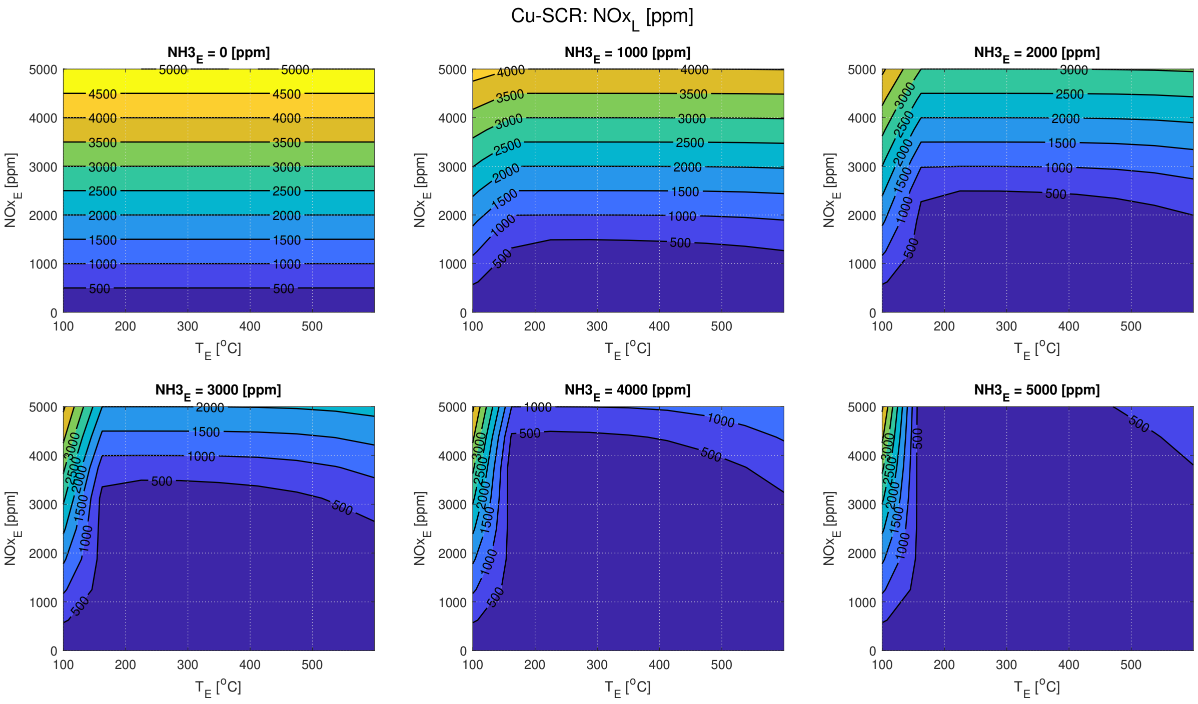

Figure I.1: NO$_X$ concentrations at outlet Cu-SCR (N$_2$O$_E$ = 100 [ppm], ϕ = 0.55, $^{NO_2}/_{NO_X}$ = 0.075).

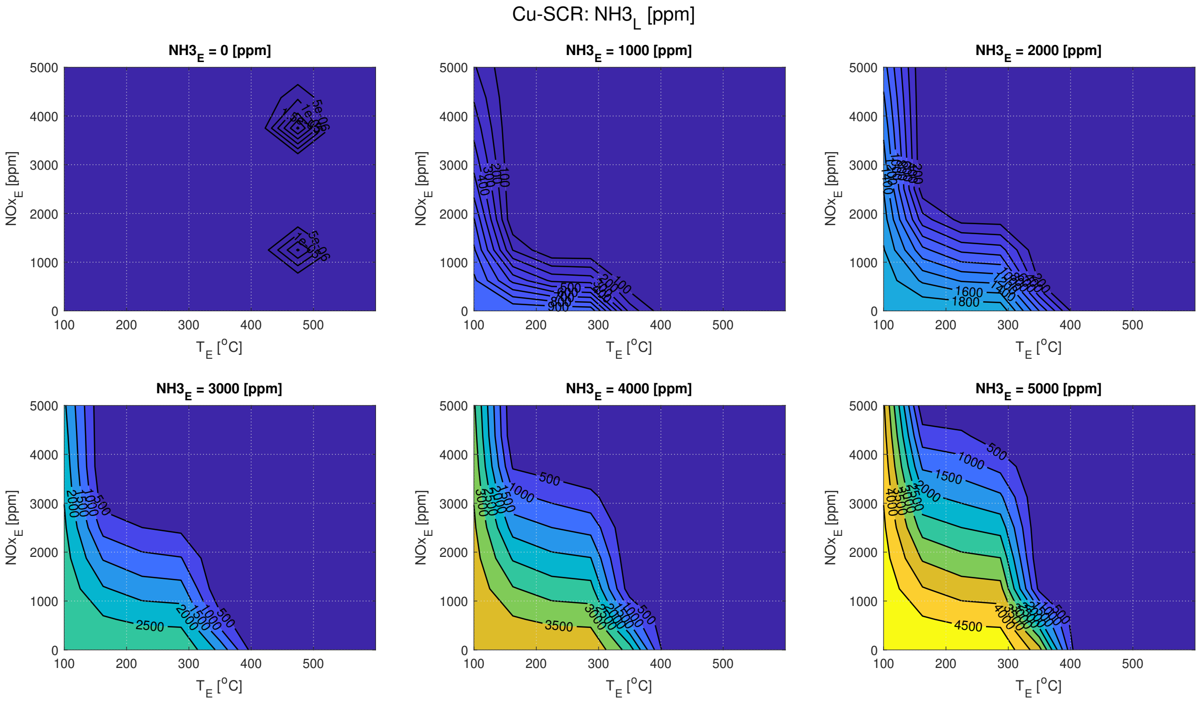

Figure I.2: NH_3 concentrations at outlet Cu-SCR (N_2O_E = 100 [ppm], ϕ = 0.55, $^{NO_2}/_{NO_x}$ = 0.075).

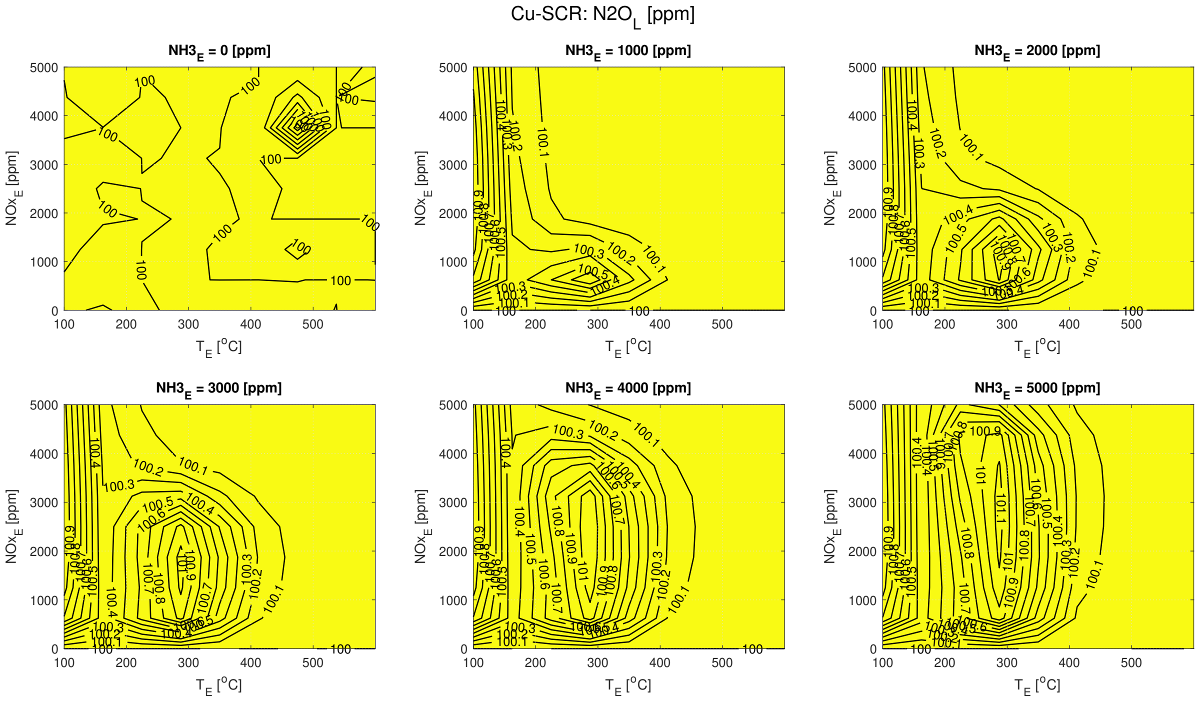

Figure I.3: N_2O concentrations at outlet Cu-SCR (N_2O_E = 100 [ppm], ϕ = 0.55, $^{NO_2}/_{NO_x}$ = 0.075).

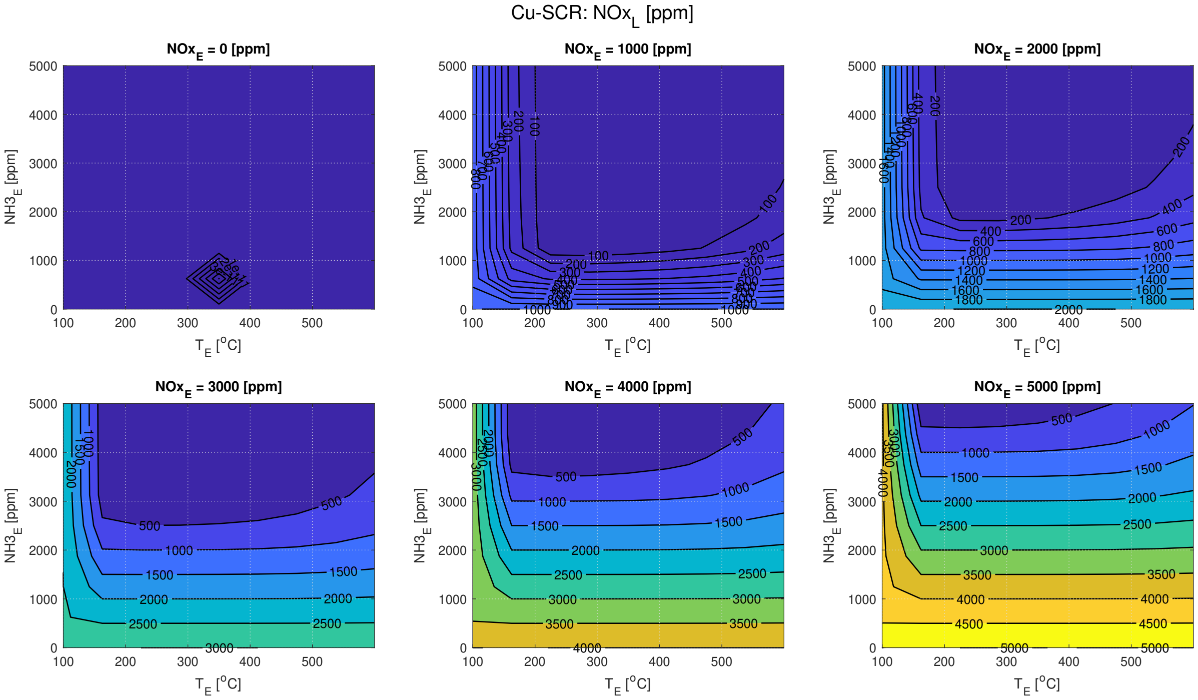

Figure I.4: NO_X concentrations at outlet Cu-SCR (N_2O_E = 100 [ppm], ϕ = 0.55, $^{NO_2}/_{NO_X}$ = 0.075).

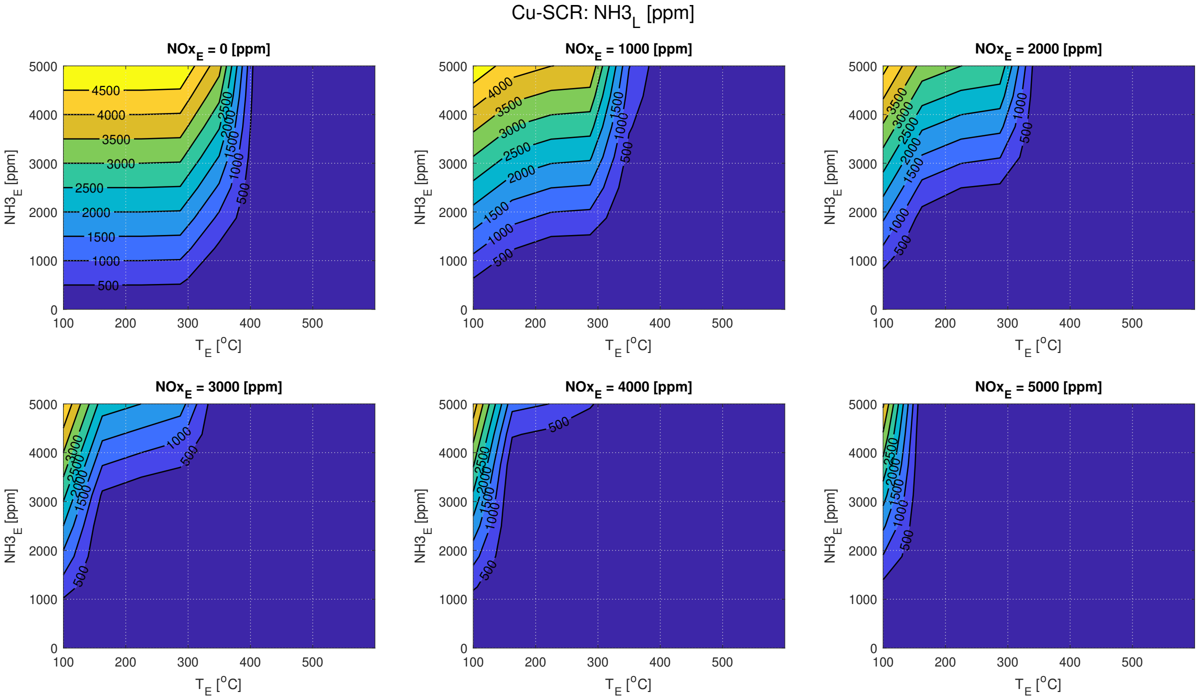

Figure I.5: NH_3 concentrations at outlet Cu-SCR (N_2O_E = 100 [ppm], ϕ = 0.55, $^{NO_2}/_{NO_X}$ = 0.075).

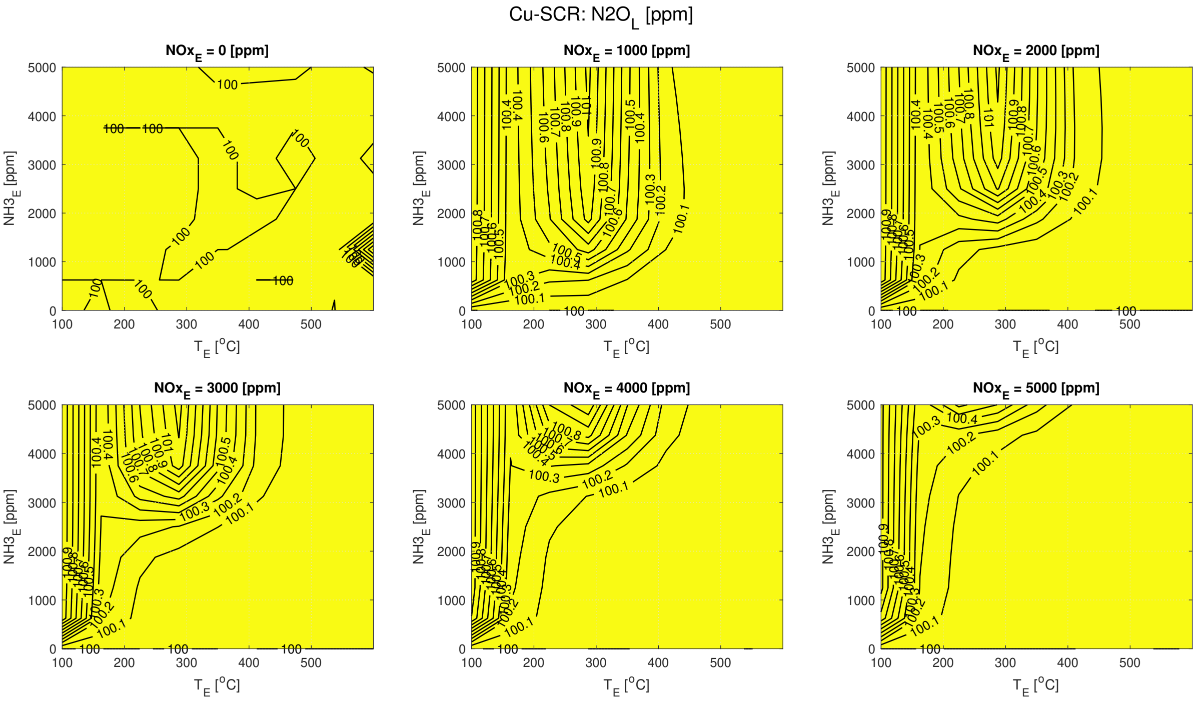

Figure I.6: N_2O concentrations at outlet Cu-SCR (N_2O_E = 100 [ppm], ϕ = 0.55, ${}^{NO_2}/_{NO_X}$ = 0.075).

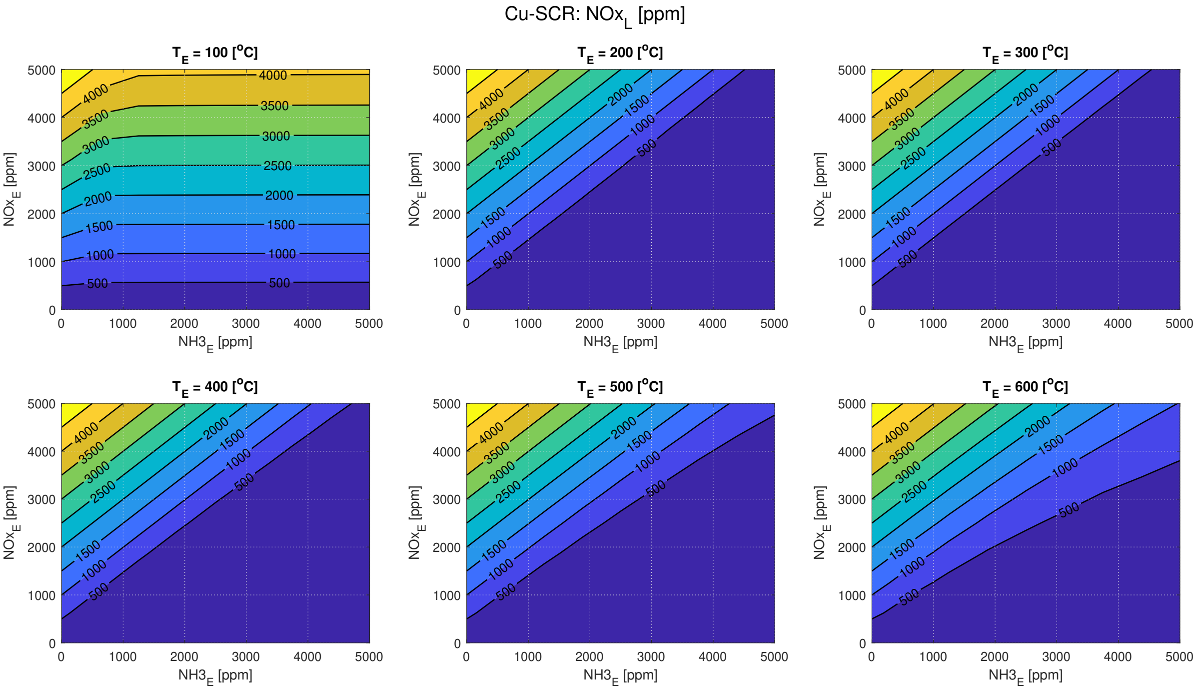

Figure I.7: NO_X concentrations at outlet Cu-SCR (N_2O_E = 100 [ppm], ϕ = 0.55, ${}^{NO_2}/_{NO_X}$ = 0.075).

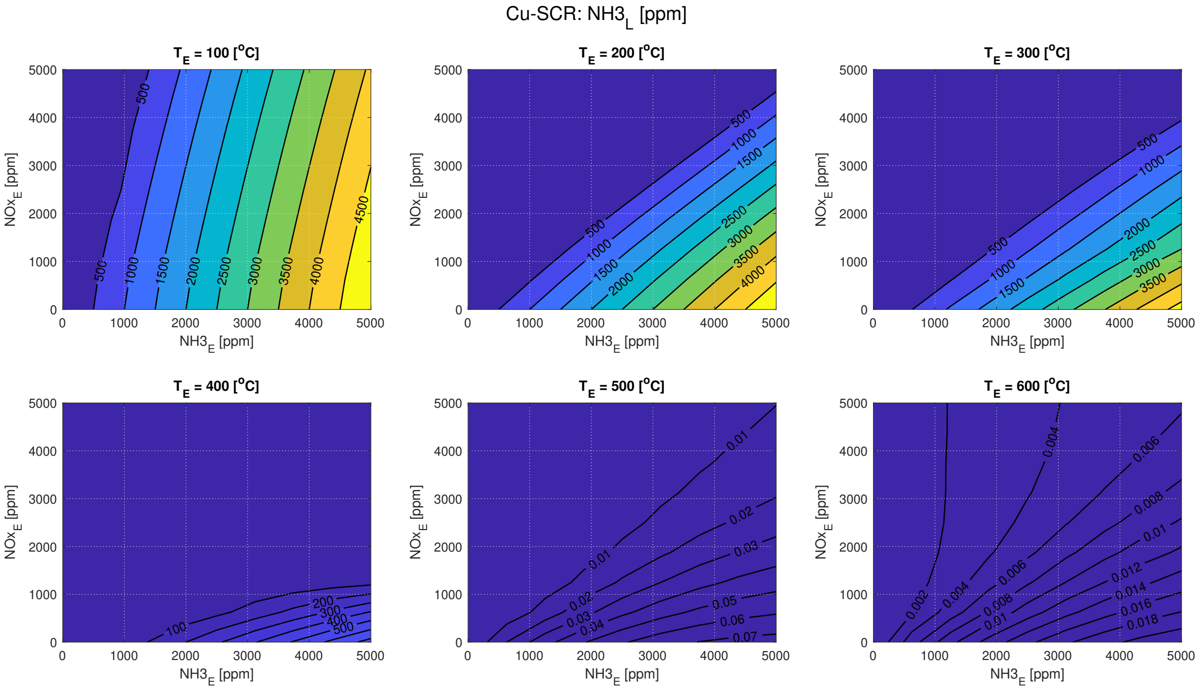

Figure I.8: NH$_3$ concentrations at outlet Cu-SCR (N$_2$O$_E$ = 100 [ppm], ϕ = 0.55, $^{NO_2}/_{NO_X}$ = 0.075).

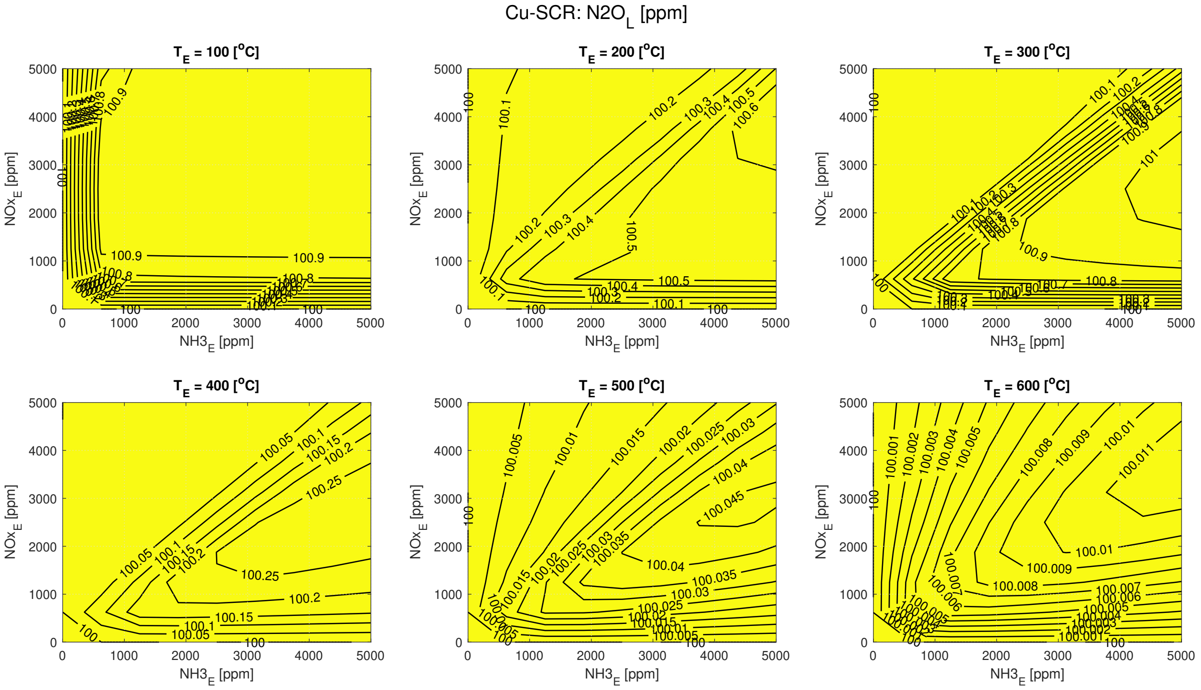

Figure I.9: N$_2$O concentrations at outlet Cu-SCR (N$_2$O$_E$ = 100 [ppm], ϕ = 0.55, $^{NO_2}/_{NO_X}$ = 0.075).

J

Operating range

J.1. Va

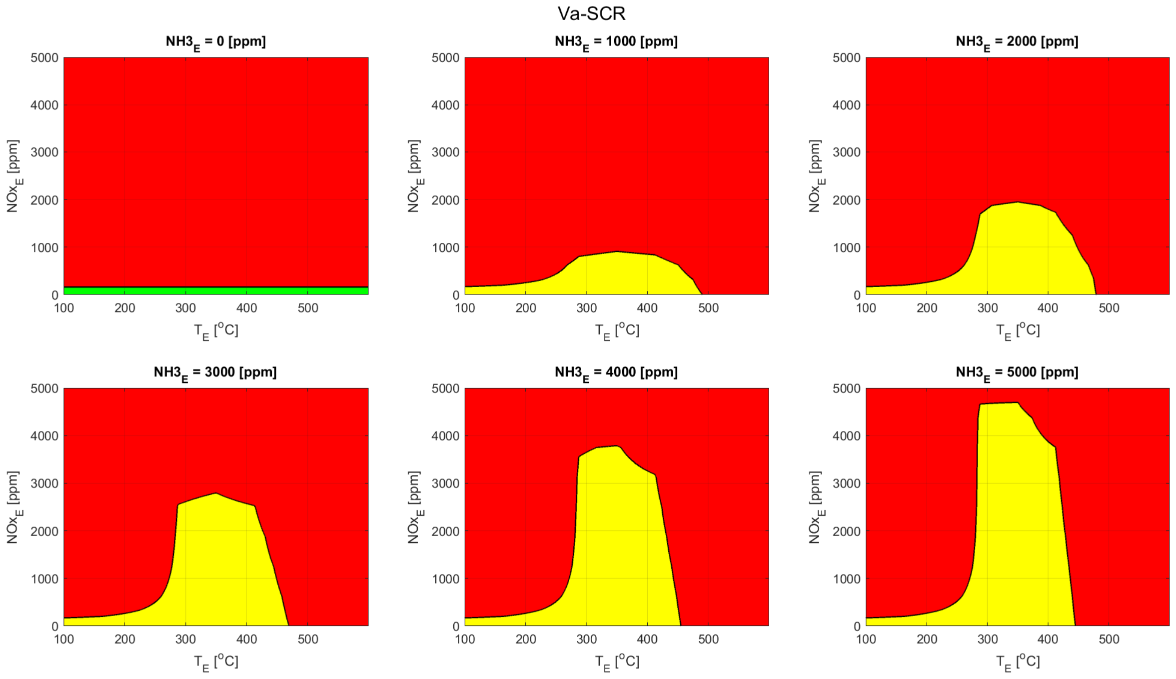

Figure J.1: Operating range Va-SCR (N_2O_E = 0 [ppm], ϕ = 0.2, $^{NO_2}/_{NO_X}$ = 0.075).

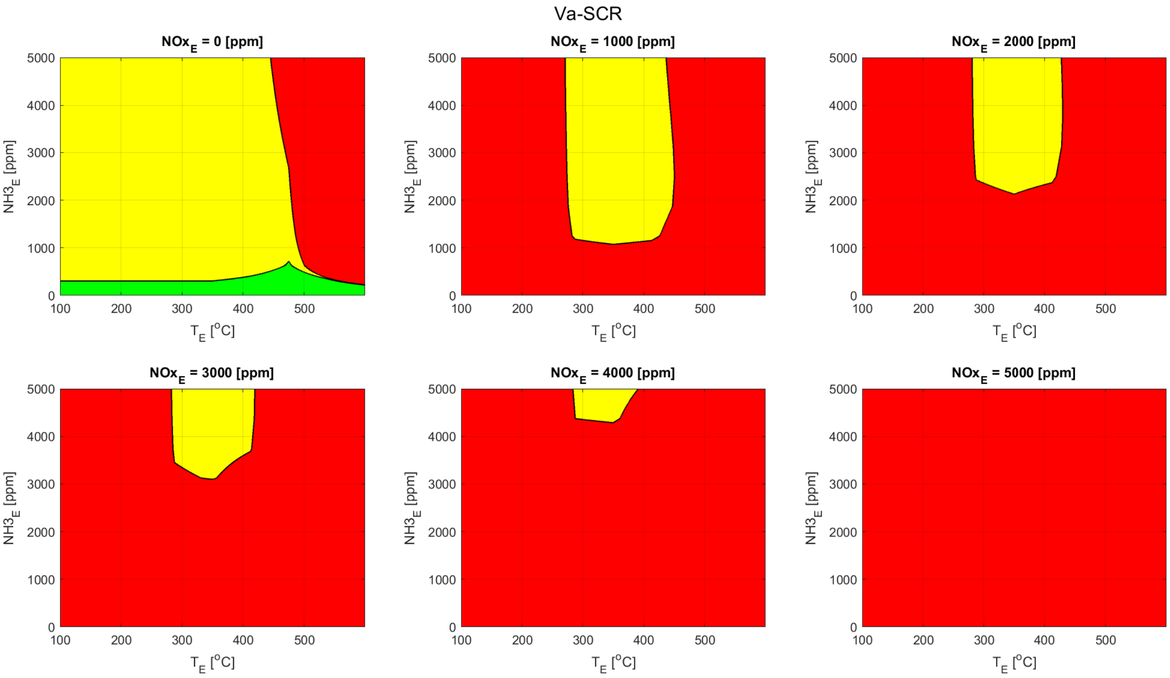

Figure J.2: Operating range Va-SCR (N_2O_E = 0 [ppm], ϕ = 0.2, $^{NO_2}/_{NO_X}$ = 0.075).

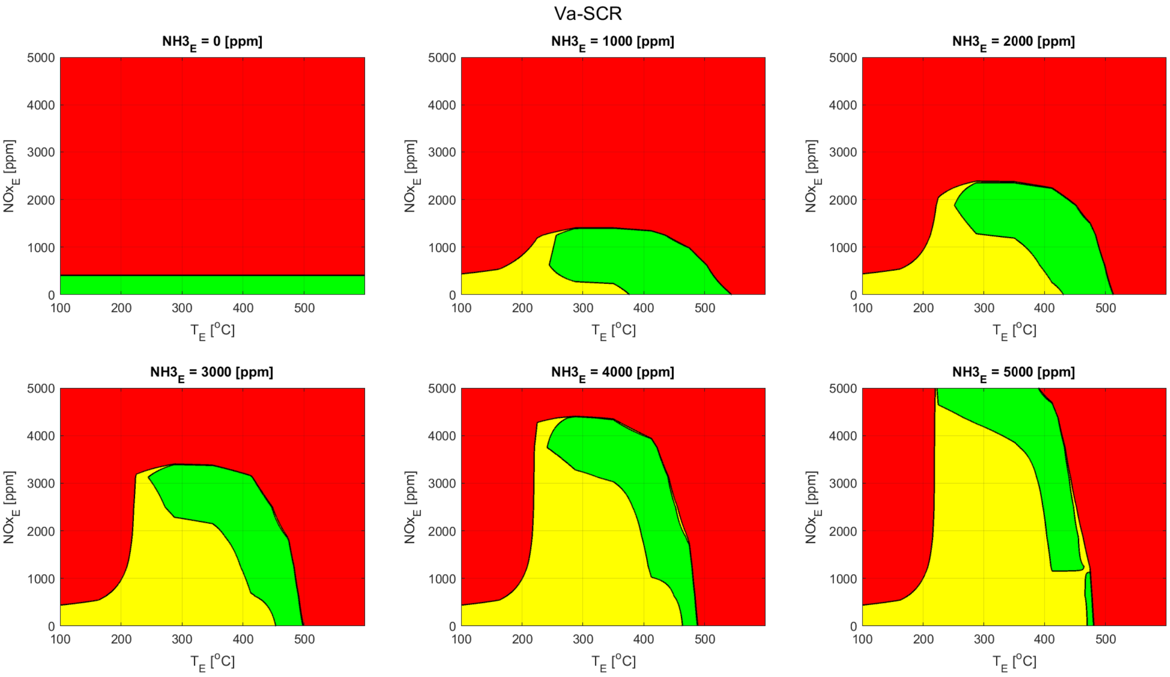

Figure J.3: Operating range Va-SCR (N_2O_E = 0 [ppm], ϕ = 0.55, $^{NO_2}/_{NO_X}$ = 0.075).

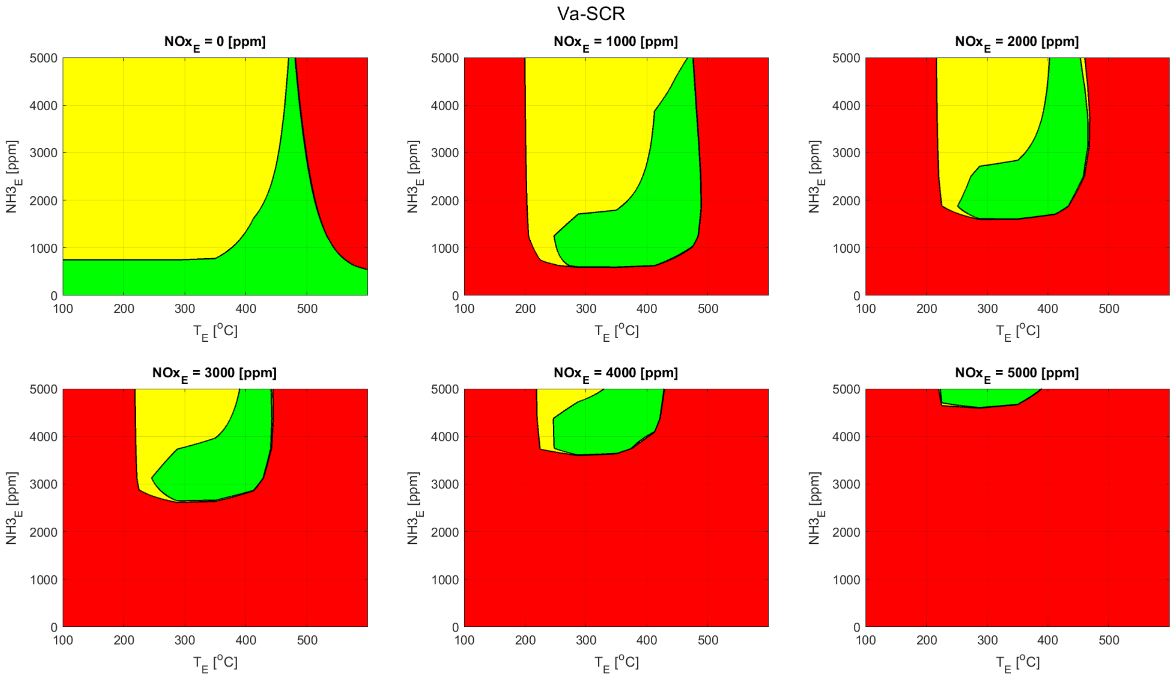

Figure J.4: Operating range Va-SCR (N_2O_E = 0 [ppm], ϕ = 0.55, $^{NO_2}/_{NO_X}$ = 0.075).

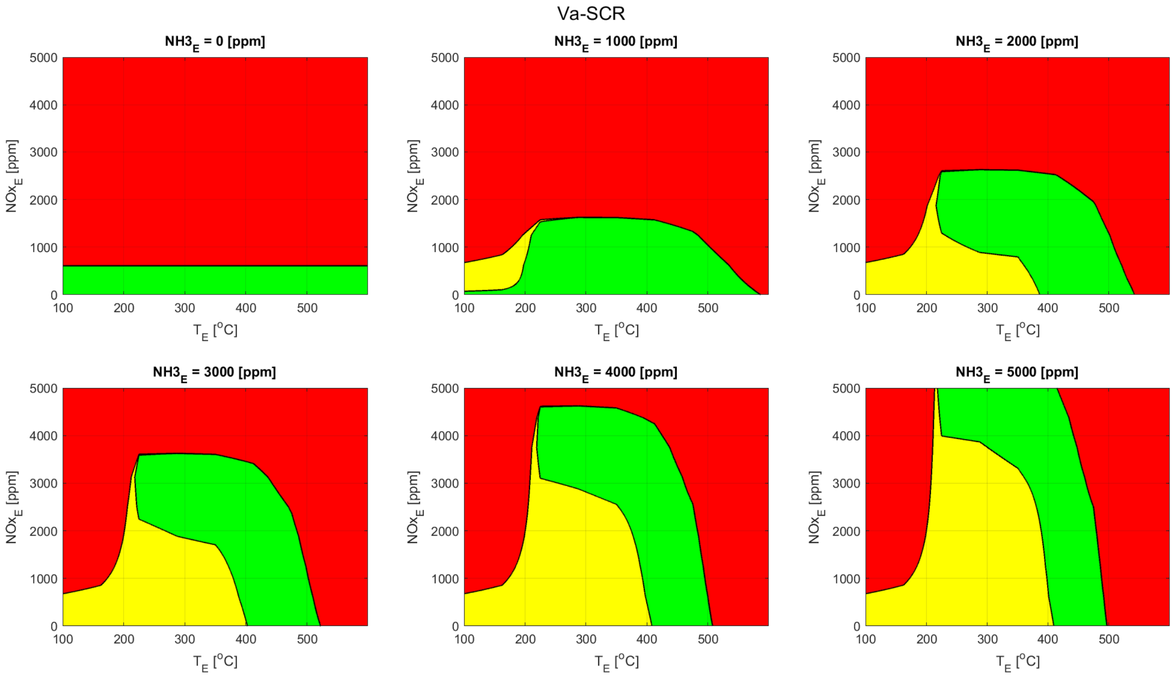

Figure J.5: Operating range Va-SCR (N_2O_E = 0 [ppm], ϕ = 0.9, $^{NO_2}/_{NO_X}$ = 0.075).

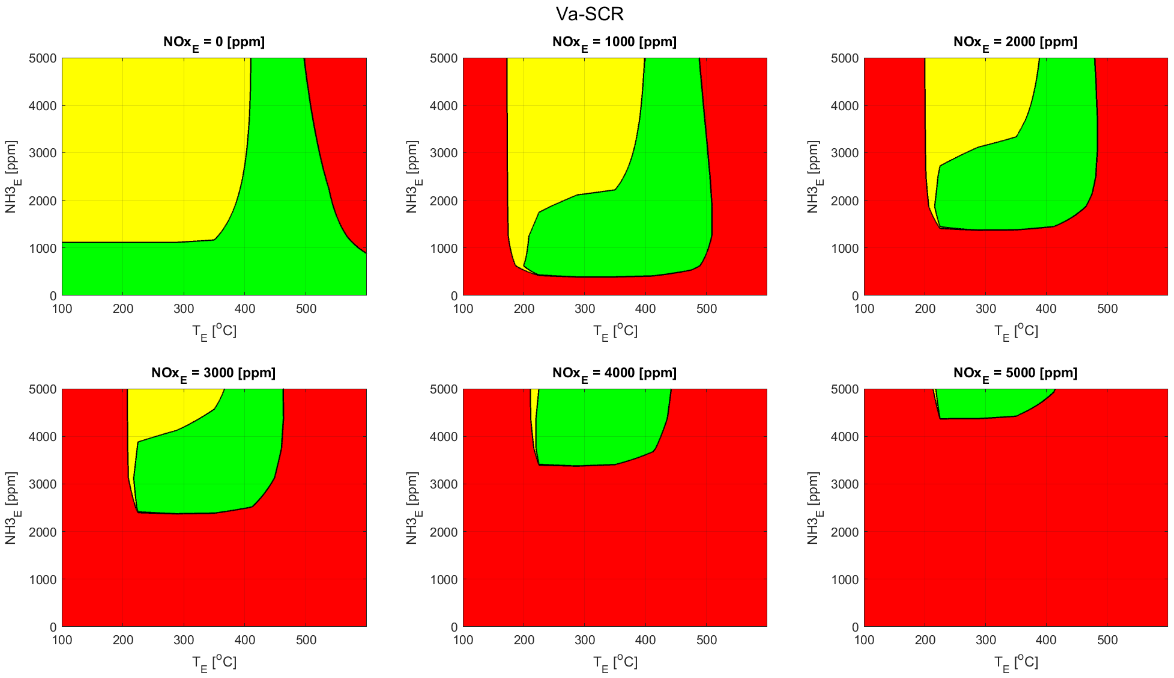

Figure J.6: Operating range Va-SCR (N_2O_E = 0 [ppm], ϕ = 0.9, ${}^{NO_2}/_{NO_X}$ = 0.075).

J.2. Fe

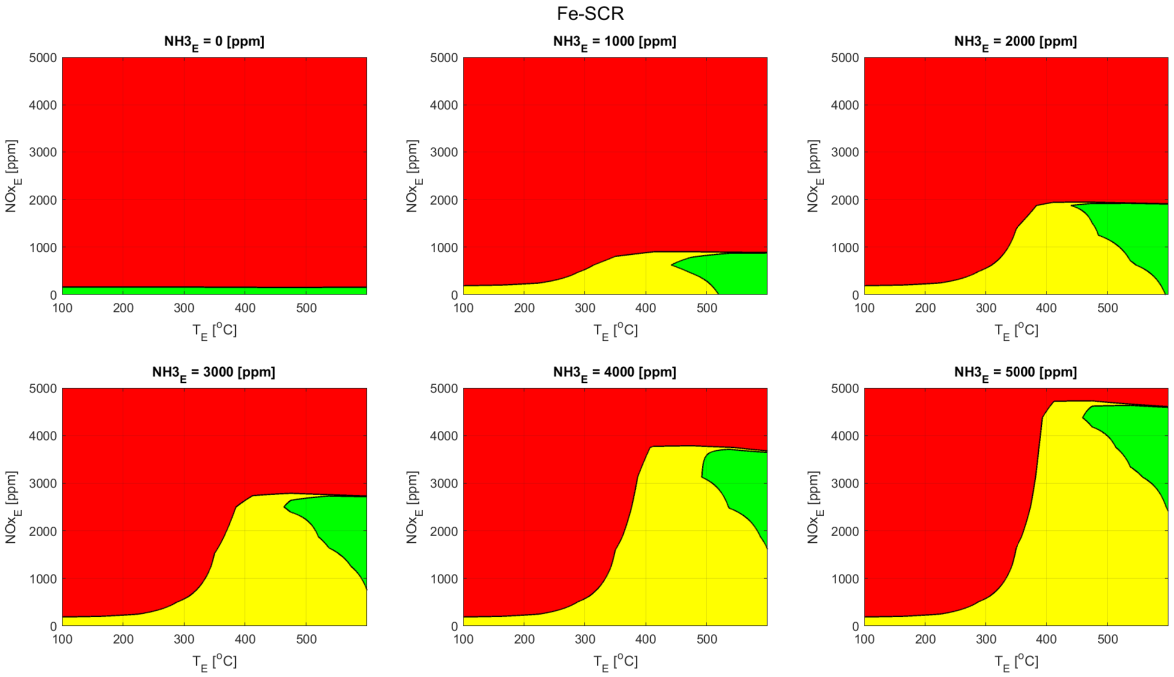

Figure J.7: Operating range Fe-SCR (N_2O_E = 0 [ppm], ϕ = 0.2, ${}^{NO_2}/_{NO_X}$ = 0.075).

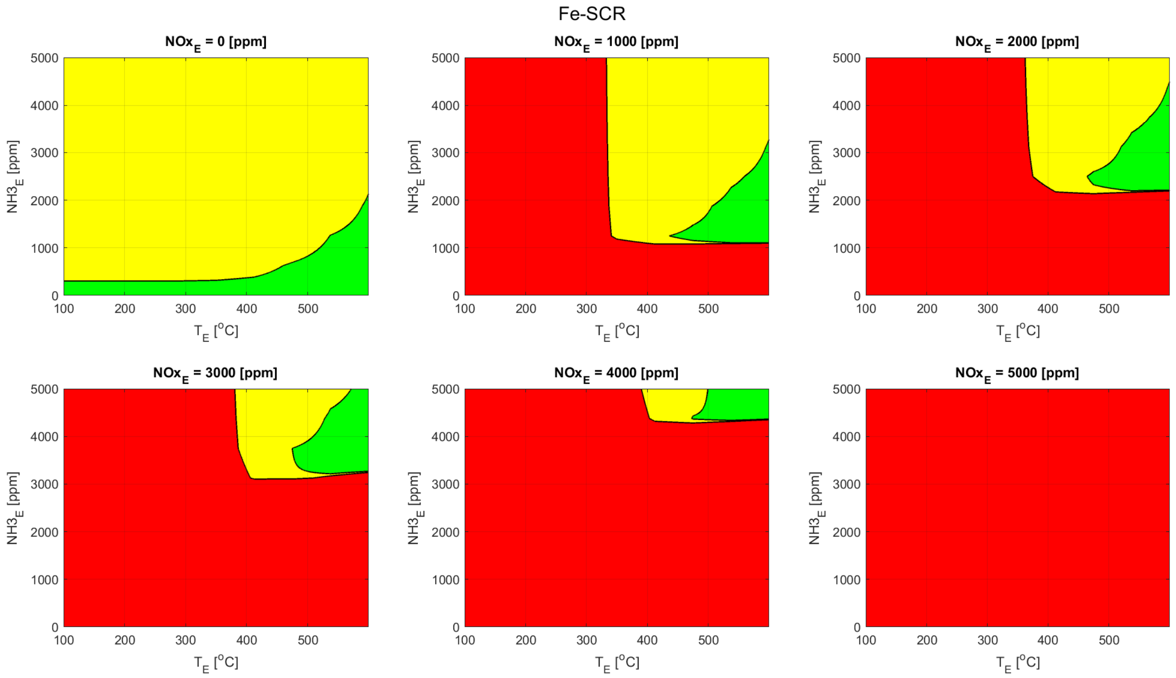

Figure J.8: Operating range Fe-SCR (N_2O_E = 0 [ppm], ϕ = 0.2, $^{NO_2}/_{NO_X}$ = 0.075).

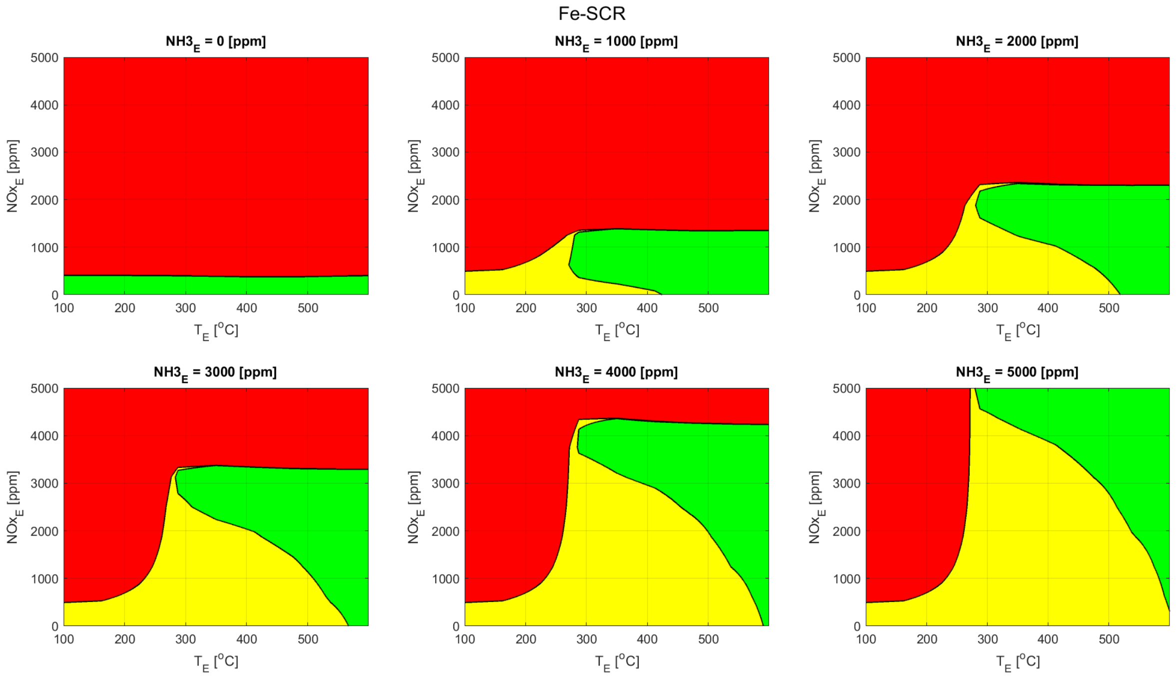

Figure J.9: Operating range Fe-SCR (N_2O_E = 0 [ppm], ϕ = 0.55, $^{NO_2}/_{NO_X}$ = 0.075).

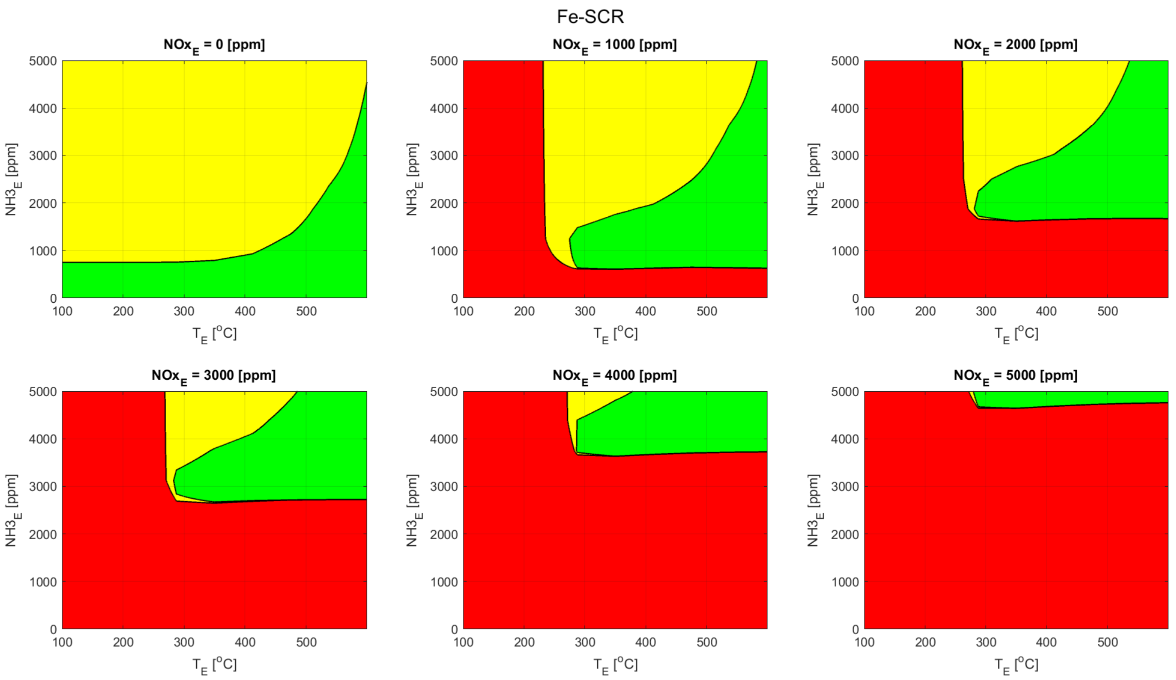

Figure J.10: Operating range Fe-SCR (N_2O_E = 0 [ppm], ϕ = 0.55, ${}^{NO_2}/_{NO_X}$ = 0.075).

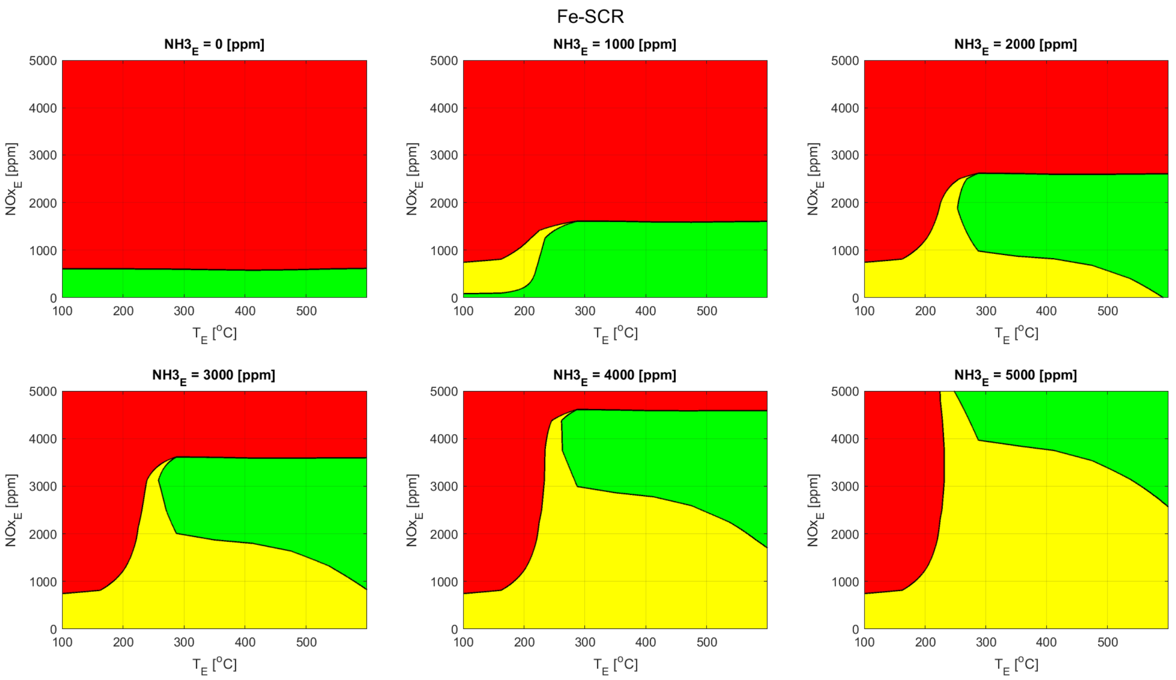

Figure J.11: Operating range Fe-SCR (N_2O_E = 0 [ppm], ϕ = 0.9, ${}^{NO_2}/_{NO_X}$ = 0.075).

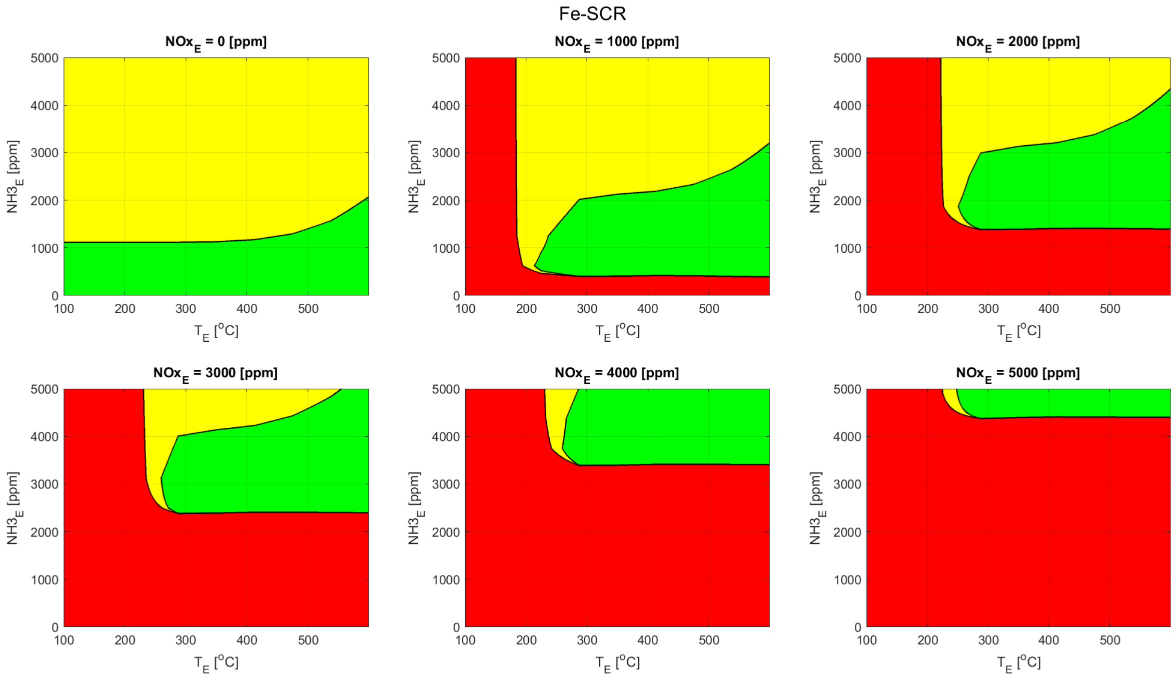

Figure J.12: Operating range Fe-SCR (N$_2$O$_E$ = 0 [ppm], ϕ = 0.9, $^{NO_2}/_{NO_X}$ = 0.075).

J.3. Cu

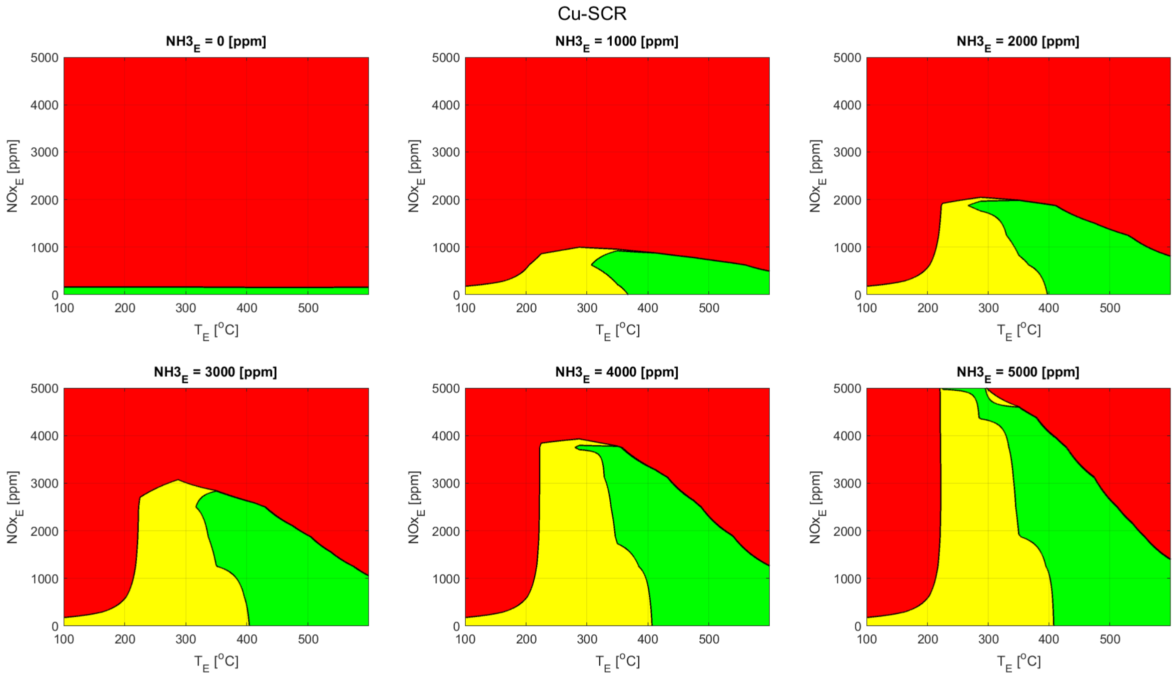

Figure J.13: Operating range Cu-SCR (N$_2$O$_E$ = 0 [ppm], ϕ = 0.2, $^{NO_2}/_{NO_X}$ = 0.075).

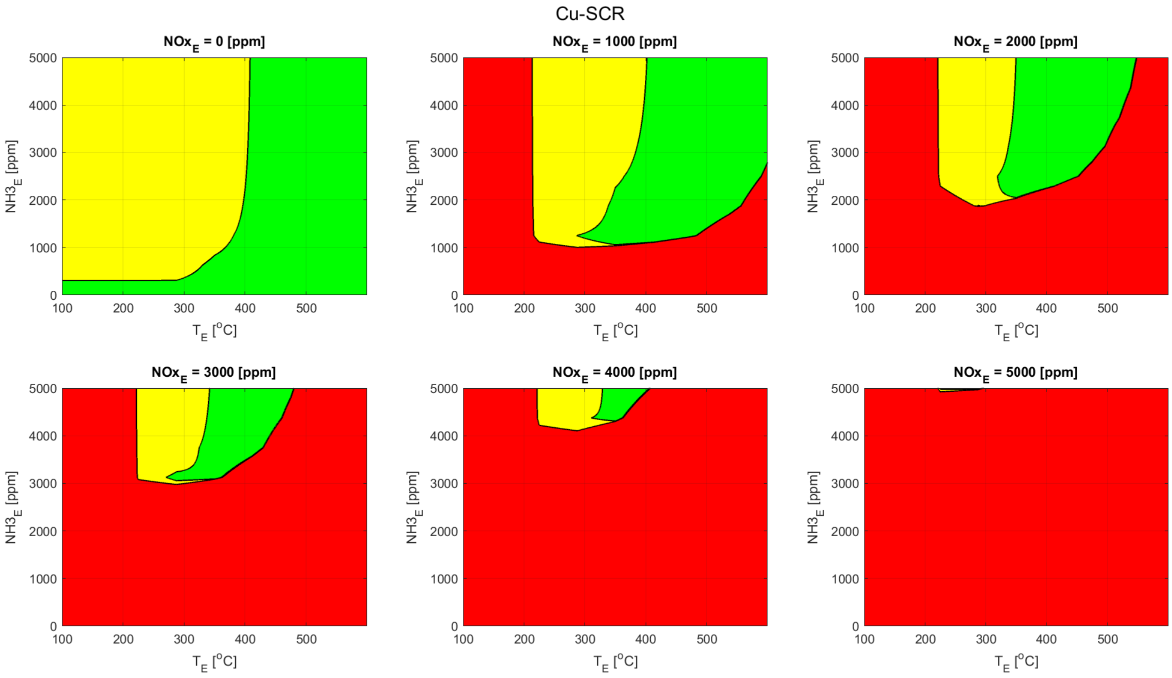

Figure J.14: Operating range Cu-SCR (N_2O_E = 0 [ppm], ϕ = 0.2, $^{NO_2}/_{NO_X}$ = 0.075).

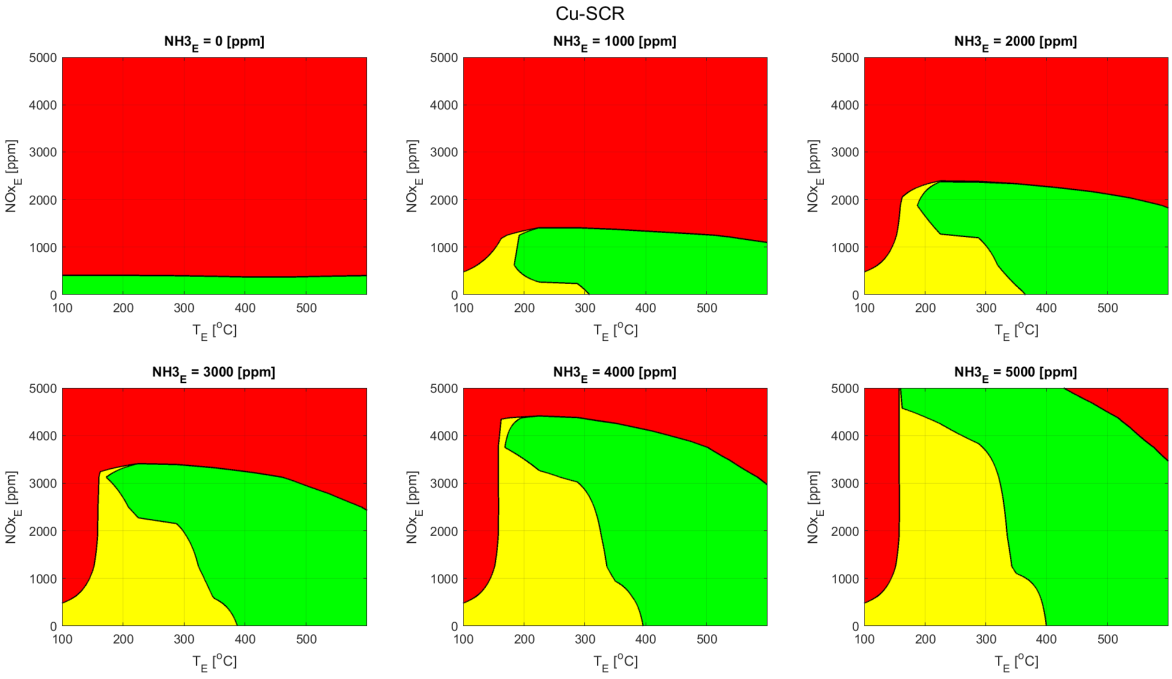

Figure J.15: Operating range Cu-SCR (N_2O_E = 0 [ppm], ϕ = 0.55, $^{NO_2}/_{NO_X}$ = 0.075).

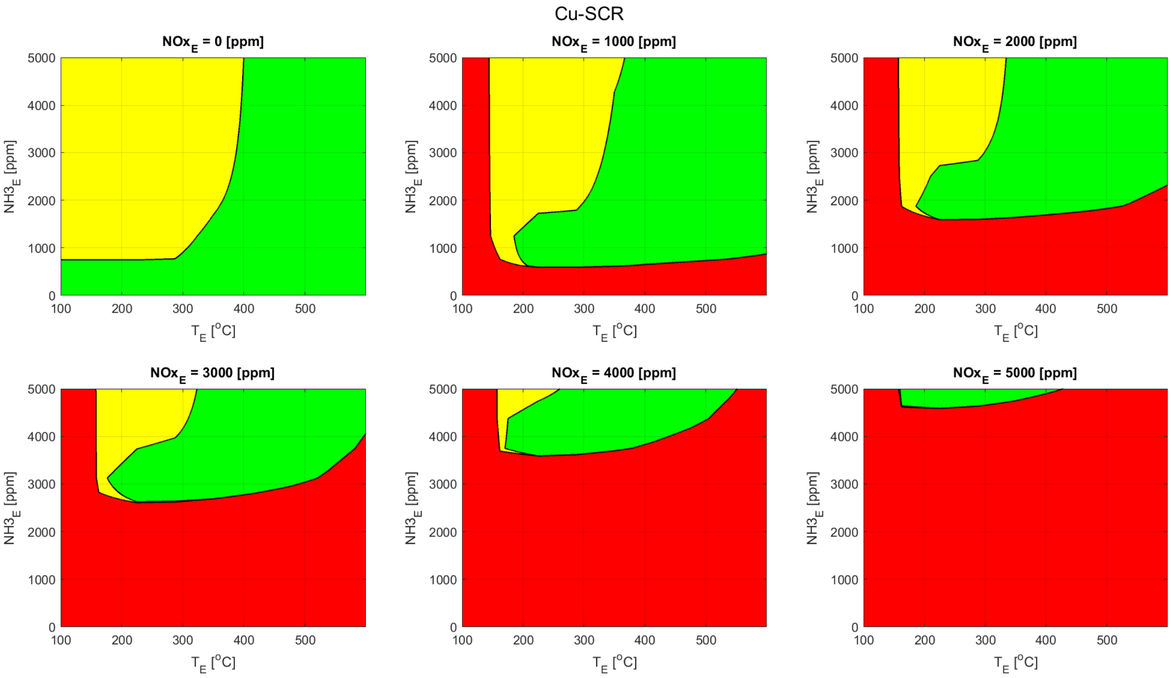

Figure J.16: Operating range Cu-SCR (N$_2$O$_E$ = 0 [ppm], ϕ = 0.55, $^{NO_2}/_{NO_X}$ = 0.075).

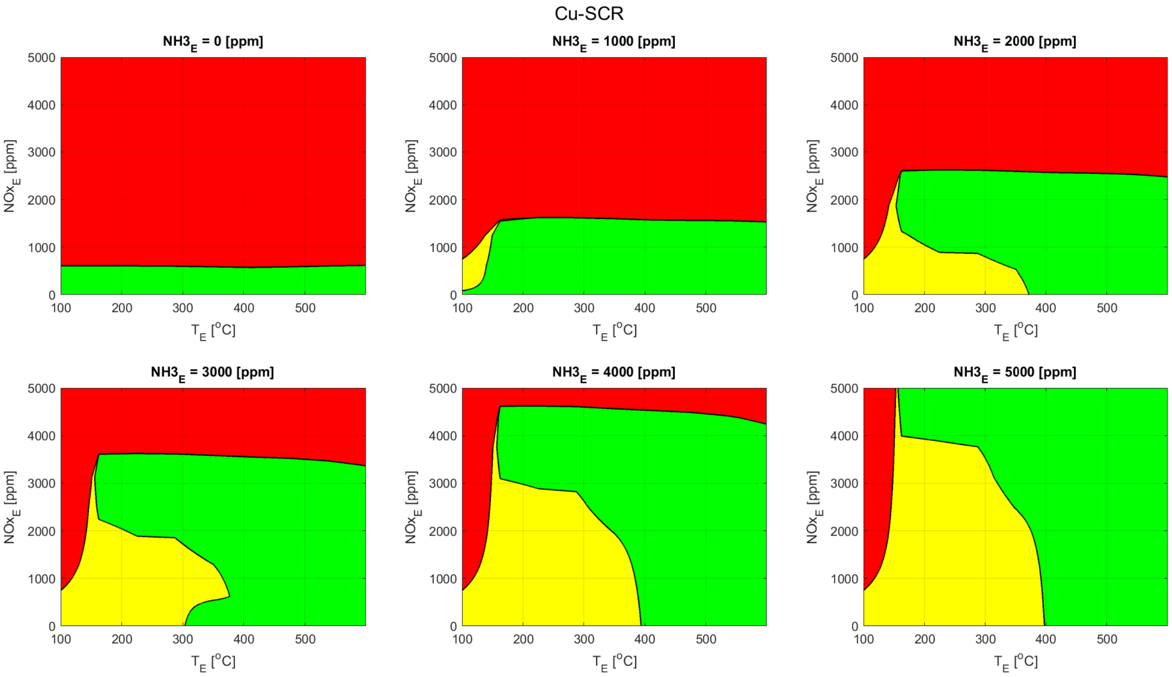

Figure J.17: Operating range Cu-SCR (N$_2$O$_E$ = 0 [ppm], ϕ = 0.9, $^{NO_2}/_{NO_X}$ = 0.075).

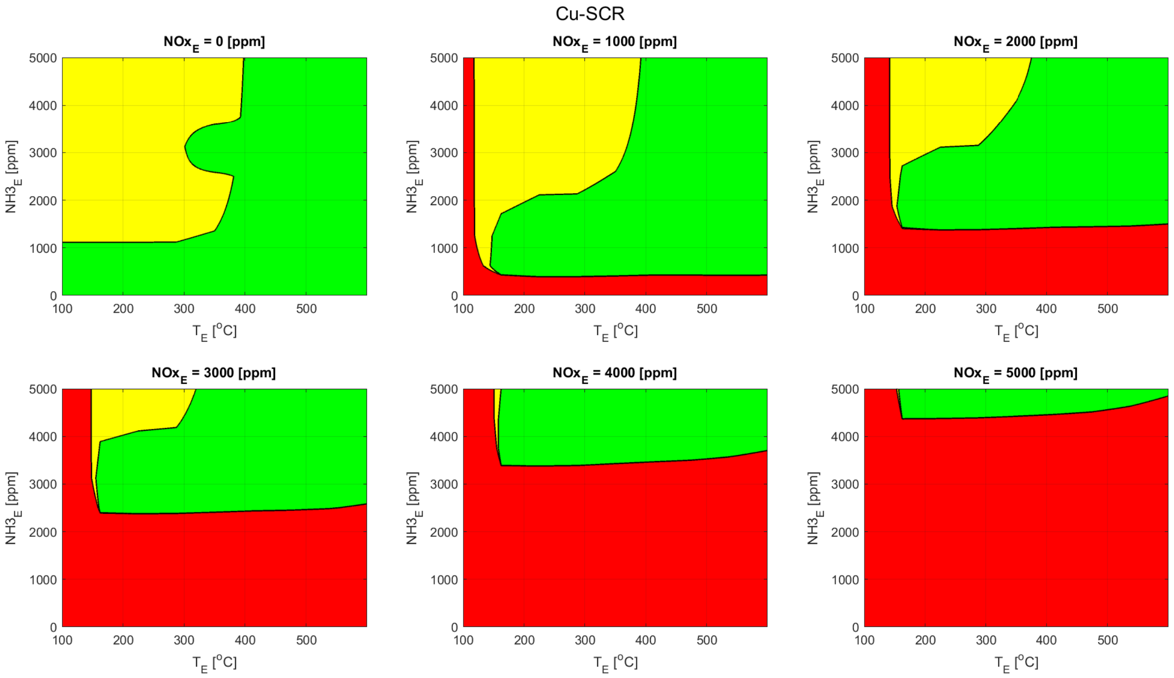

Figure J.18: Operating range Cu-SCR (N_2O_E = 0 [ppm], ϕ = 0.9, ${}^{NO_2}/_{NO_X}$ = 0.075).